Studies on chemical constituents of *Kaempferia marginata* and *Crinum asiaticum* collected from Vietnam and their NO production inhibitory activities

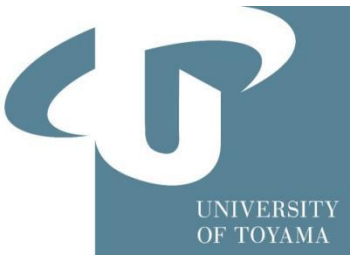

KIEP MINH DO

SECTION OF NATURAL PRODUCTS & DRUG DISCOVERY

INSTITUTE OF NATURAL MEDICINE

UNIVERSITY OF TOYAMA

2023

Table of Contents

Abbreviations

μg/mL	Microgram per milliliter
μL	Micro liter
μM	Micro molar
^{13}C NMR	Carbon Nuclear Magnetic Resonance
^{1}H NMR	Proton Nuclear Magnetic Resonance
calcd	Calculated
C.C	Column Chromatography
CD	Circular Dichroism
$CDCl_3$	Deuterated chloroform
CH_2Cl_2	Dichloromethane
CH_3	Methyl
$CHCl_3$	Chloroform
CO_2	Carbon dioxide
COSY	Correlation Spectroscopy
DMSO	Dimethylsulfoxide
ELISA	Enzyme-linked immunosorbent assay
EtOAc	Ethyl acetate
FBS	Fetal Bovine Serum
g	Gram
h	Hour
H_2O	Water
HMBC	Heteronuclear Multiple Bond Correlation
HMQC	Heteronuclear Multiple Quantum Correlation
HRESIMS	High Resolution Electron Spray Ionization Mass Spectrometry
IR	Infrared
J	Coupling Constant
KBr	Potassium bromide
L-*N*MMA	N^G-Monomethyl-L-arginine monoacetate
LPS	Lipopolysaccharide
m/z	Mass-to-charge-ratio

MeOH	Methanol
mg	Milligram
MHz	Megahertz
min	Minute
mL	Milliliter
mM	Millimolar
MRM	Multiple Reaction Monitoring
MS	Mass Spectroscopy
MTT	3-(4,5-dimethylthiazol-2-yl)-2,5-diphenyltetrazolium bromide
nm	Nanometer
NMR	Nuclear Magnetic Resonance
NOESY	Nuclear Overhauser Effect Spectroscopy
NO	Nitric oxide
OMe	Methoxy
OH	Hydroxy
PBS	Phosphate buffered saline
ppm	part per million
RCB	Riken Cell Bank
TLC	Thin Layer Chromatography
UV	Ultraviolet
αMEM	Minimum Essential Medium

Chapter 1

Introduction

Inflammation is an immune response to the living and non-living substances such as viruses, bacteria, and fungi, as well as chemical components, toxins, and drugs that occur in the body to repair the damaged tissues and maintain homeostasis.[1] Various biomolecule and cellular signal pathways are involved in the process leading to inflammation, resulting in clinical symptoms such as pain, edema, fever, and redness.[2,3] Inflammation can be classified into two types, acute and chronic. Acute inflammation is the initial, rapid response to pathogens, such as infections, toxic compounds, irritants, and tissue damage.[4,5] This process starts within minutes or hours and is of short duration, lasting for several hours or a few days. The vascular reactions of acute inflammation results in changes in the affected area, such as vasodilation, increased blood flow, exudation of fluid-containing proteins exemplified by antibodies, and migration of several different types of leukocytes, including granulocytes, monocytes, and lymphocytes.[6–9] In inflammatory response, endothelial cells are activated, and leukocytes migrate through the vessel wall. The principal leukocytes in acute inflammation are neutrophils, followed by macrophages. Activated macrophages produce a variety of inflammatory mediators, such as nitric oxide (NO), prostaglandins, and pro-inflammatory cytokines. The balance of pro-inflammatory and anti-inflammatory functions in macrophages is one of the critical regulatory factors for maintaining cell and tissue homeostasis. For example, in the macrophages, the inducible nitric oxide synthase plays a central role in producing a significant amount of NO. However, excessive NO production can be detrimental to homeostasis. The controlled inflammatory action is particularly beneficial, and it protects the body from infectious organisms, including mycobacterium tuberculosis, protozoa, fungi, and other parasites. In contrast, chronic inflammation derives from acute inflammation and is not beneficial to the body. Chronic inflammation is associated with many pathophysiologic processes and diseases, including asthma, Crohn's disease, rheumatoid arthritis, rheumatoid polymyalgia, tendonitis, bursitis, laryngitis, gingivitis, gastritis, otitis media, celiac disease, diverticulitis, and inflammatory colitis.[10,11] Furthermore, it is clear that chronic inflammation plays an essential role in the initial or progression of several age-related diseases, such as atherosclerosis, obesity, diabetes, cancer, and Alzheimer's disease.[12–14] The detailed biomechanism of chronic inflammation leading to these diseases has not yet been fully understood. However, due to the relationship between chronic

inflammation and diseases, treatments of inflammation, especially chronic inflammation, have been recognized to be an important factor in elevating human quality of life.[15]

Several non-steroidal anti-inflammatory drugs (NSAID's) such as aspirin, clinoril, diclofenac, ibuprofen, ketoprofen, and naproxen have been approved for the treatment of inflammatory diseases (Figure 1.1).[16–20] Although their structures are wildly different, they have similar antipyretic, analgesic, and anti-inflammatory properties by mitigating pain and delaying inflammatory reactions.[21–23] Nevertheless, the administration of these drugs for a long time might cause several side effects, which can be determined to be highly risk of stroke, kidney problems, and heart attack especially used in a higher dose, together with ulcers, upset stomach, and bleeding in the intestine.[24–28] Several medicinal plants have long been used in folk medicine to treat inflammatory conditions including fevers, pain, migraine, and arthritis.[29–31] Previous studies have proven that various types of natural substances such as alkaloids, diterpenoids, flavonoids, polyphenols, terpenoids, isolated from these medicinal plants exhibit potential anti-inflammatory properties and insignificant detrimental impacts (Figure 1.1).[32,33] Thus, continuous searches for the natural anti-inflammatory inhibitor from medicinal plants would be of interest for not only further discovering of promising anti-inflammatory agent, but also providing traditional usages of the medicinal plants in inflammatory-associated diseases.

Vietnam's territory stretches from North to South, with a diversity of terrestrial and aquatic ecosystems, including inland wetlands and marine ecosystems. It is estimated that more than 12,000 plant species were found in Vietnam, and about one-third of them (3,948 species) have been applied as medicinal plants in traditional medicine.[34–37] However, scientific evidences for the traditional usages of the most medicinal plants, including their active components, has been not yet fully elucidated. Identifying anti-inflammatory constituents in the medicinal plants that have been traditionally used for the inflammatory-associated diseases might lead to the discovery of novel anti-inflammatory agents. Thus, in this study, six species of plants, including *Boesenbergia pandurata* (Zingiberaceae), *Crinum asiaticum*. L. var. *anomalum* Baker (Amaryllidaceae), *Curcuma sahuynhensis* (Zingiberaceae), *Globba pendula Roxb* (Zingiberaceae), *Kaempferia champasakensis* (Zingiberaceae), and *Kaempferia marginata* Carey ex Roscoe (Zingiberaceae) were collected from Vietnam, and their

methanol, EtOAc, $CHCl_3$, and *n*-hexane extracts with the five different concentrations were tested for the NO production inhibitory activity against lipopolysaccharide (LPS)-stimulated RAW264.7 macrophage cells. The assay revealed that the $CHCl_3$ extract of *C. asiaticum* showed the most potent NO production inhibitory activities [IC_{50}: 30.89 ± 0.62 (μg/mL)], followed by the *n*-hexane extract of *K. marginata* [IC_{50} = 54.18 ± 0.61 (μg/mL)]. The *n*-hexane and EtOAc extract of *C. sahuynhensis* and the $CHCl_3$ extract of *G. pendula* showed moderate NO inhibitory activities with the IC_{50} values 74.58 ± 1.43, 72.84 ± 0.67, and 87.52 ± 4.87 (μg/mL), respectively. In contrast, the remaining extracts of *B. pandurata*, *C. asiaticum*, *C. sahuynhensis*, *G. pendula*, *K. champasakensis*, and *K. marginata* were not tested due to the cytotoxic effects (Table 1 and Table S1, Supplementary data). Based on these observations, this study aims to isolate and characterize potent compounds with the NO production inhibitory activities from the two Vietnamese medicinal plants, *K. marginata* and *C. asiaticum*. As a result, this chemical investigation led to the isolation of 36 compounds, including 15 unreported compounds (**1**−**12** and **32**−**34**) and 21 known compounds (**13**−**31, 35** and **36**). The NO production inhibitory assay revealed that *ent*-pimarane and isopimarane, together with the 9,10-seco-isopimarane diterpenoids, showed moderated NO inhibitory activities. Further investigation of the detail mechanism of the inhibitory activities of the isolated flavan and flavan-3-ol revealed their effects on NF-κB signaling pathway through the inhibition of LPS-induced IL6 production and p65 subunit phosphorylation of NF-κB. Chapter 2 will discuss the isolation and structure elucidation of new compounds (**1**−**12**) from the *K. marginata* rhizomes and the NO production inhibitory activities of all isolated compounds. Finally, the isolation and structure elucidation of new compounds (**32**−**34**) from *C. asiaticum* and their NO inhibitory activities will be discussed in Chapter 3.

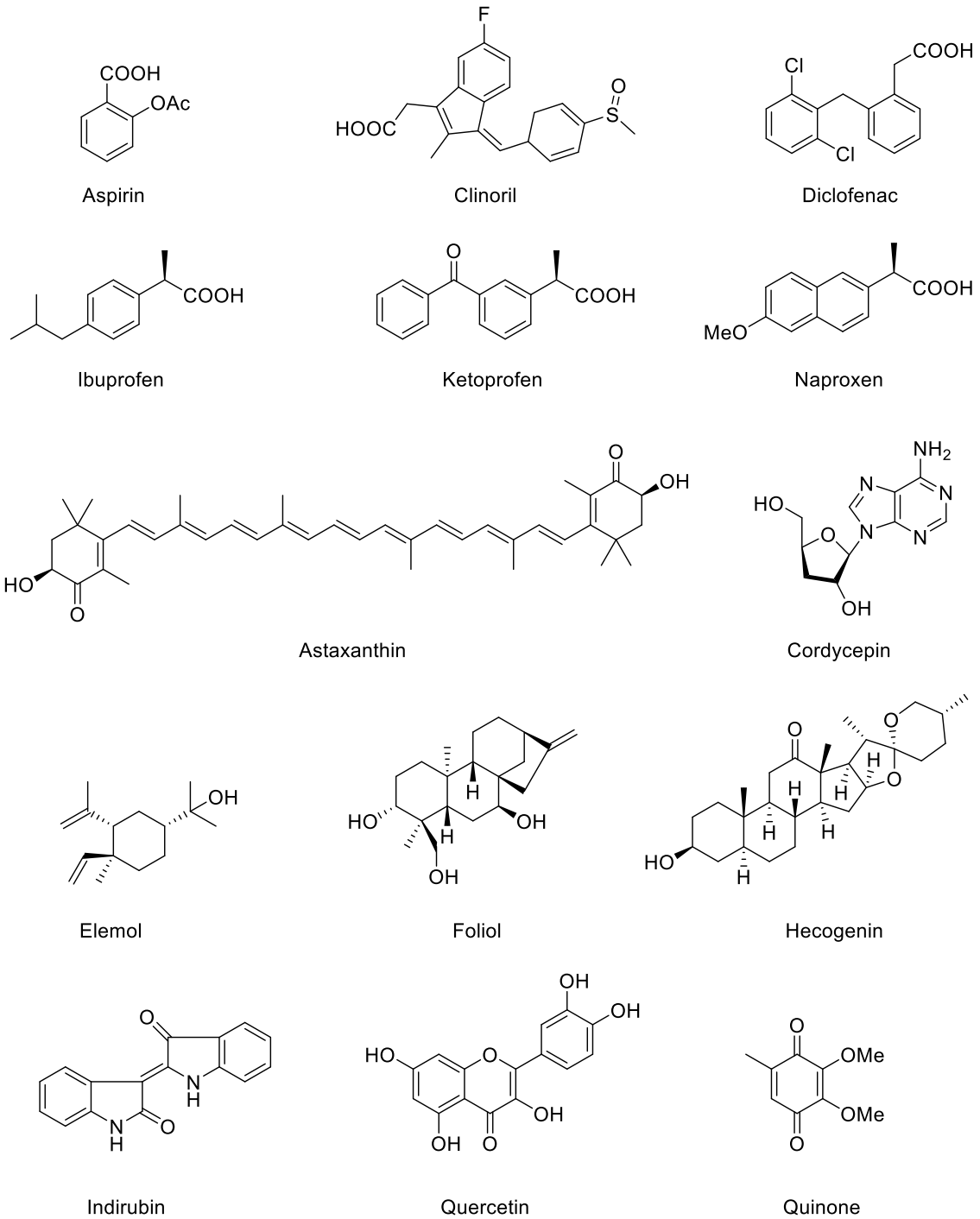

Figure 1.1 NSID's and possible natural products in treatment of inflammatory-associated diseases

Table 1. Inhibitory effects of different extracts on NO production in LPS-induced RAW264.7 cells

Extracts	IC_{50}[a] (μg/mL)	Extracts	IC_{50}[a] (μg/mL)
B. pandurata		*G. pendula*	
MeOH	NT[b]	MeOH	> 100
EtOAc	NT[b]	EtOAc	> 100
$CHCl_3$	NT[b]	$CHCl_3$	87.52 ± 4.87[c]
n-Hexane	NT[b]	*n*-Hexane	NT[b]
C. asiaticum		*K. champasakensis*	
MeOH	36.16 ± 0.28[c]	MeOH	NT[b]
EtOAc	NT[b]	EtOAc	NT[b]
$CHCl_3$	30.89 ± 0.62[c]	$CHCl_3$	NT[b]
n-Hexane	NT[b]	*n*-Hexane	NT[b]
C. sahuynhensis		*K. marginata*	
MeOH	> 100	MeOH	> 100
EtOAc	72.84 ± 0.67[c]	EtOAc	86.63 ± 2.03[c]
$CHCl_3$	NT[b]	$CHCl_3$	NT[b]
n-Hexane	74.58 ± 1.43[c]	*n*-Hexane	54.18 ± 0.61[c]
L-*N*MMA[d]	40.73 ± 0.60[c]		

[a] IC_{50}, half-maximal inhibitory concentration

[b] NT not tested due to the cytotoxicity

[c] Data are presented as mean ± SD of three independent experiments performed in duplicated

[d] L-*N*MMA was used as a positive control

Chapter 2

Constituents of the *Kaempferia marginata* Carey ex Roscoe collected from Vietnam and their NO inhibitory activities

2.1 Introduction

Kaempferia marginata Carey ex Roscoe is a small ginger of the Zingiberaceae family. In Asian countries, *K. marginata* can be found in China, India, Myanmar, and Thailand.[38,39] In Vietnam, *K. marginata* has been called *K. galanga* for a long period due to their similar characteristics. Recently, a taxonomic analysis identified *K. marginata* as a new record for the flora of Vietnam (Figure 2.1).[40] The *K. marginata* rhizomes have been locally used as an herb in food and a folk medicine for a long time. For example, local people in Thailand use the roots and leaves of *K. marginata* for curries as a flavoring, while they use the rhizomes as a medicine for treating allergy symptoms, fevers, and swollen legs.[41] Chinese traditional medicine utilizes rhizomes to cure abdominal pains, toothaches, coughs, and inflammatory tumours. In Vietnam, the local people used tubers as a food spice, while they applied the rhizomes-alcohol infusion for the relief of muscle aches and backaches.[42]

Previous phytochemical investigations of the *K. marginata* rhizomes collected from different locations detected isopimaradiene diterpenoids in extracts of this species as major components. For example, the Thailand *K. marginata* rhizomes contain pimarane diterpenoids with more than 30 sandaracopimaradienes, together with one kavalactone, one diarylheptanoid, and three sterols.[38,39,43] Meanwhile, cinnamate derivatives, monoterpenes, sandaracopimaradienes, and steroids were isolated from the Chinese *K. marginata* rhizomes.[44] Among these isolated compounds, pimarane diterpenoids showed antiplasmodial, anti-tuberculosis, antifungal,[45] and anti-inflammatory activities.[44,45] In contrast, the biological and chemical properties of the Vietnamese *K. marginata* have not yet been fully elucidated, except for the isolation of ethyl *p*-methoxycinnamate the Vietnamese *K. galanga* L. rhizomes (with the previous botanical name).[46]

As mentioned in Chapter 1, the *n*-hexane extract of the *K. marginata* rhizomes showed the NO production inhibitory activity. Thus, the isolation of the active compounds with the NO production inhibition activity from the rhizomes of *K. marginata* was performed.

2.2. Extraction and isolation

The *K. marginata* rhizomes dried powder (1.5 kg) was macerated with methanol under sonication (4 L, 90 min, × 4) at 30 °C. The methanol extract (30.3 g) was triturated in water and successively partitioned with *n*-hexane, $CHCl_3$, and EtOAc to obtain the *n*-hexane (13.6 g), $CHCl_3$ (8.4 g), and EtOAc (3.1 g) extracts after removal of the solvents using a rotatory evaporator. The *n*-hexane extract was further subjected to silica gel column chromatography (C.C), eluting with *n*-hexane:EtOAc (95:5 to 0:100, v/v), to give nine fractions F_1–F_9. These fractions were further subjected to a series of chromatographic separations, which led to the isolation of 31 compounds including twelve new diterpenoids, marginols A–K (**1**–**11**), 14-*epi*-boesenberol F (**12**), and nineteen known diterpenoids, boesenberol F (**13**), boesenberol J (**14**), kaemgalangol A (**15**), kaemgalangol C (**16**), kaempulchraols B–D (**17**–**19**), kaempulchraols E, K, L, and W (**20**–**23**), (5β,9β,10α,13α)-pimara-6,8(14)15-trien-18-oic acid (**24**), 6-actetoxysandaracopimaradien-9-ol-1-one (**25**), 6-acetoxysandaracopimaradien-1,9-diol (**26**), sandaracopimaradien-1,9-diol (**27**), sandaracopimaradien-6β,9β-diol-1-one (**28**), sandaracopimaradien-1,6,9-triol (**29**), virescenol B (**30**), and virescenol C (**31**) (Figures 2.2, 2.3, and 2.4). Analyses of the 1D and 2D NMR and HRESIMS data elucidated the chemical structures of all new compounds, and based on CD spectroscopic data, the absolute configurations of **1**–**3**, **8**, and **9**–**12** were determined. Furthermore, comparisons of NMR data with the literature previously reported identified the structures of known compounds.

Figure 2.1 *K. marginata* from Vietnam

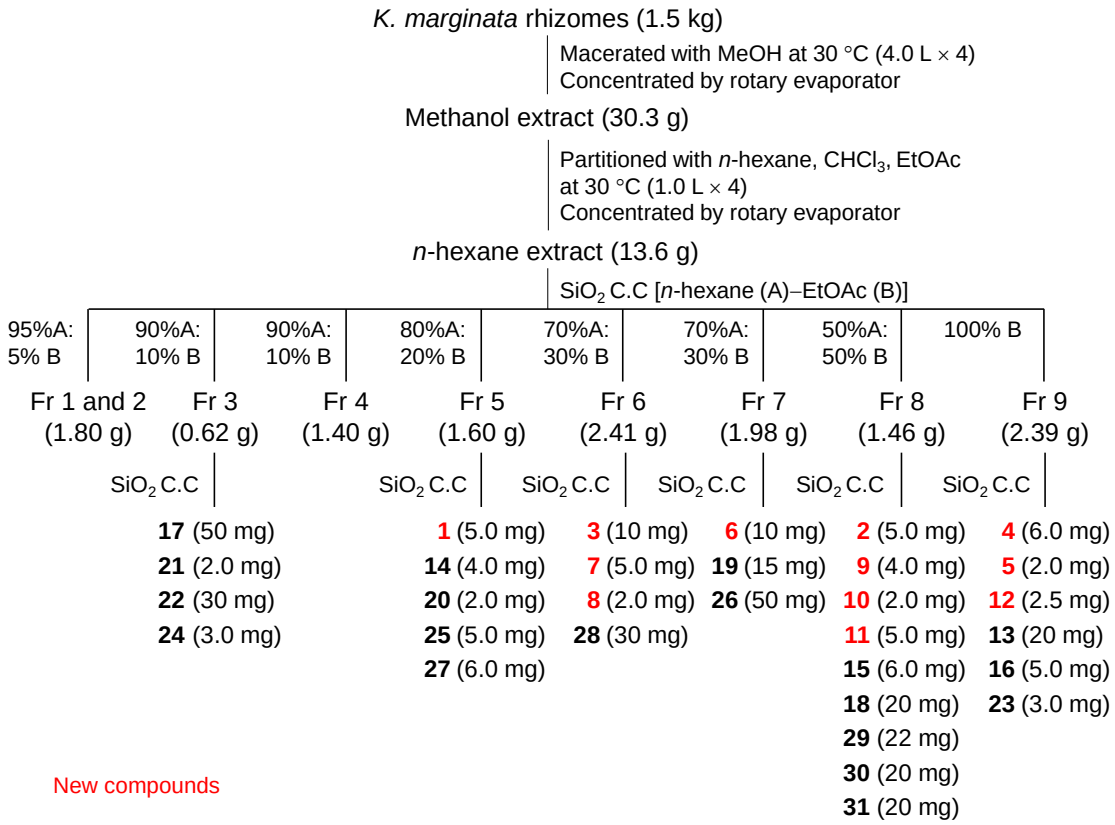

Figure 2.2 Extraction and isolation of compounds (**1**–**31**) from the *n*-hexane extract of the *K. marginata* rhizomes

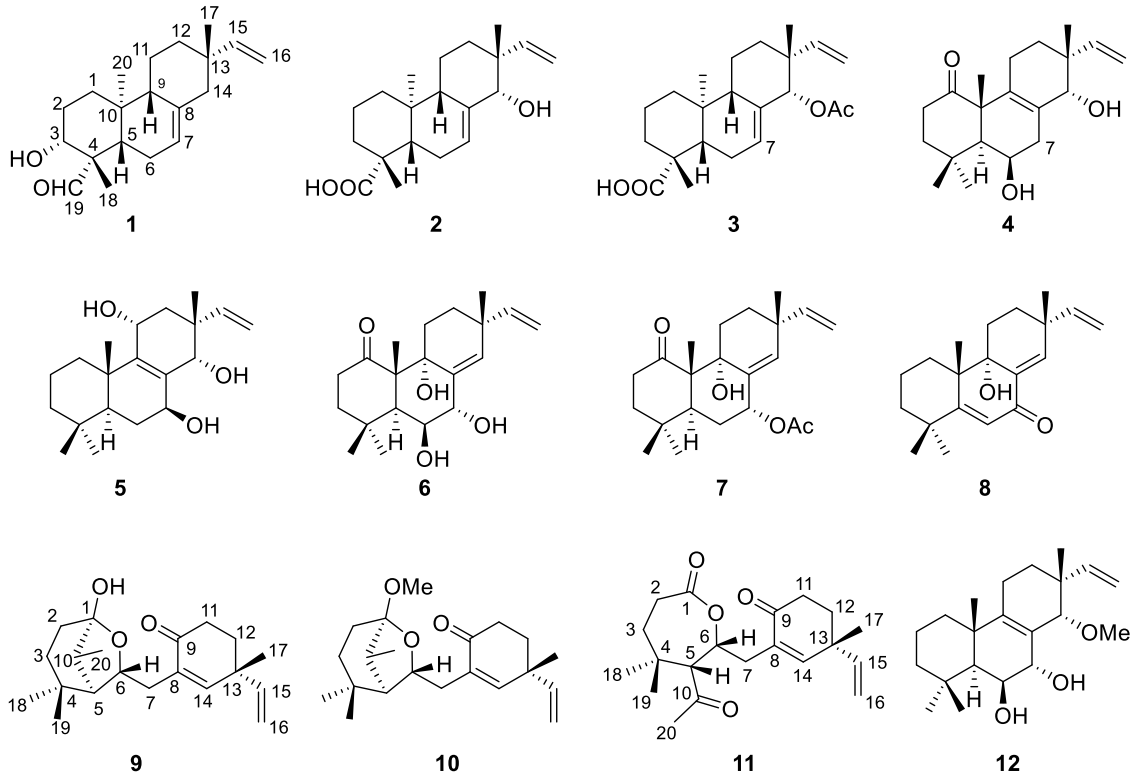

Figure 2.3 Structures of new compounds (**1**−**12**) isolated from the *n*-hexane extract of the *K. marginata* rhizomes

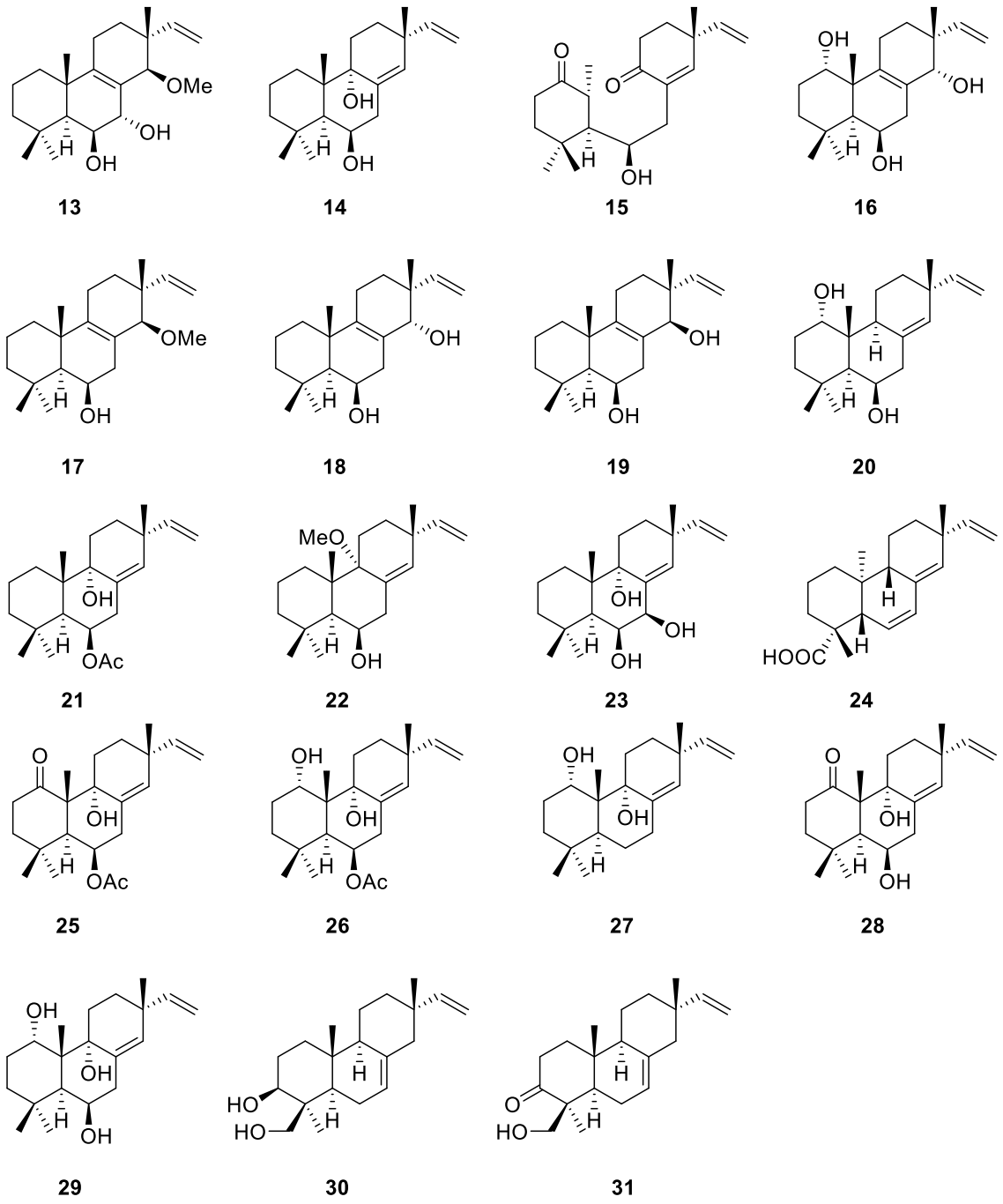

Figure 2.4 Structures of known compounds (**13**−**31**) isolated from the *n*-hexane extract of the *K. marginata* rhizomes

2.3 Structure elucidation of new compounds

2.3.1 Marginol A (1)

Compound **1** was isolated as a colorless oil. The molecular formula of **1** was determined as $C_{20}H_{30}O_2$, indicating six degrees of unsaturation, based on a cationized molecular ion peak at *m/z* 325.2134 $[M + Na]^+$ (calcd. for $C_{20}H_{30}O_2Na$, 325.2138) in HRESIMS, in conjugation with ^{13}C NMR data. Its IR spectrum showed the presence of hydroxy (3468 cm^{-1}), carbonyl (1710 cm^{-1}), and olefinic (1646 cm^{-1}) functionalities. The ^1H NMR spectrum (Figure 2.5) displayed resonances, due to the terminal vinyl protons (H-15, H-16ab), an olefinic proton (H-7), three methines including an oxygenated proton (H-3, H-5, H-9), six methylene protons (H-1$\alpha\beta$, H-2$\alpha\beta$, H-6$\alpha\beta$, H-11$\alpha\beta$, H-12$\alpha\beta$, H-14$\alpha\beta$), and three tertiary methyl singlet protons (H_3-17, H_3-18, H_3-20). The ^{13}C NMR spectrum (Figure 2.6) revealed 20 carbon resonances, which were a carbonyl carbon (C-19), four sp^2 carbons (C-7, C-8, C-15, C-16), three methines (C-3, C-5, C-9), three sp^3 quaternary carbons (C-4, C-10, C-13), six methylenes (C-1, C-2, C-6, C-11, C-12, C-14), and three tertiary methyls (C-17, C-18, C-20). These NMR spectroscopic data (Table 2.1) were highly similar to those of the *ent*-pimaradiene diterpenoid, (4*R*,5*S*,9*R*,10*S*,13*S*)-*ent*-pimara-7,15-dien-19-oic acid (**1'**).[47] Isolation of *ent*-pimarane diterpenoids have never been reported from the Thai and Chinese *K. marginata* rhizomes. The significant differences were the presence of the resonances of one oxygenated methine [δ_H 3.74 (dd, J = 11.9, 4.0 Hz)/δ_C 76.9] and a formyl group [δ_H 10.61 (s)/δ_C 207.9] in **1**, instead of the methylene and carboxylic group resonances in **1'**, suggesting **1** to be a substituent analog of **1'** with the hydroxy and formyl groups. The ^1H-^1H COSY correlations, together with the HMBC correlations from H_3-18/H_3-20 to C-5, from H_2-6/H_2-11 to C-8, from H-7 to C-9, and from H-7/H_3-17/H-15 to C-14, confirmed that **1** was a pimarane diterpenoid with a Δ^7-double bond (Figure 2.7a). Furthermore, the HMBC correlations from H_3-18 to C-3/C-4/C-5/C-19 revealed the attachment of the hydroxy and formyl groups at C-3 and C-4 in the structure of **1**, respectively. The coupling constant and the analysis of its NOESY spectrum supported the relative configuration of **1** as follows (Figure 2.7b). The large coupling constant value of 12.4 Hz at H-5 suggested the axial orientation of H-5. Furthermore, the presence of NOESY correlations from H-5 to H-3β/H_3-18/H-1β/H-9/H-14β/H_3-17/H-

12β indicated the β orientations of H-5, H-9, and the methyl groups at C-17 and C-18, respectively. In contrast, the hydroxy group at C-3, the formyl group at C-4, and the vinyl group at C-13 were assigned as α-orientation. Similarly, the methyl group at C-10 adopted α-orientation due to the NOESY correlation from H-19 to H_3-20. Thus, the structure of **1** was confirmed to be the *ent*-pimara-7,15-diene type of diterpenoid, mainly derived from *ent*-copalyl diphosphate *via* catalysis by an as-yet unidentified diterpene synthase. The comparisons of its experimental and calculated CD spectra determined the absolute configuration of **1** as follows. The CD spectrum of **1** showed a negative Cotton effect value at 266 nm and a positive Cotton effect value at 303 nm due to the presence of a formyl moiety at C-4, in good agreement with the calculated CD spectrum from the model of (3*R*,4*S*,5*S*,9*R*,10*S*,13*S*)-**1** (Figure 2.8). Thus, **1** was determined to be (3*R*,4*S*,5*S*,9*R*,10*S*,13*S*)-*ent*-pimara-3-hydroxy-7,15-dien-19-al, and was named marginol A.

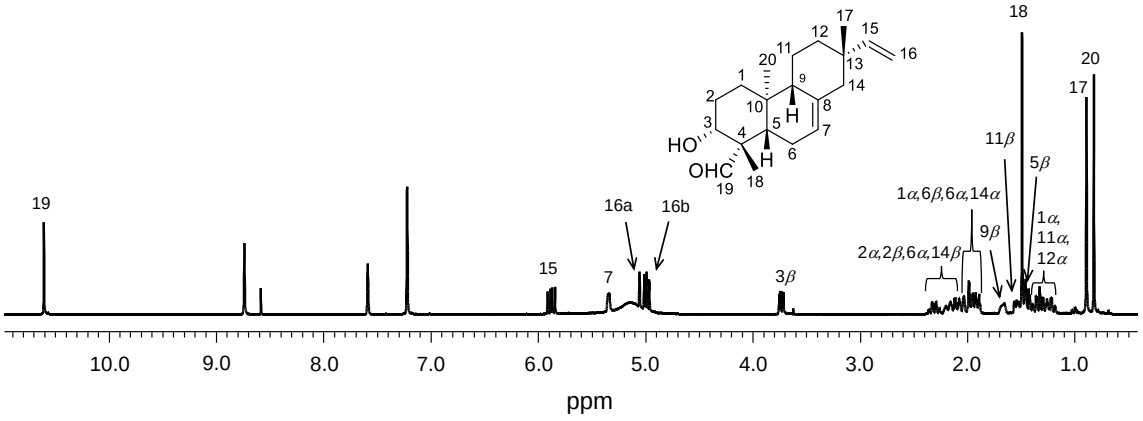

Figure 2.5 ^{1}H NMR spectrum (400 MHz) of **1** in pyridine-d_5

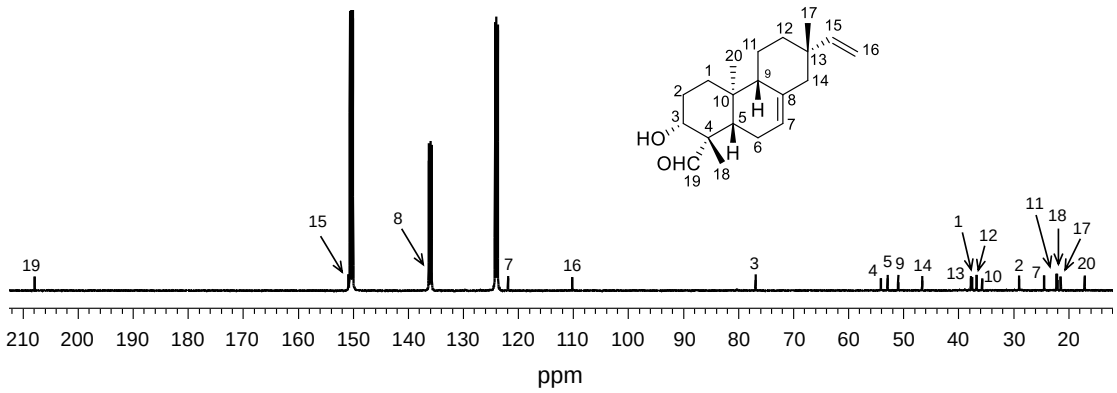

Figure 2.6 ^{13}C NMR spectrum (100 MHz) of **1** in pyridine-d_5

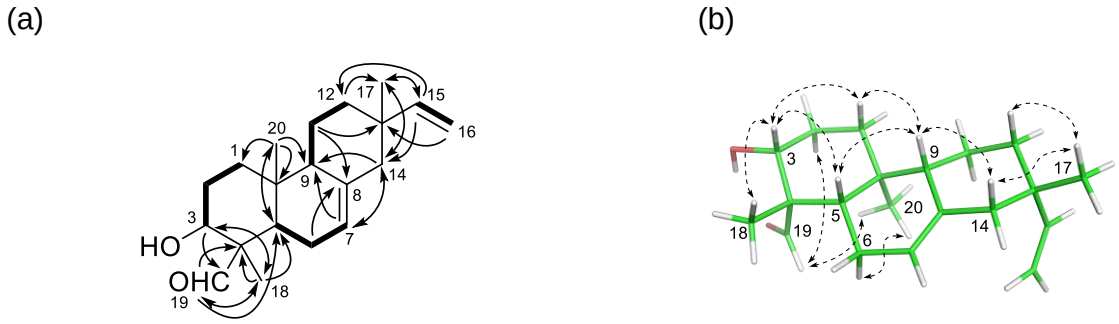

Figure 2.7 ^{1}H–^{1}H COSY correlations (bold lines) and key HMBC (arrows) (a) and NOESY (dashed arrows) correlations of **1** (b)

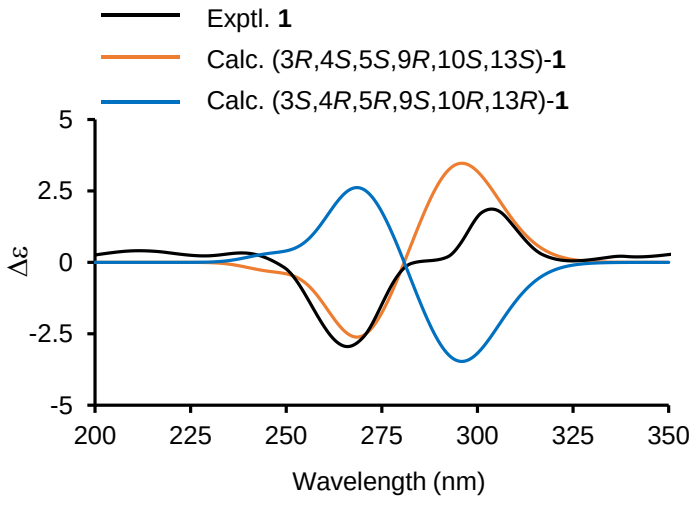

Figure 2.8 Experimental and calculated CD spectra of **1**

Table 2.1 ^{1}H (400 MHz) and ^{13}C (100 MHz) NMR spectroscopic data for **1** in pyridine-d_5 [δ in ppm and J value in (Hz) in parentheses]

Position	**1**	
	δ_H	δ_C
1α	1.91 (dt,13.3. 3.4)	37.5
1β	1.23 (m)	
2α	2.30 (m)	29.0
2β	2.10 (m)	
3β	3.74 (dd, 11.9, 4.0)	76.9
4		54.1
5β	1.43 (dd, 12.4, 4.6)	52.9
6α	2.22 (m)	24.5
6β	1.97 (m)	
7	5.35 (br d, 3.6)	121.9
8		135.8
9β	1.67 (m)	51.0
10		35.7
11α	1.29 (m)	22.2
11β	1.54 (m)	
12α	1.33 (m)	36.7
12β	1.47 (m)	
13		37.8
14α	1.94 (m)	46.6
14β	2.04 (m)	
15	5.88 (dd, 17.4, 10.5)	150.9
16a	5.04 (dd, 17.4, 1.4)	110.2
16b	4.98 (dd, 10.5, 1.4)	
17	0.89 (s)	21.5
18	1.49 (s)	22.1
19	10.61 (s)	207.9
20	0.82 (s)	17.1

2.3.2 Marginol B (2)

Compound **2** was isolated as a colorless oil. Its HRESIMS indicated an anionized molecular ion peak at *m/z* 317.2124 $[M - H]^-$ (calcd. for $C_{20}H_{29}O_3$, 317.2122) assignable to the molecular formula $C_{20}H_{30}O_3$, with an increase of 16 mass units over that of **1**. The IR spectrum of **2** displayed an absorption band at 1689 cm^{-1} assignable to the carbonyl group. In addition, it also showed a stronger and broader absorption band than that of **1** at 3440 cm^{-1} corresponding to the hydroxy group. No absorption bands corresponding to ether group(s) were observed in the IR spectrum. This information suggested that **2** could be an analog of **1** with either a carboxylic group instead of the formyl group or one more hydroxy group on the main skeleton. 1D, 2D NMR, and CD spectra analyses further proved the possibility of **2** being a structural analog of **1** (Figures 2.9 and 2.10). The 1D NMR data of **2** in conjugation with the HMQC data showed the close structural resemblance between **2** and **1** (Table 2.2), suggesting that **2** shared the *ent*-pimara-7,15-diene type of skeleton observed in **1**. The significant difference was the absence of the formyl proton as well as the change in the chemical shift at C-19, where the signal was shielded from δ_C 207.9 in **1** to δ_C 183.9 in **2**. Another difference was the presence of a singlet oxygenated methine proton signal at δ_H 3.62 in **2**, instead of the methylene resonance [δ_H 2.04/1.94 (each m)/δ_C 46.6] at C-14 of **1**. These differences suggested that **2** is not only the substituent analog of **1** with the carboxylic moiety at C-4, but also the regioisomer of **1** that shifted the hydroxy group at C-3 to C-14. The carboxylic group was attached at C-4 based on the HMBC correlations from H_3-18 to C-3/C-4/C-5/C-19. Furthermore, the HMBC correlations from H-7/H_3-17/H-15 to C-14 indicated that the hydroxy group was located at C-14 (Figure 2.11a). Therefore, the planar structure of **2** was assigned, as shown in Figure 2.3. The relative configuration of **2** was established in the same way as those of **1**, based on the coupling constant (Table 2.2) and NOESY correlations as mentioned in Figure 2.11b. Compound **2** was thus supported to be an *ent*-pimarane diterpenoid. Furthermore, the NOESY correlations from H-5 to H-3/H_3-18 and from H-14 to H_3-17 suggested α-orientations of the carboxylic and hydroxy groups at C-4 and C-14 (Figure 2.11b). In addition, ECD spectrum of **2** was consistent with the calculated one of the (4*R*,5*S*,9*S*,10*S*,13*R*,14*S*)-**2**

model (Figure 2.12). Hence, **2** was established as *ent*-pimara-14-hydroxy-7,15-dien-19-oic acid with these absolute configurations and was named marginol B.

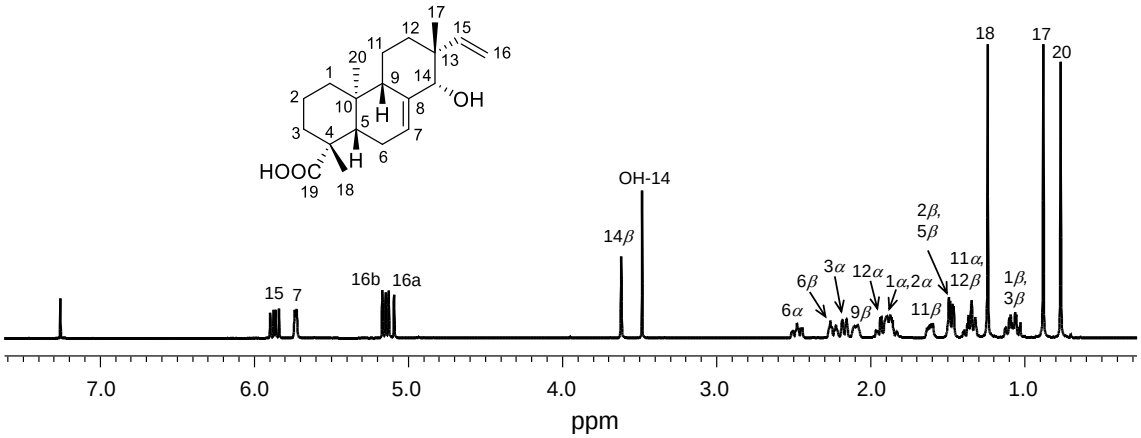

Figure 2.9 ^{1}H NMR spectrum (500 MHz) of **2** in $CDCl_3$

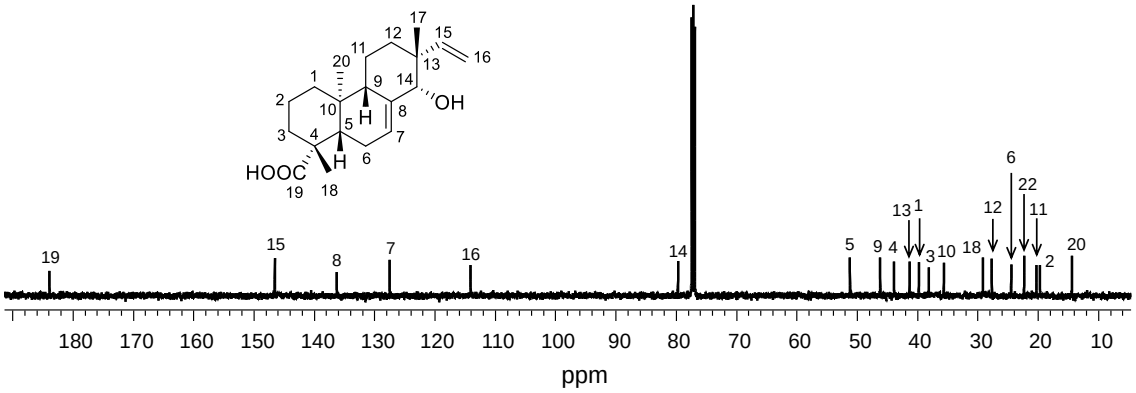

Figure 2.10 ^{13}C NMR spectrum (125 MHz) of **2** in $CDCl_3$

(a) (b)

Figure 2.11 ^{1}H–^{1}H COSY correlations (bold lines) and key HMBC (arrows) (a) and NOESY (dashed arrows) correlations of **2** (b)

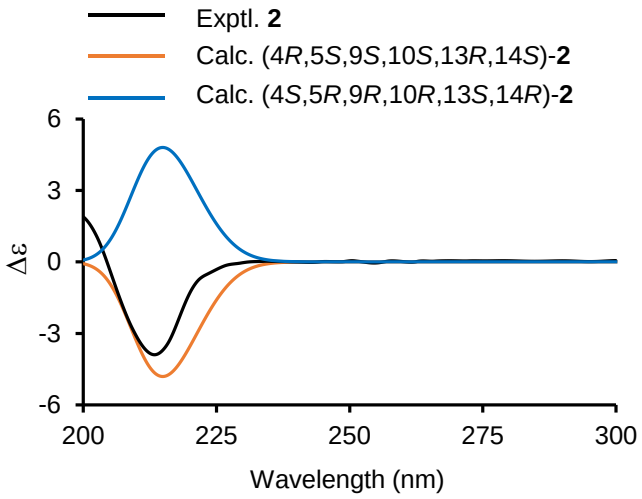

Figure 2.12 Experimental and calculated CD spectra of **2**

Table 2.2 ^{1}H (500 MHz) and ^{13}C (125 MHz) NMR spectroscopic data for **2** in $CDCl_3$ [δ in ppm and *J* value in (Hz) in parentheses]

Position	**2**	
	δ_H	δ_C
1α	1.88 (m)	39.8
1β	1.11 (dd, 14.0, 4.3)	
2α	1.87 (m)	19.7
2β	1.47 (m)	
3α	2.17 (d, 12.3)	38.1
3β	1.06 (m)	
4		43.9
5β	1.48 (dd, 12.3, 4.3)	51.2
6α	2.48 (m)	24.4
6β	2.24 (m)	
7	5.73 (br d, 5.7)	127.5
8		136.2
9β	2.10 (m)	46.2
10		35.6
11α	1.35 (m)	20.3
11β	1.62 (m)	
12α	1.93 (m)	27.5
12β	1.33 (m)	
13		41.3
14β	3.62 (s)	
15	5.87 (dd, 17.8, 10.9)	146.5
16a	5.11 (dd, 17.8, 1.1)	114.1
16b	5.16 (dd, 10.9, 1.1)	
17	0.88 (s)	22.3
18	1.24 (s)	29.1
19		183.9
20	0.76 (s)	14.4
OH-14	3.48 (s)	

2.3.3 Marginol C (3)

Compound **3** was obtained as a colorless oil with a molecular formula of $C_{22}H_{34}O_4$, 42 mass units higher than that of **2**, based on the HRESIMS analysis in conjugation with the ^{13}C NMR data, suggesting that **3** was an acetylated analog of **2**. The 1D NMR data of **3** (Table 2.3, Figures 2.13 and 2.14) was similar to those of **2**, except for the presence of resonances for the acetyl group [δ_H 2.06/δ_C 20.8 (*Me*COO-14); δ_C 170.4 (Me*C*OO-14)]. The HMBC correlations from H-14 to Me*C*OO-14/C-7/C-9/C-15 allow us to locate the acetoxy moiety at C-14 (Figure 2.15a).

NOESY and CD spectrum analyses in the same way as those of **2** confirmed the relative and absolute configurations of **3** as shown in Figures 2.15b and 2.16. Hence, **3** was determined to be (4*R*,5*S*,9*S*,10*S*,13*R*,14*S*)-*ent*-pimara-14-acetoxy-7,15-dien-19-oic acid, and was named marginol C.

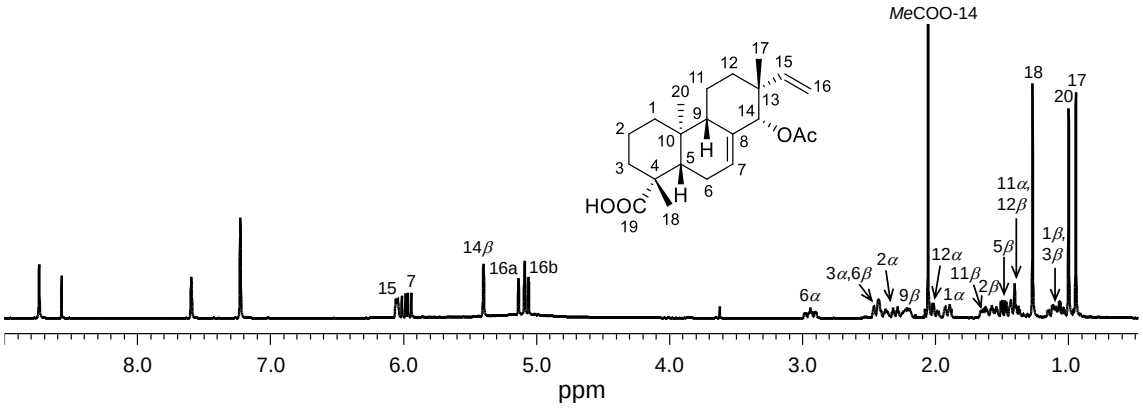

Figure 2.13 ^1H NMR spectrum (400 MHz) of **3** in pyridine-d_5

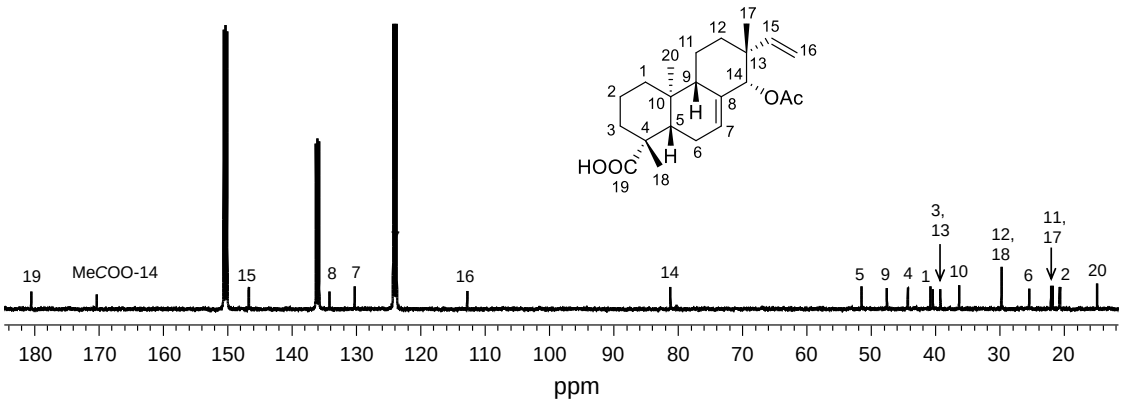

Figure 2.14 ^{13}C NMR spectrum (100 MHz) of **3** in pyridine-d_5

(a) (b)

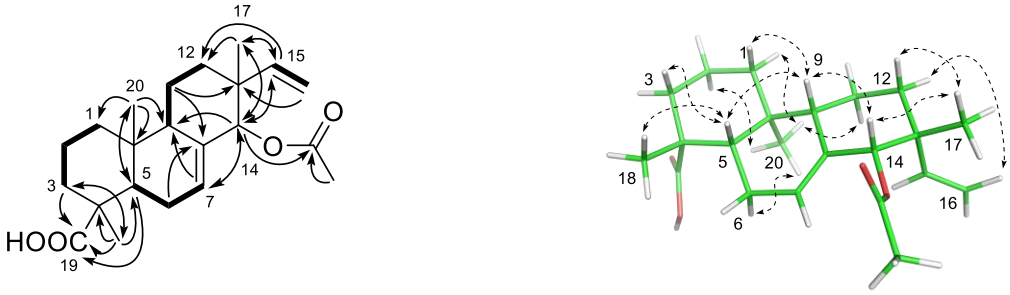

Figure 2.15 ^{1}H–^{1}H COSY correlations (bold lines) and key HMBC (arrows) (a) and NOESY (dashed arrows) correlations of **3** (b)

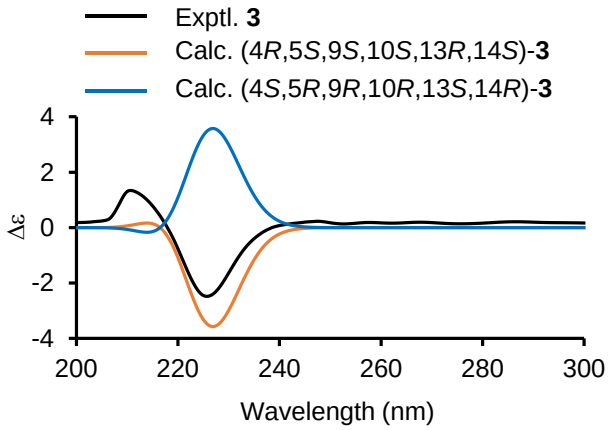

Figure 2.16 Experimental and calculated CD spectra of **3**

Table 2.3 ^{1}H (400 MHz) and ^{13}C (100 MHz) NMR spectroscopic data for **3** in pyridine-d_5 [δ in ppm and J value in (Hz) in parentheses]

Position	**3**	
	δ_H	δ_C
1α	1.91 (d, 14.2)	40.5
1β	1.14 (m)	
2α	2.30 (dt, 14.2, 3.7)	20.7
2β	1.56 (dt, 13.7, 3.3)	
3α	2.44 (m)	
3β	1.07 (m)	39.3
4		44.4
5β	1.49 (dd, 12.1, 4.4)	51.5
6α	2.94 (dddd, 18.5, 12.1, 4.4, 1.8)	25.5
6β	2.39 (m)	
7	6.05 (dd, 3.9, 2.1)	130.3
8		134.2
9β	2.23 (m)	47.6
10		36.4
11α	1.39 (m)	21.9
11β	1.64 (m)	
12α	2.00 (dd, 14.0, 4.8)	29.8
12β	1.42 (m)	
13		39.3
14β	5.40 (s)	81.2
15	5.98 (dd, 17.6, 10.8)	146.7
16a	5.11 (dd, 17.6, 1.4)	112.8
16b	5.07 (dd, 10.8, 1.4)	
17	0.95 (s)	22.1
18	1.27 (s)	29.8
19		180.5
20	1.00 (s)	14.9
*Me*COO-14	2.06 (s)	20.8
Me*C*OO-14		170.4

2.3.4 Marginol D (4)

Compound **4** was obtained as a colorless oil. HRESIMS and 1D NMR deduced the molecular formula to be $C_{20}H_{30}O_3$. The IR spectrum showed 3407 and 1706 cm^{-1} absorption bands, corresponding to hydroxy and carbonyl groups. The 1D NMR data of **4** (Table 2.4) were similar to those of the isopimara-8(9),15-diene type of diterpenoids, which have also never been isolated from the China and Thai *K. marginata* species. In particular, the 1D NMR (Figures 2.17 and 2.18) data of **4** was similar to those of kaempulchraol D (**19**),[48] which was also isolated in this study. However, the presence of the carbonyl resonance (δ_C 215.1) in **4**, instead of the absence of the methylene signal [δ_H 1.03, 1.67 (each m)/δ_C 39.7] at C-1 of **19** were observed as significant differences between **4** and **19**, indicating that **4** is a substituent analog of **19** with the keto group at C-1. The ^{1}H-^{1}H COSY and HMBC correlations shown in Figure 2.19a established the planar structure of **4** with the keto group at C-1. The relative configuration of **4** was established in the same way as those of **19**, based on the NOESY cross peaks of H-5/H_3-19/H-7α/H-6α, H_3-18/H_3-20, and H-7β/H-14/H_3-17 (Figure 2.19b). Thus, the structure of **4** was established as 6β,14α-dihydroxyisopimara-8(9),15-diene-1-one, and named marginol D.

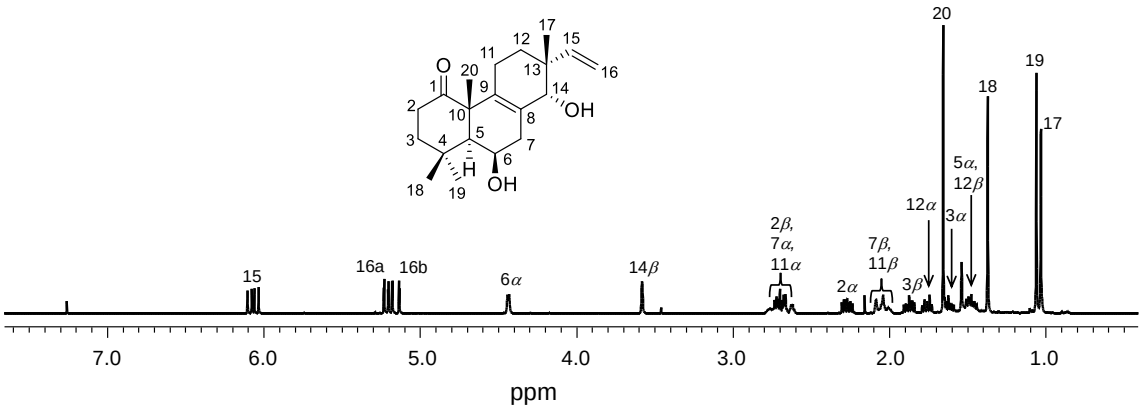

Figure 2.17 ^{1}H NMR spectrum (400 MHz) of **4** in $CDCl_3$

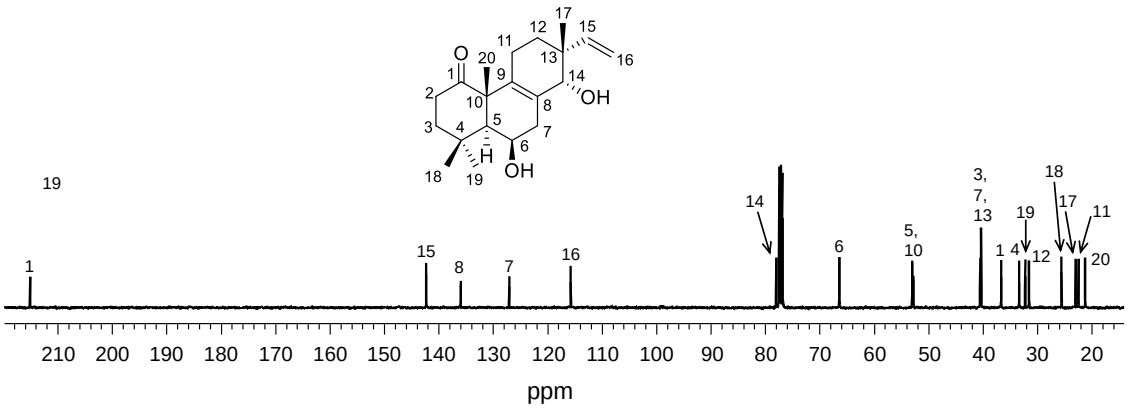

Figure 2.18 ^{13}C NMR spectrum (100 MHz) of **4** in $CDCl_3$

(a) (b)

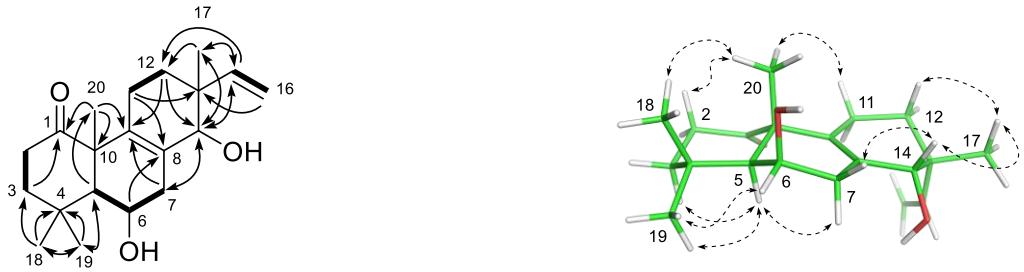

Figure 2.19 $^{1}H–^{1}H$ COSY correlations (bold lines) and key HMBC (arrows) (a) and NOESY (dashed arrows) correlations of **4** (b)

Table 2.4 ^{1}H (400 MHz) and ^{13}C (100 MHz) NMR spectroscopic data for **4** in $CDCl_3$ [δ in ppm and *J* value in (Hz) in parentheses]

Position	**4**	
	δ_H	δ_C
1		215.1
2α	2.27 (m)	36.7
2β	2.70 (m)	
3α	1.62 (td, 9.3, 4.6)	40.3
3β	1.88 (m)	
4		33.4
5α	1.54 (s)	53.0
6α	4.44 (t, 2.1)	66.5
7α	2.66 (m)	40.3
7β	2.08 (m)	
8		127.0
9		136.1
10		52.8
11α	2.75 (m)	22.5
11β	2.05 (m)	
12α	1.75 (dt,13.3, 5.7)	31.6
12β	1.48 (m)	
13		40.5
14β	3.58 (s)	78.0
15	6.07 (dd, 17.4, 11.0)	142.3
16a	5.16 (dd, 17.4, 1.6)	115.9
16b	5.22 (dd, 11.0, 1.6)	
17	1.06 (s)	23.1
18	1.37 (s)	25.6
19	1.01 (s)	32.3
20	1.66 (s)	21.3

2.3.5 Marginol E (5)

Compound **5** was obtained as an amorphous solid. HRESIMS in conjugation with 1D NMR data revealed its molecular formula to be $C_{20}H_{32}O_3$. The IR spectrum showed a characteristic absorption band indicative of the presence of the hydroxy group in **5**. The planar structure of **5** was established to be 7,11,14-trihydroxyisopimara-8(9),15-diene, based on the 1D and 2D NMR data (Table 2.5, Figures 2.20, 2.21, and 2.22a). Its structure was similar to the sphaeropsidin E.[49] Particularly remarkable differences were observed at C-7 and C-11 in the ^{13}C NMR data of **5**, where the signals for C-7 in **5** was deshielded from δ_C 65.5 in sphaeropsidin E to δ_C 69.9, while the signal for C-11 was shielded from δ_C 65.5 in sphaeropsidin E to δ_C 63.7 in **5**, suggesting that **5** is a stereoisomer of sphaeropsidin E at both C-7 and C-11 (Figures 2.20 and 2.21). The coupling constant values of 13.0 Hz and 10.1 Hz were observed at H-5 and H-7, respectively, and the NOESY correlations of H-5 to H-7 (Figure 2.22b) suggested that the hydroxy group at C-7 was β-oriented in the equatorial form. In contrast, the coupling constant values of 4.8 and 1.6 Hz between H-11 and H_2-12 and the NOESY correlations of H-5/H_3-19 and H_3-18/H_3-20/H-11 indicated the α-orientation of the hydroxy group at C-11 in the equatorial form. The α-orientation of the C-14 hydroxy group was established based on NOESY correlation between H-14 and H-7β. Hence, **5** was determined to be 7β,11α,14α-trihydroxyisopimara-8(9),15-diene, and named marginol E.

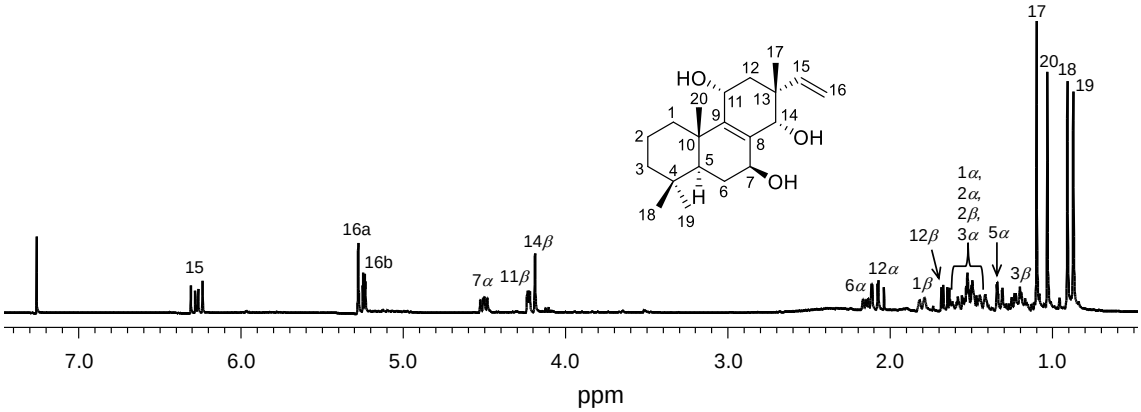

Figure 2.20 ^{1}H NMR spectrum (400 MHz) of **5** in $CDCl_3$

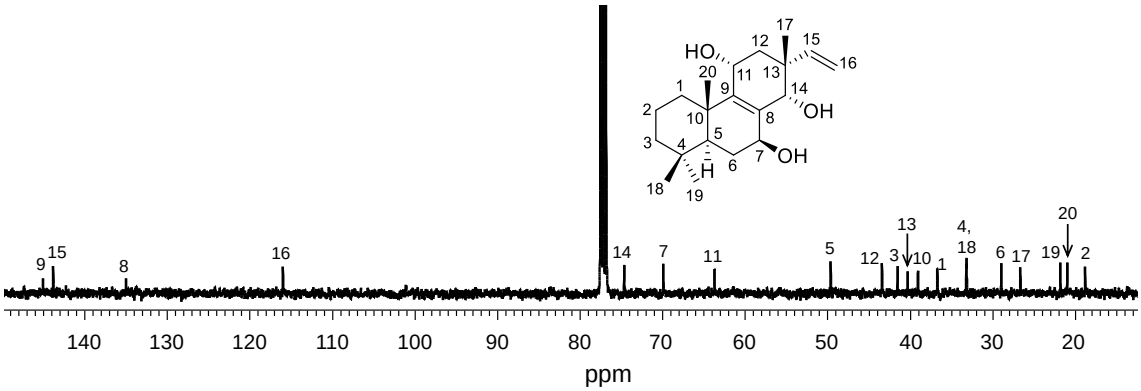

Figure 2.21 ^{13}C NMR spectrum (100 MHz) of **5** in $CDCl_3$

(a) (b)

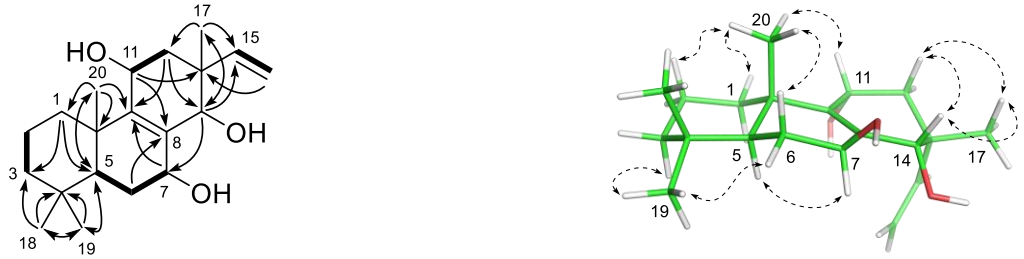

Figure 2.22 $^{1}H–^{1}H$ COSY correlations (bold lines) and key HMBC (arrows) (a) and NOESY (dashed arrows) correlations of **5** (b)

Table 2.5 ^{1}H (400 MHz) and ^{13}C (100 MHz) NMR spectroscopic data for **5** in $CDCl_3$ [δ in ppm and *J* value in (Hz) in parentheses]

Position	**5**	
	δ_H	δ_C
1α	1.49 (m)	36.7
1β	1.80 (d, 12.7)	
2α	1.58 (m)	18.8
2β	1.52 (m)	
3α	1.43 (d, 14.7)	41.5
3β	1.20 (m)	
4		33.2
5α	1.33 (dd, 13.0, 1.6)	49.6
6α	2.15 (m)	28.9
6β	1.50 (m)	69.9
7α	4.50 (dd, 10.1, 7.3)	
8		135.0
9		145.0
10		39.0
11β	4.23 (dd, 4.8, 1.6)	63.7
12α	2.09 (dd, 14.7, 1.6)	
12β	1.66 (dd,14.7, 4.8)	43.4
13		40.3
14β	4.19 (s)	74.6
15	6.22 (dd, 18.3, 10.5)	143.8
16a	5.25 (dd, 18.3, 1.2)	116.0
16b	5.26 (dd, 10.5 1.2)	
17	1.10 (s)	26.7
18	0.91 (s)	33.2
19	0.87 (s)	21.8
20	1.03 (s)	20.9

2.3.6 Marginol F (6)

Compound **6** was isolated as an amorphous solid. Its molecular formula was deduced to be $C_{20}H_{30}O_4$ with six degrees of unsaturation, based on a cationized molecular ion peak at *m/z* 357.2026 $[M + Na]^+$ (calcd. for $C_{22}H_{30}O_4Na$, 357.2036) in the HRESIMS and NMR data. The IR spectrum showed absorption bands at 3654 and 1710 cm^{-1}, indicating the presence of hydroxy and carbonyl groups, respectively. The ^1H and ^{13}C NMR data of **6** (Table 2.6) were similar to those of the 9α-hydroxysandaracopimarane type of diterpenoids.[45] In particular, the 1D NMR spectra (Figures 2.23 and 2.24) were similar to those of sandaracopimaradien-6β,9α-diol-1-one (**28**). However, the presence of an oxygenated carbon (δ_C 79.2) at C-7 in **6** instead of the methylene (δ_C 42.3) of **28** was observed, suggesting that **6** is a hydroxy derivative of **28** at this position. The ^1H-^1H COSY and HMBC correlations (Figure 2.25a) confirmed the attachment of the hydroxy group at C-7 in **6**. Furthermore, the broad singlet methine signal at H-7 suggested the axial/axial relationship between the C-5 and C-6 hydroxy groups. This allowed us to establish their relative configurations as α and β, respectively. The α-orientations of the hydroxy groups at C-9 and H-5 were established based on NOESY correlations from the hydroxy proton at C-7 to the hydroxy proton at C-9 *via* H-5, respectively (Figure 2.25b). Therefore, **6** was determined to be 6β,7α,9α-trihydroxysandaracopimaradien-1-one and was named marginol F.

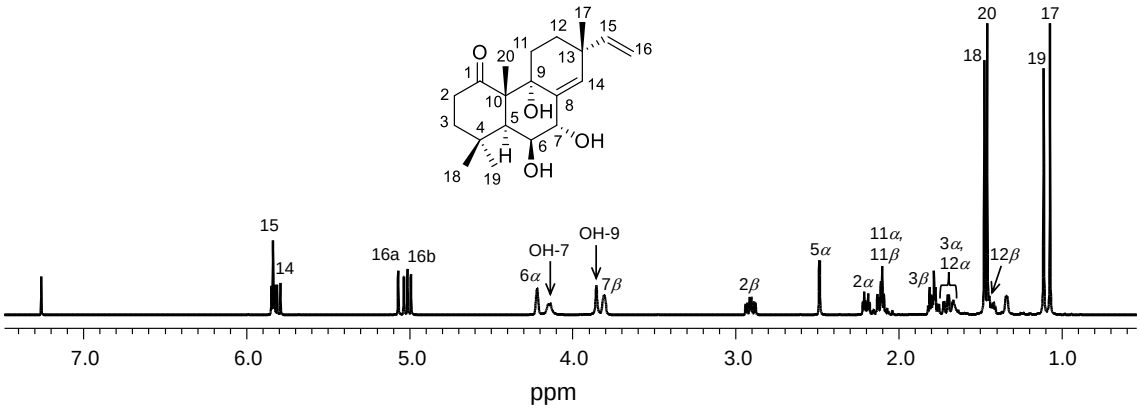

Figure 2.23 ^{1}H NMR spectrum (500 MHz) of **6** in $CDCl_3$

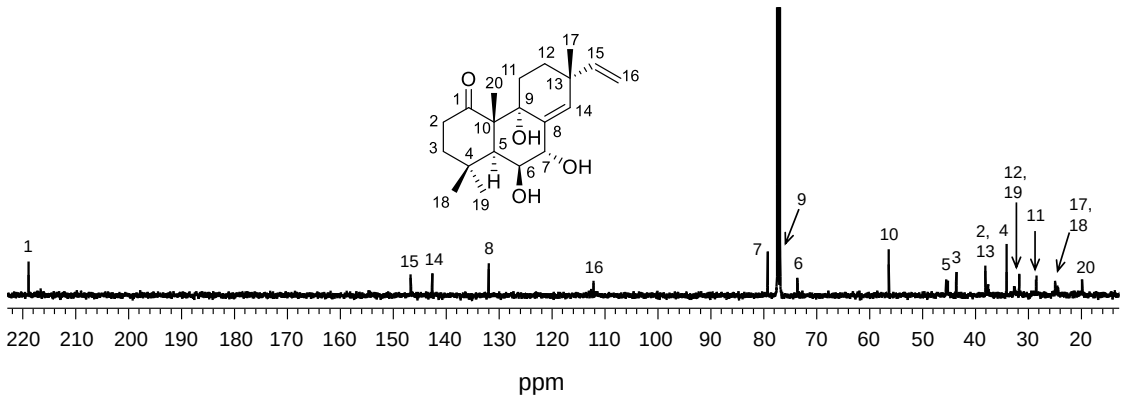

Figure 2.24 ^{13}C NMR spectrum (100 MHz) of **6** in $CDCl_3$

(a) (b)

Figure 2.25 ^{1}H–^{1}H COSY correlations (bold lines) and key HMBC (arrows) (a) and NOESY (dashed arrows) correlations of **6** (b)

Table 2.6 ^{1}H (500 MHz) and ^{13}C (125 MHz) NMR spectroscopic data for **6** in $CDCl_3$ [δ in ppm and *J* value in (Hz) in parentheses].

Position	**6**	
	δ_H	δ_C
1		218.9
2α	2.20 (ddd, 12.5, 4.6, 3.8)	37.6
2β	2.91 (ddd, 13.5, 12.5, 4.6)	
3α	1.70 (dd, 13.5, 3.8)	43.5
3β	1.81 (dd, 10.0, 4.6)	
4		34.1
5α	2.49 (d, 1.7)	45.4
6α	4.22 (br s)	73.6
7β	3.81 (br s)	79.2
8		131.9
9		77.2
10		56.4
11α	2.08 (m)	28.5
11β	2.13 (dd, 14.9, 3.8)	
12α	1.77 (dd,4.7, 2.1)	31.7
12β	1.43 (m)	
13		38.1
14	5.84 (br s)	142.6
15	5.85 (dd, 17.5, 10.5)	146.7
16a	5.06 (dd, 17.5, 1.1)	112.2
16b	5.01 (dd, 10.5, 1.1)	
17	1.08 (s)	24.6
18	1.48 (s)	24.9
19	1.11 (s)	32.6
20	1.46 (s)	19.8
OH-7	4.13 (s)	
OH-9	3.85 (br s)	

2.3.7 Marginol G (7)

Compound **7** was obtained as a colorless oil, with a molecular formula of $C_{22}H_{34}O_4$ based on the HRESIMS and ^{13}C NMR data analyses. The IR spectrum showed absorption bands indicative of hydroxy (3654 and 3436 cm^{-1}) and carbonyl (1713 cm^{-1}) groups. The 1D NMR data of **7** (Table 2.7, Figures 2.26 and 2.27) were similar to those of **6**. Notable differences between **6** and **7** were the appearance of resonances for a non-oxygenated methylene [δ_H 1.81, 1.73/δ_C 27.7] at C-6 and the acetyl group [δ_H 2.06/δ_C 21.8 (*Me*COO-7); δ_C 170.1 (Me*C*OO-7)] in **7**, in which C-6 in **6** was observed as the oxygenated methine (δ_H 4.22/δ_C 73.6). Furthermore, the signal for H-7 in **6** was deshielded from δ_H 3.81 to δ_H 5.38 in **7**, suggesting that **7** was an analog not only with an acetoxy group at C-7, but also without the hydroxy group at C-6 of **6**. The ^1H-^1H COSY spin system of C(5)H-C(6)H_2-C(7)H, as well as the cross peaks observed in the main skeleton of **7**, supported the absence of the hydroxy group at C-6 in **7**. The HMBC correlations from H-7/*Me*COO-7 to Me*C*OO-7 confirmed the attachment of the acetoxy group at C-7 (Figure 2.28a). The relative configurations of **7** were determined by the same way as those of **6**, where H-5 and the acetoxy group at C-7 adopted axial form, while H-7 was an equatorial form. Furthermore, the α-orientations of H-5, the hydroxy group at C-9, and the acetoxy moiety at C-7 were deduced from the NOESY correlations from H-5 to the hydroxy proton at C-9, in conjunction with the absence of the NOESY cross peak between H-5 and H-7 (Figure 2.28b). Consequently, **7** was identified as 7α-acetoxy-9α-hydroxysandaracopimaradien-1-one and was named marginol G.

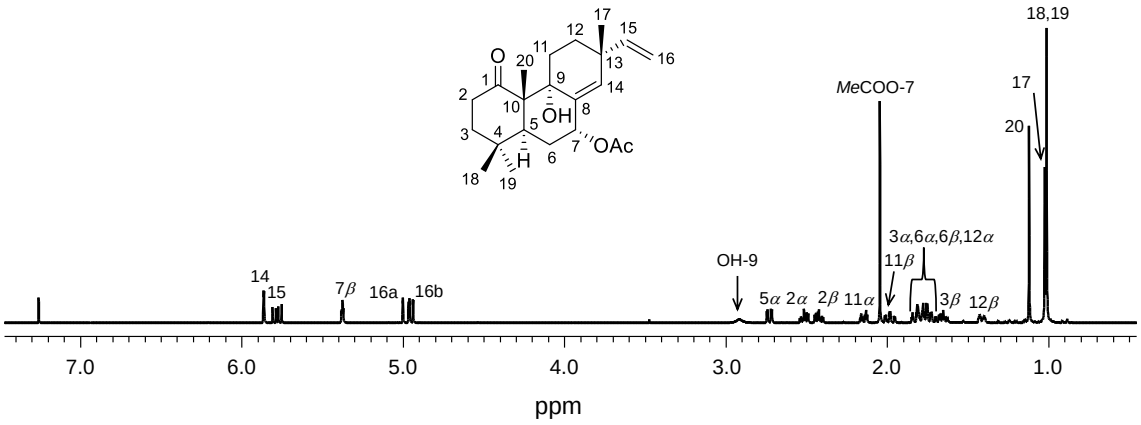

Figure 2.26 ^{1}H NMR spectrum (400 MHz) of **7** in $CDCl_3$

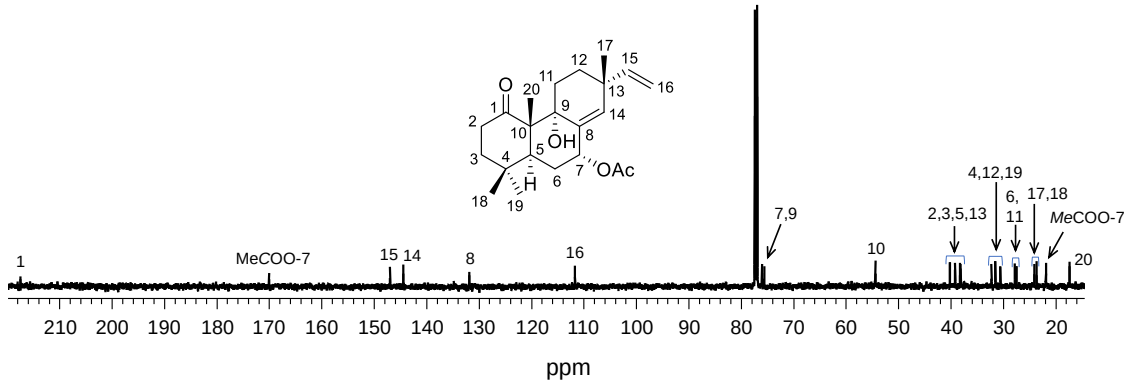

Figure 2.27 ^{13}C NMR spectrum (100 MHz) of **7** in $CDCl_3$

(a) (b)

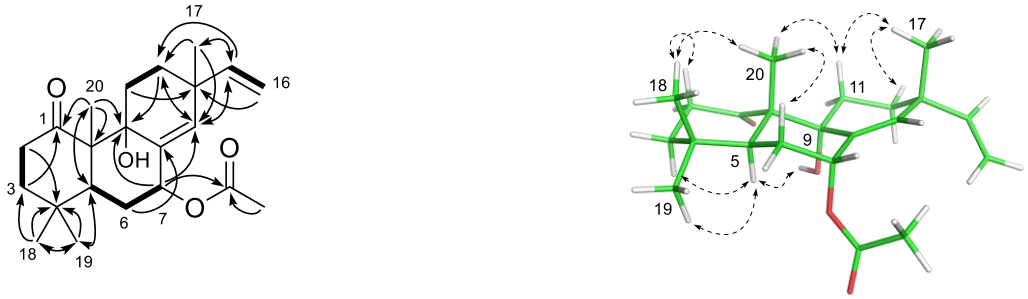

Figure 2.28 ^{1}H–^{1}H COSY correlations (bold lines) and key HMBC (arrows) (a) and NOESY (dashed arrows) correlations of **7** (b)

Table 2.7 ^{1}H (500 MHz) and ^{13}C (125 MHz) NMR spectroscopic data for **7** in $CDCl_3$ [δ in ppm and *J* value in (Hz) in parentheses]

Position	**7**	
	δ_H	δ_C
1		217.4
2α	2.43 (m)	38.1
2β	2.52 (m)	
3α	1.77 (m)	39.2
3β	1.65 (m)	
4		32.2
5α	2.74 (dd, 14.5, 3.7)	40.2
6α	1.81 (m)	27.7
6β	1.73 (m)	
7β	5.38 (t, 2.9)	76.0
8		131.8
9		75.6
10		54.4
11α	2.15 (dt, 14.5, 3.7)	27.5
11β	1.99 (td 13.9, 3.2)	
12α	1.78 (m)	30.5
12β	1.42 (m)	
13		38.3
14	5.86 (d, 1.7)	144.5
15	5.78 (dd, 17.5, 10.5)	146.9
16a	5.00 (dd, 17.5, 1.0)	111.7
16b	4.96 (dd, 10.5, 1.0)	
17	1.03 (s)	23.6
18	1.00 (s)	24.0
19	1.02(s)	31.5
20	1.12 (s)	17.3
OH-9	2.92 (br s)	
*Me*COO-7	2.05 (s)	21.8
Me*C*OO-7		170.1

2.3.8 Marginol H (8)

Compound **8** was obtained as an amorphous solid, and HRESIMS and 1D NMR data deduced the molecular formula as $C_{20}H_{28}O_2$, indicating seven degrees of unsaturation. The IR spectrum indicated the presence of hydroxy and carbonyl groups in **8**, based on the observations of absorption bands at 3482 and 1664 cm^{-1}, respectively. The ^{1}H and ^{13}C NMR data of **8** (Table 2.8, Figures 2.29 and 2.30) were similar to those of (9*R*,10*R*,13*R*)-isopimara-5,8(14),15-trien-7-one (**8'**).[50] The significant difference in **8** was the presence of the oxygenated methine resonance (δ_C 74.6), instead of the disappearance of the methine resonance (δ_H 2.54/δ_C 44.6), which is consistent with the 16 mass unit higher molecular weight of **8** than **8'**. Based on the HMBC correlations from H_3-20 to C-9, from H-14 to C-9, and the other observed correlations, the location of the hydroxy group was confirmed to be at C-9 (Figure 2.31a). Furthermore, the NOESY correlations of H_3-20/H-11β/H_3-17 determined the β-orientations of the C-10 and C-13 methyl groups, while it allow us to assign the vinyl group at C-13 as an α-orientation (Figure 2.31b). Considering the aforementioned relative configurations and the structural features of **8** with a hydroxy group at C-9 and the double bond between C-8 and C-14, **8** is considered to be a 9-hydroxysandaracopimarane derivative with an additional double bond between C-5 and C-6. Therefore, I considered the relative configuration of the hydroxy group at C-9 as α-orientation, as in the case of the previously reported sandaracopimaranes. A comparison of the experimental and calculated CD spectrum of **8** suggested the 9*S*, 10*S*, 13*R*-configurations (Figure 2.32). Hence, the structure of **8** was established as (9*S*,10*S*,13*R*)-9-hydroxyisopimara-5,8(14),15-trien-7-one, and **8** was named marginol H.

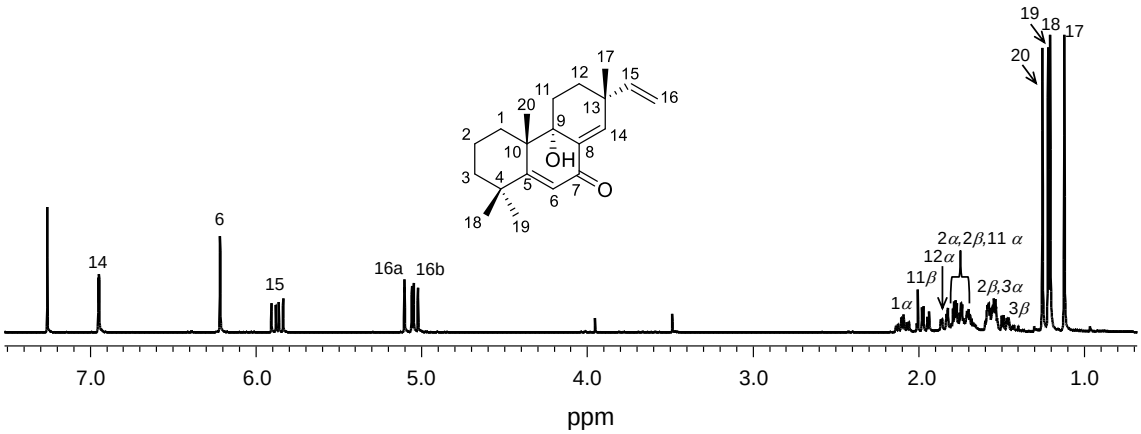

Figure 2.29 ^{1}H NMR spectrum (500 MHz) of **8** in $CDCl_3$

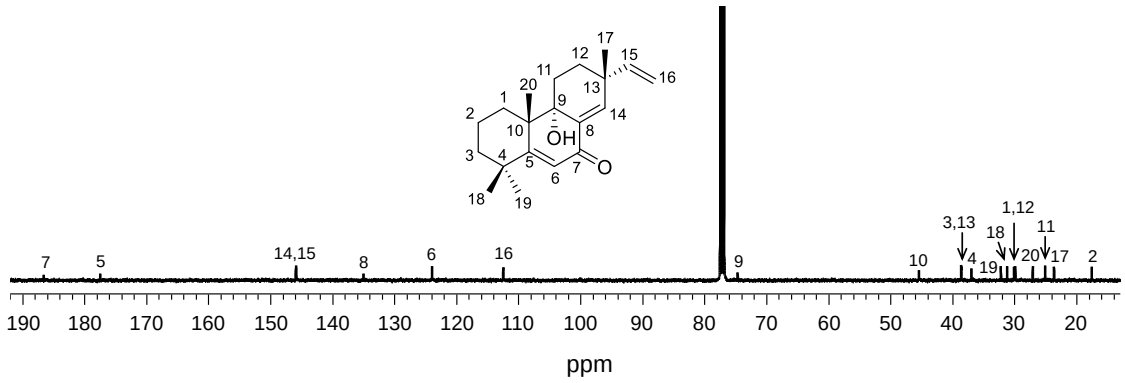

Figure 2.30 ^{13}C NMR spectrum (125 MHz) of **8** in $CDCl_3$

(a) (b)

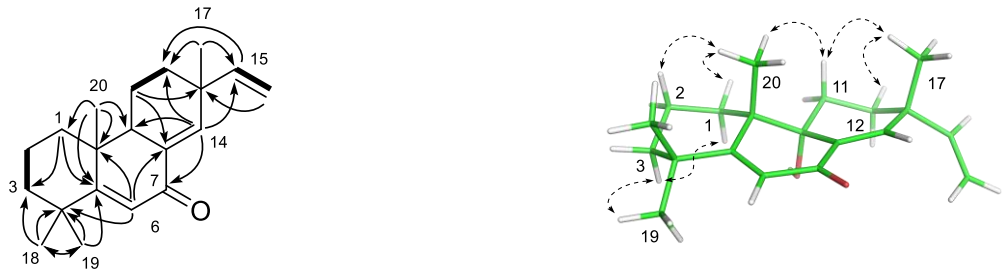

Figure 2.31 ^{1}H–^{1}H COSY correlations (bold lines) and key HMBC (arrows) (a) and NOESY (dashed arrows) correlations of **8** (b)

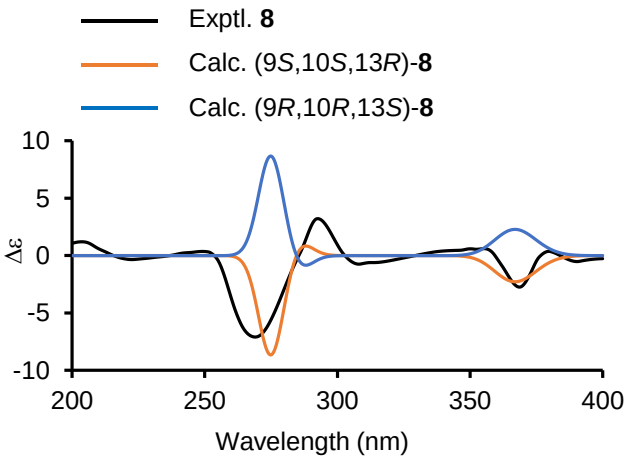

Figure 2. 32 Experimental and calculated CD spectra of **8**

Table 2.8 ^{1}H (500 MHz) and ^{13}C (125 MHz) NMR spectroscopic data for **8** in $CDCl_3$ [δ in ppm and *J* value in (Hz) in parentheses]

Position	**8**	
	δ_H	δ_C
1α	2.10 (td, 12.9, 5.3)	
1β	1.56 (m)	30.0
2α	1.68 (m)	17.5
2β	1.73 (m)	
3α	1.55 (m)	38.6
3β	1.45 (td, 12.7, 4.3)	
4		36.9
5		177.4
6	6.22 (s)	123.9
7		186.5
8		135.0
9		74.6
10		45.4
11α	1.76 (m)	25.0
11β	1.98 (td, 12.9, 3.4)	
12α	1.84 (m)	29.8
12β	1.57 (m)	
13		38.6
14	6.95 (d, 1.4)	145.9
15	5.87 (dd, 17.4, 10.6)	145.8
16a	5.08 (dd, 17.4, 0.9)	112.5
16b	5.04 (dd, 10.6, 0.9)	
17	1.10 (s)	23.6
18	1.19 (s)	31.2
19	1.24 (s)	32.1
20	1.20 (s)	27.0

2.3.9 Marginol I (9)

Marginol I (**9**) was isolated as a colorless oil with negative optical rotation ($[\alpha]^{22}_{D}$ –32.5 in $CHCl_3$). The molecular formula of **9** was established to be $C_{20}H_{30}O_3$ by a cationized molecular ion peak at *m/z* 341.2090 $[M + Na]^+$ (calcd. for $C_{20}H_{30}O_3Na$, 341.2087), implying six degrees of unsaturation in the HRESIMS analysis. The IR spectrum of **9** displayed absorption bands at 3419 cm^{-1}, 1673 cm^{-1}, and 1114 cm^{-1}, corresponding to the hydroxy group, a carbonyl group in an α,β-unsaturated six membered ring, and an ether group, respectively. The ^1H NMR spectrum of **9** (Table 2.9, Figure 2.33) indicated the presence of terminal vinyl protons (H-15, H-16ab), an olefinic proton (H-14), an oxygenated methine proton (H-6), two non-oxygenated methine protons (H-5, H-10), five methylene protons, three singlet methyl protons (H-17, H-18, H-19), and one doublet methyl proton (H-20). The ^{13}C NMR spectrum of **9** (Figure 2.34) in conjugation with the HMQC spectrum indicated 20 carbon resonances assignable to one carbonyl carbon (δ_C 199.1), four sp^2 carbons (δ_C 114.9, 136.3, 143.9, and 153.7), three quaternary carbons including a ketal or hemiketal carbon (δ_C 107.9), three methine carbons including an oxygenated one (δ_C 77.3), five methylene carbons, and four methyl carbons (δ_C 15.9, 27.0, 27.7, and 29.3) (Table 2.9). The ^1H-^1H COSY spectra disclosed four partial structures, -C(2)H_2-C(3)H_2-, -C(20)H_3-C(10)H-C(5)H-C(6)H(O)-C(7)H_2-, -C(11)H_2-C(12)H_2-, and -C(15)H=C(16)H_2, in **9** (Figure 2.35a). The HMBC correlations from H_2-2 to C-10, from H_2-3 to C-18, from H-5, H_3-20, and the hydroxy proton at C-1 (δ_H 7.74, OH-1) to C-1, from H-10 to C-4, from H_3-18 to C-3/C-4/C-5/C-19, and from H_3-19 to C-3/C-4, C-5/C-18 indicated the presence of a 3-(1-oxygenated-2-substituted-ethyl)-2,4,4-trimethylcyclohexane-1-oxygenated-1-ol ring in **9** (Figure 2.35a). The HMBC correlations from H_2-11 to C-8/C-13 and from H-14 to C-9/C-12 supported the presence of a 2,4-disubstituted cyclohex-2-en-1-one ring. Meanwhile, the methyl and terminal vinyl groups were located at C-4, based on the HMBC correlations from H-16 to C-13/C-15 and from H_3-17 to C-12/C-14. The HMBC correlations from H_2-7 to C-9/C-14 allowed us to connect two partial structures, the cyclohexane-1-oxygenated-1-ol ring and the cyclohex-2-en-1-one ring, *via* C-2 of the ethyl moiety. The structure of **9** was similar to **15**, except a C-1 dioxygenation, suggesting that **9** is a 9,10-seco-isopimarane diterpene. Thus, the remaining HMBC

correlations from H-6 to C-1 and C-10 allowed us to determine the 6-oxabicyclo[3.2.1]octane-5-ol ring, including the aforementioned cyclohexane-1-oxygenated-1-ol ring of **9**.

The NOESY correlations between H-12β and H_3-17 determined the relative configuration of **9** (Figure 2.35b). The β-orientations of H-12β and H_3-17 were established from the NOESY correlations between H-12β and H_3-17. In contrast, the NOESY correlations between H-12α and H-15 confirmed α-orientations of H-12α and the vinyl group on the cyclohex-2-en-1-one ring. Meanwhile, the exo configuration at C-6 on the 6-oxabicyclo[3.2.1]octane-5-ol ring was deduced from the NOESY cross peaks of H-6/H-3β/H_3-19. Furthermore, the NOESY cross peaks from OH-1 to H-2β, from H-2α to H-10, and from H_2-7 to H_3-20 indicated the anti configuration of C-10. A comparison of the experimental and calculated CD spectrum of **9** suggested the 1*R*,5*R*,6*R*,10*S*,13*R*-configurations (Figure 2.36). Therefore, **9** was determined to be (1*R*,5*R*,6*R*,10*S*,13*R*)-1-hydroxy-4,4,10-trimethyl-6-oxabicyclo[3.2.1]octane-9-oxo-9,10-seco-isopimarane diterpene and was named marginol I. To the best of our knowledge, only artemilavanolides A and B were reported to have the 6-oxabicyclo[3.2.1]octane-5-ol ring as the scaffold.[51] Presumably, **9** could be biogenetically derived from the sandaracopimaradien-6β,9α-diol-1-one, (**28**)[52] by a retro-aldol reaction and the subsequent nucleophilic attack of the hydroxy oxygen at C-6, leading to the C-9–C-10 bond cleavage and ether bond formation between C-1 and C-6, respectively (Figure 2.37).

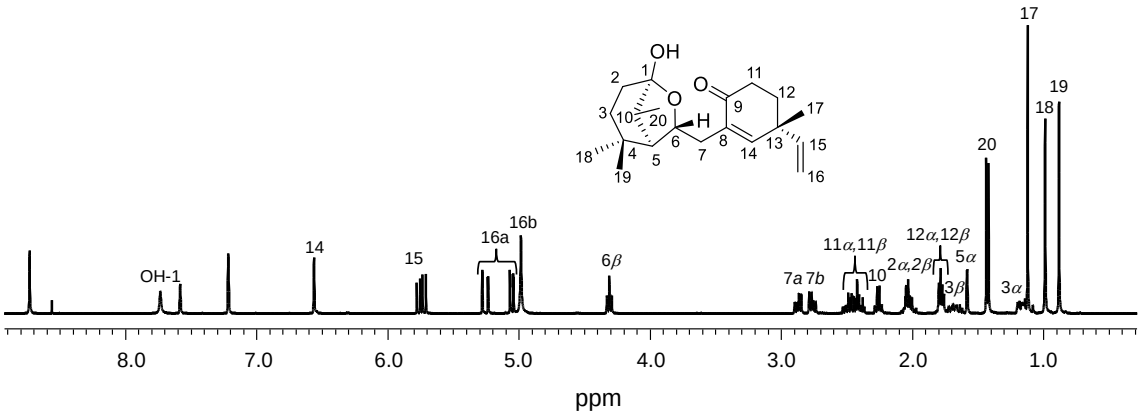

Figure 2.33 ^{1}H NMR spectrum (400 MHz) of **9** in pyridine-d_5

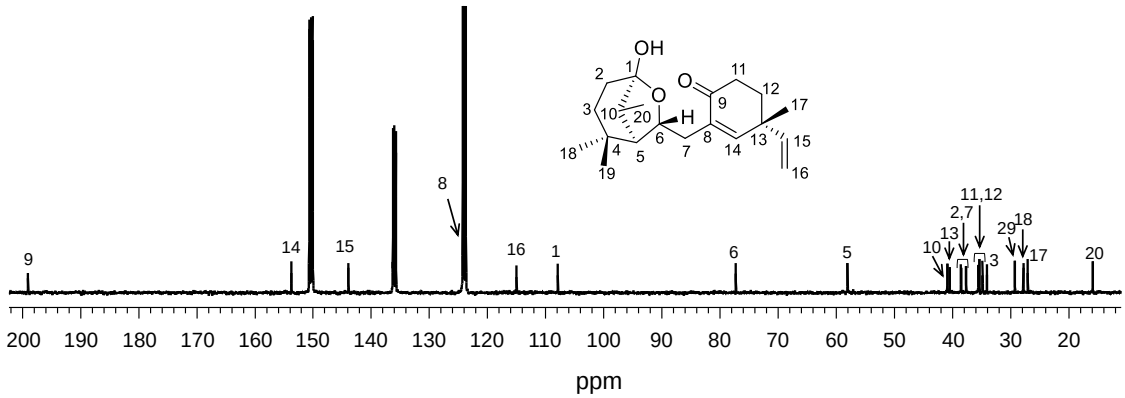

Figure 2.34 ^{13}C NMR spectrum (100 MHz) of **9** in pyridine-d_5

(a) (b)

Figure 2.35 ^{1}H–^{1}H COSY correlations (bold lines) and key HMBC (arrows) (a) and NOESY (dashed arrows) correlations of **9** (b)

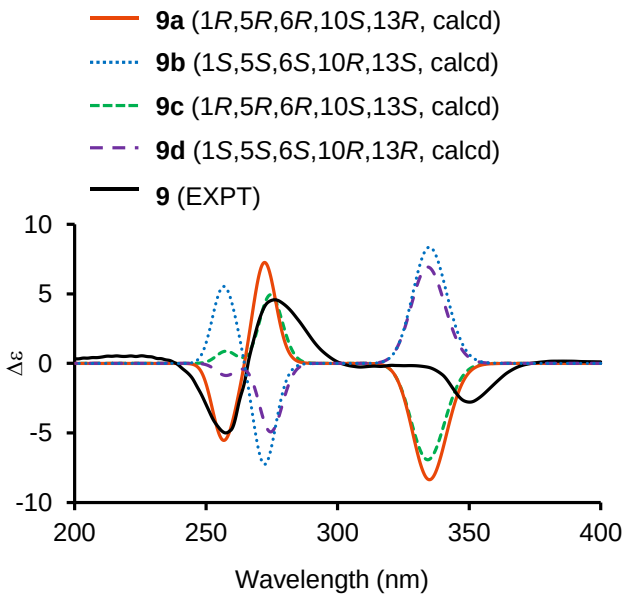

Figure 2. 36 Experimental and calculated CD spectra of **9**

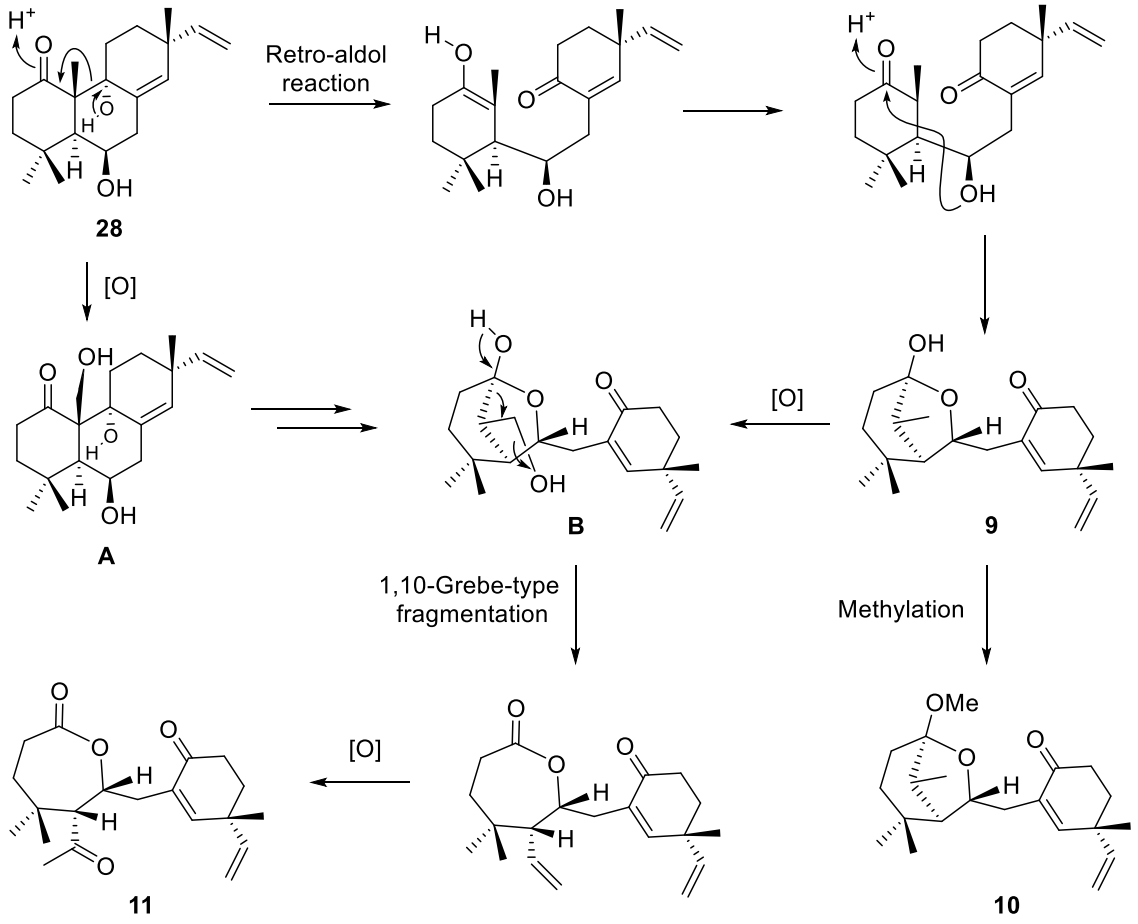

Figure 2. 37 Plausible biosynthetic pathways of **9–11**

Table 2.9 ^{1}H (400 MHz) and ^{13}C (100 MHz) NMR spectroscopic data for **9** in pyridine-d_5 [δ in ppm and J value in (Hz) in parentheses]

Position	**9**	
	δ_H	δ_C
1		107.9
2α	2.06 (m)	37.7
2β	2.04 (m)	
3α	1.18 (m)	34.1
3β	1.69 (ddd, 19.2, 14.8, 7.3)	
4		34.8
5α	1.59 (d, 1.4)	58.1
6	4.32 (dd, 7.3, 7.2)	77.3
7a	2.88 (ddd, 13.1, 7.3, 0.8)	38.5
7b	2.77 (ddd, 13.1, 7.1, 0.6)	
8		136.3
9		199.1
10	2.27 (q, 7.2)	40.9
11α	2.50 (ddd, 16.5, 10.1, 6.5)	35.5
11β	2.41 (m)	
12α	1.80 (m)	35.5
12β	1.78 (m)	
13		40.7
14	6.57 (s)	153.7
15	5.75 (dd, 17.4, 10.5)	143.9
16a	5.27 (dd, 17.4, 1.4)	114.9
16b	5.06 (dd, 10.5, 1.4)	
17	1.13 (s)	27.0
18	1.00 (s)	27.7
19	0.89 (s)	29.3
20	1.43 (d, 7.2)	15.9
OH-1	7.74 (s)	

2.3.10 Marginol J (10)

Marginol J (**10**) was obtained as a colorless oil with negative optical rotation ($[\alpha]^{22}_{D}$ –77.5 in $CHCl_3$). A cationized molecular ion peak at *m/z* 355.2239 $[M + Na]^+$ (calcd. for $C_{21}H_{32}O_3Na$, 355.2244) with 14 mass units higher than that of **9** was observed in the HRESIMS of **10**. Thus, I determined the molecular formula of **10** to be $C_{21}H_{32}O_3$. The IR spectrum showed absorption bands at 1676 cm^{-1} and 1119 cm^{-1} corresponding to carbonyl and ether groups, respectively, while it lacked any bands assignable to a hydroxy group, in contrast to the case of **9**. The 1D NMR data of **10** (Table 2.10, Figures 2.38 and 2.39) was similar to those of **9**. The only difference was the presence of the methoxy group [δ_H 3.39 (s), δ_C 48.9, OMe-1] in **10** instead of the hydroxy group at C-1 in **9**. The presence of the methoxy group at C-1 in **10** was in agreements with its HMBC correlations from H_2-2 to C-1/C-4/C-10, from H_2-3 to C-1/C-18, from H_3-20 to C-1/C-5, and from the methyl proton of OMe-1 to C-1(Figures 2.40a). Based on NOESY correlations and comparison of the calculated ECD spectra, the relative and absolute configurations of **10** were determined (Figures 2.40b and 2.41). Thus, **10** was elucidated as 1-methoxy-4,4,10-trimethyl-6-oxabicyclo[3.2.1]octane-9-oxo-9,10-seco-isopimarane, which is biogenetically derivable from **9** and was named marginol J (Figure 2.37).

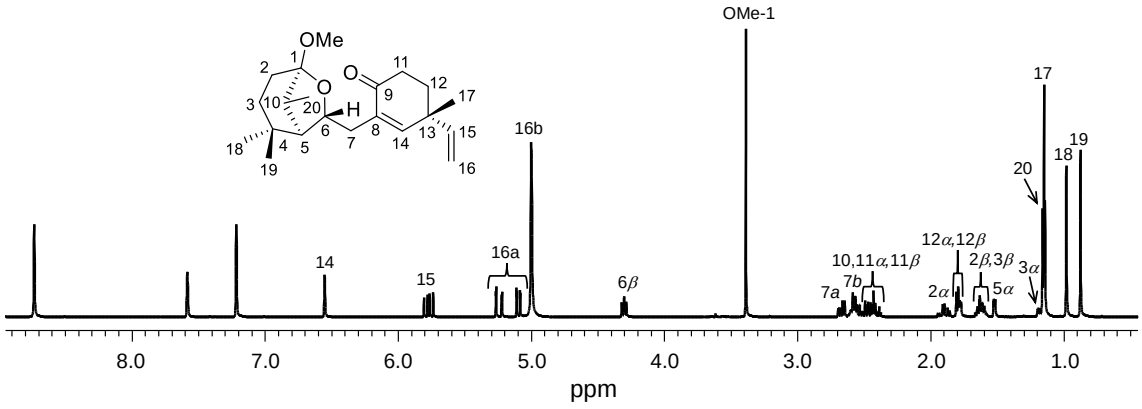

Figure 2.38 ^{1}H NMR spectrum (500 MHz) of **10** in pyridine-d_5

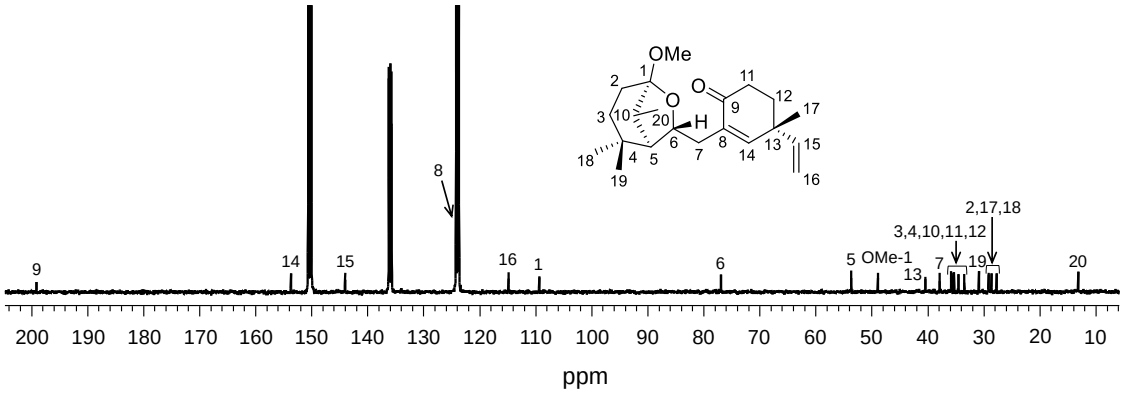

Figure 2.39 ^{13}C NMR spectrum (100 MHz) of **10** in pyridine-d_5

(a) (b)

Figure 2.40 ^{1}H–^{1}H COSY correlations (bold lines) and key HMBC (arrows) (a) and NOESY (dashed arrows) correlations of **10** (b)

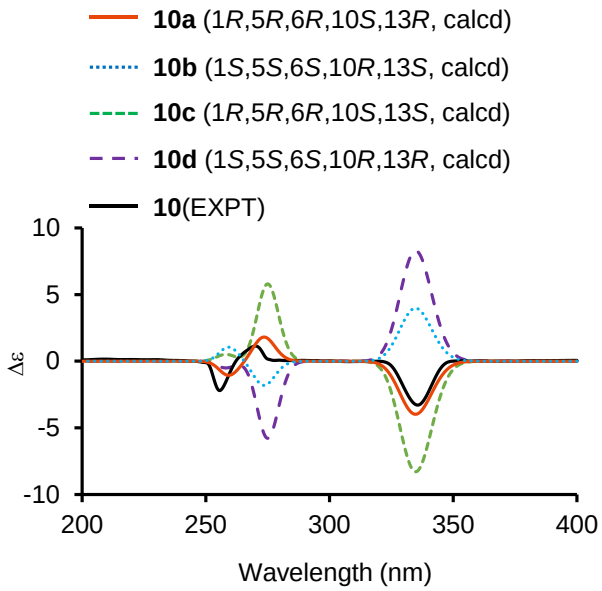

Figure 2. 41 Experimental and calculated CD spectra of **10**

Table 2.10 ^{1}H (400 MHz) and ^{13}C (100 MHz) NMR spectroscopic data for **10** in pyridine-d_5 [δ in ppm and J value in (Hz) in parentheses]

Position	**10**	
	δ_H	δ_C
1		109.4
2α	1.89 (dd, 15.3, 6.2)	29.2
2β	1.64 (m)	
3α	1.20 (m)	34.5
3β	1.60 (m)	
4		33.5
5α	1.53 (dd, 4.4, 1.6)	53.7
6	4.31 (dd, 7.4, 6.4)	76.9
7a	2.68 (dd, 12.4, 6.4)	37.9
7b	2.55 (m)	
8		135.8
9		199.1
10	2.58 (m)	35.9
11α	2.47 (dd, 10.3, 3.4)	35.3
11β	2.41 (m)	
12α	1.80 (m)	35.5
12β	1.78 (m)	
13		40.5
14	6.56 (s)	153.8
15	5.78 (dd, 17.4, 10.5)	144.0
16a	5.25 (dd, 17.4, 0.9)	114.9
16b	5.06 (dd, 10.5, 0.9)	
17	1.15 (s)	27.8
18	0.99 (s)	28.7
19	0.88 (s)	30.9
20	1.17 (d, 7.3)	13.2
OMe-1	3.39	48.9

2.3.11 Marginol K (11)

Marginol K (**11**) was obtained as an amorphous powder. Its molecular formula was established as $C_{20}H_{28}O_4$, accounting for seven degrees of unsaturation, based on a cationized molecular ion peak at *m/z* 355.1881 $[M + Na]^+$ (calcd. for $C_{20}H_{28}O_4Na$, 355.1880) in HRESIMS, in conjugation with ^{13}C NMR data. Its IR spectrum displayed absorption bands at 1739, 1712, 1673, and 1152 cm^{-1}, in which the first three and the last one suggested the presence of carbonyl and ether groups in **11**, respectively. The spectroscopic data of **11** was similar to those of **9** (Table 2.11, Figures 2.42 and 2.43). The notable differences in these spectra were the appearances of resonances assignable to lactone [δ_C 173.9 (C-1)] and acetyl [δ_H 2.22 (s, H-20)/δ_C 35.9 (C-20), δ_C 207.7 (C-10)] moieties in **11**, instead of the disappearances of those of the C-1 hemiketal and C-10 methine groups in **9**. The presence of a 4-methyl-2-methylene-4-vinylcyclohex-2-en-1-one ring in **11** was established based on ^1H-^1H COSY and HMBC correlations, as in the case of **9** and **10** (Figure 2.44a). Moreover, the NOESY correlations between H-12β and H_3-17 revealed the β-orientations of H-12β and H_3-17. In contrast, the NOESY cross peak between H-12α and H-15 suggested the α-orientations of H-12α and the vinyl group at C-13 of the cyclohex-2-en-1-one ring (Figure 2.44b). These data suggested that **11** was a bicyclic ring-rearranged analogue of **9**, and were further supported by the observation of a linear spin system between H_2-2 and H_2-3 in the ^1H-^1H COSY spectrum and cross peaks from H_2-2 to C-1 and C-4, from H_2-3 to C-1 and C-5, and from H-6 to C-1 and C-4. The rearranged ring in **11** was thus determined to be the oxepan-2-one ring. Furthermore, the attachment of the germinal methyl groups at C-4 and acetyl moiety at C-5 were established from the HMBC correlations from H_2-3 to C-18/C-19, from H_3-18 and H_3-19 to C-3/C-4/C-5, from H-6 to C-10, and from H_3-20 to C-5. The NOESY correlations between H-6 and H_3-19 and between H_3-18 and H_3-20 suggested the β-orientations of H-5, H-6, and H_3-19. The absolute configuration of **11** was assigned as shown in Figure 2.45. Based on these results, the structure of **11** was confirmed as (5*R*,6*R*,13*R*)-4,4,10-trimethyl-1-oxepanone-9,10-diketo-9,10-seco-isopimara-8(14),15-diene with the rare oxepanone ring and **11** was named marginol K. Presumably, **11** could be a biogenetical product obtained *via* hydroxylation of **9** at C-20 or, as in case of **9**, *via* 9,10-bond cleavage bicyclic ring formation of **A** to form **B**,

followed by 1,10-Grebe-type bond cleavage of **B** and oxidation of the resulting olefin (Figure 2.37).

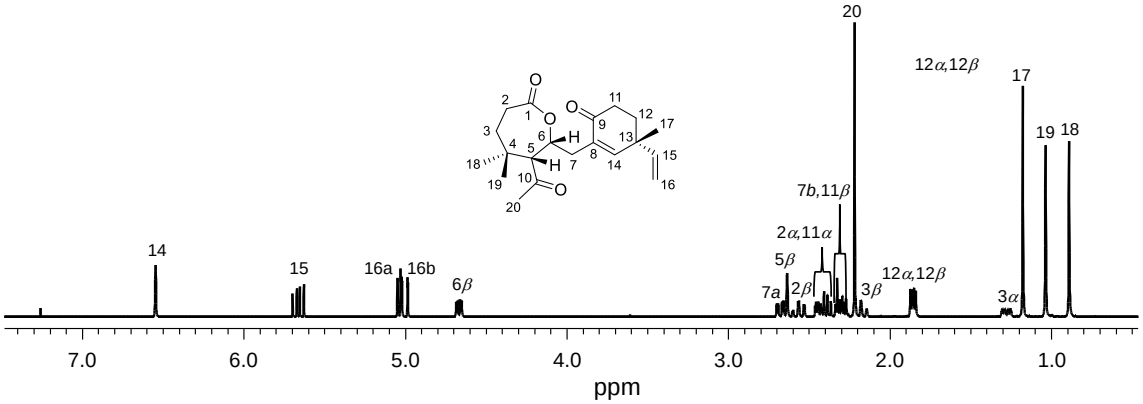

Figure 2.42 ^{1}H NMR spectrum (400 MHz) of **11** in $CDCl_3$

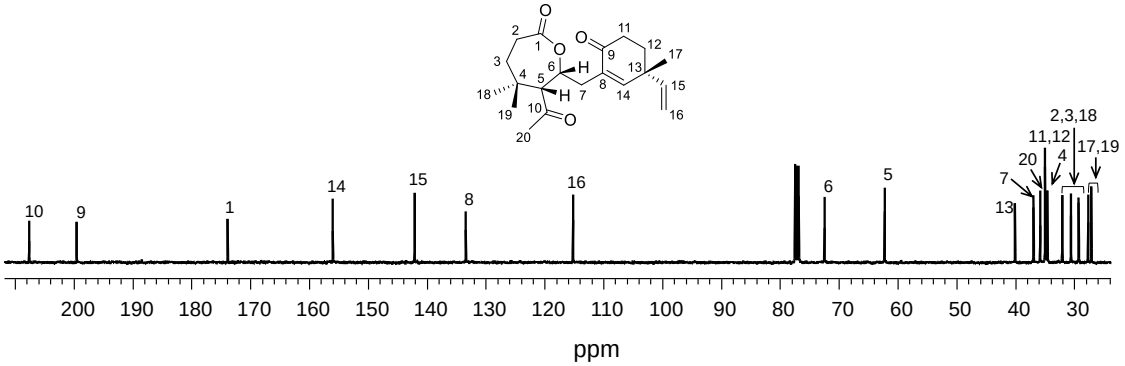

Figure 2.43 ^{13}C NMR spectrum (100 MHz) of **11** in in $CDCl_3$

(a) (b)

Figure 2.44 ^{1}H–^{1}H COSY correlations (bold lines) and key HMBC (arrows) (a) and NOESY (dashed arrows) correlations of **11** (b)

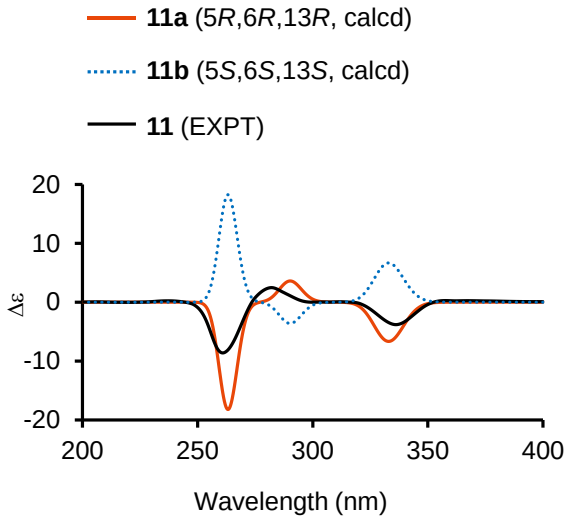

Figure 2. 45 Experimental and calculated CD spectra of **11**

Table 2.11 ^{1}H (400 MHz) and ^{13}C (100 MHz) NMR spectroscopic data for **11** in $CDCl_3$ [δ in ppm and J value in (Hz) in parentheses]

Position	**11**	
	δ_H	δ_C
1		173.9
2α	2.45 (m)	30.6
2β	2.58 (td, 13.9, 2.2)	
3α	1.28 (m)	32.1
3β	2.16 (m)	
4		34.6
5β	2.64 (br s)	62.4
6	4.66 (dd, 9.8, 3.9)	72.5
7a	2.68 (ddd, 13.5, 3.9, 1.0)	37.0
7b	2.28 (m)	
8		133.6
9		199.6
10		207.7
11α	2.41 (m)	35.0
11β	2.33 (m)	
12α	1.87 (m)	35.0
12β	1.85 (m)	
13		40.1
14	6.55 (s)	1156.1
15	5.67 (dd, 17.4, 10.5)	142.1
16a	5.05 (dd, 17.4, 1.0)	115.2
16b	5.02 (dd, 10.5, 1.0)	
17	1.17 (s)	27.7
18	0.89 (s)	29.3
19	1.04 (s)	27.2
20	1.22 (s)	35.9

2.3.12 14-*epi*-boesenberol F (12)

Compound **12** was obtained as a white powder, and its molecular formula was assigned to be $C_{21}H_{34}O_3$ on the basis of HRESIMS. The IR spectrum of **12** displayed absorption bands at 3331, 2925, and 1460 cm^{-1}, indicative of hydroxy and olefinic groups in **12**. The planar structure of **12** was similar to that of boesenberol F (**12′**)[54] as supported by the ^1H and ^{13}C NMR data (Table 2.12, Figures 2.46 and 2.47) and the cross peaks observed in the ^1H-^1H COSY and HMBC spectra (Figure 2.48a). The hydroxy group at C-7 was deduced as the α-orientation, based on the NOESY cross peaks from H-5α to H-1α, H-3α, and the hydroxy proton of OH-7. Similarly, the methoxy group at C-14 was adopted as α-orientation due to the NOESY correlations from H-1β to H_3-20 and from H-7β to H-14β, as well as from H-14β to H_3-17 (Figure 2.48b). Thus, **12** was determined to be 14-*epi*-boesenberol F.

The previous study successfully determined the absolute configuration of the isopimarane diterpenoid without significant chromophore, by using acetonitrile with lower absorption as the solvent.[55] Accordingly, the absolute configuration of **12** was determined by comparing the ECD spectrum measured in acetonitrile with the calculated CD spectra of models of 5*S*,6*S*,7*S*,10*S*,13*R*,14*S* (**12a**) and its enantiomer (**12b**). The calculated spectrum of **12** showed the negative Cotton effect on the short-wavelength side, consistent with the calculated CD curve for **12a** (Figure 2.49). Therefore, **12** was determined to be (5*S*,6*S*,7*S*,10*S*,13*R*,14*S*)-14-methoxyisopimara-8,15-dien-6,7-diol, and was named 14-*epi*-bosenberol F.

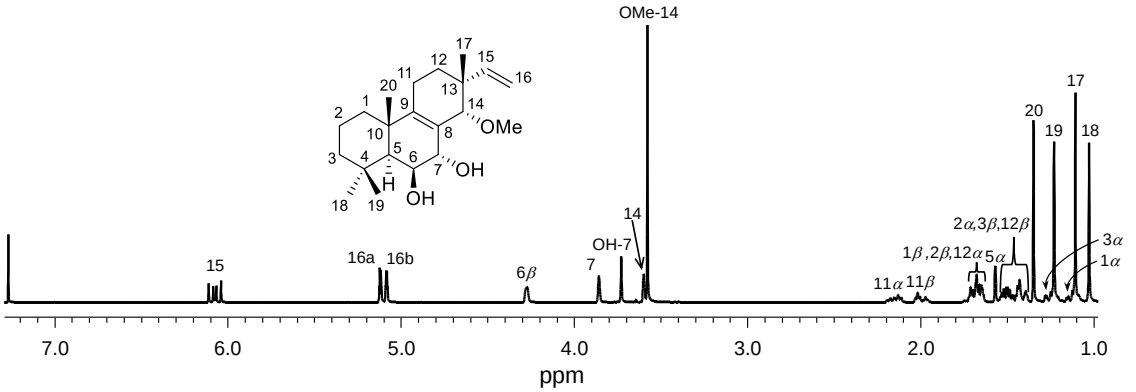

Figure 2.46 ^{1}H NMR spectrum (400 MHz) of **12** in $CDCl_3$

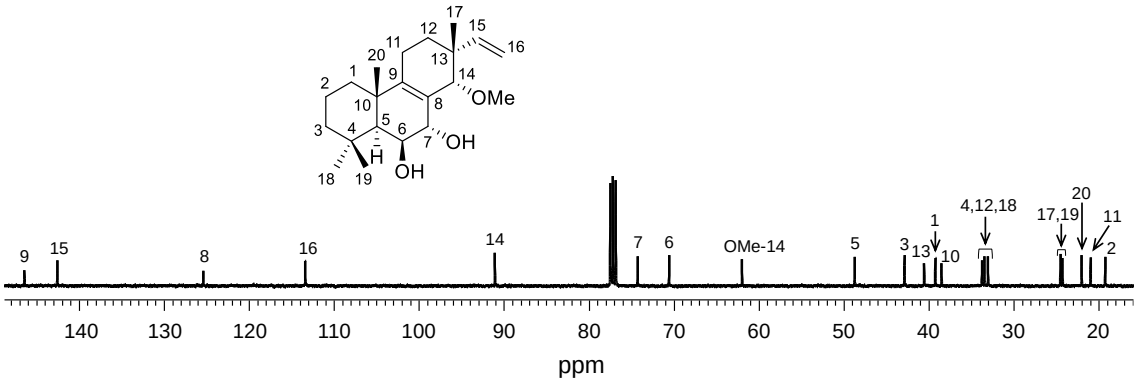

Figure 2.47 ^{13}C NMR spectrum (100 MHz) of **12** in $CDCl_3$

(a) (b)

Figure 2.48 ^{1}H–^{1}H COSY correlations (bold lines) and key HMBC (arrows) (a) and NOESY (dashed arrows) correlations of **12** (b)

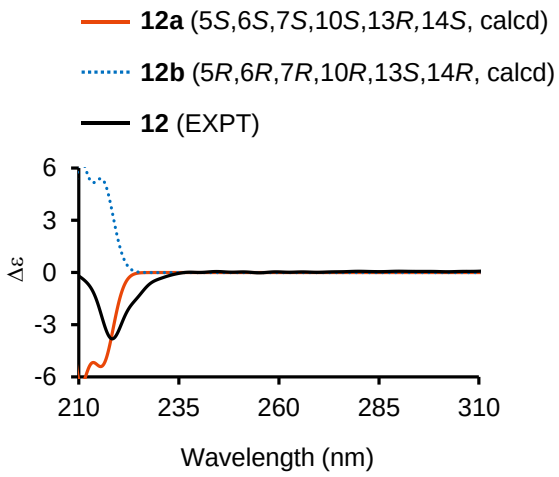

Figure 2. 49 Experimental and calculated CD spectra of **12**

Table 2.12 ^{1}H (400 MHz) and ^{13}C (100 MHz) NMR spectroscopic data for **12** in $CDCl_3$ [δ in ppm and J value in (Hz) in parentheses]

Position	**12**	
	δ_H	δ_C
1α	1.13 (m)	39.2
1β	1.65 (m)	
2α	1.51 (m)	19.2
2β	1.69 (m)	
3α	1.29 (m)	42.9
3β	1.40 (m)	
4		33.8
5α	1.56 (d, 1.4)	48.8
6α	4.26 (br s)	70.7
7β	3.75 (br s)	74.2
8		125.4
9		146.5
10		38.5
11α	2.19 (m)	21.0
11β	1.99 (td, 12.9, 3.4)	
12α	1.67 (m)	33.1
12β	1.47 (m)	
13		40.6
14β	3.59 (br s)	91.2
15	6.07 (dd, 18.1, 10.8)	142.6
16a	5.12 (dd, 18.1, 1.7)	113.4
16b	5.08 (dd, 10.8, 1.7)	
17	1.10 (s)	24.3
18	1.03 (s)	33.5
19	1.22 (s)	24.5
20	1.34 (s)	22.1
OH-7	3.72 (br s)	
OMe-14	3.58 (s)	

2.4 Contents of isolated compounds 9–11 and 15 in extracts

It is noted that the 9,10-seco-isopimarane diterpenoids **9**–**11** and **15** have never been isolated from the *K. marginata* species in the world. To confirm that these isolated compounds were not artificial, the LC-MS analysis of the *n*-hexane, $CHCl_3$, and EtOAc extracts of the rhizomes of the *K. marginata* were performed. The results showed that **9**–**11** and **15** were found in three extracts (Figures S1 and S2). The qualifications and contents of these isolated compounds in the extracts are summarized in Table S2. Namely, compounds **9**–**11** were mainly found in the *n*-hexane extract, with amounts of 6.63 ± 0.04 mg/g, 0.78 ± 0.02 mg/g, and 6.78 ± 0.10 mg/g, respectively. Compound **15** was found to be mainly distributed in the $CHCl_3$ extract at 5.38 ± 0.10 mg/g, in the EtOAc extract at 4.15 ± 0.08 mg/g, and the *n*-hexane extract at 3.50 ± 0.13 mg/g.

2.5 NO production inhibitory activities of isolated compounds from the *K. marginata* rhizomes

To evaluate the NO production inhibitory activities, all of the isolated compounds were tested for the cytotoxic effects on RAW264.7 macrophage cells. The isolated compounds **2**, **4**–**7**, **9**–**12**, **15**, **16**, **20**, **21**, **25**, **27**, and **28** without showing cytotoxicity against the RAW264.7 cells (Table S3, Supplementary data) were further investigated for the NO production inhibitory activities against LPS-stimulated RAW274.7 cells. L-*N*MMA was used as a positive control (IC_{50} = 40.73 ± 0.60 μM). As shown in Table 2.13, compounds **2**, **4**–**7**, **9**, **11**, **12**, **15**, **25**, and **28** exhibited potent activities for the NO production inhibitory in LPS-stimulated RAW264.7 cells, with the IC_{50} values ranging from 65.04 to 96.10 μM. In contrast, **10**, **16**, **20**, **21**, and **27** did not show any NO production inhibitory activity.

Table 2.13 Inhibition of NO production of **1**–**31** from the *K. marginata* rhizomes and positive control, L-*N*MMA

Compounds	IC_{50}[a] (μM)	Compounds	IC_{50}[a] (μM)
1	NT[b]	**17**	NT[b]
2	86.59 ± 1.93[c]	**18**	NT[b]
3	NT	**19**	NT[b]
4	89.02 ± 2.13[c]	**20**	> 100
5	96.10 ± 4.64[c]	**21**	> 100
6	68.51 ± 1.86[c]	**22**	NT[b]
7	74.97 ± 0.73[c]	**23**	NT[b]
8	NT[b]	**24**	NT[b]
9	81.93 ± 0.58[c]	**25**	78.03 ± 1.13[c]
10	> 100	**26**	NT[b]
11	87.70 ± 3.38[c]	**27**	> 100
12	65.04 ± 0.76[c]	**28**	86.63 ± 2.03[c]
13	NT[b]	**29**	NT[b]
14	NT[b]	**30**	NT[b]
15	84.97 ± 1.74[c]	**31**	NT[b]
16	> 100	L-*N*MMA[d]	40.73 ± 0.60[c]

[a] IC_{50}, half-maximal inhibitory concentration

[b] NT not tested due to the cytotoxicity

[c] Data are presented as mean ± SD of three independent experiments performed in duplicated

[d] L-*N*MMA was used as a positive control

2.6 Summary of chapter 2

Twelve undescribed diterpenoids, including eight isopimarane diterpenoids, marginols A–H (**1**–**8**), three 9,10-seco-ispimarane diterpenes, marginols I–K (**9**–**11**), and one isopimara-8(9),15-diene diterpene, 14-*epi*-boesenberol F (**12**), together with 19 known diterpenoids (**13**–**31**) were isolated from the *n*-hexane extract of the Vietnamese *K. marginata* rhizomes. The isolated compounds **2**, **4**–**7**, **9**, **11**, **12**, **15**, **25**, and **28** displayed potent NO production inhibitory activity against LPS-stimulated RAW264.7 cells, with the IC_{50} values ranging from 65.04 to 96.10 μM. These findings shed light on the chemodiversity of the *K. marginata* rhizomes in Vietnam and their traditional use in the treatment of inflammatory-associated diseases in terms of chemical compositions.

Chapter 3

Constituents of the *Crinum asiaticum* L. var. *anomalum* Baker collected from Vietnam and their NO inhibitory activities

3.1 Introduction

Crinum asiaticum L. var. *anomalum* Baker is a perennial plant that belongs to the genus *Crinum* (Figure 3.1).[56] Vietnamese *C. asiaticum* was known as "Ngai to" or "Nang", and the local people use the leaf extracts for the treatment of coughs, fevers, and inflammation, without scientific evidence.[37,57] The genus *Crinum* has been investigated due to their alkaloid components with various biological activities, including antiplasmodial,[58] antibacterial,[59] antiviral,[60] anti-malarial,[61] and cytotoxic activities.[62] However, to the best of our knowledge, the chemical constituents and biological activities have never been reported for any parts of *C. asiaticum* var. *anomalum*.

3.2 Extraction and isolation

The dried powder of *C. asiaticum* (0.5 kg) was sonicated in methanol for 48 h (4.0 L × 3) (Figure 3.2). Then, the methanol extract (32.8 g) was suspended in distilled water, and partitioned successively with *n*-haxane (500 mL × 4), $CHCl_3$ (500 mL × 4), and EtOAc (500 mL × 4), to give 4.95, 12.8, and 3.5 g of the *n*-hexane, $CHCl_3$, and EtOAc extracts, respectively. Open silica gel C.C of the $CHCl_3$ extract, eluted with $CHCl_3$:MeOH (100:0 to 60:40, v/v) afforded 21 fractions (500 mL each), and the fractions were combined, based on the TLC profiles. As a result, eleven fractions F_1–F_{11} were obtained. Serial chromatographic separations from these fractions led to isolation of five compounds, including three new flavanols, (2*R*,3*S*)-7-methoxy-flavan-3-ol (**32**), (2*R*,3*S*)-7-hydroxy-flavan-3-ol (**33**) and (2*R*,3*S*)-2′-hydroxy-7-methoxy-flavan-3-ol (**34**), and two known flavans, (2*S*)-4′-hydroxy-7-methoxyflavan (**35**) and (2*S*)-7,4′-dihydroxyflavan (**36**). Structure elucidation of new compounds **32**–**34** were achieved by analyses of 1D and 2D NMR and HRESIMS data, in conjunction with the CD spectra analysis. Meanwhile, comparisons of their spectroscopic data with those reported in literatures identified structures of the known compounds **35** and **36**.

Figure 3.1 *Crinum asiaticum* L. var. *anomalum* Baker

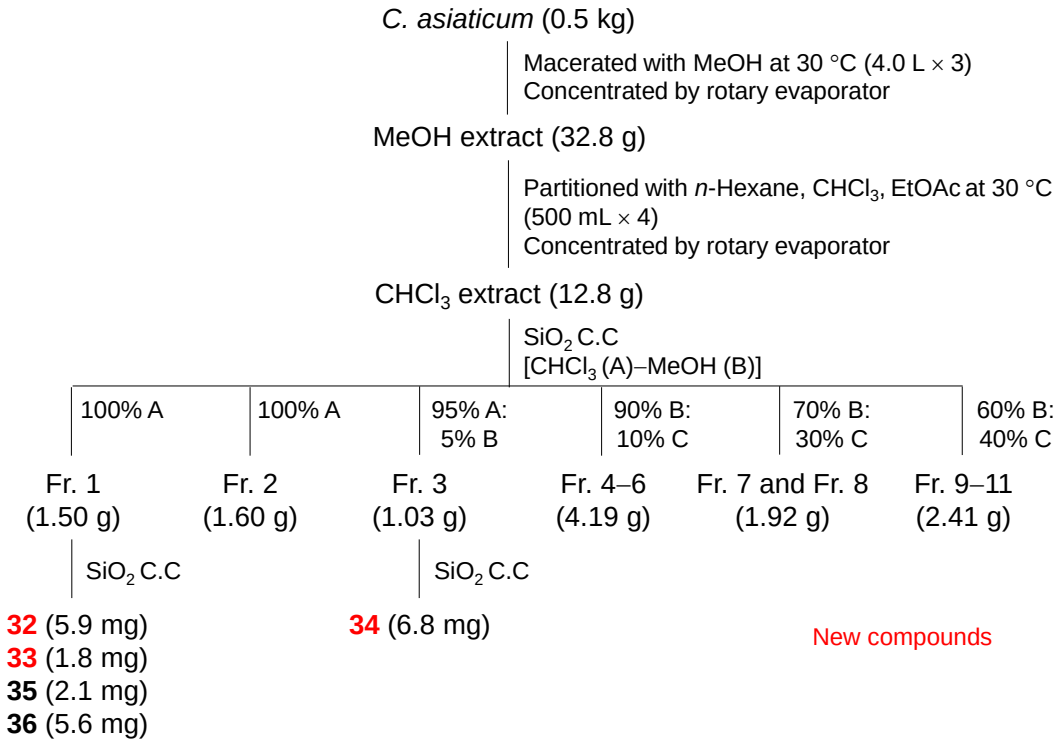

Figure 3.2 Extraction and isolation procedure of compounds from $CHCl_3$ extract of *C. asiaticum*

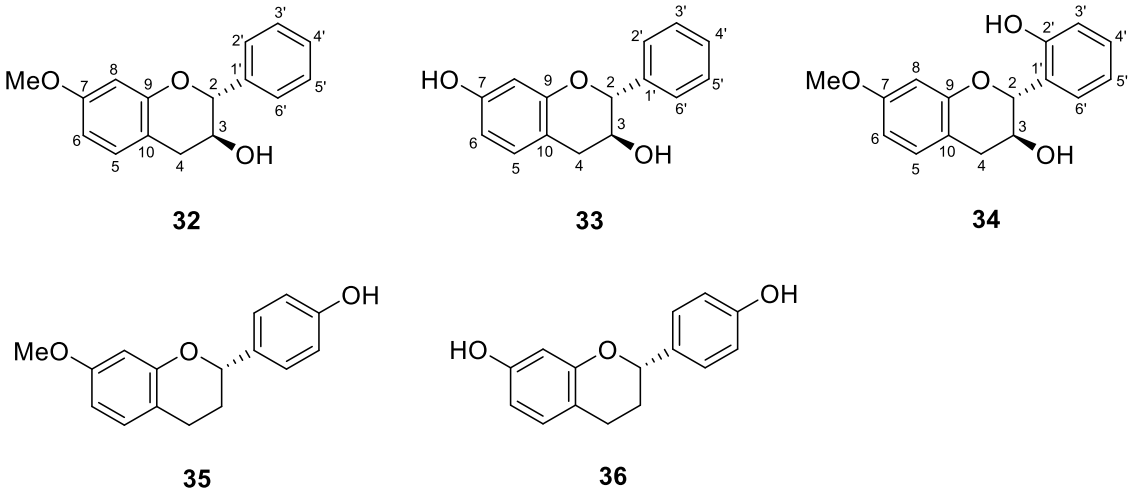

Figure 3.3 Structures of new compounds (**32**–**34**) and known compounds (**35** and **36**) isolated from the chloroform extract of *C. asiaticum*

3.3 Structure elucidation of new compounds

3.3.1 (2*R*,3*S*)-7-Methoxy-flavan-3-ol (32)

Compound **32** was obtained as a colorless oil, with a negative optical rotation $[\alpha]^{22}_{D}$ −26.5 (*c* 0.1, MeOH). The IR spectrum indicated the presence of the hydroxy group (3428 cm^{-1}) and the aromatic ring (1624 and 1588 cm^{-1}) in **32**. The UV spectrum showed absorption maxima at 209, 218, and 282 nm, which are characteristic of the flavan skeleton. The molecular formula of **32** was determined to be $C_{16}H_{16}O_3$, on the basis of the quasi-molecular ion peak at *m/z* 279.0984 $[M + Na]^+$ (calcd. for $C_{16}H_{16}NaO_3$, 279.0992) observed in the HRESIMS and ^{13}C NMR data. The ^1H NMR spectrum displayed signals corresponding to a methoxy group (OMe-7), a methylene group (H-4ax and H-4eq), two oxygenated protons (H-2 and H-3), and eight aromatic protons (H-5, H-6, H-8, H-2′, H-3′, H-4′, H-5′, H-6′) (Figure 3.4). The ^{13}C NMR and HMQC spectra indicated 16 carbon resonances, which are a methoxy (OMe-7), a methylene (C-4), two oxygenated methines (C-2 and C-3), and twelve aromatic carbons including four non-protonated carbons (C-7, C-9, C-10, and C-1′) and eight methine carbons (C-5, C-6, C-8, C-2′, C-3′, C-4′, C-5′, C-6′) (Figure 3.5). The 1D NMR data of **32** (Table 3.1) were similar to those of (2*R*,3*R*)-7-methoxy-flavan-3-ol (**32′**).[61] The COSY correlations between H-5 and H-6, in conjunction with the correlation of the methoxy protons (δ_H 3.73) to C-7 (δ_C 160.9) in the HMBC analysis, indicated that the methoxy group was attached to C-7 (Figure 3.6a). Significant differences were the changes in the chemical shifts at C-2 (δ_C 83.1) and C-3 (δ_C 68.7) in **32**, as compared with those of C-2 (δ_C 80.4) and C-3 (δ_C 67.7) in **32′**, suggested that **32** was a stereoisomer of **32′**. The relative configuration of **32** was assigned *via* the coupling constant values, in conjunction with the NOSEY correlations. The coupling constants between H-3 and H-4eq (J = 5.1 Hz) and between H-3 and H-4ax (J = 8.0 Hz) suggested that H-3 was a *pseudo*-equatorial orientation. In contrast, the coupling constant between H-2 and H-3 (J = 7.2 Hz) and the NOESY correlations between H-2 and H-4ax suggested that H-2 was a *pseudo*-axial orientation (Figure 3.6b).[63–65] The CD spectrum analysis of **32**, which showed positive and negative Cotton effects at 241 and 285 nm, similar to those of (2*R*,3*S*)-catechin-7-*O*-*β*-D-glucopyranoside, respectively, suggested the absolute configurations of C-2 and C-3 in **32** to be *R* and *S*, respectively

(Figure 3.7).[66] Thus, structure of **32** was determined to be (2*R*,3*S*)-7-methoxy-flavan-3-ol.

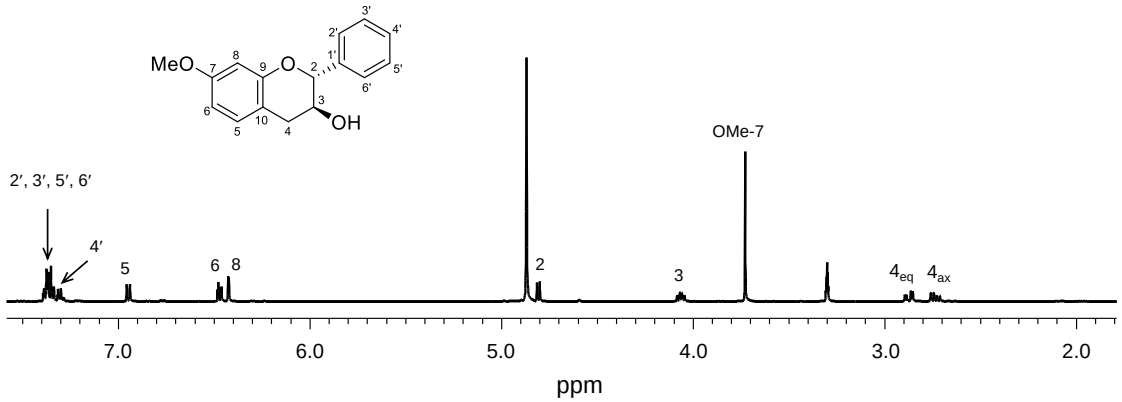

Figure 3.4 [1]H NMR spectrum (500 MHz) of **32** in methanol-d_4

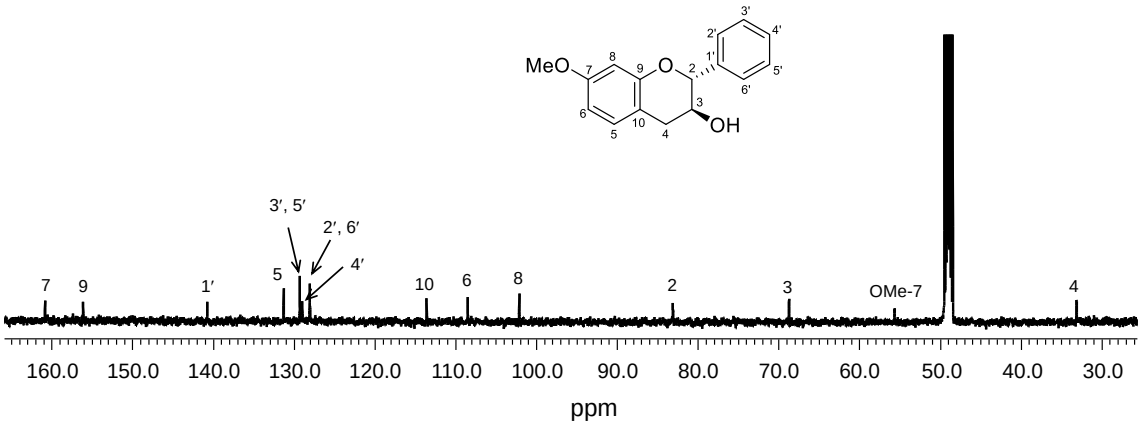

Figure 3.5 [13]C NMR spectrum (125 MHz) of **32** in methanol-d_4

(a) (b)

Figure 3.6 $^{1}H–^{1}H$ COSY correlations (bold lines) and key HMBC (arrows) (a) and NOESY (dashed arrows) correlations of **32** (b)

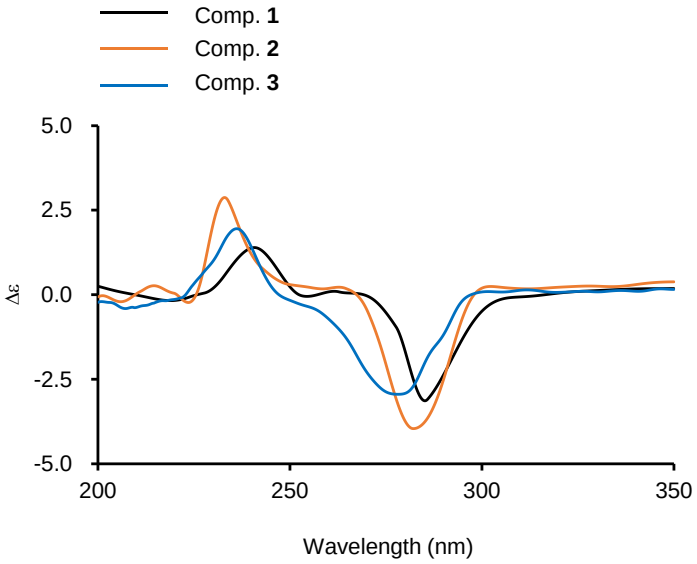

Figure 3.7 Experimental CD spectra of **32**–**34**

Table 3.1 ^{1}H (500 MHz) and ^{13}C (125 MHz) NMR spectroscopic data for **32** in methanol-d_4 [δ in ppm and J value in (Hz) in parentheses]

Position	**32**	
	δ_H	δ_C
2	4.82, d (7.2)	83.1
3	4.08, ddd (8.0, 7.2, 5.1)	67.1
4_{ax}	2.73, dd (15.8, 8.0)	33.2
4_{eq}	2.90, dd (15.8, 5.1)	
5	6.96, d (8.4)	131.3
6	6.48, dd (8.4. 2.4)	108.5
7		160.9
8	6.42, d (2.4)	102.1
9		156.1
10		113.6
1′		140.8
2′	7.39[a], m	128.1
3′	7.39[a], m	129.3
4′	7.30, m	129.0
5′	7.39[a], m	129.3
6′	7.39[a], m	128.1
OMe-7	3.73, s	55.7

[a] Overlapping resonances within the same column

3.3.2 (2*R*,3*S*)-7-Hydroxy-flavan-3-ol (33)

Compound **33** was isolated as a colorless oil, with a negative optical rotation $[\alpha]^{22}_{D}$ –51.0 (*c* 0.1, MeOH). Its IR spectrum indicated the presence of the hydroxy (3436 cm^{-1}) group and an aromatic ring (1627 and 1512 cm^{-1}) in the molecule. Its molecular formula was assigned as $C_{15}H_{14}O_3$, on the basis of the quasi-molecular ion peak at *m/z* 241.0867 $[M - H]^-$ (calcd. for $C_{15}H_{13}O_3$, 241.0870) observed in the HRESIMS and ^{13}C NMR data. The ^1H and ^{13}C NMR data of **33** recorded in DMSO-d_6 (Table 3.2, Figures 3.8 and 3.9) showed similar patterns to those of **32**. The significant difference was the presence of the hydroxy group [δ_H 9.20 (br s, OH-7); δ_C 156.7 (C-7)], instead of the methoxy group.

The HMBC correlations from the hydroxy proton to C-6/C-7/C-8 indicated the location of the hydroxy group at C-7 (Figure 3.10a). The observation of the coupling constant of 7.6 Hz between H-2 and H-3 in the ^1H NMR data and the NOESY correlations determined the same relative configurations at C-2 and C-3 of **33** as those of **32** (Figure 3.10b). The CD spectrum of **33** showed similar Cotton effects to those of **32**, indicating that both compounds shared the same absolute configuration (Figure 3.7). Consequently, **33** was determined as (2*R*,3*S*)-7-hydroxy-flavan-3-ol.

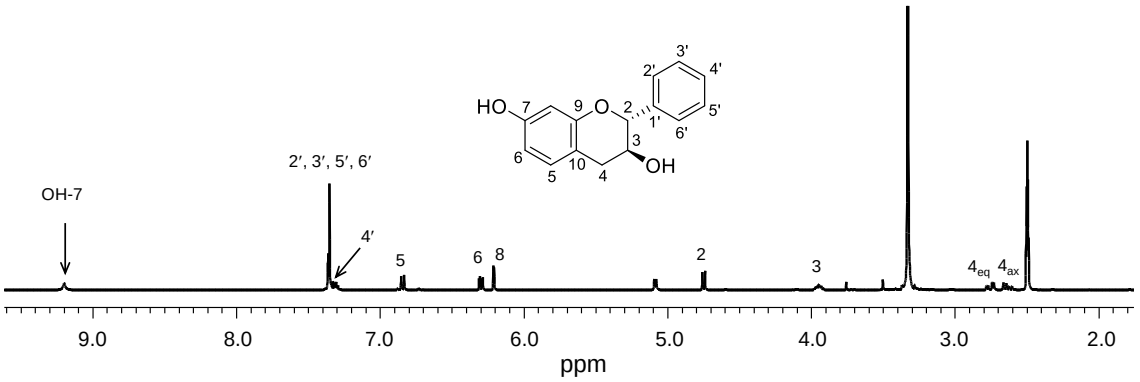

Figure 3.8 ^1H NMR spectrum (400 MHz) of **33** in DMSO-d_6

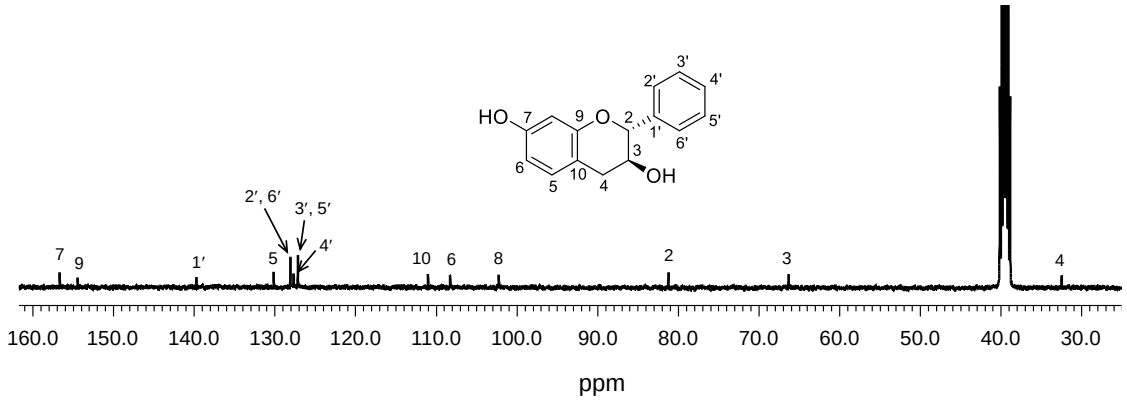

Figure 3.9 ^{13}C NMR spectrum (125 MHz) of **33** in DMSO-d_6

(a) (b)

Figure 3.10 ^{1}H–^{1}H COSY correlations (bold lines) and key HMBC (arrows) (a) and NOESY (dashed arrows) correlations of **33** (b)

Table 3.2 ^{1}H (400 MHz) and ^{13}C (100 MHz) NMR spectroscopic data for **33** in DMSO-d_6 [δ in ppm and J value in (Hz) in parentheses]

Position	**33**	
	δ_H	δ_C
2	4.77, d (7.6)	81.2
3	3.98, ddd (8.1, 7.6, 5.0)	66.4
4_{ax}	2.66, dd (15.8, 8.1)	32.5
4_{eq}	2.74, dd (15.8, 5.0)	
5	6.86, d (8.2)	130.2
6	6.31, dd (8.2. 2.5)	108.3
7		156.7
8	6.21, d (2.5)	102.3
9		154.5
10		111.0
1′		139.7
2′	7.39[a], m	128.1
3′	7.39[a], m	127.2
4′	7.32, m	127.7
5′	7.39[a], m	127.2
6′	7.39[a], m	128.1
OH-7	9.20, br s	

[a] Overlapping resonances within the same column

3.3.3 (2*R*,3*S*)-2′-hydroxy-7-methoxy-flavan-3-ol (34)

Compound **34** was obtained as a colorless oil, with a negative optical rotation $[\alpha]^{22}_{D}$ −42.0 (*c* 0.1, MeOH). Its molecular formula was deduced as $C_{16}H_{16}O_4$ from the NMR and negative-ion HRESIMS data (*m/z* 271.0972 $[M - H]^-$, calcd. for $C_{16}H_{15}O_4$, 271.0976), and was 16 amu higher than that of **32**. The NMR spectroscopic data (Table 3.3) (Figures 3.11 and 3.12) were similar to those of **32**, except for the appearance of an additional hydroxy group [δ_H 9.60 (br s, OH-2′); C-2′ δ_C (154.5)]. The HMBC correlations from H-2 to C-2 and from H-4′ and H-6′ to C-2′ indicated that an additional hydroxy group was attached at C-2′ (Figure 3.13a). The relative configuration of **34** was assigned to be the same as those of **32**, based on the ^{1}H NMR and the NOESY correlations (Figure 3.13b). The CD spectrum of **34** was also quite similar to those of **32** and **33** (Figure 3.7). Thus, **34** was determined to be (2*R*,3*S*)-2′-hydroxy-7-methoxy-flavan-3-ol.

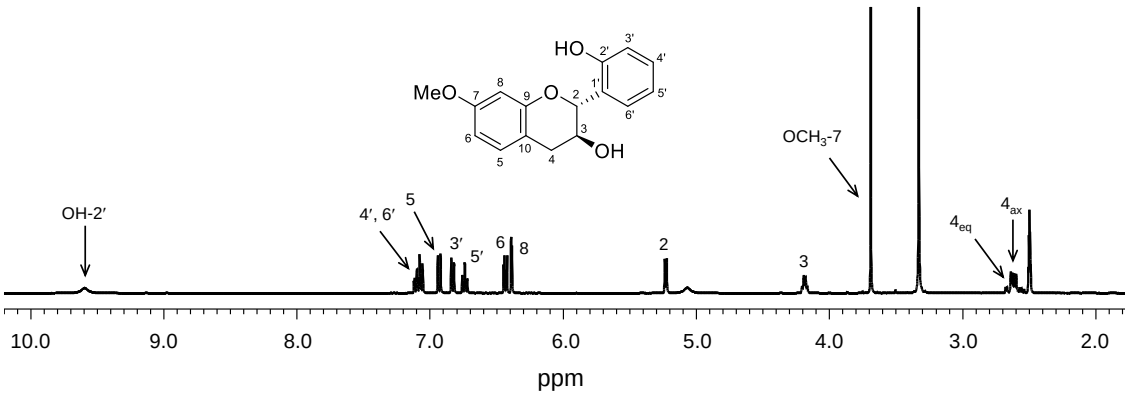

Figure 3.11 ^{1}H NMR spectrum (400 MHz) of **34** in DMSO-d_6

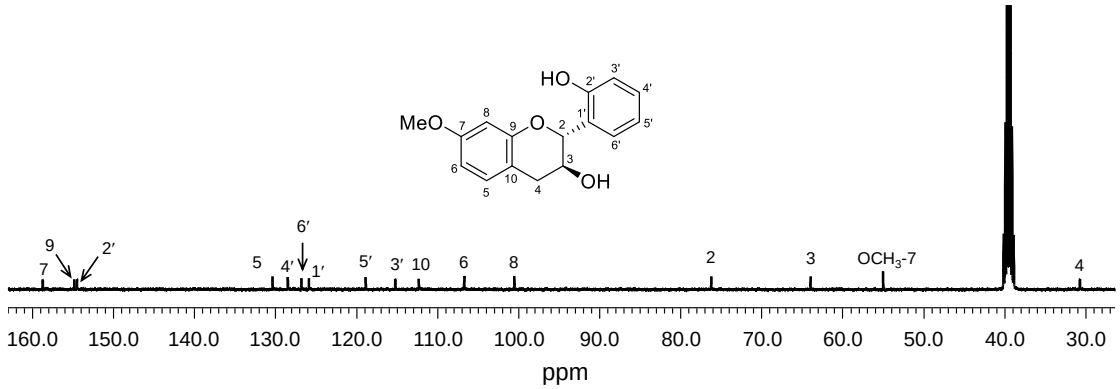

Figure 3.12 ^{13}C NMR spectrum (100 MHz) of **34** in DMSO-d_6

(a) (b)

Figure 3.13 ^{1}H–^{1}H COSY correlations (bold lines) and key HMBC (arrows) (a) and NOESY (dashed arrows) correlations of **34** (b)

Table 3.3 ^{1}H (400 MHz) and ^{13}C (100 MHz) NMR spectroscopic data for **34** in DMSO-d_6 [δ in ppm and J value in (Hz) in parentheses]

Position	**34**	
	δ_H	δ_C
2	5.24, d (5.5)	76.2
3	4.21, ddd (6.2, 5.5, 4.4)	64.0
4ax	2.61, dd (15.9, 6.2)	30.7
4eq	2.68, dd (15.9, 4.4)	
5	6.94, d (8.5)	130.4
6	6.45, dd (8.5. 2.5)	106.7
7		158.8
8	6.39, d (2.5)	100.5
9		154.9
10		112.3
1′		125.9
2′		154.5
3′	6.84, dd (8.1, 1.1)	115.2
4′	7.08, m	128.5
5′	6.76, td (7.4, 1.1)	118.8
6′	7.12, m	126.8
OMe-7	3.69, s	55.0
OH-2′	9.60, br s	

3.4 Contents of isolated compounds in extracts

The LC-MS/MS analysis determined the presence of the isolated compounds **32**–**36** in the extracts. The results indicated that **32**–**36** were distributed in the $CHCl_3$ extract. In contrast, only trace amounts of **32** and **33** were found in the EtOAc extract, confirming the good extraction with the $CHCl_3$ during the liquid/liquid partition process (Figure S3, Supplementary data). MRM method determined the contents of each compound in the $CHCl_3$ extract, which showed contents of 1.23 ± 0.01 mg/g (**32**), 1.01 ± 0.07 mg/g (**33**), 0.85 ± 0.02 mg/g (**34**), 1.44 ± 0.01 mg/g (**35**), and 1.09 ± 0.01 mg/g (**36**) (Table S4, Supplementary data).

3.5 NO inhibitory activities of isolated compounds from *C. asiaticum*

The isolated compounds, except **33** due to low amount, were investigated for NO production inhibitory activity against the LPS-stimulated RAW264.7 cells. Compounds **32** and **34**–**36** showed significant inhibitory effects on NO production with IC_{50} values ranging from 11.15 μM to 12.43 μM, as compared to the positive control L-*N*MMA (IC_{50}: 39.30 μM) (Table 3.4). Meanwhile, **35** did not exhibit any cytotoxicity against the RAW264.7 cells at 3.13 μM (Table S5, Supplementary data). Furthermore, these active compounds were tested for their inhibition of specific cytokine production IL-6 using immunosorbent assay. The result indicated that compounds **32** and **34**–**36** inhibited the IL-6 production at 10 μM (Figure 3.14). In addition, **32** and **34**–**36** suppressed the LPS-induced phosphorylation of the p65 subunit of NF-κB in RAW264.7 cells at 10 μM, without significantly affecting the phosphorylation status of p65 under the unstimulated conditions (Figures 3.15a and 3.15b). These results suggested that **32** and **34**–**36** have potential anti-inflammatory effects by inhibiting the activation of the NF-κB signaling pathway toward LPS-stimulation.

Table 3.4 Inhibition of NO production of **32** and **34**–**36** from the *C. asiaticum*

Compounds	IC_{50}[a] (μM)
32	11.60 ± 0.27[b]
34	12.33 ± 0.40[b]
35	12.43 ± 0.16[b]
36	11.15 ± 0.69[b]
L-*N*MMA[c]	39.30 ± 2.23[b]

[a] IC_{50}, half-maximal inhibitory concentration

[b] Data are presented as mean ± SD of three independent experiments performed in duplicated

[c] L-*N*MMA was used as a positive control

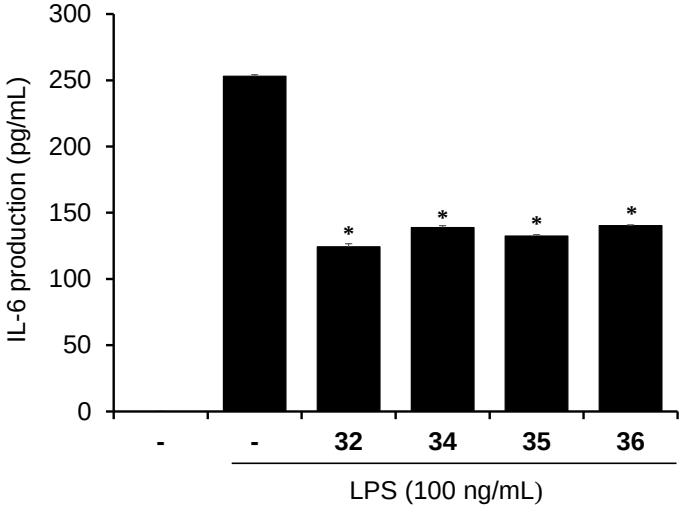

Figure 3.14 Inhibitory effects of **32** and **34**–**36** on IL-6 production. RAW264.7 cells were treated with 10 μM of **32** and **34**–**36** for 1 h, then stimulated with LPS (100 ng/mL) for 24 h, supernatants were collected, and IL-6 levels were measured by ELISA as described in materials and methods. Data are expressed as mean ± SD of three independent experiments. *p <0.05 as compared with LPS alone

(a)

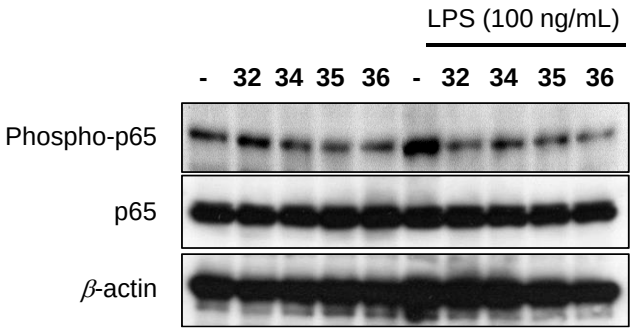

(b)

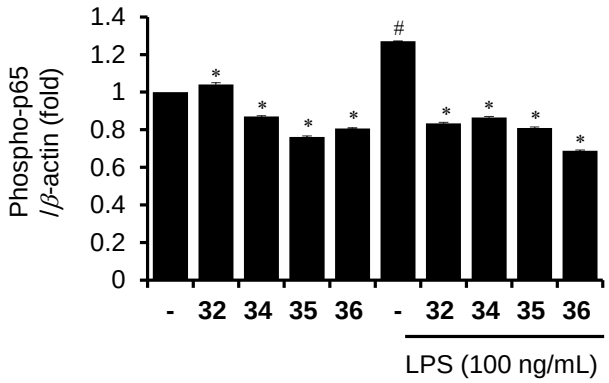

Figure 3.15 Inhibitory effects of **32** and **34**–**36** on NF-κB pathway. RAW264.7 cells were pre-treated with 10 μM of **32** and **34**–**36** for 1 h and stimulated with or without LPS (100 ng/mL) for 15 min. Western blot analysis was performed using antibodies against phospho-NF-κB p65 (a). The relative expression of phospho-NF-κB p65 (b). The data are expressed as the means ± SD of three independent experiments. #$p < 0.05$ as compared with untreated group, *$p < 0.05$ as compared with LPS alone

3.5 Summary of chapter 3

Phytochemical investigation of the $CHCl_3$ extract of *C. asiaticum* resulted in the isolation of three new flavanols (**32**–**34**) and two known flavans (**35** and **36**). Further investigation of the anti-inflammatory effects of the NF-κB pathway showed that **32** and **34**–**36** inhibited the LPS-induced NO production and IL-6 expression, as well as phosphorylation of p65. Thus, this study provides new insight into the chemical constituents of *C. asiaticum* and the biological activities of flavanols and flavans. It was also suggested that flavanols (**32**–**34**) and flavans (**35** and **36**) exhibit anti-inflammatory effects by suppressing LPS-induced NF-κB activation and IL-6 cytokine expression.

Conclusion

In this study, the chemical investigation of the active *n*-hexane and $CHCl_3$ extracts of the *K. marginata* rhizomes and the *C. asiaticum* whole plants led to the isolation of 36 compounds including 15 new ones, marginols A–K (**1**–**11**), 14-*epi*-boesenberol (**12**), (2*R*,3*S*)-7-methoxy-flavan-3-ol (**32**), (2*R*,3*S*)-7-mydroxy-flavan-3-ol (**33**), and (2*R*,3*S*)-2′-hydroxy-7-methoxy-flavan-3-ol (**34**), and 21 known compounds **13**–**31**, and **35** and **36**.

Furthermore, isolation of the *ent*-pimaranes, marginols A–C (**1**–**3**), together with the 9,10-seco-isopimarane diterpenes, marginols I–K (**9**–**11**) makes a great contribution to the chemodiversity of the *K. marginata* species. In addition, the isolation of flavanols (**32**–**34**) and flavanes **35** and **36** were reported for the first time from the *C. asiaticum* L. var. *anomalum* Baker.

The isopimarane and 9,10-seco-isopimarane diterpenoids isolated from the *K. marginata* rhizomes, especially compounds, **2**, **4**–**7**, **9**, **11**, **12**, **15**, **25**, and **28** showed potent NO production inhibitory activities. On the other hand, the flavanols **32** and **34**, together with flavanes **35** and **36** showed significant NO production inhibitory activities as compared to the positive control, L-*N*MMA.

These findings provide insights into not only the chemodiversity of the diterpenoid and flavonoid skeletons, but also the anti-inflammatory effects of the two Vietnamese plants, *K. marginata* and *C. asiaticum*, in their traditional usage for treatment of inflammatory-associated diseases.

Experimental

I. Chemicals and reagents

RAW264.7 macrophage cell line (RCB 0535) was obtained from the RCB. L-*N*MMA was obtained from Enzo. LPS from *E. coli*, α-MEM with L-glutamine and phenol red, *N*-1-naphthylethylene diamine dihydrochloride, penicillin–streptomycin solution, and sulfanilamide were obtained from Wako. Phosphoric acid was purchased from Nacalai Tesque. MTT was purchased from BLDpharm. ELISA MAX Standard Set Mouse IL-6 kits were purchased from BioLegend. The primary antibodies used in western blotting analysis were obtained from Cell Signaling Technology. The β-actin antibodies were obtained from Santa Cruz Biotechnology.

II. General experimental procedures

NMR spectra were recorded on ECX-400P and ECA500II spectrometers (JEOL) in $CDCl_3$, DMSO-d_6, methanol-d_4, and pyridine-d_5. HRESIMS data were obtained on a LCMS-IT-TOF spectrometer (Shimadzu). Optical rotations were measured on a P2100 polarimeter (JASCO). UV spectra were measured on a NanoDrop 2000c spectrophotometer (Thermofisher). IR spectra were recorded as KBr pellets on an FTIR-460 Plus spectrometer (JASCO). CD spectra were recorded on a J-805 spectropolarimeter (JASCO). Open C.C was performed with silica gel 60N (40–50 μM) (Kanto Chemical). TLC was performed using silica gel GF_{254} precoated plates, spot detection by visualization under UV, spraying with $Ce(SO_4)_2$ stain, and heating at 120 ^oC for 10 min in a drying cabinet.

Cell culture

RAW264.7 macrophage cells were grown in α-MEM including 1% penicillin-streptomycin and 10% FBS. The cells were collected when cell confluence was about 70% and seeded in 96 well plate at a density of 4×10^4 cells/well. After 24 h of incubation, the samples were treated with various concentrations for 1 h, then stimulated with LPS (400 ng/mL) at a final volume of 50 μL/well and incubated for another 24 h.

Cell viability assay

MTT assay performed cytotoxicity of the test samples to RAW264.7 cells.[67] In detail, the remaining cells in the 96-well plate were washed with PBS (100 μL/well). A solution of 10% MTT (5 mg/mL) was then added to each well (100 μL) and incubated for 3 h. After removing the supernatant, 100 μL of DMSO was added to each well and incubated for another 15 min. The absorbance at 570 nm was measured using a microplate reader SH-1200 (Corona).

The percentages of cell viability were calculated using the following formula:

% cell survival (A) = 100 × [Abs (treated cell + LPS)/Abs (control cell + LPS)].

NO production inhibitory assay

Griess assay determined the nitrite concentration in the supernatant layer.[68] 100 μL of the Griess reagent containing 0.5% sulfanilamide and 0.05% naphthalenediamide dihydrochloride in 2.5% H_3PO_4 was added to each well and incubated for 15 min. The coloration corresponding to NO concentration was recorded at 540 nm.

The percentages of NO inhibition were calculated using the following formula:

% NO inhibition = 100 × [Abs (control cell + LPS) − Abs (treated cell + LPS)]/Abs (control cell + LPS) × [Abs (treated cell + LPS)/Abs (control cell + LPS)].

ELISA

The supernatants of RAW264.7 cells (5×10^5 cells/well) seeded in 12-well plates were collected. The ELISA MAX Standard Set Mouse IL-6 kit, was used for determining the IL-6 production, according to the manufacturer's instructions. The absorbance was recorded at 450/570 nm using an SH-1200 microplate reader.

Western blotting

RAW264.7 cells were seeded in 12-well plates and incubated for 24 h, then treated cells stimulated with LPS (100 ng/mL) for 15 min (10 μM compounds), and unstimulated treated cells. After stimulation, the treated cells were collected and lysed in whole-cell lysis buffer. 10% Sodium dodecyl sulfate-polyacrylamide gel electrophoresis (SDS-PAGE) separated cell lysates and proteins were transferred to

polyvinylidene difluoride (PVDF) membranes. Membranes were blocked with Block Age for 2 h and immunoblotted at 4 ^{o}C with primary antibodies specific for phospho-NF-κB p65, NF-κB phospho-p65, and β-actin. Before using for immunoblotting, primary antibodies were diluted in 10^3 folds (v/v) with PBS containing 0.1% Tween 20 (PBST). After incubation for 24 h, the membrane blots were further incubated with horseradish peroxidase (HRP)-conjugated secondary antibody diluted 2×10^3 folds in 0.1% PBST for 1 h at room temperature, washed with PBST, and the bands were detected using the Pierce ECL Western Blotting Substrate to detect bands. Immunoreactive proteins were visualized on X-ray film. After scanning, the protein bands were quantified with ImageJ software. Equal loading of proteins was confirmed with β-actin.

Experimental detail of chapter 2

Plant material

Rhizomes of *Kaempferia marginata* Carey ex Roscoe were collected from Dong Nai Province, Vietnam during the rainy season in September 2020. Dr. Dang Van Son, botanist at the Institute of Tropical Biology, Vietnam performed identification of the specimens. The voucher specimens (20605) are kept in the Museum for Materia Medica, Analytical Research Center for Ethnomedicines, Institute of Natural Medicine, University of Toyama, Japan.

Extraction and isolation procedure

Dried powder (1.5 kg) of the *K. marginata* rhizomes was macerated in MeOH under sonication (4 L, 90 min, × 4) at 30 °C. The extract was evaporated under vacuum and the remaining aqueous residue was successively partitioned with *n*-hexane, $CHCl_3$ and EtOAc. The *n*-hexane extract (13.6 g) was subjected to silica gel C.C and eluted with *n*-hexane:EtOAc (from 95:5 to 0:100, v/v) to yield nine fractions, F_1 (869 mg), F_2 (939 mg), F_3 (618 mg), F_4 (1.40 g), F_5 (1.60 g), F_6 (2.41 g), F_7 (1.98 g), F_8 (1.46 g), and F_9 (2.39 g). Fraction F_3 (618 mg) was loaded on open silica gel C.C and eluted with *n*-hexane:EtOAc (95:5 to 85:15, v/v) to yield three subfractions, $F_{3–1}$ (196 mg), $F_{3–2}$ (240 mg), and $F_{3–3}$ (176 mg). *n*-Hexane:EtOAc isocratic system (90:10, v/v) was used to purify subfraction $F_{3–1}$ (196 mg) on an open silica gel C.C to separate **21** (2.0 mg) and **22** (30 mg). Subfraction $F_{3–2}$ (240 mg) was further purified with open silica gel C.C [*n*-hexane:EtOAc (90:10 to 85:15, v/v)] to give **24** (2.0 mg) and **17** (50 mg). Fraction F_5 (1.60 g) was fractionated on an open silica gel C.C and eluted with *n*-hexane:EtOAc (90:10 to 70:30, v/v) to obtain four subfractions, $F_{5–1}$ (200 mg), $F_{5–2}$ (160 mg), $F_{5–3}$ (900 mg), and $F_{5–4}$ (240 mg). Subfraction $F_{5–2}$ (160 mg) was separated via open silica gel C.C using an *n*-hexane:EtOAc isocratic system (90:10, v/v) to separate **1** (5.0 mg), **25** (5.0 mg), and **27** (6.0 mg). Compounds **14** (4.0 mg) and **20** (2.0 mg) were separated from fractionton $F_{5–3}$ (900 mg) using the *n*-hexane:EtOAc isocratic system (80:20, v/v) *via* open silica gel C.C. Fraction F_6 (2.41 g) was fractionated on open silica gel C.C, eluting with *n*-hexane:EtOAc (from 80:20 to 60:40, v/v) to yield six subfractions, $F_{6–1}$ (340 mg), $F_{6–2}$ (720 mg), $F_{6–3}$ (410 mg), $F_{6–4}$ (210 mg), $F_{6–5}$ (523 mg), and $F_{6–6}$ (200

mg). Subfraction $F_{6–1}$ (340 mg) was purified on open silica gel C.C with *n*-hexane: EtOAc (80:20, v/v) to give **3** (10.0 mg) and **7** (5.0 mg). Using the same method for subfraction $F_{6–4}$ (210 mg), compounds **8** (3.0 mg) and **28** (30.0 mg) were isolated. Fraction F_7 (1.98 g) was rechromatographed on open silica gel C.C and eluted with *n*-hexane:EtOAc (70:30 to 50:50, v/v) to yield five subfractions, $F_{7–1}$ (260 mg), $F_{7–2}$ (311 mg), $F_{7–3}$ (408 mg), $F_{7–4}$ (270 mg), and $F_{7–5}$ (721 mg). $F_{7–3}$ (408 mg) was purified on open column C.C and eluted with an *n*-hexane:EtOAc isocratic system (60:40, v/v) to isolate **6** (10.0 mg), **19** (15.0 mg), and **26** (50.0 mg). Fraction F_8 (1.46 g) was subjected to open silica gel C.C eluting with *n*-hexane:EtOAc (70:30 to 40:60) to yield five subfractions, $F_{8–1}$ (376 mg), $F_{8–2}$ (216 mg), $F_{8–3}$ (431 mg), $F_{8–4}$ (266 mg), and $F_{8–5}$ (158 mg). Subfraction $F_{8–1}$ (376 mg) was separated on open silica gel C.C and eluted with an *n*-hexane:EtOAc isocratic system (70:30, v/v) to give **2** (2.0 mg), **30** (20.0 mg), and **31** (20.0 mg). Subfraction $F_{8\text{-}2}$ (216 mg) was separated *via* open silica gel open C.C using the *n*-hexane:EtOAc isocratic system (60:40, v/v) to yield **9** (10.0 mg) and **10** (2.0 mg). Further purification of subfraction $F_{8–3}$ (431 mg) with *n*-hexane:EtOAc (60:40 to 50:50, v/v) gave **29** (22.0 mg) and **18** (20.0 mg). Using the same method for subfration $F_{8–4}$ (266 mg), compounds **11** (20.0 mg) and **15** (15.0 mg) were isolated. Fraction F_9 (2.39 g) was separated on an open silica gel C.C performed in *n*-hexane:EtOAc (60:40 to 30:70, v/v) to give five subfractions of $F_{9–1}$ (430 mg), $F_{9–2}$ (310 mg), $F_{9–3}$ (512 mg), $F_{9–4}$ (576 mg), and $F_{9–5}$ (560 mg). Subfraction $F_{9–1}$ (430 mg) was further purified with a mixture of *n*-hexane:EtOAc (50:50, v/v) to give **4** (6.0 mg) and **5** (2.0 mg). Subfraction $F_{9–3}$ (512 mg) was rechromatographed on an open silica gel C.C and eluted with an isocratic system of *n*-hexane:EtOAc (40:60, v/v) to give **13** (14.0 mg), **23** (3.0 mg), and **16** (3.0 mg). Normal phase silica gel C.C of subfraction $F_{9–4}$ (576 mg), eluting with *n*-hexane:EtOAc isocratic system (40:60, v/v), gave **12** (2.5 mg).

Marginol A (1): Colorless oil; $[\alpha]^{22}_{D}$ −114.0 (*c* 0.1, $CHCl_3$); UV (MeOH) λ_{max} 260, 214, 212, and 207 nm; CD (*c* 0.01, MeOH) ($\Delta\varepsilon$) 303 (1.87), and 266 (−2.95) nm; IR (KBr) 3632, 3468, 2948, 1887, 1710, 1646, and 1090 cm^{-1}; ^{1}H and ^{13}C NMR data, see Table 2.1; HRESIMS *m/z* 325.2134 $[M + Na]^+$ (calcd. for $C_{20}H_{30}O_2Na$, 325.2138).[52]

Marginol B (2): Colorless oil; $[\alpha]^{22}_{D}$ −22.5 (*c* 0.06, $CHCl_3$); UV (MeOH) λ_{max} 240, 218, and 211 nm; CD (*c* 0.01, MeOH) ($\Delta\varepsilon$) 226 (−2.47), and 211 (1.34) nm; IR (KBr) 3440, 2942, 1689, 1637, and 1007 cm^{-1}; ^{1}H and ^{13}C NMR data, see Table 2.2; HRESIMS *m/z* 317.2124 $[M - H]^-$ (calcd. for $C_{20}H_{29}O_3$, 317.2122).[52]

Marginol C (3): Colorless oil; $[\alpha]^{22}_{D}$ −16.5 (*c* 0.05, $CHCl_3$); UV (MeOH) λ_{max} 248, 211, and 208 nm; CD (*c* 0.01, MeOH) ($\Delta\varepsilon$) 220 (−3.94), and 203 (1.72) nm; IR (KBr) 3450, 2390, 1731, 1693, 1370, and 1239 cm^{-1}; ^{1}H and ^{13}C NMR data, see Table 2.3; HRESIMS *m/z* 383.2193 $[M + Na]^+$ (calcd. for $C_{22}H_{34}O_4Na$, 383.2193).[52]

Marginol D (4): Amorphous solid; $[\alpha]^{22}_{D}$ −29.6 (*c* 0.1, MeOH); UV (MeOH) λ_{max} 213, 209, and 205 nm; IR (KBr) 3424, 3336, 2925, 1704, 1462, 1372, and 1081 cm^{-1}; ^{1}H and ^{13}C NMR data, see Table 2.4; HRESIMS *m/z* 341.2092 $[M + Na]^+$ (calcd. for $C_{20}H_{30}O_3Na$, 341.2087).[52]

Marginol E (5): Amorphous solid; $[\alpha]^{22}_{D}$ −8.4 (*c* 0.1, MeOH); UV (MeOH) λ_{max} 263, and 208 nm; IR (KBr) 3408, 3336, 2948, 2360, 1706, 1665, 1460, 1383, and 1062 cm^{-1}; ^{1}H and ^{13}C NMR data, see Table 2.5; HRESIMS *m/z* 343.2227 $[M + Na]^+$ (calcd. for $C_{20}H_{32}O_3Na$, 343.2244).[52]

Marginol F (6): Amorphous solid; $[\alpha]^{22}_{D}$ −125.0 (*c* 0.1, MeOH); UV (MeOH) λ_{max} 271, 218, and 211 nm; IR (KBr) 3654, 3523, 2958, 1890, 1710, 1642, and 1089 cm^{-1}; ^{1}H and ^{13}C NMR data, see Table 2.6; HRESIMS *m/z* 357.2026 $[M + Na]^+$ (calcd. for $C_{20}H_{30}O_4Na$, 357.2036).[52]

Marginol G (7): Amorphous solid; $[\alpha]^{22}_{D}$ −9.3 (*c* 0.1, MeOH); UV (MeOH) λ_{max} 213, 210, and 206 nm; IR (KBr) 3654, 3436, 2964, 2365, 1713, 1371, and 1242 cm^{-1}; ^{1}H and ^{13}C NMR data, see Table 2.7; HRESIMS *m/z* 383.2194 $[M + Na]^{+}$ (calcd. for $C_{22}H_{32}O_4Na$, 383.2193).[52]

Marginol H (8): Amorphous solid; $[\alpha]^{22}_{D}$ −44.4 (*c* 0.1, MeOH); UV (MeOH) λ_{max} 263, and 208 nm. CD (*c* 0.01, MeOH) ($\Delta\varepsilon$) 369 (−2.21), 294 (3.09), and 267 (−6.99) nm; IR (KBr) 3482, 2965, 1664, 1615, 1294, and 1062 cm^{-1}; ^{1}H and ^{13}C NMR data, see Table 2.8; HRESIMS *m/z* 323.1983 $[M + Na]^{+}$ (calcd. for $C_{20}H_{28}O_2Na$, 323.1982).[52]

Marginol I (9): Colorless oil; $[\alpha]^{22}_{D}$ −32.5 (*c* 0.1, $CHCl_3$); UV (MeOH) λ_{max} 239 and 284 nm; CD (*c* 0.1, MeOH) ($\Delta\varepsilon$) 350 (−2.78), 276 (4.57), and 258 (−5.00) nm; IR (KBr) 3419, 2931, 1673, and 1114 cm^{-1}; ^{1}H and ^{13}C-NMR data, see Table 2.9; HRESIMS *m/z* 341.2090 $[M + Na]^{+}$ (calcd. for $C_{20}H_{30}O_3Na$, 341.2087).[53]

Marginol J (10): Colorless oil; $[\alpha]^{22}_{D}$ −77.5 (*c* 0.1, $CHCl_3$); UV (MeOH) λ_{max} 211, 232, and 243 nm; CD (*c* 0.1, MeOH) ($\Delta\varepsilon$) 336 (– 3.29), 270 (1.13), and 256 (−2.20) nm; IR (KBr) 2952, 1676, 1119 cm^{-1}; ^{1}H and ^{13}C-NMR data, see Table 2.10; HRESIMS *m/z* 355.2239 $[M + Na]^{+}$ (calcd. for $C_{21}H_{32}O_3Na$, 355.2244).[53]

Marginol K (11): Amorphous powder; $[\alpha]^{22}_{D}$ −27.5 (*c* 0.1, $CHCl_3$); UV (MeOH) λ_{max} 233 and 285 nm; CD (*c* 0.1, MeOH) ($\Delta\varepsilon$) 346 (−3.82), 282 (2.48), and 261 (−8.62) nm; IR (KBr) 2958, 1739, 1712, 1673, and 1152 cm^{-1}; ^{1}H and ^{13}C-NMR data, see Table 2.11; HRESIMS *m/z* 355.1881 $[M + Na]^{+}$ (calcd. for $C_{20}H_{28}O_4Na$, 355.1880).[53]

14-*Epi*-boesenberol F (12): Amorphous powder; $[\alpha]^{22}_{D}$ −22.6 (*c* 0.1, $CHCl_3$); UV (MeCN) λ_{max} 204, 208, and 212 nm; CD (*c* 0.1, MeCN) ($\Delta\varepsilon$) 218 (−3.81) nm, IR (KBr) 3331, 2925, 1460, and 1084 cm^{-1}; ^{1}H and ^{13}C-NMR data, see Table 2.13; HRESIMS *m/z* 357.2401 $[M + Na]^{+}$ (calcd. for $C_{21}H_{34}O_3Na$, 357.2400).[53]

Boesenberol F (13): An amorphous solid; ^{1}H NMR (400 MHz, $CDCl_3$) δ_H 1.03 (m, H-1α),1.66 (m, H-1β), 1.50 (m, H-2α), 1.70 (m, H-2β), 1.16 (m, H-3α), 1.40 (m, H-3β), 1.29 (d, J = 1.8 Hz, H-5α), 4.29 (t, J = 1.8 Hz, H-6α), 3.99 (br s, H-7β), 1.97 (m, H-11α), 1.97 (m, H-11β), 1.65 (m, H-12α), 1.40 (m, H-12β), 3.51 (s, H-14α), 5.74 (dd, J = 17.4, 11.0 Hz, H-15), 5.06 (dd, J = 17.4, 1.4 Hz, H-16a), 4.99 (dd, J = 11.0, 1.4 Hz, H-16b), 1.11 (s, H_3-17), 1.23 (s, H_3-18), 1.01 (s, H_3-19), 1.34 (s, H_3-20), 3.56 (s, OMe-14); δ_C 39.2 (C-1), 19.2 (C-2), 42.9 (C-3), 33.8 (C-4), 49.3 (C-5), 71.9 (C-6), 71.7 (C-7), 125.7 (C-8), 147.1 (C-9), 38.2 (C-10), 21.5 (C-11), 29.9 (C-12), 40.2 (C-13), 81.9 (C-14), 144.1 (C-15), 112.9 (C-16), 23.8 (C-17), 24.2 (C-18), 33.6 (C-19), 22.0 (C-20), 62.2 (OMe-14). The above data and those of boesenberol F in the literature are identical.[54]

Boesenberol J (14): An amorphous solid; ^{1}H NMR (400 MHz, $CDCl_3$) δ_H 1.70 (m, H-1α), 1.34 (m, H-1β), 1.55 (m, H-2α), 1.45 (m, H-2β), 1.35 (m, H-3α), 1.20 (m, H-3β), 1.78 (d, J = 1.8 Hz, H-5α), 4.30 (br s, H-6α), 2.72 (ddd, J = 14.9, 4.0, 2.7 Hz, H-7α), 2.05 (m, H-7β), 1.52 (m, H-11α), 2.04 (m, H-11β), 1.48 (m, H-12α), 1.53 (m, H-12β), 5.44 (d, J = 1.2 Hz, H-14), 5.78 (dd, J = 17.4, 10.5 Hz, H-15), 4.96 (d, J = 17.4 Hz, H-16a), 4.92 (d, J = 10.5 Hz, H-16b), 1.05 (s, H_3-17), 1.24 (s, H_3-18), 1.00 (s, H_3-19), 1.22 (s, H_3-20); ^{13}C NMR (100 MHz, $CDCl_3$) δ_C 34.3 (C-1), 18.9 (C-2), 43.6 (C-3), 34.3 (C-4), 48.0 (C-5), 68.4 (C-6), 41.9 (C-7), 134.3 (C-8), 75.0 (C-9), 42.5 (C-10), 27.2 (C-11), 32.0 (C-12), 38.1 (C-13), 134.8 (C-14), 148.1 (C-15), 110.9 (C-16), 24.3 (C-17), 24.6 (C-18), 34.0 (C-19), 22.2 (C-20). The above data and those of boesenberol J in the literature are identical.[71]

Kaemgalangol A (15): White crystals; ^{1}H NMR (400 MHz, $CDCl_3$) δ_H 2.27 (m, H-2α), 2.48 (m, H-2β), 1.56 (td, J = 13.5, 4.7 Hz, H-3α), 1.74 (qd, J = 6.6, 3.4 Hz, H-3β), 1.30 (d, J = 11.0 Hz, H-5α), 3.92 (q, J = 4.6 Hz, H-6α), 2.58 (dd, J = 13.5, 9.4 Hz, H-7α), 2.21 (dd, J = 13.5, 4.6 Hz, H-7β), 2.73 (dd, J = 10.5, 6.4 Hz, H-11α), 2.38 (m, H-11β), 1.92 (m, H-12α), 1.90 (m, H-12β), 6.42 (s, H-14), 5.78 (dd, J = 17.4, 10.5 Hz, H-15), 5.01 (dd, J = 17.4, 0.9, H-16*a*), 5.09 (dd, J = 10.5, 0.9 Hz, H-16*b*), 1.23 (s, H_3-

17), 1.10 (s, H_3-18), 0.93 (s, H_3-19), 1.20 (s, H_3-20); ^{13}C NMR (100 MHz, $CDCl_3$) δ_C 215.1 (C-1), 37.6 (C-2), 40.9 (C-3), 34.2 (C-4), 57.7 (C-5), 70.5 (C-6), 41.5 (C-7), 136.2 (C-8), 201.2 (C-9), 42.2 (C-10), 34.6 (C-11), 34.8 (C-12), 39.9 (C-13), 154.5 (C-14), 142.8 (C-15), 114.4 (C-16), 27.5 (C-17), 21.1 (C-18), 30.1 (C-19), 15.3 (C-20). The above data and those of kaemgalangol A in the literature are identical. [72]

Kaemgalangol C (16): White amorphous powder; ^{1}H NMR (400 MHz, $CDCl_3$) δ_H 3.75 (d, J = 3.2 Hz, H-1β), 1.60 (ddd, J = 14.5, 7.7, 3.3 Hz, H-2α), 1.85 (m, H-2β), 1.67 (m, H-3α), 1.13 (m, H-3β), 1.67 (m, H-5α), 4.58 (d, J = 4.6 Hz, H-6α), 2.76 (dt, J = 17.9, 1.7 Hz, H-7α), 1.97 (d, J = 18.3 Hz, H-7β), 2.12 (m, H-11α), 2.07 (m, H-11β), 1.78 (q, J = 6.6 Hz, H-12α), 1.44 (m, H-12β), 3.22 (s, H-14β), 6.03 (dd, J = 17.4, 11.0 Hz, H-15), 5.10 (dd, J = 17.4, 1.6 Hz, H-16a), 5.06 (dd, J = 11.0, 1.6 Hz, H-16b), 1.07 (s, H_3-17), 1.20 (s, H_3-18), 1.01 (s, H_3-19), 1.36 (s, H3-20), 3.48 (s, OMe-14); δ_C 73.0 (C-1), 24.6 (C-2), 35.9 (C-3), 33.8 (C-4), 46.4 (C-5), 66.0 (C-6), 40.2 (C-7), 129.5 (C-8), 136.9 (C-9), 43.1 (C-10), 20.0 (C-11), 31.3 (C-12), 40.6 (C-13), 89.0 (C-14), 143.5 (C-15), 112.7 (C-16), 24.2 (C-17), 24.0 (C-18), 33.7 (C-19), 21.7 (C-20), 62.2 (OMe-14). The above data and those of kaemgalangol C in the literature are identical.[73]

Kaempulchraol B (17): A colorless needles; ^{1}H NMR (400 MHz, $CDCl_3$) δ_H 1.01 (m, H-1α), 1.66 (dd, J = 14.4, 3.4 Hz, H-1β), 1.46 (m, H-2α), 1.66 (dd, J = 14.4, 3.4 Hz, H-2β), 1.14 (m, H-3α), 1.38 (m, H-3β), 1.14 (m, H-5α), 4.48 (d, J = 4.6 Hz, H-6α), 2.32 (m, H-7α), 2.32 (m, H-7β), 1.96 (m, H-11α), 1.96 (m, H-11β), 1.60 (m, H-12α), 1.38 (m, H-12β), 2.92 (br s, H-14α), 5.74 (dd, J = 17.4, 11.0 Hz, H-15), 4.96 (dd, J = 11.0, 1.4 Hz, H-16a), 4.92 (dd, J = 17.4, 1.4 Hz, H-16b), 1.09 (s, H_3-17), 1.22 (s, H_3-18), 0.97 (s, H_3-19), 1.35 (s, H_3-20), 3.50 (OMe-14); δ_C 39.7 (C-1), 19.2 (C-2), 43.2 (C-3), 34.2 (C-4), 53.9 (C-5), 65.9 (C-6), 40.7 (C-7), 122.7 (C-8), 141.5 (C-9), 37.4 (C-10), 21.2 (C-11), 30.4 (C-12), 40.5 (C-13), 85.2 (C-14), 144.4 (C-15), 112.2 (C-16), 23.3 (C-17), 23.8 (C-18), 33.7 (C-19), 21.4 (C-20), 61.8 (OMe-14). The above data and those of kaempulchraol B in the literature are identical.[48]

Kaempulchraol C (18): A colorless needles; ^{1}H NMR (400 MHz, $CDCl_3$) δ_H 1.15 (t, J = 3.9 Hz, H-1α), 1.64 (m, H-1β), 1.44 (m, H-2α), 1.64 (m, H-2β), 1.09 (dd, J = 16.3, 3.4 Hz, H-3α), 1.44 (m, H-3β), 1.20 (m, H-5α), 4.47 (d, J = 5.0 Hz, H-6α), 2.68 (m, H-7α), 1.93 (m, H-7β), 2.11 (m, H-11α), 1.97 (m, H-11β), 1.65 (m, H-12α), 1.45 (m, H-12β), 3.57 s, H-14β), 5.94 (dd, J = 17.4, 11.0 Hz, H-15), 5.14 (dd, J = 11.0, 1.4 Hz, H-16a), 5.10 (dd, J = 17.4, 1.4 Hz, H-16b), 1.00 (s, H_3-17), 1.18 (s, H_3-18), 0.93 (s, H_3-19), 1.34 (s, H_3-20); ^{13}C NMR (100 MHz, $CDCl_3$) δ_C 39.9 (C-1), 19.2 (C-2), 43.0 (C-3), 34.0 (C-4), 53.5 (C-5), 65.4 (C-6), 40.2 (C-7), 123.8 (C-8), 140.5 (C-9), 37.5 (C-10), 20.2 (C-11), 30.7 (C-12), 40.1 (C-13), 77.3 (C-14), 142.7 (C-15), 115.2 (C-16), 22.9 (C-17), 23.9 (C-18), 33.5 (C-19), 21.4 (C-20). The above data and those of kaempulchraol C in the literature are identical.[48]

Kaempulchraol D (19): A colorless needles; ^{1}H NMR (400 MHz, $CDCl_3$) δ_H 1.03 (m, H-1α), 1.71 (m, H-1β), 1.46 (m, H-2α), 1.72 (m, H-2β), 1.16 (m, H-3α), 1.34 (m, H-3β), 1.13 (m, H-5α), 4.48 (d, J = 4.9 Hz, H-6α), 2.26 (m, H-7α), 2.51 (m, H-7β), 2.02 (m, H-11α), 2.02 (m, H-11β), 1.46 (m, H-12α), 1.58 (m, H-12β), 3.33 (br s, H-14β), 5.72 (dd, J = 17.5, 11.2 Hz, H-15), 4.95 (dd, J = 17.5, 1.4 Hz, H-16a), 4.92 (dd, J = 11.2, 1.4 Hz, H-16b), 1.04 (s, H_3-17), 1.19 (s, H_3-18), 0.97 (s, H_3-19), 1.33 (s, H_3-20); δ_C 39.5 (C-1), 19.1 (C-2), 43.1 (C-3), 34.1 (C-4), 53.9 (C-5), 65.5 (C-6), 40.2 (C-7), 123.3 (C-8), 141.6 (C-9), 37.5 (C-10), 20.9 (C-11), 29.0 (C-12), 39.6 (C-13), 74.3 (C-14), 144.0 (C-15), 112.4 (C-16), 23.8 (C-17), 23.9 (C-18), 33.7 (C-19), 21.3 (C-20). The above data and those of kaempulchraol D in the literature are identical.[48]

Kaempulchraol E (20): A colorless oil; ^{1}H NMR (500 MHz, $CDCl_3$) δ_H 3.64 (t, J = 2.9 Hz, H-1α), 1.56 (m, H-2α), 1.93 (q, J = 2.9 Hz, H-2β), 1.70 (d, J = 3.4 Hz, H-3α), 1.14 (m, H-3β), 1.48 (t, J = 1.7 Hz, H-5α), 4.37 (d, J = 1.7 Hz, H-6α), 2.33 (t, J = 1.7 Hz, H-7α), 2.24 (dd, J = 14.3, 2.9 Hz, H-7β), 1.67 (m, H-11α), 1.62 (m, H-11β), 1.41 (m, H-12α), 1.51 (td, J = 8.3, 4.0 Hz, H-12β), 5.43 (br s, H-14), 5.78 (dd, J = 17.8, 10.3 Hz, H-15), 4.93 (dd, J = 17.8, 1.7 Hz, H-16a), 4.90 (dd, J = 10.3, 1.7 Hz, H-16b), 1.10 (s, H_3-17), 1.26 (s, H_3-18), 1.03 (s, H_3-19), 1.10 (s, H_3-20); ^{13}C NMR (100 MHz,

$CDCl_3$) δ_C 73.4 (C-1), 26.1 (C-2), 35.9 (C-3), 34.1 (C-4), 50.1 (C-5), 68.9 (C-6), 45.8 (C-7), 133.9 (C-8), 43.0 (C-9), 42.7 (C-10), 17.9 (C-11), 34.2 (C-12), 37.8 (C-13), 133.0 (C-14), 148.4 (C-15), 110.9 (C-16), 26.8 (C-17), 24.4 (C-18), 33.9 (C-19), 19.0 (C-20). The above data and those of kaempulchraol E in the literature are identical.[48]

Kaempulchraol K (21): An amorphous solid; ^{1}H NMR (400 MHz, $CDCl_3$) δ_H 1.71 (dd, *J* = 12.4, 4.1 Hz, H-1α), 1.38 (m, H-1β), 1.55 (m, H-2α), 1.55 (m, H-2β), 1.26 (dd, *J* = 12.8, 3.7 Hz, H-3α), 1.38 (m, H-3β), 2.00 (d, *J* = 3.7 Hz, H-5α), 5.36 (m, H-6α), 2.66 (dq, *J* = 15.5, 2.1 Hz, H-7α), 2.19 (dd, *J* = 15.5, 2.3 Hz, H-7β), 1.57 (m, H-11α), 2.11 (m, H-11β), 1.57 (m, H-12α), 1.51 (m, H-12β), 5.34 (d, *J* = 1.8 Hz, H-14), 5.80 (dd, *J* = 17.6, 10.8 Hz, H-15), 4.97 (dd, *J* = 17.6, 1.6 Hz, H-16a), 4.93 (dd, *J* = 10.8, 1.6 Hz, H-16b), 1.07 (s, H_3-17), 1.01 (s, H_3-18), 0.99 (s, H_3-19), 1.20 (s, H_3-20), 2.00 (s, *Me*COO-6); ^{13}C NMR (100 MHz, $CDCl_3$) δ_C 33.4 (C-1), 18.6 (C-2), 43.6 (C-3), 34.1 (C-4), 46.5 (C-5), 70.1 (C-6), 37.8 (C-7), 133.9 (C-8), 74.5 (C-9), 42.7 (C-10), 26.9 (C-11), 32.0 (C-12), 37.8 (C-13), 133.8 (C-14), 147.6 (C-15), 110.9 (C-16), 24.2 (C-17), 23.6 (C-18), 33.6 (C-19), 21.1 (C-20), 21.6 (*Me*COO-6), 170.4 (Me*C*OO-6). The above data and those of kaempulchraol K in the literature are identical.[74]

Kaempulchraol L (22): A colorless oil; ^{1}H NMR (400 MHz, $CDCl_3$) δ_H 1.82 (m, H-1α), 1.29 (m, H-1β), 1.45 (dt, *J* = 13.7, 3.4 Hz, H-2α), 1.58 (m, H-2β), 1.21 (m, H-3α), 1.29 (m, H-3β), 1.88 (m, H-5α), 4.28 (br s, H-6α), 2.44 (dd, *J* = 13.7, 2.3 Hz, H-7α), 2.02 (dd, *J* = 13.7, 2.3 Hz, H-7β), 1.66 (m, H-11α), 1.82 (m, H-11β), 1.58 (m, H-12α), 1.62 (q, *J* = 4.4 Hz, H-12β), 5.70 (br s, H-14), 5.81 (dd, *J* = 17.5, 10.3 Hz, H-15), 4.97 (dd, *J* = 17.5, 1.6 Hz, H-16a), 4.94 (dd, *J* = 10.3, 1.6 Hz, H-16b), 1.07 (s, H_3-17), 1.22 (s, H_3-18), 1.00 (s, H_3-19), 1.23 (s, H_3-20), 3.09 (s, OMe-9); ^{13}C NMR (100 MHz, $CDCl_3$) δ_C 33.8 (C-1), 19.0 (C-2), 43.7 (C-3), 34.3 (C-4), 48.2 (C-5), 68.9 (C-6), 42.6 (C-7), 132.4 (C-8), 79.5 (C-9), 44.5 (C-10), 22.3 (C-11), 34.7 (C-12), 37.6 (C-13), 138.0 (C-14), 147.7 (C-15), 111.3 (C-16), 26.9 (C-17), 22.3 (C-18), 34.1 (C-19), 24.5 (C-20), 51.0 (OMe-9). The above data are identical and those of kaempulchraol L in the literature are identical.[74]

Kaempulchraol W (23): An amorphous solid; ^{1}H NMR (400 MHz, $CDCl_3$) δ_H 1.78 (dd, *J* = 13.1, 3.9 Hz, H-1α), 1.35 (m, H-1β), 1.50 (m, H-2α), 1.61 (m, H-2β), 1.35 (m, H-3α), 1.42 (m, H-3β), 1.96 (d, *J* = 1.8 Hz, H-5α), 4.26 (br s, H-6α), 3.95 (d, *J* = 2.7 Hz, H-7α), 1.50 (m, H-11α), 2.01 (m, H-11β), 1.71 (m, H-12α), 1.50 (m, H-12β), 5.79 (d, *J* = 1.4 Hz, H-14), 5.85 (dd, *J* = 17.6, 10.8 Hz, H-15), 5.05 (dd, *J* = 17.6, 0.9 Hz, H-16a), 5.00 (dd, *J* = 10.8, 0.9 Hz, H-16b), 1.08 (s, H_3-17), 1.29 (s, H_3-18), 1.06 (s, H_3-19), 1.21 (s, H_3-20), 2.92 (s, 9-OH); ^{13}C NMR (100 MHz, $CDCl_3$) δ_C 34.4 (C-1), 18.8 (C-2), 43.8 (C-3), 34.1 (C-4), 43.1 (C-5), 72.8 (C-6), 79.5 (C-7), 134.5 (C-8), 76.5 (C-9), 42.8 (C-10), 26.8 (C-11), 31.5 (C-12), 38.4 (C-13), 140.7 (C-14), 147.5 (C-15), 111.6 (C-16), 23.7 (C-17), 25.0 (C-18), 34.0 (C-19), 21.7 (C-20). The above data and those of kaempulchraol W in the literature are identical.[75]

(5β,9β,10α,13α)-pimara-6,8(14)15-trien-18-oic acid (24): While amorphous powder; ^{1}H NMR (400 MHz, $CDCl_3$) δ_H 1.75 (d, *J* = 12.8 Hz, H-1α), 1.03 (m, H-1β), 1.53 (m, H-2α), 1.43 (m, H-2β), 2.21 (d, *J* = 13.3 Hz, H-3α), 1.11 (m, 3β), 2.17 (m, H-5β), 6.06 (dd, *J* = 10.1, 1.8 Hz, H-6), 5.98 (dd, *J* = 10.1, 2.7 Hz, H-7), 1.98 (d, *J* = 8.7 Hz, H-9β), 1.84 (m, H-11α), 1.60 (m, H-11β), 1.66 (m, H-12α), 1.43 (m, H-12β), 5.32 (s, H-14), 5.82 (dd, *J* = 17.6, 10.8 Hz, H-15), 4.96 (dd, *J* = 17.6, 1.4 Hz, H-16a), 4.90 (dd, *J* = 10.8, 1.4 Hz, H-16b), 1.07 (s, H_3-17), 1.32 (H_3-18), 0.64 (H_3-20); ^{13}C NMR (100 MHz, $CDCl_3$) δ_C 37.2 (C-1), 18.9 (C-2), 37.8 (C-3), 43.4 (C-4), 55.5 (C-5), 127.6 (C-6), 128.4 (C-7), 134.7 (C-8), 49.2 (C-9), 37.8 (C-10), 19.6 (C-11), 34.9 (C-12), 38.3 (C-13), 132.7 (C-14), 148.8 (C-15), 110.3 (C-16), 26.5 (C-17), 28.3 (C-18), 182.8 (C-19), 11.9 (C-20). The above data are identical with those of (5β,9β,10α,13α)-pimara-6,8(14)15-trien-18-oic acid in the literature.[76]

6β-acetoxysandaracopimaradien-9α-ol-1-one (25): An amorphous solid; ^{1}H NMR (400 MHz, $CDCl_3$) δ_H 2.09−2.29 (m, H-2α), 2.77 (td, *J* = 14.9, 5.0 Hz, H-2β), 2.09−2.29 (m, H-3α), 2.09−2.29 (m, H-3β), 2.48 (d, *J* = 1.7 Hz, H-5α), 5.32 (m, H-6α), 2.66 (ddd, *J* = 14.9, 3.3, 2.3 Hz, H-7α), 1.71 (m, H-7β), 2.09−2.29 (m, H-11α), 2.09−2.29 (m, H-11β), 2.09−2.29 (m, H-12α), 2.09−2.29 (m, H-12β), 5.38 (s, H-14),

5.78 (dd, *J* = 17.5, 10.6 Hz, H-15), 4.97 (dd, *J* = 17.5, 1.1 Hz, H-16a), 4.94 (dd, *J* = 10.6, 1.1 Hz, H-16b), 1.07 (s, H_3-17), 1.43 (s, H_3-18), 1.18 (s, H_3-19), 1.07 (s, H_3-20), 2.03 (s, *Me*COO-6), 2.93 (s, 9-OH); ^{13}C NMR (100 MHz, $CDCl_3$) δ_C 218.0 (C-1), 37.9 (C-2), 37.8 (C-3), 31.8 (C-4), 48.7 (C-5), 71.0 (C-6), 41.9 (C-7), 131.8 (C-8), 75.0 (C-9), 56.5 (C-10), 28.4 (C-11), 37.7 (C-12), 33.8 (C-13), 136.3 (C-14), 147.4 (C-15), 111.4 (C-16), 24.7 (C-17), 32.4 (C-18), 20.3 (C-19), 24.4 (C-20), 21.8 (*Me*COO-6), 170.4 (Me*C*OO-6). The above data and those of 6β-acetoxysandaracopimaradien-9α-ol-1-one in the literature are identical.[77]

6β-acetoxysandaracopimaradien-1α,9α-diol (26): An amorphous solid; ^{1}H NMR (400 MHz, $CDCl_3$) δ_H 4.00 (d, *J* = 2.7 Hz, H-1β), 1.80 (m, H-2α), 1.48 (m, H-2β), 2.02 (m, H-3α), 1.35 (m, H-3β), 2.40 (d, *J* = 2.3 Hz, H-5α), 5.40 (q, *J* = 2.3 Hz, H-6α), 2.73 (dq, *J* = 15.2, 2.3 Hz, H-7α), 2.12 (m, (m, H-7β), 2.16 (dq, *J* = 13.3, 3.7 Hz, H-11α), 1.80 (m, H-11β), 1.67 (td, *J* = 13.3, 3.7 Hz, H-12α), 1.48 (m, H-12β), 5.29 (br s, H-14), 5.79 (dd, *J* = 17.4, 10.5 Hz, H-15), 4.96 (dd, *J* = 17.4, 1.4 Hz, H-16a), 4.92 (dd, *J* = 10.5, 1.4 Hz, H-16b), 1.02 (s, H_3-17), 1.11 (s, H_3-18), 1.04 (s, H_3-19), 1.06 (s, H_3-20), 1.99 (s, *Me*COO-6); ^{13}C NMR (100 MHz, $CDCl_3$) δ_C 74.0 (C-1), 26.4 (C-2), 37.3 (C-3), 33.7 (C-4), 42.1 (C-5), 70.7 (C-6), 35.7 (C-7), 133.6 (C-8), 77.3 (C-9), 44.0 (C-10), 26.9 (C-11), 31.5 (C-12), 37.8 (C-13), 133.5 (C-14), 148.0 (C-15), 110.9 (C-16), 24.7 (C-17), 21.7 (C-18), 33.7 (C-19), 24.0 (C-20), 22.0 (*Me*COO-6), 170.7 (Me*C*OO-6). The above data and those of 6β-acetoxysandaracopimaradien-1α,9α-diol in the literature are identical.[77]

Sandaracopimaradien-1α,9α-diol (27): An amorphous solid; ^{1}H NMR (400 MHz, $CDCl_3$) δ_H 4.03 (m, H-1β), 1.40−1.90 (m, H-2α), 1.40−1.90 (m, H-2β), 1.40−1.90 (m, H-3α), 1.13 (m, H-3β), 2.23 (dd, *J* = 12.7, 3.1 Hz, H-5α), 1.40 − 1.90 (m, H-6α), 1.36 (m, H-6β), 2.51 (m, H-7α), 2.08 (m, H-7β), 1.40−1.90 (m, H-11α), 2.02 (dd, *J* = 14.2, 3.7 Hz, H-11β), 1.40−1.90 (m, H-12α), 1.40−1.90 (m, H-12β), 5.28 (t, *J* = 1.8 Hz, H-14), 5.80 (dd, *J* = 17.5, 10.5 Hz, H-15), 4.97 (dd, *J* = 17.5, 1.3 Hz, H-16a), 4.92 (dd, *J* = 10.5, 1.3 Hz, H-16b), 1.03 (s, H_3-17), 0.90 (s, H_3-18), 0.85 (s, H_3-19), 0.97

(s, H_3-20); ^{13}C NMR (100 MHz, $CDCl_3$) δ_C 74.0 (C-1), 26.4 (C-2), 33.9 (C-3), 32.9 (C-4), 39.8 (C-5), 22.3 (C-6), 31.2 (C-7), 136.9 (C-8), 77.5 (C-9), 43.6 (C-10), 27.0 (C-11), 31.6 (C-12), 37.8 (C-13), 131.5 (C-14), 148.5 (C-15), 110.6 (C-16), 23.7 (C-17), 33.7 (C-18), 18.7 (C-19), 22.8 (C-20). The above data and those of sandaracopimaradien-1α,9α-diol in the literature are identical.[77]

Sandaracopimaradien-6β,9α-diol-1-one (28): A white amorphous powder; ^{1}H NMR (400 MHz, $CDCl_3$) δ_H 2.17 (m, H-2α), 2.84 (m, H-2β), 1.64 (dd, J = 13.3, 3.7 Hz, H-3α), 1.74 (m, H-3β), 2.25 (d, J = 1.8 Hz, H-5α), 4.28 (d, J = 1.8 Hz, H-6α), 2.80 (m, H-7α), 2.06 (m, (m, H-7β), 2.11 (m, H-11α), 2.15 (m, H-11β), 1.41 (m, H-12α), 1.69 (m, H-12β), 5.47 (s, H-14), 5.79 (dd, J = 17.4, 10.5 Hz, H-15), 4.98 (dd, J = 17.4, 1.4 Hz, H-16a), 4.94 (dd, J = 10.5, 1.4 Hz, H-16b), 1.06 (s, H_3-17), 1.43 (s, H_3-18), 1.08 (s, H_3-19), 1.45 (s, H_3-20), 3.17 (br s, 9-OH); ^{13}C NMR (100 MHz, $CDCl_3$) δ_C 37.7 (C-1), 42.8 (C-2), 33.9 (C-3), 34.4 (C-4), 50.4 (C-5), 68.9 (C-6), 42.3 (C-7), 132.0 (C-8), 75.2 (C-9), 56.4 (C-10), 28.5 (C-11), 32.0 (C-12), 38.0 (C-13), 136.9 (C-14), 147.5 (C-15), 111.3 (C-16), 24.8 (C-17), 24.7 (C-18), 32.6 (C-19), 20.7 (C-20). The above data and those of sandaracopimaradien-6β,9α-diol-1-one in the literature are identical.[77]

Sandaracopimaradien-1α,6β,9α-triol (29): An amorphous powder; ^{1}H NMR (500 MHz, $CDCl_3$) δ_H 3.95 (d, J = 3.8 Hz, H-1β), 1.47 (d, J = 3.8 Hz, H-2α), 1.68 (td, J = 13.2, 3.8 Hz, H-2β), 1.79 (dt, J = 14.5, 3.8 Hz, H-3α), 1.39 (d, J = 14.5 Hz, H-3β), 2.21 (br s, H-5α), 4.38 (d, J = 1.5 Hz, H-6α), 2.86 (dq, J = 14.5, 1.5 Hz, H-7α), 2.13 (m, (d, J = 13.8, 3.6 Hz, H-7β), 2.03 (dd, J = 14.5, 2.3 Hz, H-11α), 1.86 (m, H-11β), 1.87 (m, H-12α), 1.49 (m, H-12β), 5.41 (br s, H-14), 5.81 (dd, J = 17.2, 10.3 Hz, H-15), 4.98 (dd, J = 17.2, 1.4 Hz, H-16a), 4.94 (dd, J = 10.3, 1.4 Hz, H-16b), 1.07 (s, H_3-17), 1.28 (s, H_3-18), 1.08 (s, H_3-19), 1.13 (s, H_3-20); ^{13}C NMR (125 MHz, $CDCl_3$) δ_C 75.8 (C-1), 26.7 (C-2), 35.6 (C-3), 34.0 (C-4), 43.3 (C-5), 68.4 (C-6), 41.5 (C-7), 133.9 (C-8), 77.6 (C-9), 43.8 (C-10), 27.1 (C-11), 31.5 (C-12), 38.0 (C-13), 134.4 (C-14), 148.2 (C-15), 110.9 (C-16), 25.3 (C-17), 22.2 (C-18), 34.0 (C-19), 24.0 (C-20). The above data and those of sandaracopimaradien-1α,6β,9α-triol in the literature are identical.[77]

Virescenol B (30): An amorphous solid; ^{1}H NMR (400 MHz, $CDCl_3$) δ_H 1.25 (dd, *J* = 12.6, 4.2 Hz, H-1α), 1.80 (dd, *J* = 13.8, 11.5 Hz, H-1β), 1.72 (qd, *J* = 8.3, 3.6 Hz, H-2α), 1.72 (qd, *J* = 8.3, 3.6 Hz, H-2β), 4.32 (d, *J* = 10.7 Hz, H-3α), 1.15 (td, *J* = 13.4, 3.8 Hz, H-5α), 1.97 (m, H-6α), 1.97 (m, H-6β), 5.33 (d, *J* = 5.4 Hz, H-7), 1.61 (br s, H-9α), 1.53 (m, H-11α), 1.32 (t, *J* = 8.4 Hz, H-11β), 1.32 (t, *J* = 8.4 Hz, H-12α), 1.45 (d, *J* = 8.4 Hz, H-12β), 1.88 (m, H-14α), 1.88 (m, H-14β), 5.77 (dd, *J* = 17.6, 10.7 Hz, H-15), 4.90 (d, *J* = 17.6 Hz, H-16a), 4.85 (d, *J* = 10.7 Hz, H-16b), 0.79 (s, H_3-17), 1.21 (s, H_3-18), 3.89 (s, H-19a), 3.44 (q, *J* = 5.4 Hz, H-19b), 0.83 (s, H_3-20); ^{13}C NMR (100 MHz, $CDCl_3$) δ_C 37.8 (C-1), 27.9 (C-2), 81.2 (C-3), 42.0 (C-4), 51.2 (C-5), 23.0 (C-6), 121.3 (C-7), 135.6 (C-8), 51.9 (C-9), 35.1 (C-10), 20.4 (C-11), 36.1 (C-12), 36.9 (C-13), 45.9 (C-14), 150.2 (C-15), 109.4 (C-16), 21.6 (C-17), 22.8 (C-18), 64.6 (C-19), 16.3 (C-20). The above data and those of virescenol B in the literature are identical.[78]

Virescenol C (31): An amorphous solid; ^{1}H NMR (400 MHz, $CDCl_3$) δ_H 1.50 (td, *J* = 5.7, 2.5 Hz, H-1α), 1.38 (m, H-1β), 2.56 (m, H-2α), 2.42 (dq, *J* = 16.4, 3.1 Hz, H-2β), 1.76 (dd, *J* = 12.2, 3.8 Hz, H-5α), 2.08 (dq, *J* = 6.6, 3.8 Hz, H-6α), 1.96 (m, H-6β), 5.38 (q, *J* = 2.5 Hz, H-7), 1.76 (dd, *J* = 12.2, 3.8 Hz, H-9α), 1.62 (m, H-11α), 1.62 (m, H-11β), 2.08 (dq, *J* = 6.6, 3.8 Hz, H-12α), 1.38 (m, H-12β), 1.96 (m, H-14α), 1.96 (m, H-14β), 5.79 (dd, *J* = 17.6, 10.7 Hz, H-15), 4.93 (dd, *J* = 17.6, 1.5 Hz, H-16a), 4.87 (dd, *J* = 10.7, 1.5 Hz, H-16b), 0.86 (s, H_3-17), 1.17 (s, H_3-18), 3.95 (d, *J* =11.5 Hz, H-19a), 3.59 (d, *J* = 11.5 Hz, H-19b), 0.97 (s, H_3-20); ^{13}C NMR (100 MHz, $CDCl_3$) δ_C 36.1 (C-1), 35.2 (C-2), 218.2 (C-3), 52.3 (C-4), 51.9 (C-5), 23.9 (C-6), 121.4 (C-7), 135.8 (C-8), 50.4 (C-9), 35.1 (C-10), 20.8 (C-11), 36.0 (C-12), 37.0 (C-13), 46.0 (C-14), 150.1 (C-15), 109.6 (C-16), 21.6 (C-17), 22.5 (C-18), 66.2 (C-19), 15.6 (C-20). The above data and those of virescenol C in the literature are identical.[79]

Conformational analyses and ECD calculations

The conformational analysis was performed in the same way as for conventional methods.[69] The molecular force field MMFF94 was applied using the Avogadro 1.2 program. The selected conformers were optimized at the B3LYP level of theory using

the 6-31G(d) basis set. Optimized geometries were calculated to minimum the energy of the structure. The geometry used for the ECD calculations was Gaussian 16 at the B3LYP/6-31G(d) level; GaussSum generated the ECD curve with a width at half maximum of 0.2 eV. All spectra of the lowest energy conformations were averaged. The final ECD spectra were compared to the CD experimental spectra.

LC-MS/MS instrumentation and chromatographic conditions

The concentrations of isolated compounds were adjusted to **9** (200 μg/mL), **10** (200 μg/mL), **11** (200 μg/mL), **15** (400 μg/mL), and each extract (10 mg/mL) using a mixture of MeOH:H_2O (80:20, v/v). Calibration curves for all compounds were prepared for concentrations ranging from 200 to 6,000 mg/L. LC-MS/MS analyses of compounds **9**–**11** and **15** and extracts were performed according to conventional methods with some modifications.[70] The LC-MS analyses were performed on a 6420 Triple Quad LC/MS spectrometer (Agilent) with a Discovery C-18 5μm column (4.6 mm × 250 mm). The compounds were separated using mobile phases A (H_2O and 0.1% HCOOH) and B (MeOH and 0.1% HCOOH) at a flow rate of 0.5 mL/min with the following gradient program: solvent B: 0–5 min, 75–80%; 5–20 min, 80–90%; 25–30 min, 90–100%. The injection volume settled at 5 μL, and the column temperature was maintained at 40 ^oC.

The MRM and ESI positive mode were performed as previous literature.[70] In detail, the precursor to product ion of each compound was: *m/z* 341 → *m/z* 136 for **9** and **11**, *m/z* 333 → *m/z* 137 for **10** and **15**. Quantifications of **9**–**11**, and **15** in the extracts was determined from retention time, precursor-to-product ions, and peak area. The content of the quantified compounds is expressed in mg/g of dry weight.

Experimental detail of chapter 3

Plant material

The *C. asiaticum* whole plants (10.0 kg) were collected from Dong Thap province, Vietnam, in May 2019, and Dr. Dang Van Son, botanist at the Institute of Tropical Biology, Vietnam identified the sample. The voucher specimens (TMPW 30719) were deposited at the Museum for Materia Medica, Analytical Research Center for Ethnomedicines, Institute of Natural Medicine, University of Toyama, Japan.

Extraction and isolation procedure

Dried powder of *C. asiaticum* (0.5 kg) was extracted with MeOH for 48 h (4 L × 3) and the solvent was evaporated under reduced pressure to obtain a methanol extract (32.8 g). The extract was triturated with water and sequentially partitioned with *n*-hexane, $CHCl_3$, and EtOAc to give 4.95, 12.8, and 3.5 g of *n*-hexane, $CHCl_3$, and EtOAc extracts, respectively. The $CHCl_3$ extract (12.8 g) was fractionated on open silica gel C.C using $CHCl_3$:MeOH (100:0 to 60:40, v/v) as solvent to yield 21 fractions (500 mL each). Similar fractions were combined based on TLC profiles to obtain, F_1 (1.50 g), F_2 (1.60 g), F_3 (1.02 g), F_4 (1.68 g), F_5 (1.25 g), F_6 (1.26 g), F_7 (1.10 g), F_8 (0.82 g), F_9 (0.41 g), F_{10} (0.68 g), and F_{11} (1.32 g). Fraction F_1 (1.50 g) was separated on an open silica gel C.C using *n*-hexane:EtOAc (95:5 to 70:30, v/v) solvent system and four subfractions, $F_{1–1}$ (146.0 mg), $F_{1–2}$ (250.0 mg), $F_{1–3}$ (580.2 mg), and $F_{1–4}$ (519.5 mg) were obtained. Open silica gel C.C of subfraction $F_{1–1}$ (146.0 mg) using the isocratic solvent system *n*-hexane:EtOAc (80:20, v/v) afforded **32** (5.9 mg) and **35** (2.4 mg). Purification of subfraction $F_{1–2}$ (250.0 mg) by open silica gel C.C eluting with *n*-hexane:EtOAc (90:10 to 70:30, v/v) gave **33** (1.8 mg) and **36** (5.6 mg). Open silica gel C.C of the fraction F_3 (1.02 g) using a gradient system of of *n*-hexane:EtOAc (80:20 to 40:60, v/v) yielded five subfractions $F_{3–1}$ (81.0 mg), $F_{3–2}$ (380.6 mg), $F_{3–3}$ (165.2 mg), $F_{3–4}$ (240.0 mg), and $F_{3–5}$ (140.8 mg). Subfraction $F_{3–2}$ (380.6 mg) was further separated on open silica gel C.C using *n*-hexane:EtOAc (70:30 to 50/50, v/v) to give **34** (6.8 mg).

(2*S*,3*R*)-7-methoxy-flavan-3-ol (32): colorless oil; $[\alpha]^{22}_{D}$ −26.5 (*c* 0.1, MeOH); UV (MeOH) λ_{max} 209, 218, and 282 (3.45) nm; IR (KBr) 3428, 2925, 2860, 1624, 1588, 1507, 1446, 1390, 1158, 1119, 1034, and 843 cm^{-1}; CD (*c* 0.1, MeOH) ($\Delta\varepsilon$) 241 (1.39), 285 (−3.14) nm; ^{1}H and ^{13}C NMR data (500 MHz, methanol-d_4), see Table 3.1; HRESIMS *m/z*: 279.0984 $[M + Na]^+$ (calcd. for $C_{16}H_{16}O_3Na$, 279.0992); ^{1}H NMR (400 MHz, DMSO-d_6) δ_H 4.82 (d, *J* = 7.4 Hz, H-2), 4.01 (ddd, *J* = 8.1, 7.4, 5.1 Hz, H-3), 2.71 (dd, *J* = 15.8, 8.1 Hz, H-4ax), 2.81 (dd, *J* = 15.8, 5.1 Hz, H-4eq), 6.99 (d, *J* = 8.3 Hz, H-5), 6.48 (dd, *J* = 8.3, 2.5 Hz, H-6), 6.41 (d, *J* = 2.5 Hz, H-8), 7.38 (m, H-2′, H-3′, H-5′, H-6′), 7.35 (m, H-4′), 3.69 (s, OMe-7); ^{13}C NMR (100 MHz, DMSO-d_6) δ_C 81.3 (C-2), 66.2 (C-3), 32.4 (C-4), 130.3 (C-5), 107.2 (C-6), 158.8 (C-7), 100.8 (C-8), 154.6 (C-9), 112.7 (C-10), 139.6 (C-1′), 127.1 (C-2′ and C-6′), 128.1 (C-3′ and C-5′), 127.8 (C-4′), 55.1 (OMe-7).[70]

(2*S*,3*R*)-7-hydroxy-flavan-3-ol (33): colorless oil; $[\alpha]^{22}_{D}$ −51.0 (*c* 0.1, MeOH); UV (MeOH) λ_{max} 207, 219, 228, and 282 nm; IR (KBr) 3436, 2926, 2848, 1627, 1512, 1457, 1159, 1390, 1119, 1029, 850, and 700 cm^{-1}; CD (*c* 0.1, MeOH) ($\Delta\varepsilon$) 233 (2.87), 282 (−3.96) nm; ^{1}H and ^{13}C NMR data (400 MHz, DMSO-d_6), see Table 3.2; HRESIMS *m/z*: 241.0867 $[M - H]^-$ (calcd. for $C_{15}H_{15}O_3$, 241.0870).[70]

(2*S*,3*R*)-2′-hydroxy-7-methoxy-flavan-3-ol (34): colorless oil; $[\alpha]^{22}_{D}$ −42.0 (*c* 0.1, MeOH); UV (MeOH) λ_{max} 208, 218, and 280 nm; IR (KBr) 3507, 3436, 2931, 1622, 1591, 1507, 1157, 1122, 1036, 947, 843, and 758 cm^{-1}; CD (*c* 0.1, MeOH) ($\Delta\varepsilon$) 236 (1.95), 278 (−2.94) nm; ^{1}H and ^{13}C NMR (400 MHz, DMSO-d_6), see Table 3.3; HRESIMS *m/z*: 271.0972 $[M - H]^-$ (calcd. for $C_{16}H_{15}O_4Na$, 271.0976).[70]

(2*S*)-4′-hydroxy-7-methoxyflavan (35): colorless crystals; ^{1}H NMR (400 MHz, Acetone-d_6) δ_H 4.97 (dd, *J* = 10.2, 2.4 Hz, H-2), 2.15 (m, H-3), 2.93 (m, H-4), 6.96 (d, *J* = 8.2 Hz, H-5), 6.43 (dd, *J* = 8.2, 2.5 Hz, H-6), 6.36 (d, *J* = 2.5 Hz, H-8), 7.28 (m, H-2′, H-6′), 6.88 (m, H-3′, H-5′), 8.36 (s, OH); ^{13}C NMR (100 MHz, Acetone-d_6) δ_C 78.4 (C-2), 25.1 (C-3), 30.8 (C-4), 130.7 (C-5), 107.8 (C-6), 160.2 (C-7), 102.3 (C-8), 156.9 (C-

9), 114.8 (C-10), 133.8 (C-1′), 128.2 (C-2′ and C-6′), 115.9 (C-3′ and C-5′), 157.9 (C-4′). The above data and those of (2*S*)-4′-hydroxy-7-methoxyflavan in the literature are identical.[80]

(2*S*)-7,4′-dihydroxyflavan (36): colorless crystals; ^{1}H NMR (500 MHz, Acetone-d_6) δ_H 4.95 (dd, J = 10.4, 2.1 Hz, H-2), 2.12 (m, H-3), 2.83 (m, H-4), 6.85 (d, J = 8.2 Hz, H-5), 6.33 (dd, J = 8.2, 2.4 Hz, H-6), 6.27 (d, J = 2.4 Hz, H-8), 7.25 (d, J = 8.5 Hz, H-2′, H-6′), 6.82 (d, J = 8.5 Hz, H-3′, H-5′); ^{13}C NMR (125 MHz, Acetone-d_6) δ_C 78.4 (C-2), 25.2 (C-3), 31.0 (C-4), 130.8 (C-5), 108.8 (C-6), 157.0 (C-7), 104.1 (C-8), 157.6 (C-9), 113.8 (C-10), 134.0 (C-1′), 128.4 (C-2′ and C-6′), 115.9 (C-3′ and C-5′), 157.9 (C-4′). The above data and those of (2*S*)-7,4′-dihydroxyflavan in the literature are identical.[80]

Quantitative analysis of *C. asiaticum* extracts

The isolated compounds **32**−**36** were prepared in MeOH:H_2O (80:20, v/v) at concentrations ranging from 0.02 to 0.80 mg/mL to obtain a five point calibration curve. The $CHCl_3$ and EtOAc extracts were then dissolved in the same solvent at a final concentration of 10 mg/mL. The each sample (5 μL) was injected on a 6420 Triple Quad LC/MS spectrometer with an Union US-C18 5 μm (4.6 × 150 mm) column. The mobile phase consisted of H_2O and MeOH, both containing 0.1% HCOOH. Parameters were set as follows: flow rate of 0.5 mL/min: 0−10 min, 60−70% MeOH; 10−30 min, 70−100% MeOH. The separation temperature was maintained at 28 °C. Detection was performed in ESI positive ion mode [drying gas (N_2) flow rate, 12 L/min; drying gas temperature, 350 °C; nebulizer, 55 psi; capillary voltage, 3,500 V; fragmentor, 135 V; collision energy, 20 eV]. MRM was applied for the quantification of **32**–**36**. The monovalent precursor and product ion pairs were *m/z* 257 and 137 for **32**, *m/z* 243 and 123 for **33**, *m/z* 273 and 131 for **34**, *m/z* 257 and 133 for **35**, and *m/z* 243 and 133 for **36**.

References

1. Marshall JS, Warrington R, Watson W, Kim HL (2018) An introduction to immunology and immunopathology. *Allergy Asthma Clin Immunol* 14: 49.
2. Libby P (2007) Inflammatory mechanisms: the molecular basis of inflammation and disease. *Nutr Rev* 65: S140–S146.
3. Calder PC (2006) Polyunsaturated fatty acids and inflammation. *Prostaglandins Leukot Essent Fatty Acids* 75: 197–202.
4. Fritsch J, Abreu MT. (2019) The microbiota and the immune response: What is the chicken and what is the egg? *Gastrointest Endosc Clin North America* 29: 381–393.
5. Waisman A, Liblau RS, Becher B. (2015) Innate and adaptive immune responses in the CNS. *Lancet Neurol* 14: 945–955.
6. Scott A, Khan KM, Roberts CR, Cook JL, Duronio V (2004) What do we mean by the term "inflammation"? A contemporary basic science update for sports medicine. *Br J Sports Med* 38: 372–380.
7. Majno G, Joris I (2014) Cells, tissues, and disease: principles of general pathology. *Oxford University Press. New York.*
8. Medzhitov R (2010) Inflammation 2010: new adventures of an old flame. *Cell* 140: 771–776.
9. Artis D, Spits H (2015) The biology of innate lymphoid cells. *Nature* 517: 293–301.
10. Kumar V, Abbas AK, Aster JC (2017) *Robbins basic pathology e-book*. Elsevier Health Sciences.
11. Freund A, Orjalo AV, Desprez PY, Campisi J (2010) Inflammatory networks during cellular senescence: causes and consequences. *Trends Mol Med* 16: 238–246.
12. Taniguchi K, Karin M (2018) NF-κB, inflammation, immunity and cancer: coming of age. *Nat Rev Immunol* 18: 309–324.
13. Jin C, Henao-Mejia J, Flavell RA (2013) Innate immune receptors: key regulators of metabolic disease progression. *Cell Metab* 17: 873–882.

14. Vasto S, Candore G, Balistreri CR, Caruso M, Colonna-Romano G, Grimaldi MP, Listi F, Nuzzo D, Lio D, Caruso C (2007) Inflammatory networks in ageing, age-related diseases and longevity. *Mech Ageing Dev* 128: 83–91.
15. Hunter P (2012) The inflammation theory of disease: The growing realization that chronic inflammation is crucial in many diseases opens new avenues for treatment. *EMBO Rep* 13: 968–970.
16. Duron J, Monconduit L, Avan P (2020) Auditory brainstem changes in timing may underlie hyperacusis in a salicylate-induced acute rat model. *Neuroscience* 426: 129–140.
17. Gupta R, Saxena R, Malviya N (2019) Investigation of anti-inflammatory activity of ethanolic extract of *Aconitum napellus* Linn against carrageenan induced paw edema in rats. *J Drug Deliv Ther* 9: 470–472.
18. Haley RM, von Recum HA (2019) Localized and targeted delivery of NSAIDs for treatment of inflammation: A review. *Exp Biol Med* 244: 433–444.
19. Rifai Y, Wahyuni S, Yulianty R, Yusrini Y (2019) Gastroulcerogenic evaluation of ibuprofen ester conjugates. *J Phys Conf Ser.* IOP Publishing 1341: 072007.
20. Satani N, Giridhar K, Cai C, Wewior N, Norris DD, Olson SD, Aronowski J, Savitz SI (2019) Aspirin in stroke patients modifies the immunomodulatory interactions of marrow stromal cells and monocytes. *Brain Res* 1720: 146298.
21. Lucas S (2016). The pharmacology of indomethacin. *Headache: J Head Face Pain* 56: 436–446.
22. Lundgren M, Steed LJ, Tamura R, Jonsdottir B, Gesualdo P, Crouch C, Sjöberg M, Hansson G, Hagopian WA, Ziegler AG, Rewers MJ (2017) Analgesic antipyretic use among young children in the TEDDY study: no association with islet autoimmunity. *BMC Pediatr* 17: 127.
23. Sullivan JE, Farrar HC (2011) Section on clinical pharmacology and therapeutics, committee on drugs: Fever and antipyretic use in children. *Pediatrics* 127: 580–587.
24. Bensman A (2020) Non-steroidal anti-inflammatory drugs (NSAIDs) systemic use: The risk of renal failure. *Front Pediatr* 7: 517.
25. Bradley M (2020) Reducing the risk of NSAID related gastrointestinal problems: an update. *Drug Ther Bull* 58: 89–92.

26. Gosavi TP, Ghosh P, Kandhare AD, Bodhankar SL (2011) Unwrapping homeopathic principles in the wake of research: serendipity, placebo or true therapeutic milestones. *Pharmacologyonline* 1: 894–906.
27. Shah AS, Alagawadi KR (2011) Anti-inflammatory, analgesic and antipyretic properties of *Thespesia populnea* Soland ex. Correa seed extracts and its fractions in animal models. *J Ethnopharmacol* 137:1504–1509.
28. Tambewagh UU, Kandhare AD, Honmore VS, Kadam PP, Khedkar VM, Bodhankar SL., Rojatkar SR (2017) Anti-inflammatory and antioxidant potential of guaianolide isolated from *Cyathocline purpurea*: Role of COX-2 inhibition. *Int Immunopharmacol* 52: 110–118.
29. Klessig DF, Tian M, Choi HW (2016) Multiple targets of salicylic acid and its derivatives in plants and animals. *Front Immunol* 7: 206.
30. Patidar A, Birla D, Patel V, Chaturvedi M, Manocha N (2014) A review on advantages of natural analgesics over conventional synthetic analgesics. *Int J Pharm Life Sci* 5:3534−3539.
31. Kocaadam B, Şanlier N (2017) Curcumin, an active component of turmeric (*Curcuma longa*), and its effects on health. *Crit Rev Food Sci Nutr* 57: 2889–2895.
32. Wu S, Pang Y, He Y, Zhang X., Peng L, Guo J, Zeng J (2021) A comprehensive review of natural products against atopic dermatitis: Flavonoids, alkaloids, terpenes, glycosides and other compounds. *Biomed Pharmacother* 140: 111741.
33. Castrillo A, De las Heras B, Hortelano S, Rodrıguez B, Villar A, Boscá L (2001) Inhibition of the nuclear factor κB (NF-κB) pathway by tetracyclic kaurene diterpenes in macrophages: specific effects on NF-κB-inducing kinase activity and on the coordinate activation of ERK and p38 MAPK. *J Biol Chem* 276: 15854–15860.
34. Bravo F, Sierra-de-Grado R, Van Sam H (2022) Global biodiversity-related conventions on facilitating biodiversity conservation in Vietnam. *For Soc* 6: 489–502.
35. Trieu VH, Pham TT, Dao TL (2020) Vietnam Forestry Development Strategy: Implementation results for 2006–2020 and recommendations for the 2021–2030 strategy. *CIFOR* 213.

36. Kurian J (2012) Ethno-medicinal plants of India, Thailand and Vietnam. *J Biodiver* 3: 61–75.
37. Organization WH (1990) Medicinal Plants in Viet Nam. *WHO Regional Office for the Western Pacific.*
38. Chokchaisiri R, Chaichompoo W, Chunglok W, Cheenpracha S, Ganranoo L, Phutthawong N, Bureekaew S, Suksamrarn A (2019) Isopimarane diterpenoids from the rhizomes of *Kaempferia marginata* and their potential anti-inflammatory activities. *J Nat Prod* 83: 14–19.
39. Kaewkroek K, Wattanapiromsakul C, Matsuda H, Nakamura S, Tewtrakul S (2017) Anti-inflammatory activity of compounds from *Kaempferia marginata* rhizomes. *Songklanakarin J Sci Technol* 39: 91–99.
40. Nguyen HT, Nguyen DD (2017) *Kaempferia marginata* Carey ex Roscoe (Zingiberaceae)-A new record of medicinal plant species for Vietnam. *J Med Materials* 22: 322–324.
41. Picheansoonthon C, Koonterm S (2008) Notes on the genus *Kaempferia* L. (Zingiberaceae) in Thailand. *J Thai Tradit Altern Med* 6: 73–79.
42. Pham NK, Nguyen HT, Nguyen QB (2021) A review on the ethnomedicinal uses, phytochemistry and pharmacology of plant species belonging to *Kaempferia* L. genus (Zingiberaceae). *Pharm Sci Asia* 48: 1–24.
43. Kaewkroek K, Wattanapiromsakul C, Kongsaeree P, Tewtrakul S (2013) Nitric oxide and tumor necrosis factor-alpha inhibitory substances from the rhizomes of *Kaempferia marginata*. *Nat Prod Commun* 8: 1934578X1300800904.
44. Jingguang Y, Donglei Y, Lan S, Shu Z, Caicheng Z, Yuheng C (2001) The chemical constituents of diterpenoids from *Kaempferia marginata* Carey. *J Chin Pharm Sci* 10: 61–64.
45. Thongnest S, Mahidol C, Sutthivaiyakit S, Ruchirawat S (2005) Oxygenated pimarane diterpenes from *Kaempferia marginata*. *J Nat Prod* 68: 1632–1636.
46. Luger P, Weber M, Dung N, Tuyet N (1996) Ethyl *p*-methoxycinnamate from *Kaempferia galanga* L. in Vietnam. *Acta Crystallographica Section C: Crystal Structure Communications* 52: 1255–1257.

47. Zidorn C, Horak S, Weavers RT, Ellmerer EP, Stuppner H, Klink VJW (2006) Diterpenoids and phenolics from *Pseudopanax simplex*. *J Serb Chem Soc* 71: 121–125.
48. Win NN, Ito T, Aimaiti S, Imagawa H, Ngwe H, Abe I, Morita H (2015) Kaempulchraols A–H, diterpenoids from the rhizomes of *Kaempferia pulchra* collected in Myanmar. *J Nat Prod* 78: 1113–1118.
49. Evidente A, Sparapano L, Bruno G, Motta A (2002) Sphaeropsidins D and E, two other pimarane diterpenes, produced in vitro by the plant pathogenic fungus *Sphaeropsis sapinea* f. sp. *cupressi*. *Phytochemistry* 59: 817–823.
50. Jiang K, Chen LL, Wang SF, Wang Y, Li Y, Gao K (2015) Anti-inflammatory terpenoids from the leaves and twigs of *Dysoxylum gotadhora*. *J Nat Prod* 78: 1037–1044.
51. Ding LF, Peng LY, Zhou HF, Song LD, Wu XD, Zhao QS (2020) Artemilavanolides A and B, two sesquiterpenoids with a 6-oxabicyclo [3.2.1] octane scaffold from *Artemisia lavandulaefolia*. *Tetrahedron Lett* 61: 151872.
52. Do KM, Kodama T, Shin, MK, Ton Nu LH, Nguyen HM, Dang SV, Shiokawa K, Hayakawa Y, Morita H (2022) Marginols A–H, unprecedented pimarane diterpenoids from *Kaempferia marginata* and their NO inhibitory activities. *Phytochemistry* 196: 113109.
53. Do KM, Kodama T, Nguyen HM, Ikumi N, Soeda C, Shiokawa K, Morita H (2023) Seco-and isopimarane diterpenoids from *Kaempferia marginata* rhizomes and their NO inhibition activities. *Phytochemistry* 205: 113510.
54. Karmakar UK, Ishikawa N, Arai MA, Ahmed F, Koyano T, Kowithayakorn T, Ishibashi M (2016) Boesenberols, pimarane diterpenes with TRAIL-resistance-overcoming activity from *Boesenbergia pandurata*. *J Nat Prod* 79: 2075–2082.
55. El-Desoky AHH, Inada N, Maeyama Y, Kato H, Hitora Y, Sebe M, Nagaki M, Kai A, Eguchi K, Iznazumi T, Sugimoto Y, Frisvad JC, William RM, Tsukamoto S (2021) Taichunins E-T, isopimarane diterpenes and a 20-*nor*-isopimarane, from *Aspergillus taichugensis* (IBT 194004): structures and inhibitory effects on RANKL-induced formation of multinuclear osteoclasts. *J Nat Prod* 84: 2475–2485.
56. Ji Z, Meerow A (2000) Amaryllidaceae. *Flora of China* 24: 264–273.

57. Tram NTN, Khanh TC (2012) *Crinum latifolium* L. var. crilae Tram & Khanh, var. *n*. A new variety of the species *Crinum latifolium* L. (Amaryllidaceae) in Vietnam. *Acad J Biol* 34: 190–193.
58. Van Dyk S, Griffiths S, Van Zyl RL, Malan SF (2009) The importance of including toxicity assays when screening plant extracts for antimalarial activity. *Afr J Biotechnol* 8: 5595–5601.
59. Adesanya S, Olugbade T, Odebiyl O, Aladesanmi J (1992) Antibacterial alkaloids in *Crinum jagus*. *Int J Pharmacogn* 30: 303–307.
60. Gabrielsen B, Monath TP, Huggins JW, Kefauver DF, Pettit GR, Groszek G, Hollingshead M, Kirsi JJ, Shannon WM, Schubert EM (1992) Antiviral (RNA) activity of selected Amaryllidaceae isoquinoline constituents and synthesis of related substances. *J Nat Prod* 55: 1569–1581.
61. Likhitwitayawuid K, Angerhofer CK, Chai H, Pezzuto JM, Cordell GA, Ruangrungsi N (1993) Cytotoxic and antimalarial alkaloids from the bulbs of *Crinum amabile*. *J Nat Prod* 56: 1331–1338.
62. Antoun MD, Mendoza NT, Ríos YR, Proctor GR, Wickramaratne DM, Pezzuto JM, Kinghorn AD (1993) Cytotoxicity of *Hymenocallis expansa* alkaloids. *J Nat Prod* 56: 1423–1425.
63. Zhan G, Zhou J, Liu T, Zheng G, Aisa HA, Yao G (2016) Flavans with potential anti-inflammatory activities from *Zephyranthes candida*. *Bioorg Med Chem Lett* 26: 5967–5970.
64. Ramadan M, Kamel M, Ohtani K, Kasai R, Yamasaki K (2000) Minor phenolics from *Crinum bulbispermum* bulbs. *Phytochemistry* 54: 891–896.
65. Jitsuno M, Yokosuka A, Sakagami H, Mimaki Y (2009) Chemical constituents of the bulbs of *Habranthus brachyandrus* and their cytotoxic activities. *Chem Pharm Bull* 57: 1153–1157.
66. Friedrich W, Galensa R (2002) Identification of a new flavanol glucoside from barley (*Hordeum vulgare* L.) and malt. *Eur Food Res Technol* 214: 388–393.
67. Mosmann T (1983) Rapid colorimetric assay for cellular growth and survival: application to proliferation and cytotoxicity assays. *J Immunol Methods* 65: 55–63.
68. Dirsch VM, Stuppner H, Vollmar AM (1998) The Griess assay: suitable for a bio-guided fractionation of anti-inflammatory plant extracts? *Planta Med* 64: 423–426.

69. Hoang NN, Kodama T, Win NN, Do KM, Abe I, Morita H (2021) A new monoterpene from the rhizomes of *Alpinia galanga* and its anti-Vpr activity. *Chem Biodivers* 18: e2100401.
70. Do KM, Shin MK, Kodama T, Win NN, Prema, Nguyen HM, Hayakawa Y, Morita H (2022) Flavanols and flavanes from *Crinum asiaticum* and their effects on LPS signaling pathway through the inhibition of NF-κB activation. *Planta Med* 88: 913–920.
71. Karmakar UK, Arai MA, Koyano T, Kowithayakorn T, Ishibashi M (2017) Boesenberols I–K, new isopimarane diterpenes from *Boesenbergia pandurata* with TRAIL-resistance overcoming activity. *Tetrahedron Lett* 58: 3838–3841.
72. Swapana N, Tominaga T, Elshamy AI, Ibrahim MA, Hegazy MEF, Singh CB, Suenaga M, Imagawa H, Noji M, Umeyama A (2018) Kaemgalangol A: Unusual seco-isopimarane diterpenoid from aromatic ginger *Kaempferia galanga. Fitoterapia* 129: 47–53.
73. Elshamy AI, Mohamed TA, Swapana N, Yoneyama T, Noji M, Efferth T, Hegazy MEF, Umeyama A (2020) Cytotoxic polyoxygenated isopimarane diterpenoids from the edible rhizomes of *Kaempferia galanga* (kencur). *Ind Crops Prod* 158: 112965.
74. Win NN, Ito T, Aimaiti S, Kodama T, Imagawa H, Ngwe H, Asakawa Y, Abe I, Morita H (2015) Kaempulchraols I–O: new isopimarane diterpenoids from *Kaempferia pulchra* rhizomes collected in Myanmar and their antiproliferative activity. *Tetrahedron* 71: 4707–4713.
75. Win NN, Ito T, Matsui T, Aimaiti S, Kodama T, Ngwe H, Okamoto Y, Tanaka M, Asakawa Y, Abe I, Morita H (2016) Isopimarane diterpenoids from *Kaempferia pulchra* rhizomes collected in Myanmar and their Vpr inhibitory activity. *Bioorg Med Chem Lett* 26: 1789–1793.
76. Yang CT, Hou SQ, Tian K, Hu QF, Huang XZ, Jiang ZY (2016) New *ent*-pimarane diterpenes from the roots of *Aralia dumetorum*. *Helv Chim Acta* 99: 220–224.
77. Prawat U, Tuntiwachwuttikul P, Taylor WC, Engelhardt LM, Skelton B, White A (1993) Diterpenes from a *Kaempferia* species. *Phytochemistry* 32: 991–997.

78. Polonsky J, Baskevitch Z, Bellavita NC, Ceccherelli P (1968) The structures of virescenol A and B, metabolites of *Oospora virescens* (Link) Wallr. *Chem Comm* 22: 1404–1405.
79. Cagnoli-Bellavita N, Ceccherelli P, Mariani R, Polonsky J, Baskevitch Z (1970) Structure of virescenoside C, a new metabolite of *Oospora virescens* (Link) Wallr. *Eur J Biochem* 15: 356–359.
80. Achenbach H, Stöcker M, Constenla MA (1988) Flavonoid and other constituents of *Bauhinia manca*. *Phytochemistry* 27: 1835–1841.

List of publications

This doctoral thesis summarizes the full contents of the following publications.

1) Do KM, Kodama T, Shin MK, Ton Nu LH, Nguyen HM, Dang SV, Shiokawa K, Hayakawa Y, Morita H (2022) Marginols A–H, unprecedented pimarane diterpenoids from *Kaempferia marginata* and their NO inhibitory activities. *Phytochemistry* 196: 113109.

2) Do KM, Kodama T, Nguyen HM, Ikumi N, Soeda C, Shiokawa K, Morita H (2022) Seco-and isopimarane diterpenoids from *Kaempferia marginata* rhizomes and their NO inhibition activities. *Phytochemistry* 205: 113510.

3) Do KM, Shin MK, Kodama T, Win NN, Prema, Nguyen HM, Hayakawa Y, Morita H (2022) Flavanols and flavanes from *Crinum asiaticum* and their effects on LPS signaling pathway through the inhibition of NF-κB activation. *Planta Med* 88: 913–920.

Acknowledgements

I would like to express my deepest gratitude to my supervisor Professor Dr. Hiroyuki Morita, Division of Natural Products Chemistry, Institute of Natural Medicine, University of Toyama, Japan, for his valuable instruction, guidance, suggestion, and encouragements on my research to achieve my PhD degree.

I would like to express my sincere appreciation to Prof. Dr Yoshihiro Hayakawa, Institute of Natural Medicine, University of Toyama, Japan, for the assistant of biological activity.

I would like to acknowledge my sincere thanks to Ministry of Education, Culture, Sports, Science, and Technology (MEXT) Japan for the scholarship grant and financial support.

I am greatly indebted to Assistant Prof. Takeshi Kodama, Division of Natural Products Chemistry, Institute of Natural Medicine, University of Toyama, Japan, for his precious suggestions, patient guidance, and comments throughout this study.

I am also extremely grateful to Assistant Prof. Yu Nakashima, Division of Natural Products Chemistry, Institute of Natural Medicine, University of Toyama, Japan, for his helpful advice, constant encouragement, and kindness during my research work.

I would like to thanks to Dr. Min-Kyoung Shin, Institute of Natural Medicine, University of Toyama, Japan, for the assistant of biological activity. My thanks are extended to teacher, Ken-ichi Shiokawa (Japan Preventive Medical Laboratory Company, Japan), Notaka Ikumi (AFC-HD AMS Life Science, Japan), and Chigusa Soeda (Japan Preventive Medical Laboratory Company, Japan), for their great support during my research time.

I would like to thanks to my beloved teacher, Dr. Lien Huong Ton Nu (Can Tho University, Vietnam), Dr. Son Van Dang (Institute of Tropical Biology, Vietnam Academy of Science and Technology, Vietnam), for their supports, sample collection and identification. My thanks are extended to Dr. Hien Minh Nguyen, Faculty of Pharmacy, Ton Duc Thang University, Vietnam.

I extend my special thanks to all members in Division of Natural Products Chemistry for their support and friendship during my course in the University of Toyama, Japan.

Last but not least, I am greatly indebted to my family for their love, understanding, support, and encouragement throughout the whole of my life.

Kiep Minh Do

Toyama, Japan

Supplementary data

List of Supporting Information

Table S1. Viability of RAW264.7 cells treated with the different extracts during LPS-induced NO production

Extracts	% Cell survival				
	6.25 (μg/mL)	12.5 (μg/mL)	25 (μg/mL)	50 (μg/mL)	100 (μg/mL)
B. pandurata					
MeOH	75.26 ± 1.00	67.75 ± 2.15	66.04 ± 0.70	65.15 ± 2.15	48.31 ± 0.94
EtOAc	74.02 ± 2.80	78.51 ± 2.22	75.42 ± 0.96	69.20 ± 2.03	23.29 ± 1.43
$CHCl_3$	82.53 ± 1.00	68.06 ± 3.03	44.03 ± 3.72	8.27 ± 0.10	4.09 ± 0.14
n-Hexane	77.28 ± 2.54	68.79 ± 0.86	31.62 ± 0.86	5.82 ± 0.49	3.27 ± 0.05
C. asiaticum					
MeOH	146.15 ± 1.30	127.35 ± 0.46	118.07 ± 3.34	106.76 ± 2.22	73.98 ± 1.66
EtOAc	108.38 ± 5.49	106.85 ± 3.00	109.58 ± 5.27	101.05 ± 3.08	47.57 ± 0.38
$CHCl_3$	148.49 ± 4.46	123.89 ± 5.75	113.28 ± 3.04	112.67 ± 1.97	64.60 ± 3.41
n-Hexane	88.51 ± 3.97	71.90 ± 1.74	63.81 ± 0.76	60.85 ± 1.31	23.78 ± 1.73
C. sahuynhensis					
MeOH	79.01 ± 2.68	76.20 ± 3.28	89.36 ± 3.94	102.96 ± 1.91	84.72 ± 1.75
EtOAc	76.82 ± 1.81	81.49 ± 0.32	81.97 ± 2.19	101.94 ± 1.52	119.45 ± 3.13
$CHCl_3$	68.02 ± 0.65	68.91 ± 1.79	87.00 ± 4.03	100.12 ± 4.65	12.02 ± 0.20
n-Hexane	83.41 ± 0.68	87.60 ± 3.92	91.47 ± 0.87	106.32 ± 0.92	120.15 ± 2.94
G. pendula					
MeOH	57.25 ± 0.93	55.34 ± 4.60	60.22 ± 2.01	68.00 ± 4.48	73.87 ± 2.05
EtOAc	53.09 ± 4.16	65.50 ± 4.08	66.71 ± 2.52	78.42 ± 4.27	110.80 ± 4.75
$CHCl_3$	72.22 ± 3.68	69.42 ± 2.38	76.66 ± 2.21	94.39 ± 0.91	114.43 ± 2.07
n-Hexane	72.99 ± 1.81	71.13 ± 1.80	78.18 ± 2.49	95.19 ± 4.89	31.74 ± 0.81
K. champasakensis					
MeOH	78.52 ± 1.98	74.78 ± 1.96	55.65 ± 1.69	5.56 ± 0.18	3.82 ± 0.19
EtOAc	67.64 ± 0.47	70.18 ± 3.07	72.46 ± 3.65	75.81 ± 2.90	39.53 ± 2.90
$CHCl_3$	81.51 ± 1.88	75.30 ± 0.79	68.14 ± 0.32	15.66 ± 0.44	10.09 ± 0.63
n-Hexane	70.85 ± 4.50	59.27 ± 4.10	12.74 ± 0.84	3.94 ± 0.18	3.14 ± 0.36
K. marginata					
MeOH	76.72 ± 3.21	74.81 ± 0.46	73.89 ± 2.47	68.04 ± 2.42	21.48 ± 0.19
EtOAc	83.21 ± 3.00	84.62 ± 2.30	89.76 ± 2.35	95.91 ± 4.71	102.49 ± 1.91
$CHCl_3$	97.62 ± 1.56	90.48 ± 1.42	88.06 ± 0.16	83.29 ± 1.21	44.35 ± 0.86
n-Hexane	108.71 ± 0.94	96.56 ± 2.26	94.90 ± 2.88	74.17 ± 1.17	72.40 ± 1.71

The data are presented as mean value ± SD for n = 3

Table S2. Identification and qualification of **9**–**11**, and **15** from extracts of *K. marginata* rhizomes

Compounds	Qualification (mg/g extract ± SD)				
	Parent ion	MS/MS	*n*-Hexane	$CHCl_3$	EtOAc
9	341[a]	136	6.63 ± 0.04	0.12 ± 0.01	0.11 ± 0.01
10	333[b]	137	0.78 ± 0.02	0.08 ± 0.01	0.29 ± 0.01
11	341[a]	147	6.78 ± 0.10	0.89 ± 0.04	0.27 ± 0.04
15	333[b]	137	3.50 ± 0.13	5.38 ± 0.10	4.15 ± 0.08

[a] Parent ion: $[M + Na]^+$. [b] Parent ion: $[M + H]^+$. SD: standard deviation. NT: not detect.

Table S3. Viability of RAW264.7 cells treated with the isolated compounds **1**–**31** of *K. marginata* rhizomes during LPS-induced NO production

Compounds	% Cell survival				
	6.25 (μM)	12.5 (μM)	25 (μM)	50 (μM)	100 (μM)
1	92.27 ± 0.89	79.88 ± 2.95	25.97 ± 1.26	12.73 ± 0.40	4.43 ± 0.03
2	95.34 ± 0.49	98.05 ± 1.56	98.26 ± 1.67	99.68 ± 2.20	104.66 ± 1.30
3	101.77 ± 4.37	91.26 ± 1.67	90.62 ± 2.54	73.52 ± 0.42	40.81 ± 1.51
4	92.71 ± 0.84	99.42 ± 2.95	98.53 ± 2.09	98.99 ± 2.16	104.88 ± 2.71
6	96.15 ± 3.47	96.89 ± 4.04	99.51 ± 0.93	101.99 ± 2.64	103.94 ± 3.40
7	95.59 ± 2.71	96.60 ± 1.99	97.94 ± 4.03	101.46 ± 2.41	104.06 ± 1.61
8	97.60 ± 0.37	97.86 ± 0.27	93.86 ± 2.41	86.65 ± 4.15	29.09 ± 1.75
9	101.53 ± 3.12	103.34 ± 3.25	109.04 ± 2.11	117.16 ± 2.87	117.26 ± 2.09
10	88.97 ± 2.31	88.50 ± 2.94	90.07 ± 3.82	97.01 ± 2.87	84.35 ± 1.30
11	94.00 ± 0.96	93.74 ± 3.92	99.76 ± 4.14	113.37 ± 2.34	116.05 ± 4.17
12	101.87 ± 2.16	107.75 ± 6.99	107.78 ± 1.59	115.18 ± 2.95	116.33 ± 3.34
13	79.43 ± 2.90	69.56 ± 4.62	62.49 ± 2.39	46.86 ± 0.77	18.40 ± 0.34
14	111.55 ± 0.89	97.52 ± 1.94	92.17 ± 1.29	91.36 ± 4.59	23.15 ± 4.82
15	102.98 ± 5.40	108.03 ± 1.16	107.07 ± 3.51	113.59 ± 3.00	114.48 ± 1.34
16	92.40 ± 0.83	95.40 ± 1.72	95.67 ± 2.98	95.98 ± 1.44	100.38 ± 0.55
17	113.04 ± 0.74	110.21 ± 3.60	102.63 ± 0.75	97.33 ± 1.26	12.77 ± 0.34
18	100.46 ± 0.49	100.59 ± 0.88	98.98 ± 2.50	92.06 ± 2.31	7.32 ± 0.05
19	112.53 ± 2.69	108.85 ± 0.36	105.60 ± 8.09	23.60 ± 3.43	6.14 ± 0.05
20	98.05 ± 4.29	98.05 ± 4.29	95.32 ± 1.35	95.19 ± 1.26	92.15 ± 1.07
21	99.15 ± 5.16	95.84 ± 1.60	95.32 ± 1.35	95.19 ± 1.26	92.15 ± 1.07
22	105.64 ± 3.04	106.28 ± 3.69	103.87 ± 3.91	98.13 ± 2.50	23.62 ± 0.21
23	103.55 ± 1.52	103.28 ± 0.96	99.98 ± 5.49	76.09 ± 2.57	17.32 ± 0.59
24	99.48 ± 2.49	98.91 ± 2.04	83.15 ± 1.69	73.42 ± 1.27	31.58 ± 5.22
25	103.60 ± 3.00	98.50 ± 0.89	97.78 ± 2.00	93.42 ± 3.77	70.86 ± 3.40
26	94.54 ± 1.96	91.62 ± 3.55	92.49 ± 2.28	45.75 ± 3.44	20.08 ± 1.25
27	82.80 ± 2.36	82.29 ± 2.03	86.97 ± 2.86	95.55 ± 0.30	104.60 ± 2.25
28	88.54 ± 2.60	89.98 ± 0.85	90.98 ± 0.98	91.74 ± 1.65	94.38 ± 0.54
29	99.48 ± 2.49	98.91 ± 2.04	83.15 ± 1.69	73.42 ± 1.27	31.58 ± 5.22
30	97.01 ± 1.07	91.84 ± 3.05	71.80 ± 0.47	24.68 ± 0.77	9.85 ± 1.24
31	96.14 ± 3.45	88.86 ± 1.16	52.86 ± 0.87	13.17 ± 0.18	4.77 ± 0.20
L-*N*MMA	104.88 ± 2.89	114.35 ± 1.43	118.27 ± 2.20	126.11 ± 0.25	135.79 ± 2.01

The data are presented as mean value ± SD for n = 3

Table S4. Contents of the isolated compounds **32**–**36** in $CHCl_3$ and EtOAc extracts of *C. asiaticum*

Compounds	Concentration of the isolated compounds (mg/g dry plant material weight ± SD)	
	$CHCl_3$	EtOAc
32	1.23 ± 0.01	< LOQ
33	1.01 ± 0.07	< LOQ
34	0.85 ± 0.02	ND
35	1.44 ± 0.01	ND
36	1.09 ± 0.01	ND

LOQ: Limit of quantitation. ND: Not detect. SD: Standard deviation

Table S5. Viability of RAW264.7 cells treated with the isolated compounds **32**, and **34**–**36** of *C. asisticum* during LPS-induced NO production

Compounds	% Cell survival				
	3.13 (μM)	6.25 (μM)	12.5 (μM)	25 (μM)	50 (μM)
32	82.00 ± 1.76	78.54 ± 5.62	76.39 ± 5.12	71.85 ± 0.29	8.78 ± 0.44
34	84.05 ± 1.34	80.24 ± 3.50	76.67 ± 5.90	69.62 ± 5.10	11.00 ± 1.80
35	103.41 ± 6.80	87.89 ± 3.93	85.14 ± 6.35	72.50 ± 3.88	12.41 ± 2.52
36	73.00 ± 1.72	72.23 ± 0.56	69.62 ± 2.63	57.16 ± 1.76	10.38 ± 2.34
L-*N*MMA	77.58 ± 5.38	85.40 ± 3.70	87.00 ± 4.65	89.82 ± 3.54	101.80 ± 6.80

The data are presented as mean value ± SD for n = 3

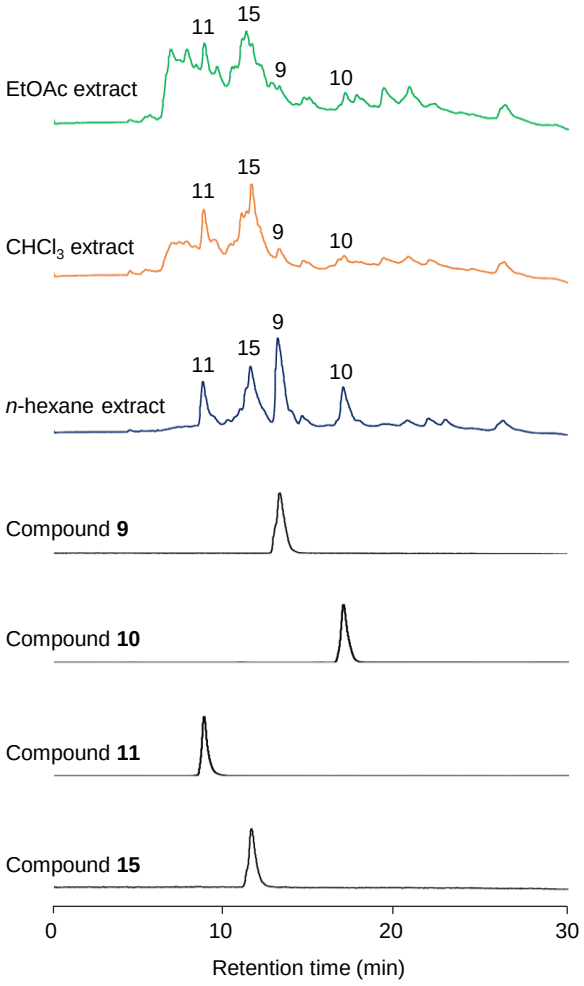

Figure S1. LC-MS total ion chromatograms of **9**–**11**, and **15**, and *n*-hexane, $CHCl_3$, and EtOAc extracts

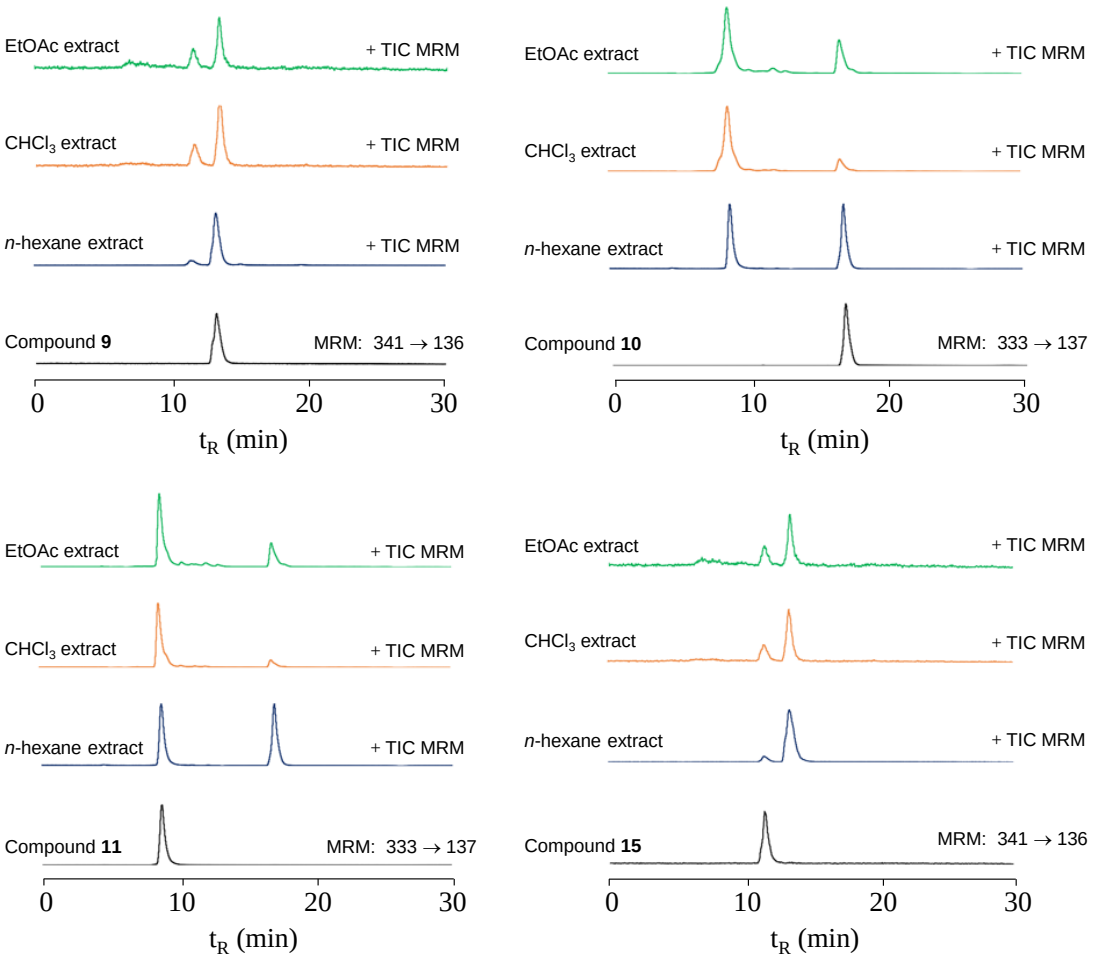

Figure S2. MRM chromatograms of **9**–**11**, and **15**, and *n*-hexane, $CHCl_3$, and EtOAc extracts corresponding to precursor-to-product ion transition

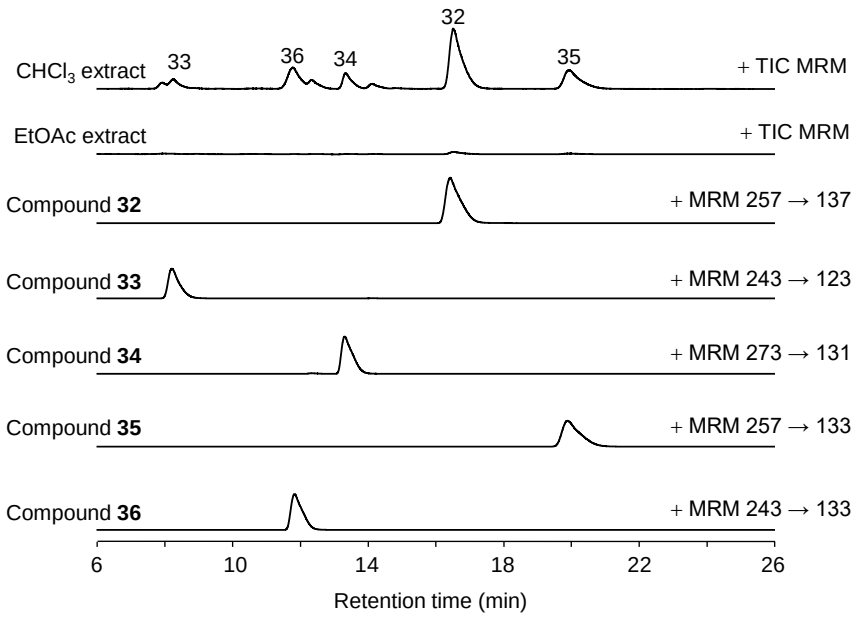

Figure S3. Chromatogram of MRM transitions of $CHCl_3$, EtOAc extracts, and compounds **32**–**36**

Figure S4. ^{1}H NMR spectrum (pyridine-d_5, 400 MHz) of **1**

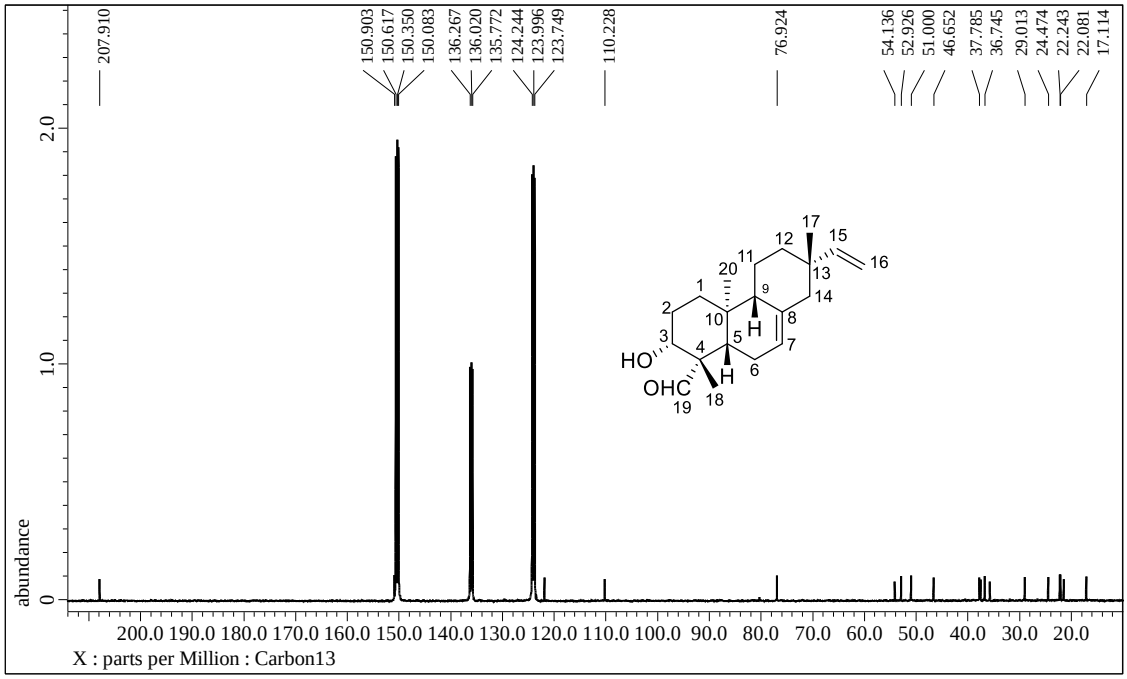

Figure S5. ^{13}C NMR spectrum (pyridine-d_5, 100 MHz) of **1**

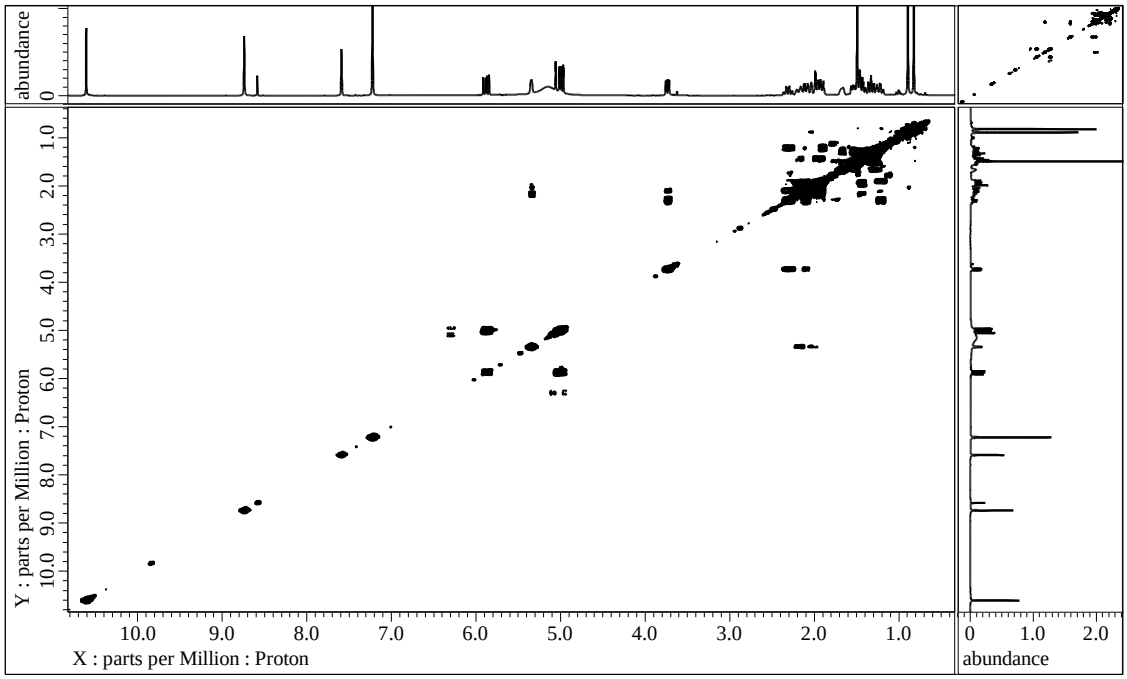

Figure S6. ^{1}H–^{1}H COSY spectrum of **1** in pyridine-d_5

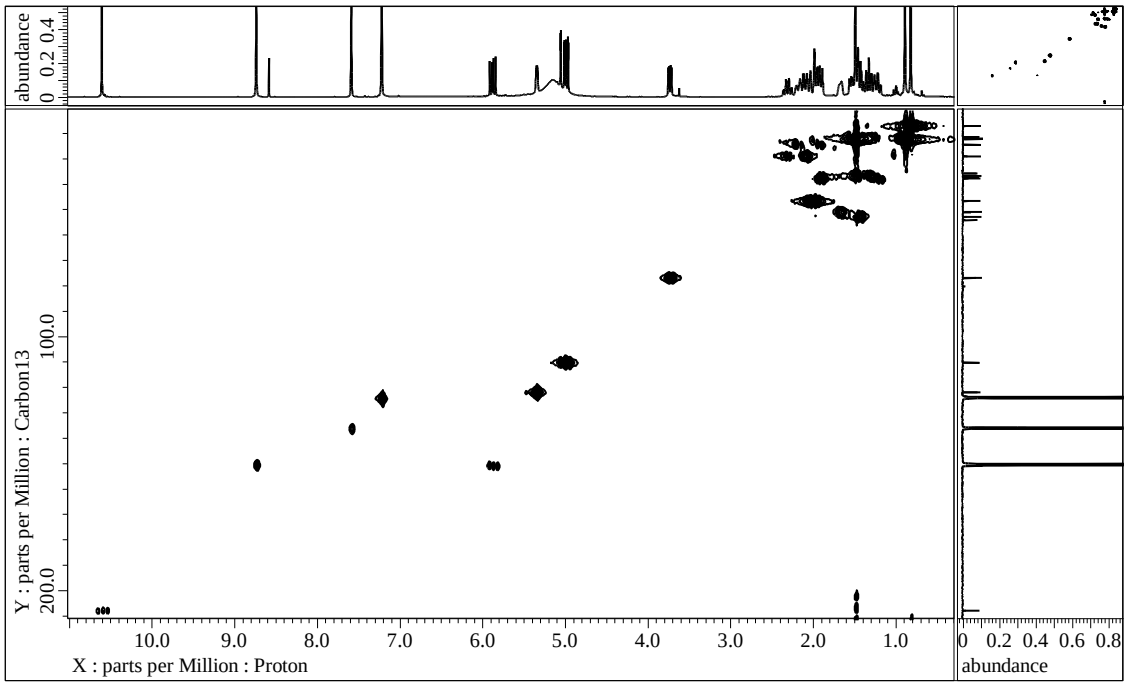

Figure S7. HMQC spectrum of **1** in pyridine-d_5

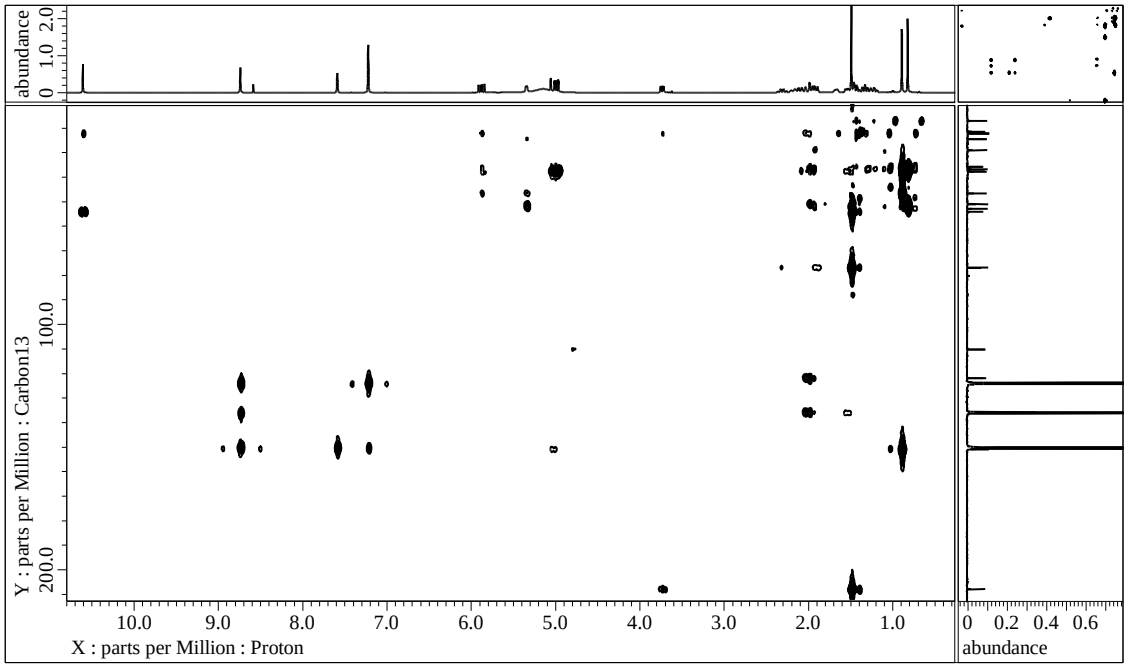

Figure S8. HMBC spectrum of **1** in pyridine-d_5

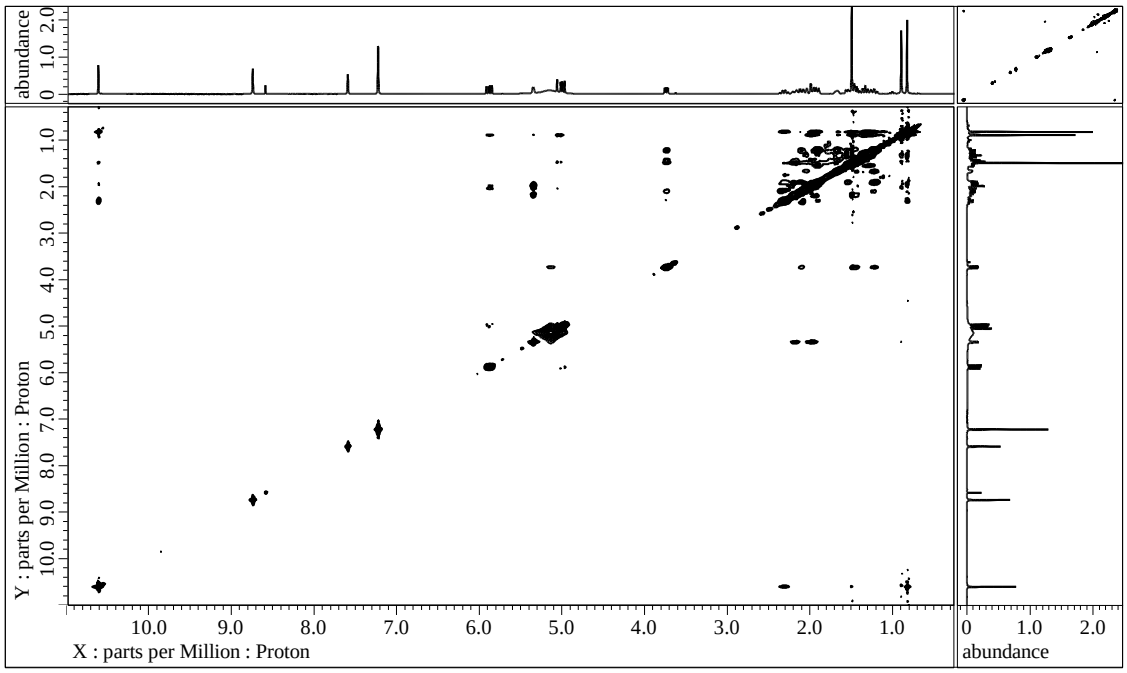

Figure S9. NOESY spectrum of **1** in pyridine-d_5

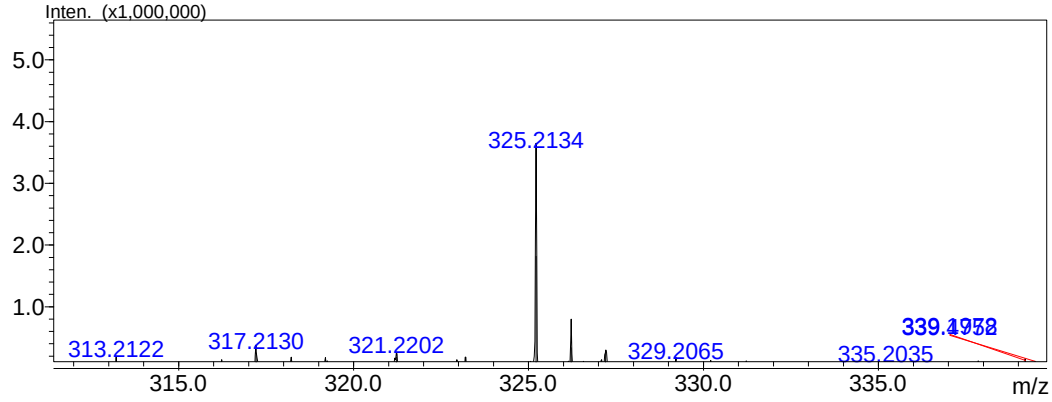

Figure S10. HRESIMS of **1**

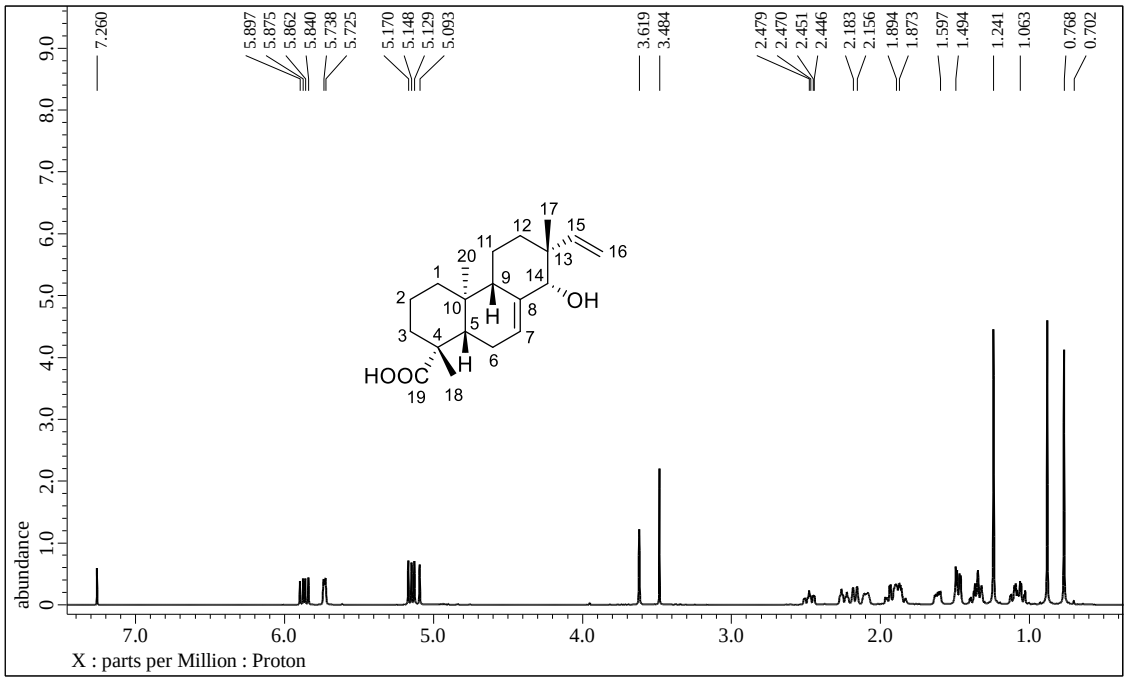

Figure S11. ^{1}H NMR spectrum ($CDCl_3$, 500 MHz) of **2**

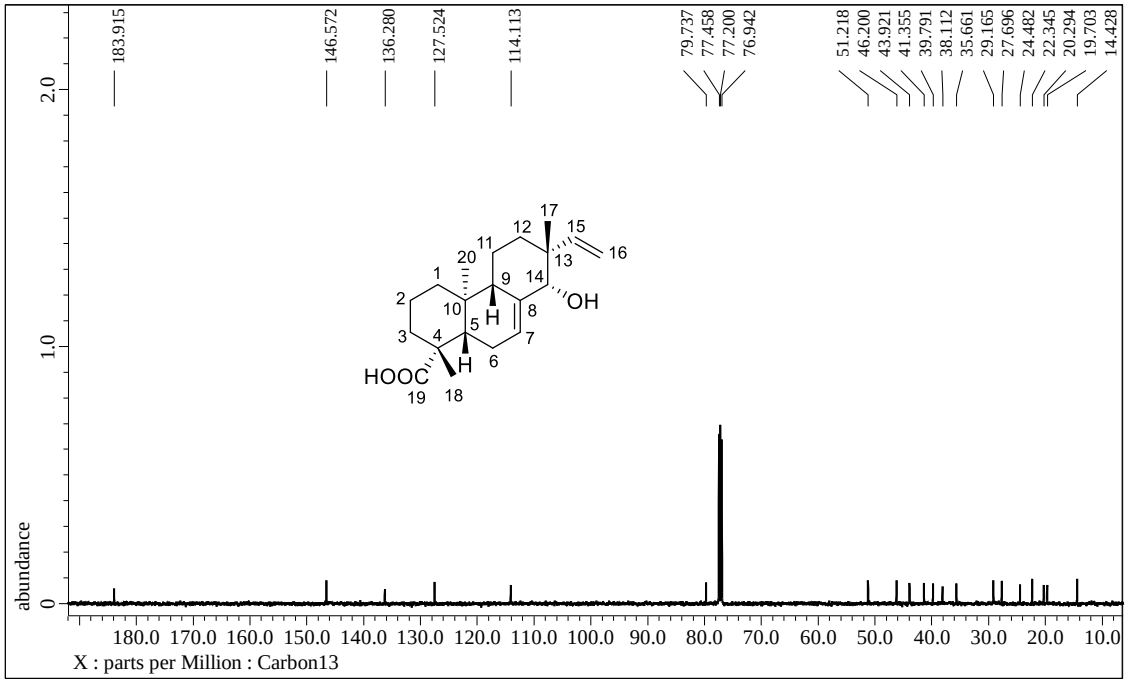

Figure S12. ^{13}C NMR spectrum ($CDCl_3$,125 MHz) of **2**

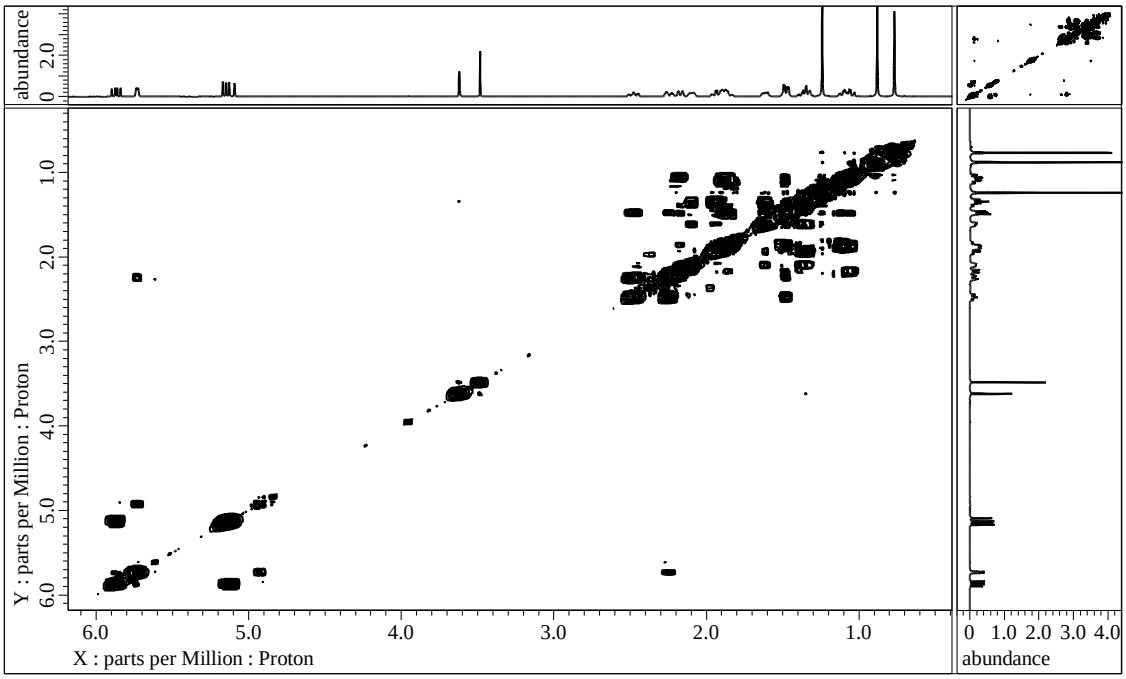

Figure S13. $^{1}H–^{1}H$ COSY spectrum of **2** in $CDCl_3$

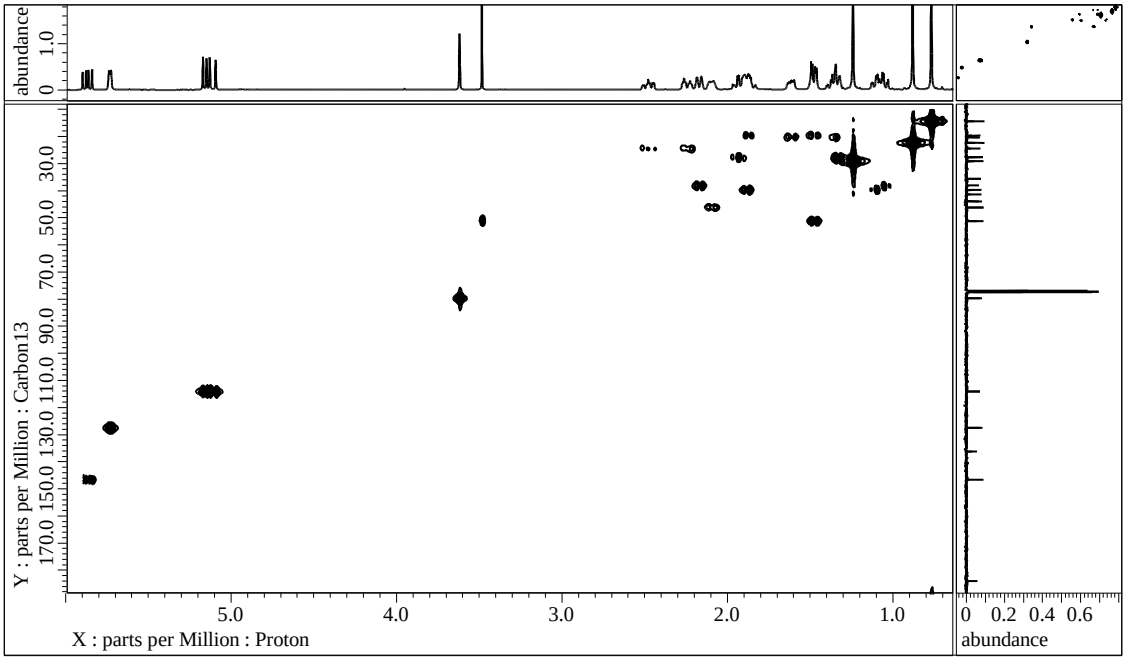

Figure 14. HMQC spectrum of **2** in $CDCl_3$

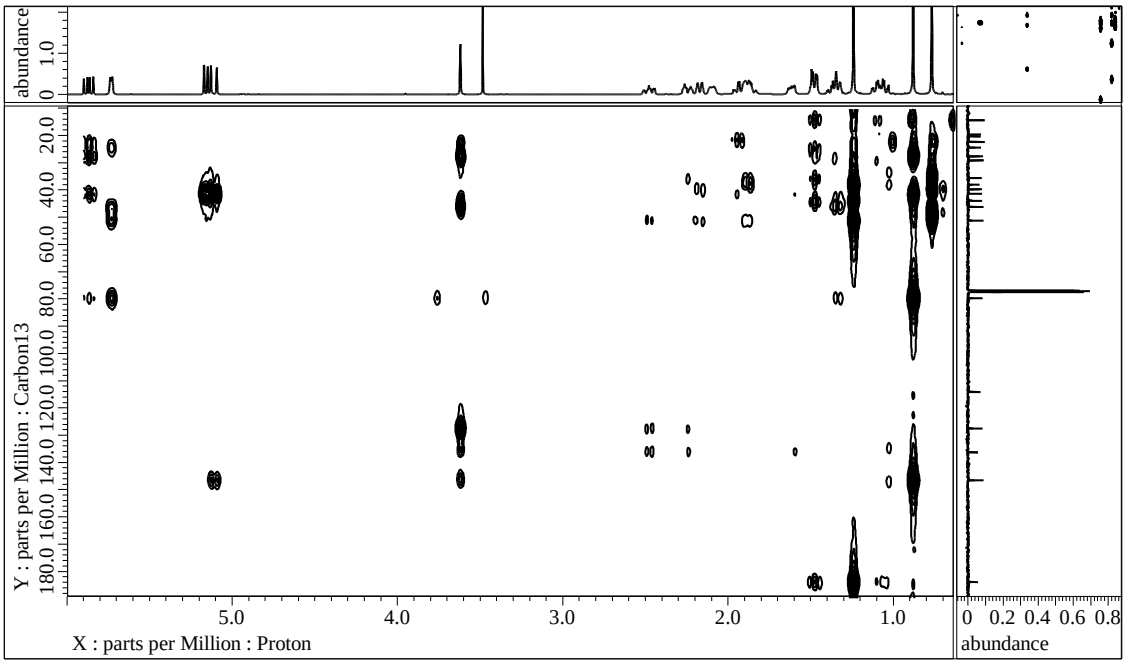

Figure S15. HMBC spectrum of **2** in $CDCl_3$

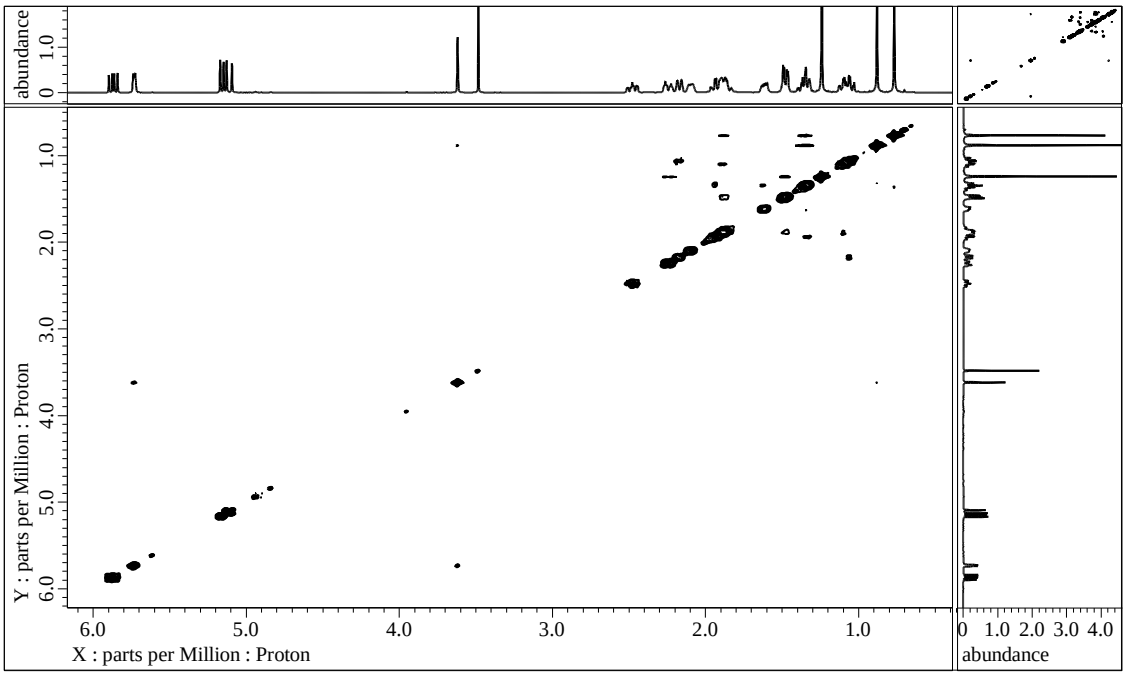

Figure S16. NOESY spectrum of **2** in $CDCl_3$

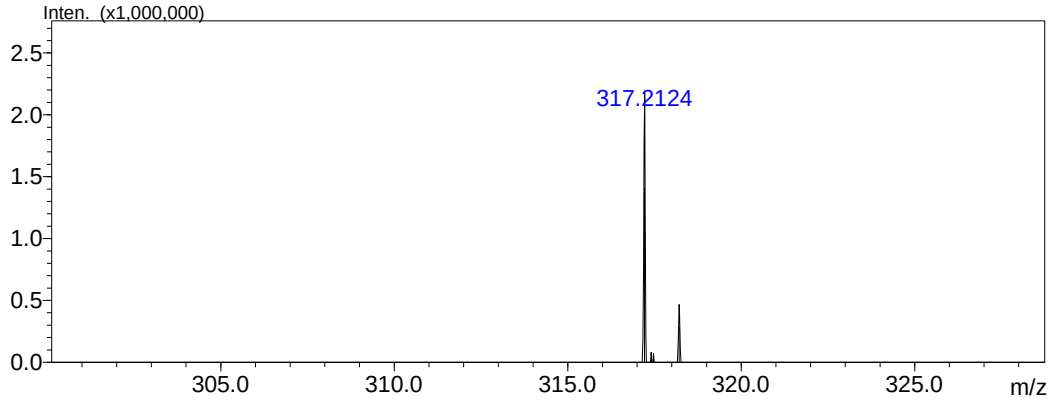

Figure S17. HRESIMS of **2**

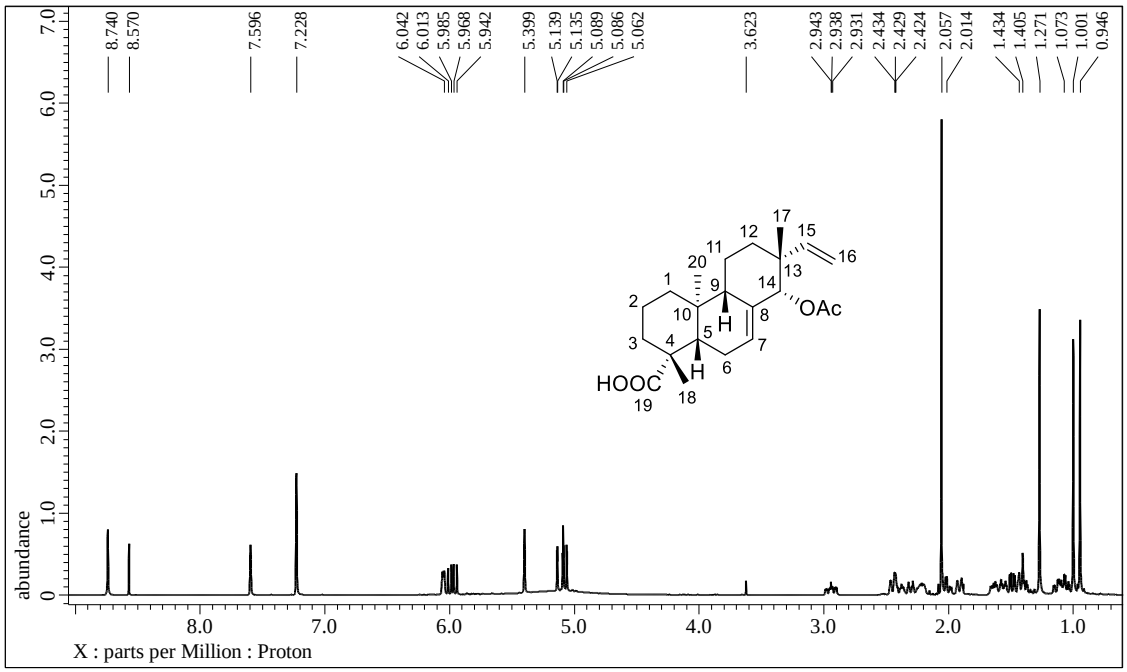

Figure S18. ^{1}H NMR spectrum (pyridine-d_5, 400 MHz) of **3**

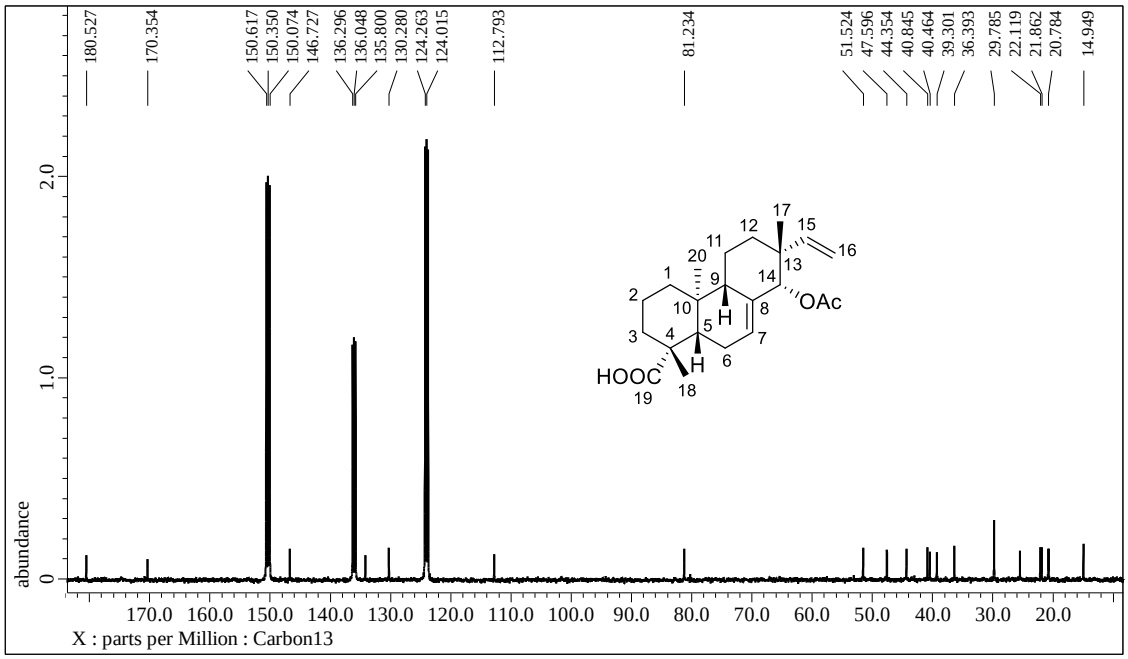

Figure S19. ^{13}C NMR spectrum (pyridine-d_5, 100 MHz) of **3**

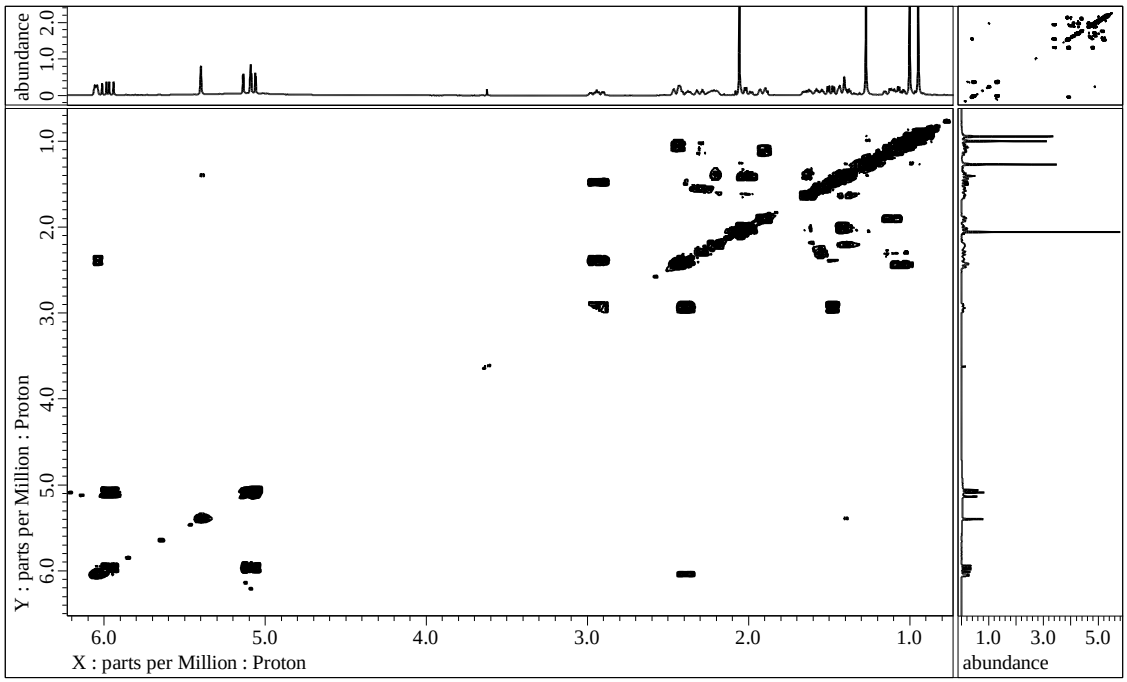

Figure S20. ^{1}H–^{1}H COSY spectrum of **3** in pyridine-d_5

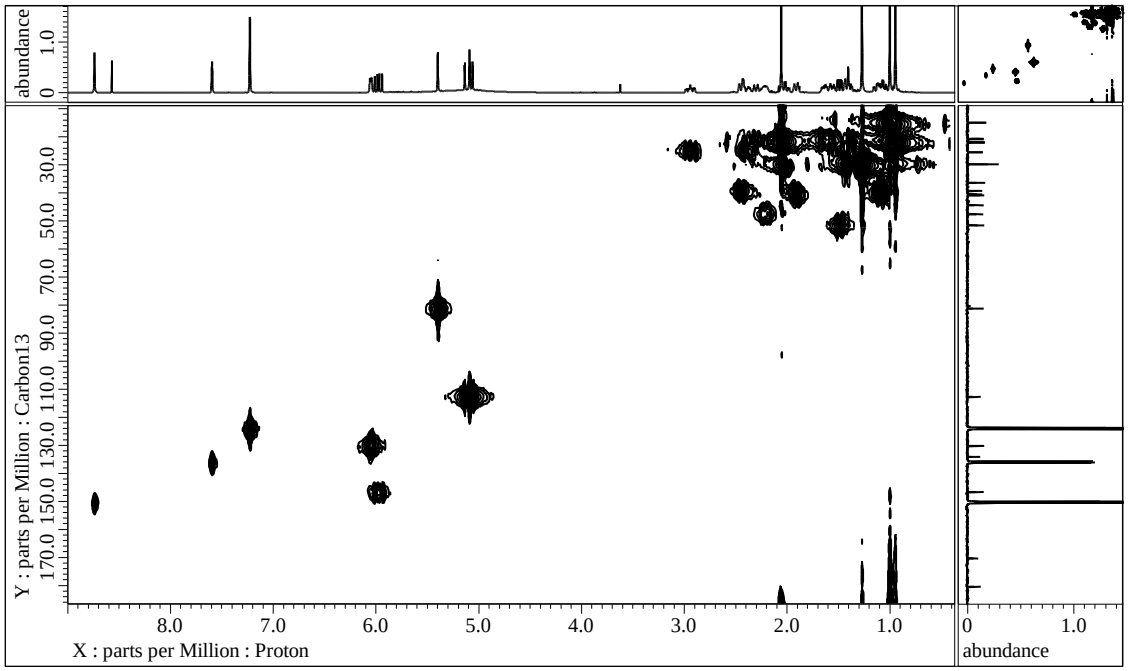

Figure S21. HMQC spectrum of **3** in pyridine-d_5

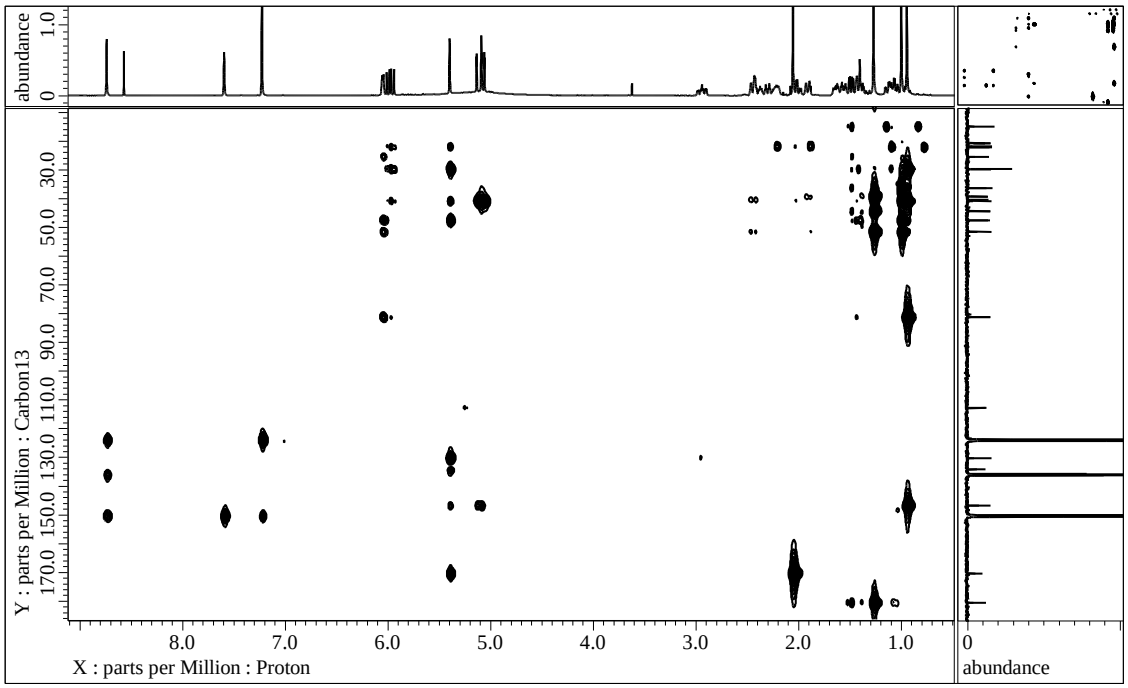

Figure S22. HMBC spectrum of **3** in pyridine-d_5

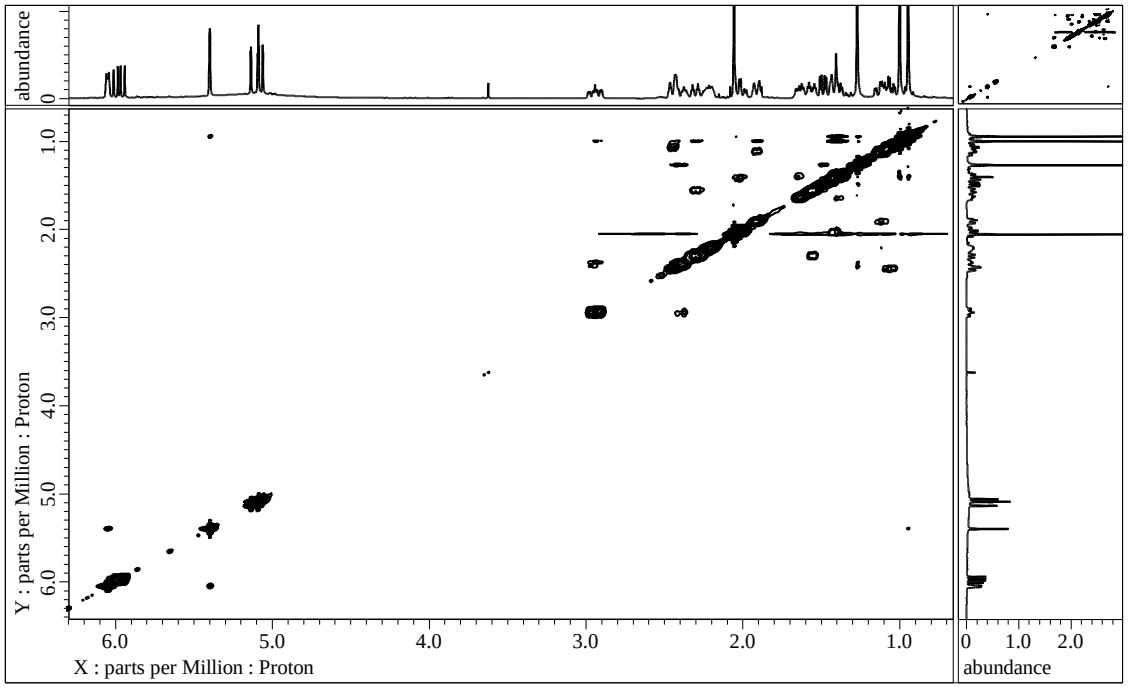

Figure S23. NOESY spectrum of **3** in pyridine-d_5

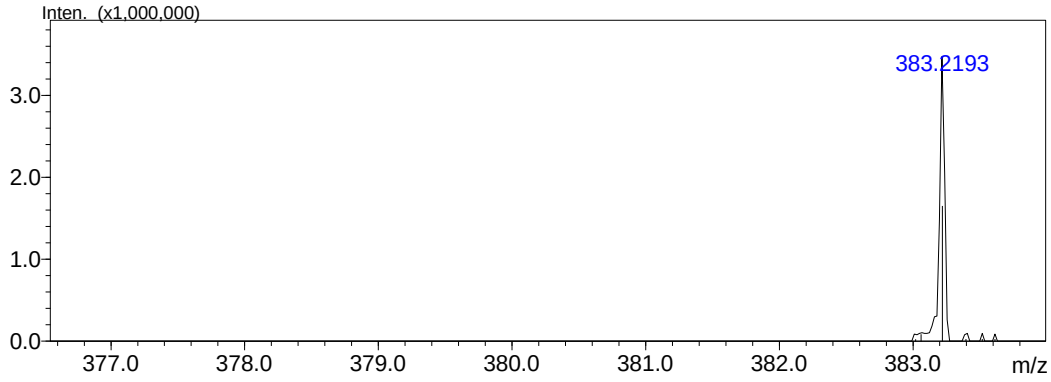

Figure S24. HRESIMS of **3**

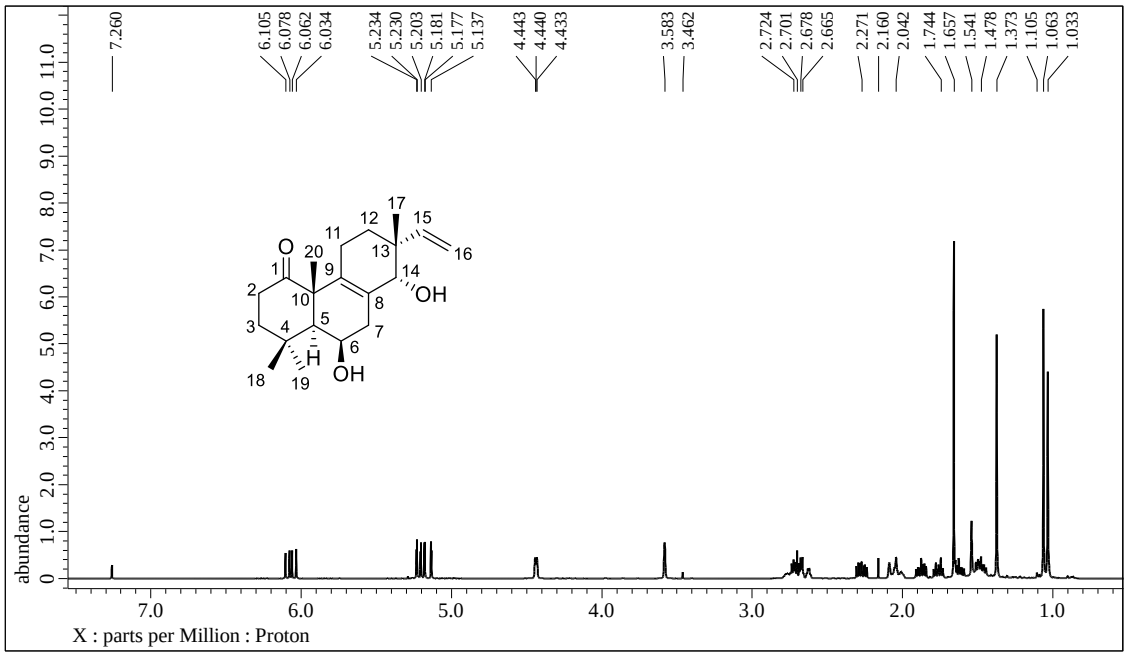

Figure S25. ^{1}H NMR spectrum ($CDCl_3$, 400 MHz) of **4**

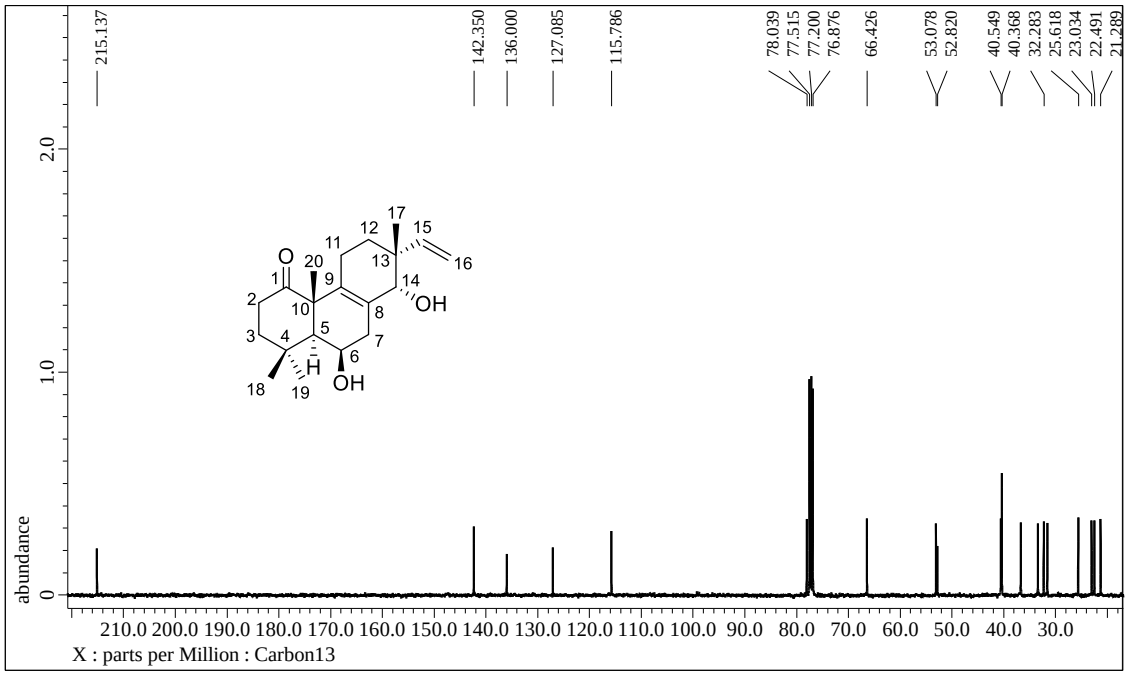

Figure S26. ^{13}C NMR spectrum ($CDCl_3$, 100 MHz) of **4**

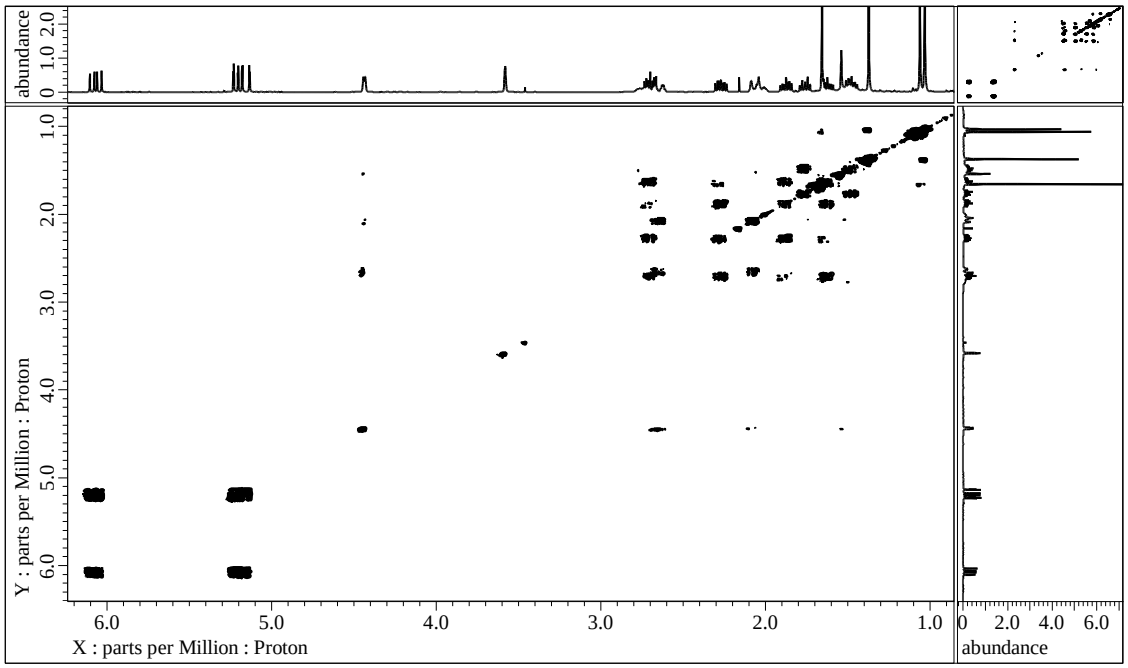

Figure S27. $^{1}H–^{1}H$ COSY spectrum of **4** in $CDCl_3$

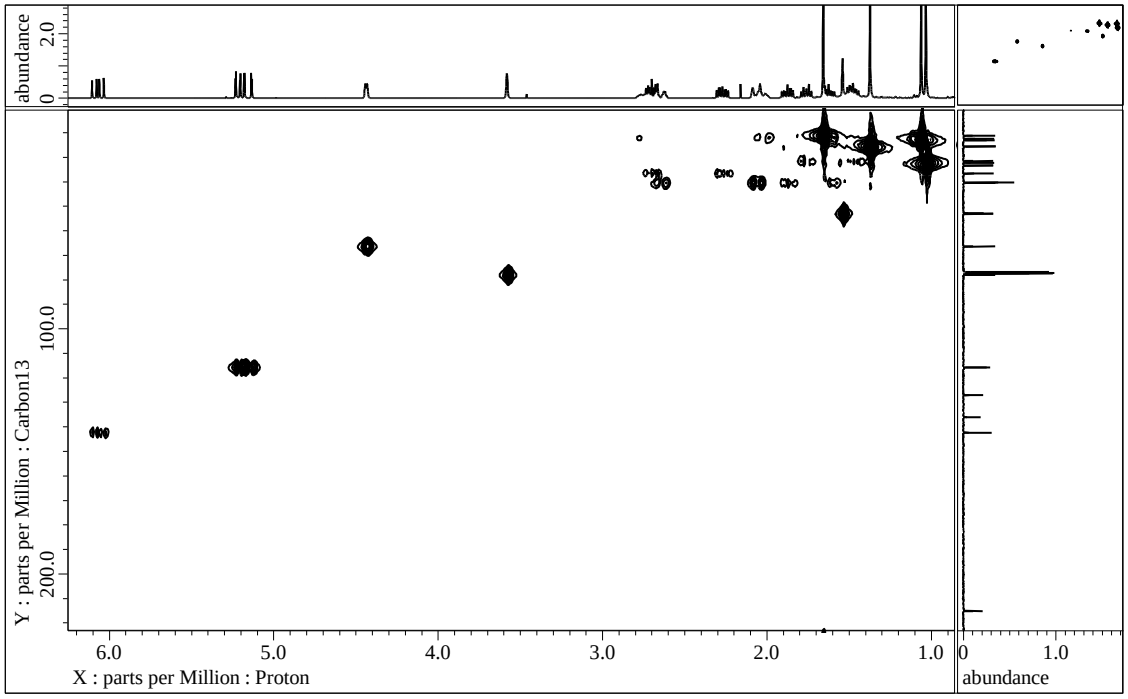

Figure S28. HMQC spectrum of **4** in $CDCl_3$

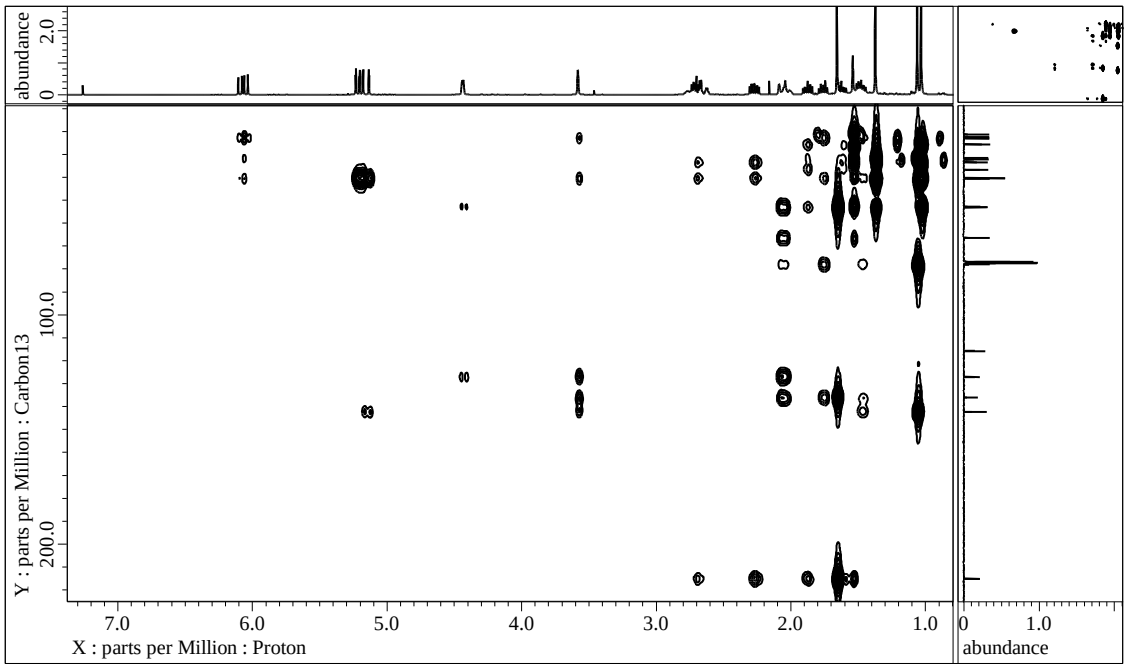

Figure S29. HMBC spectrum of **4** in $CDCl_3$

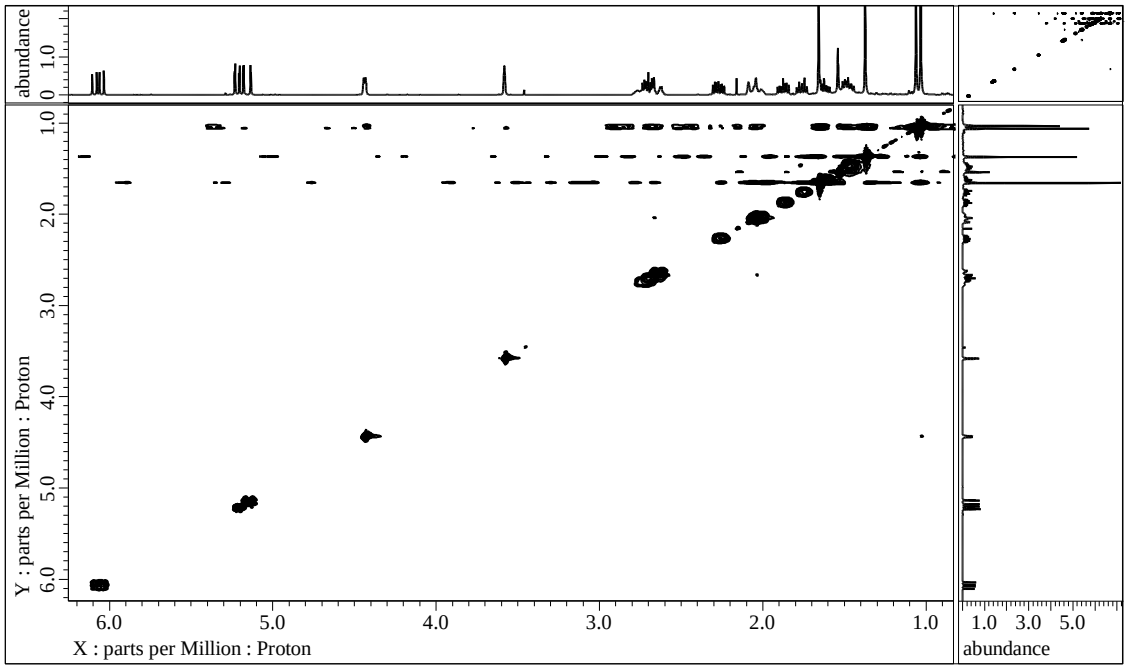

Figure S30. NOESY spectrum of **4** in $CDCl_3$

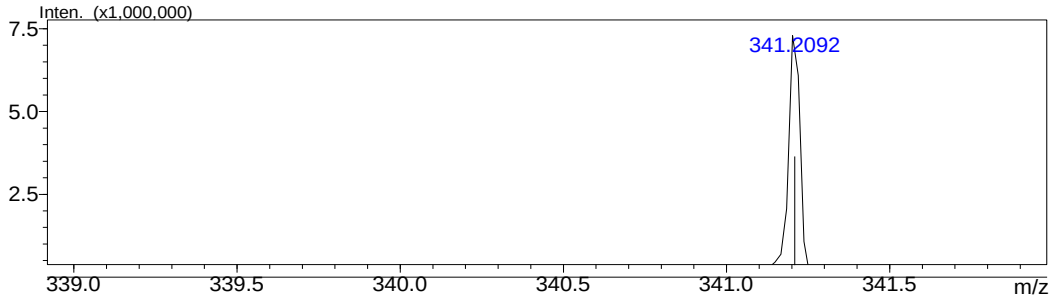

Figure S31. HRESIMS of **4**

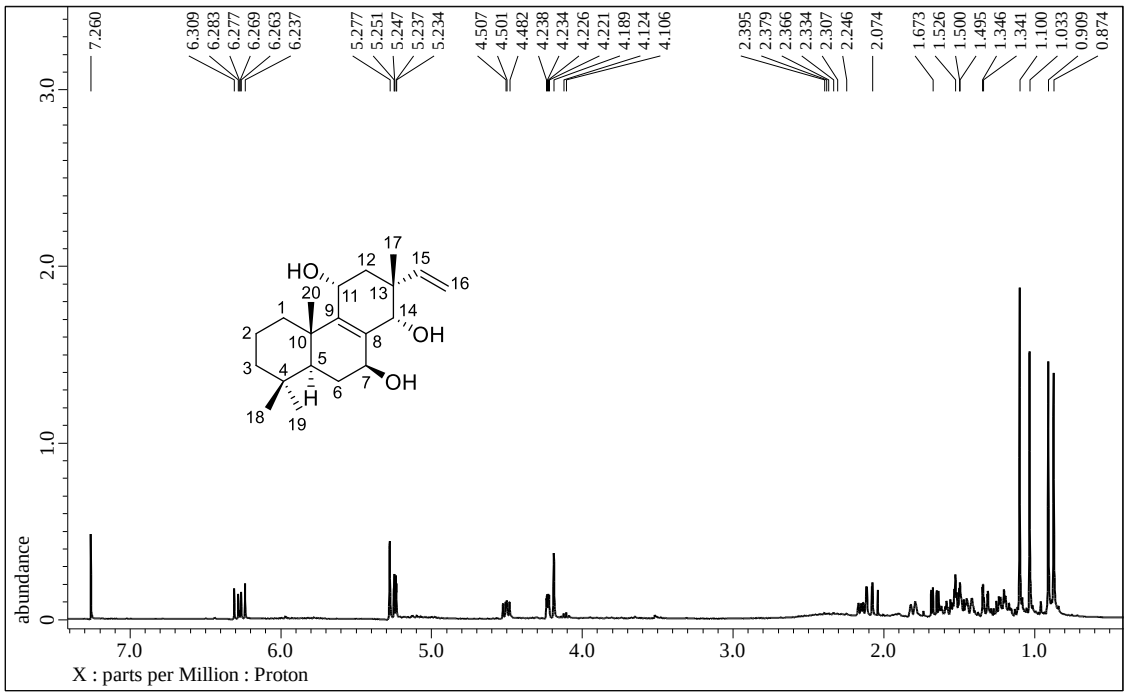

Figure S32. ^{1}H NMR spectrum ($CDCl_3$, 500 MHz) of **5**

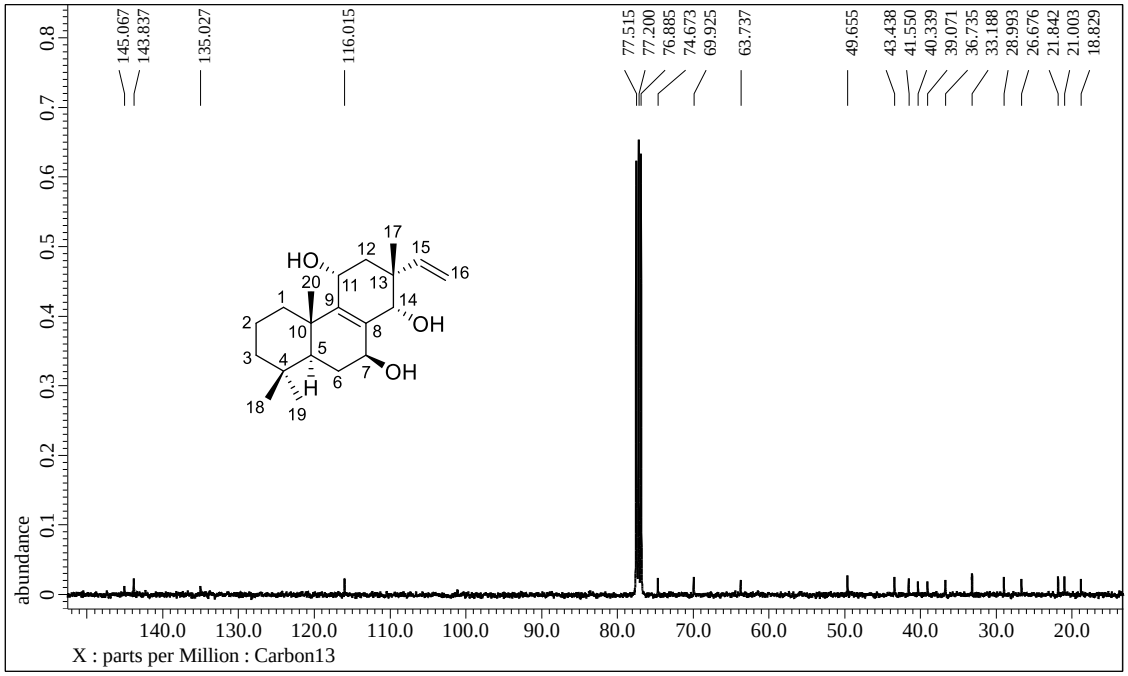

Figure S33. ^{13}C NMR spectrum ($CDCl_3$, 125 MHz) of **5**

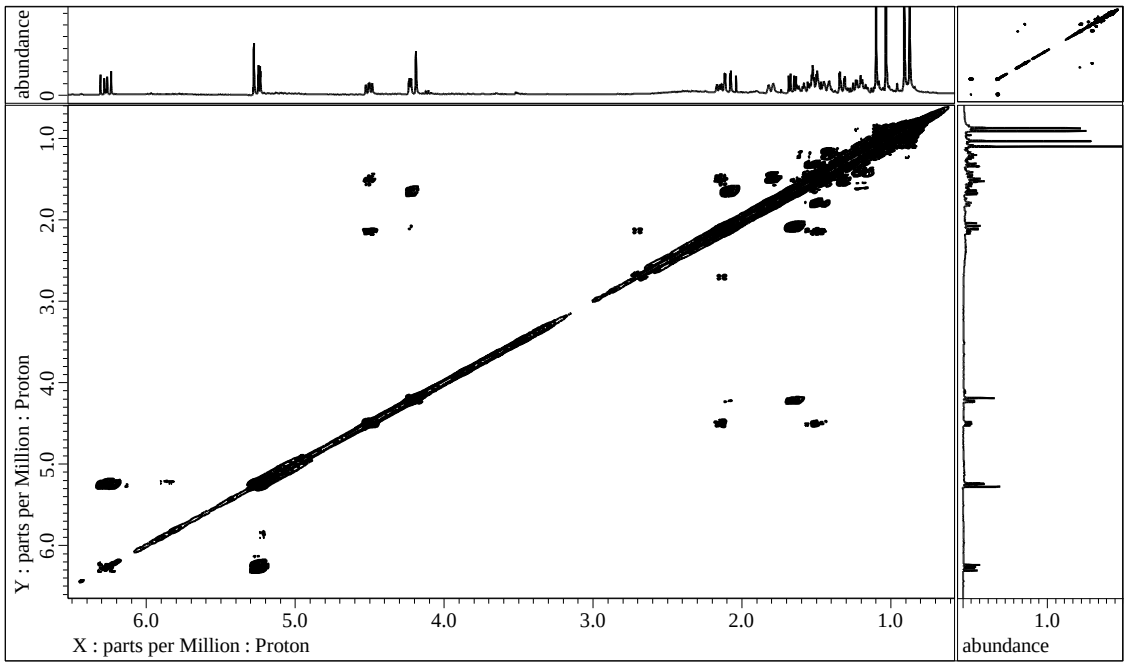

Figure S34. $^{1}H–^{1}H$ COSY spectrum of **5** in $CDCl_3$

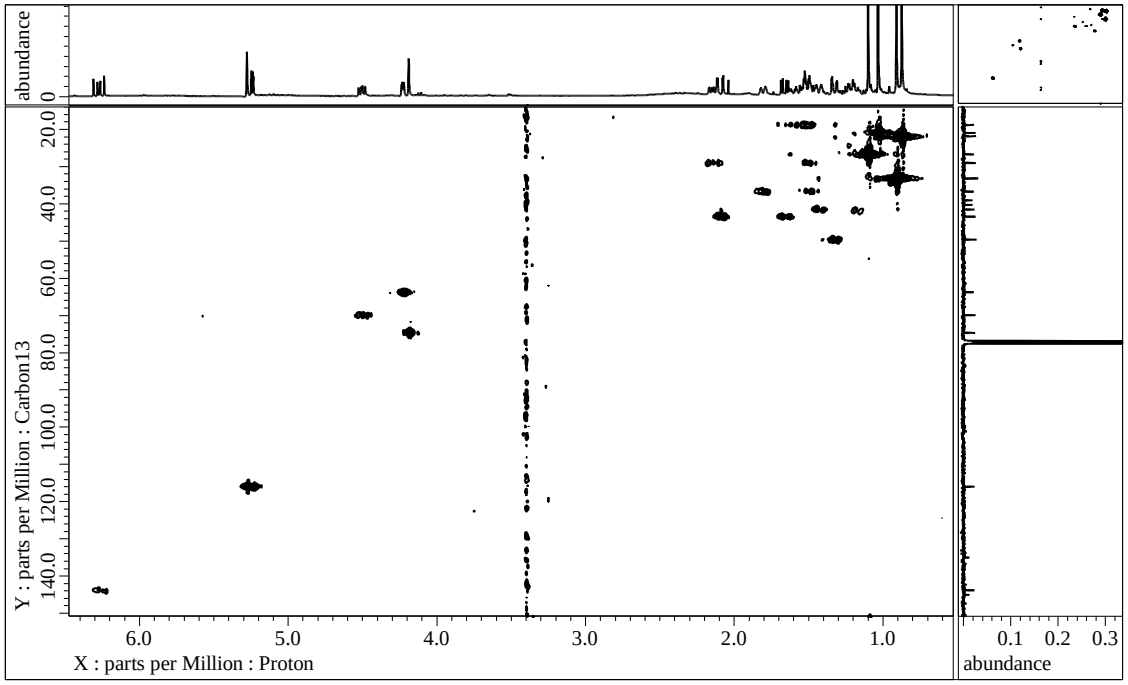

Figure S35. HMQC spectrum of **5** in $CDCl_3$

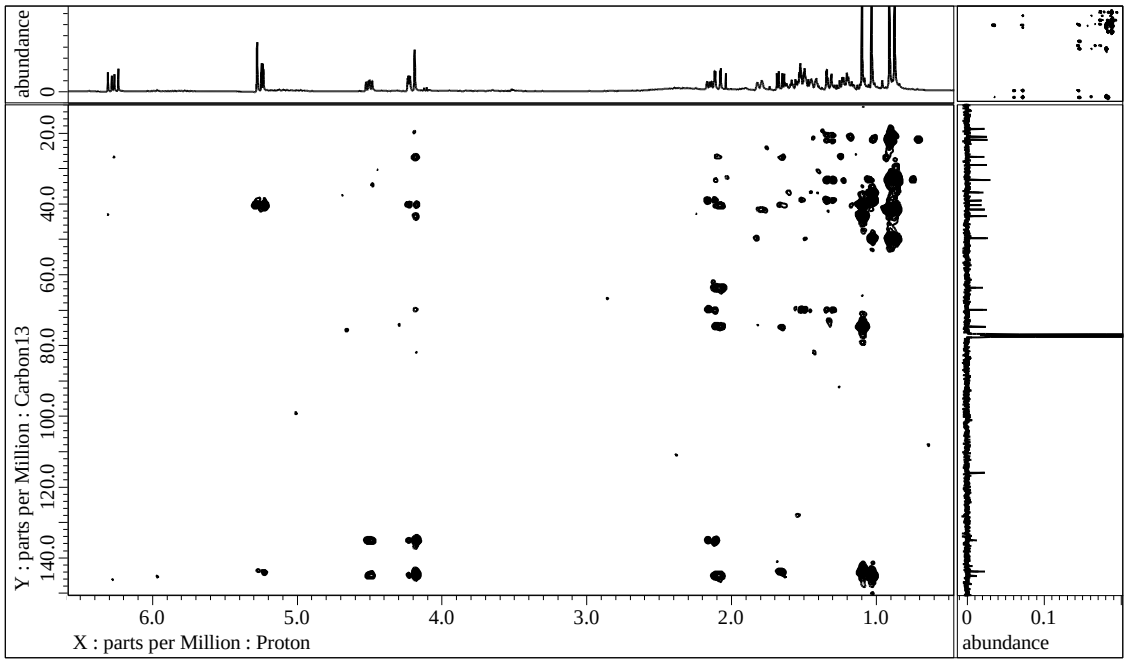

Figure S36. HMBC spectrum of **5** in $CDCl_3$

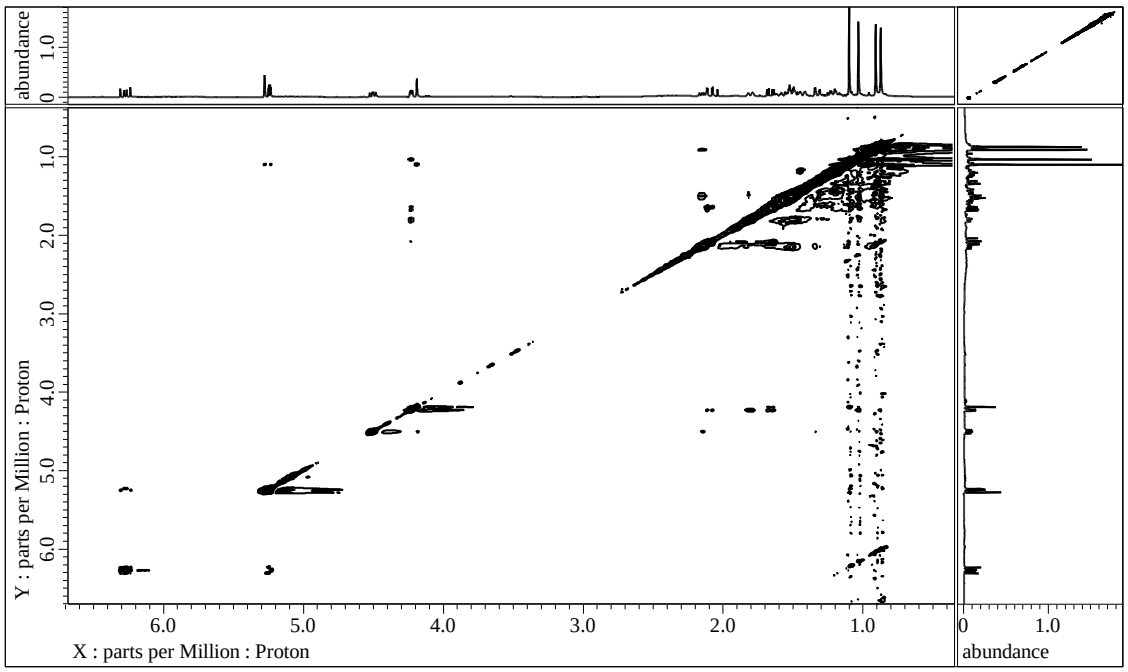

Figure S37. NOESY spectrum of **5** in $CDCl_3$

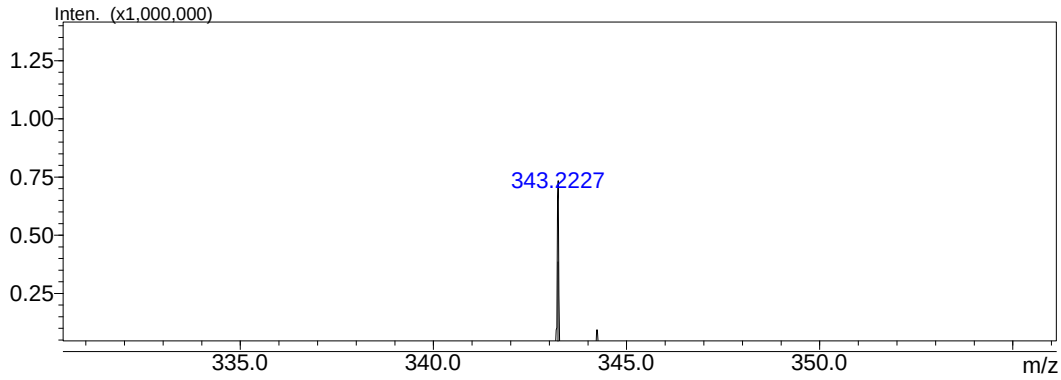

Figure S38. HRESIMS of **5**

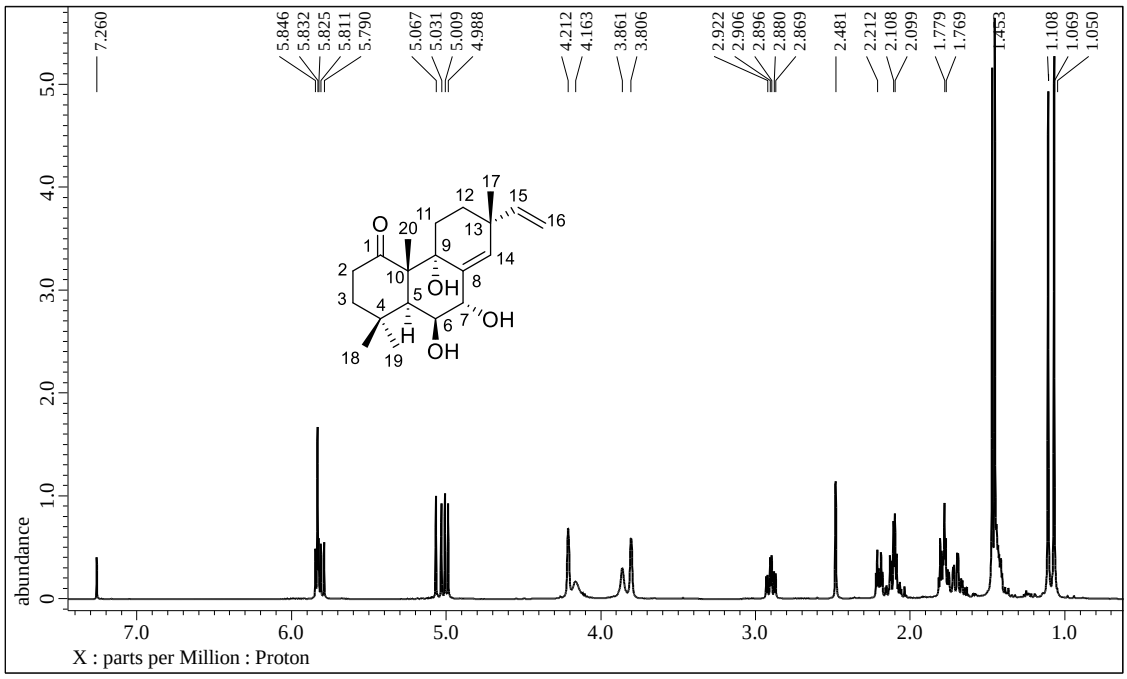

Figure S39. ^{1}H NMR spectrum ($CDCl_3$, 500 MHz) of **6**

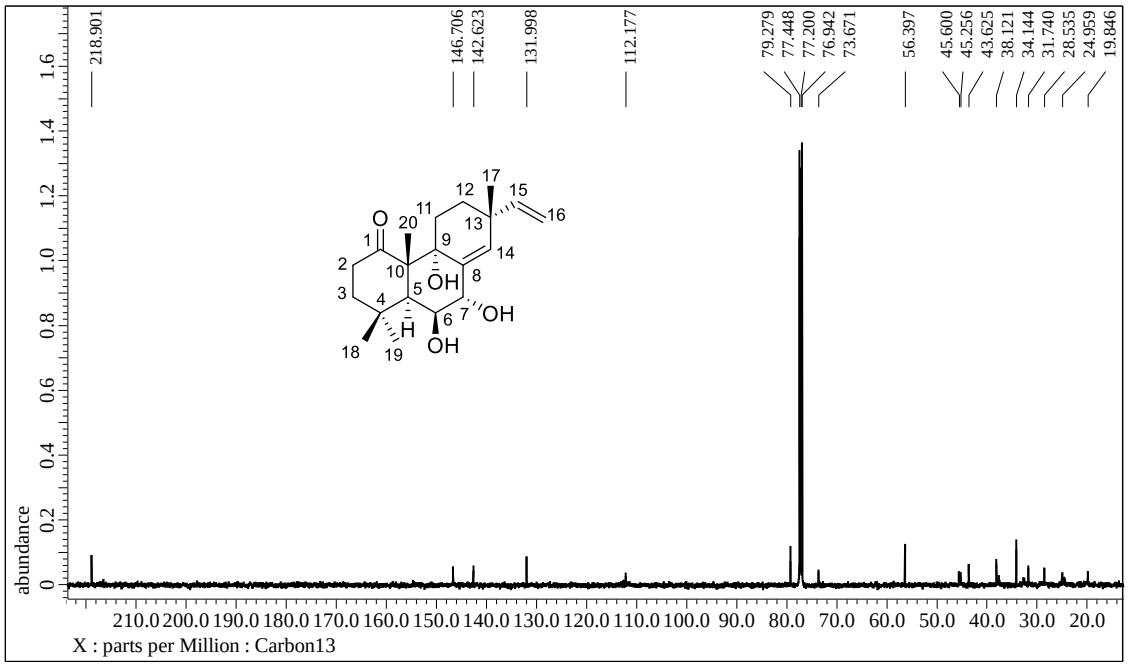

Figure S40. ^{13}C NMR spectrum ($CDCl_3$, 125 MHz) of **6**

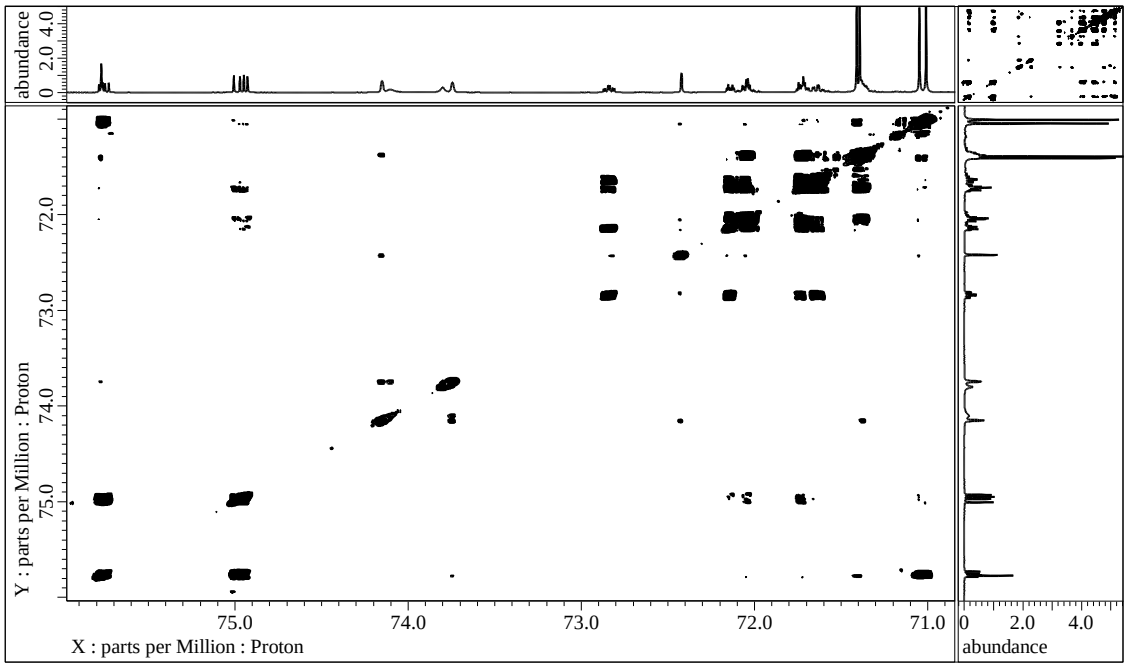

Figure S41. $^{1}H–^{1}H$ COSY spectrum of **6** in $CDCl_3$

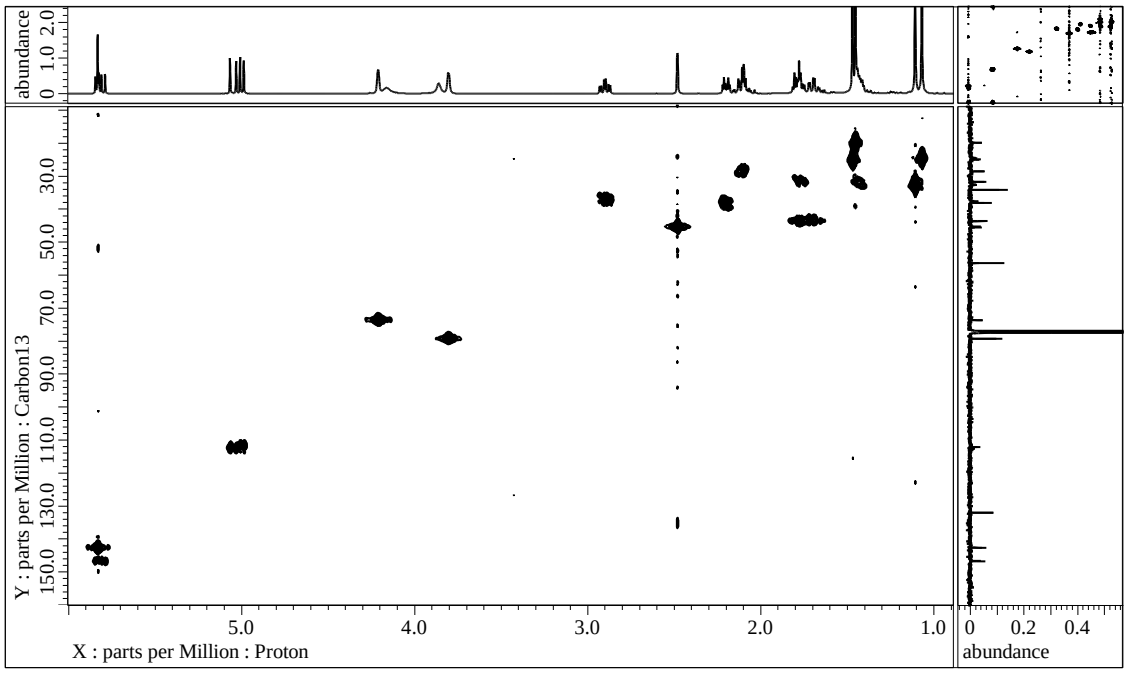

Figure S42. HMQC spectrum of **6** in $CDCl_3$

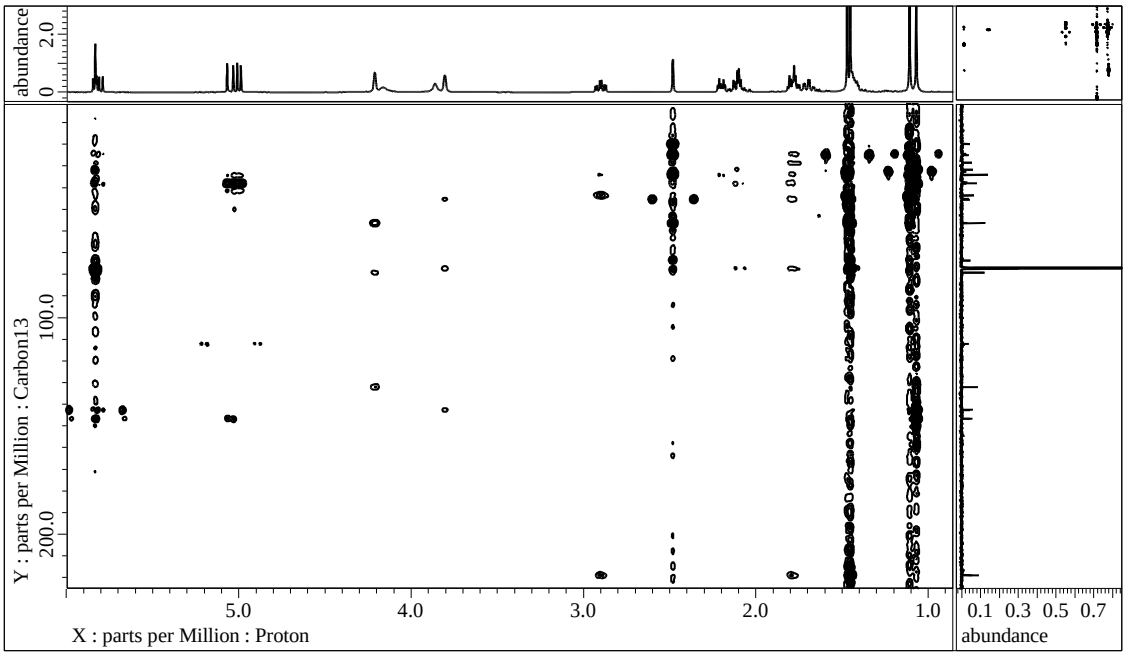

Figure S43. HMBC spectrum of **6** in $CDCl_3$

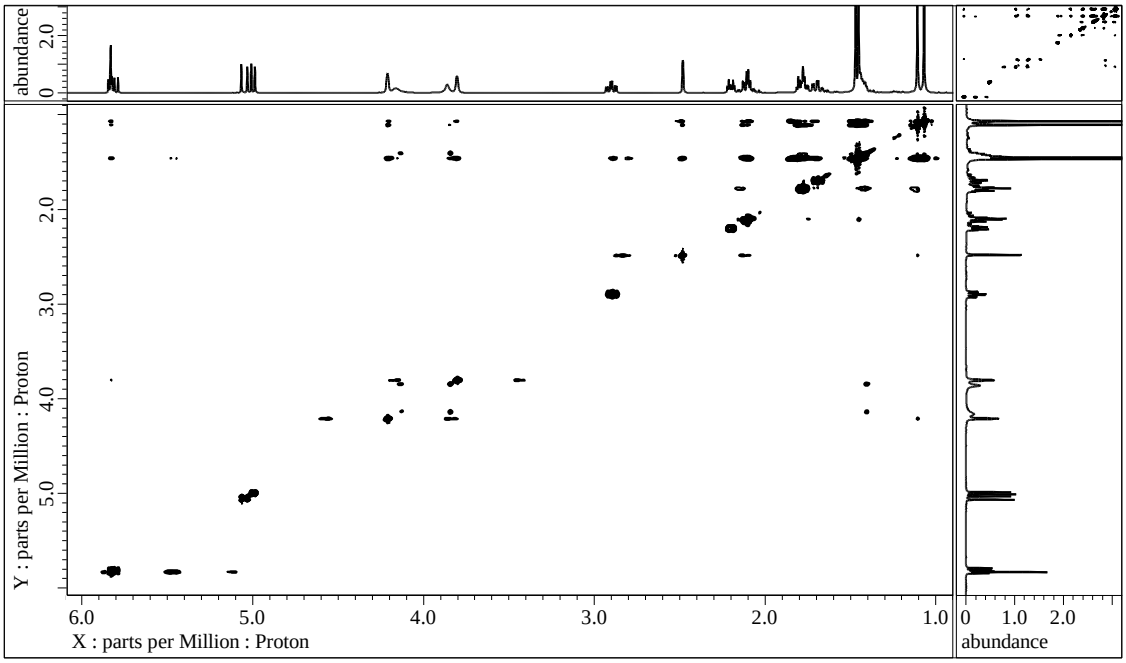

Figure S44. NOESY spectrum of **6** in $CDCl_3$

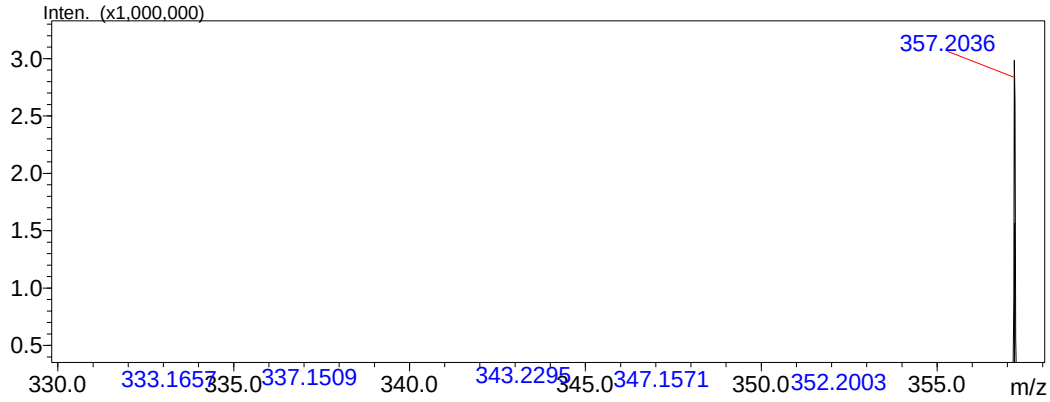

Figure S45. HRESIMS of **6**

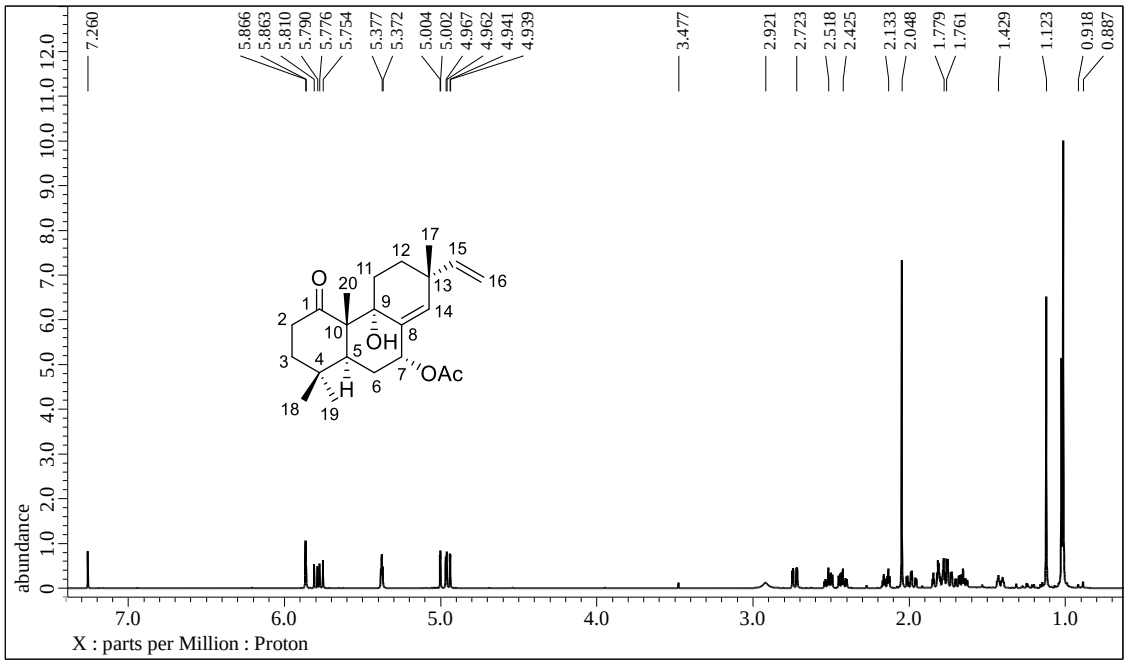

Figure S46. ^{1}H NMR spectrum ($CDCl_3$, 500 MHz) of **7**

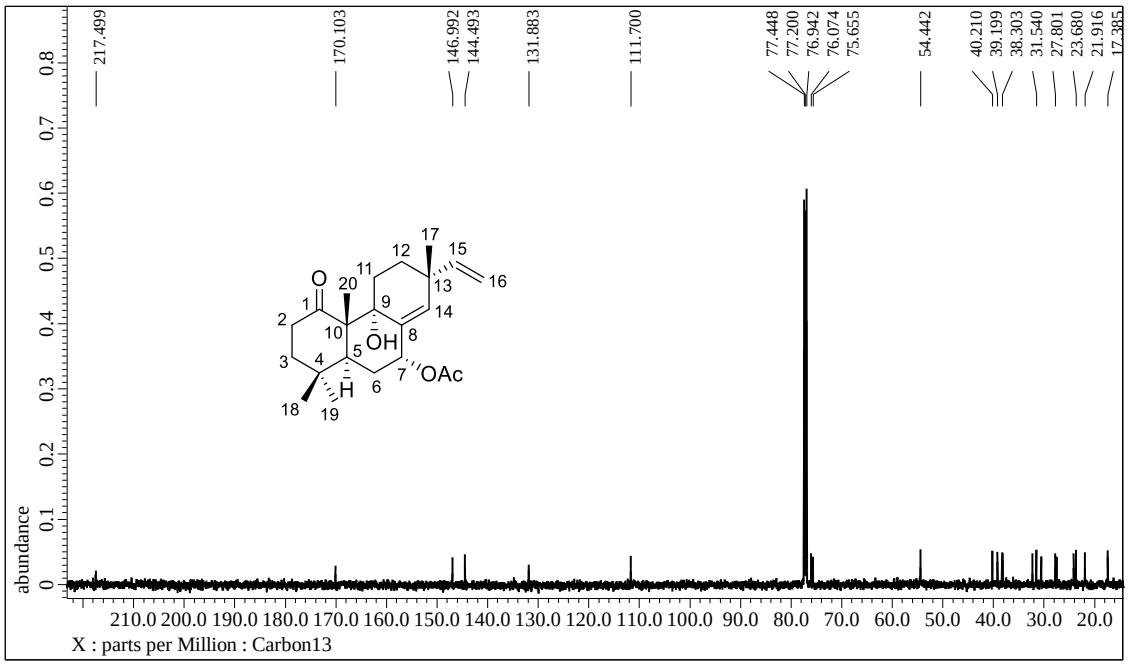

Figure S47. ^{13}C NMR spectrum ($CDCl_3$, 125 MHz) of **7**

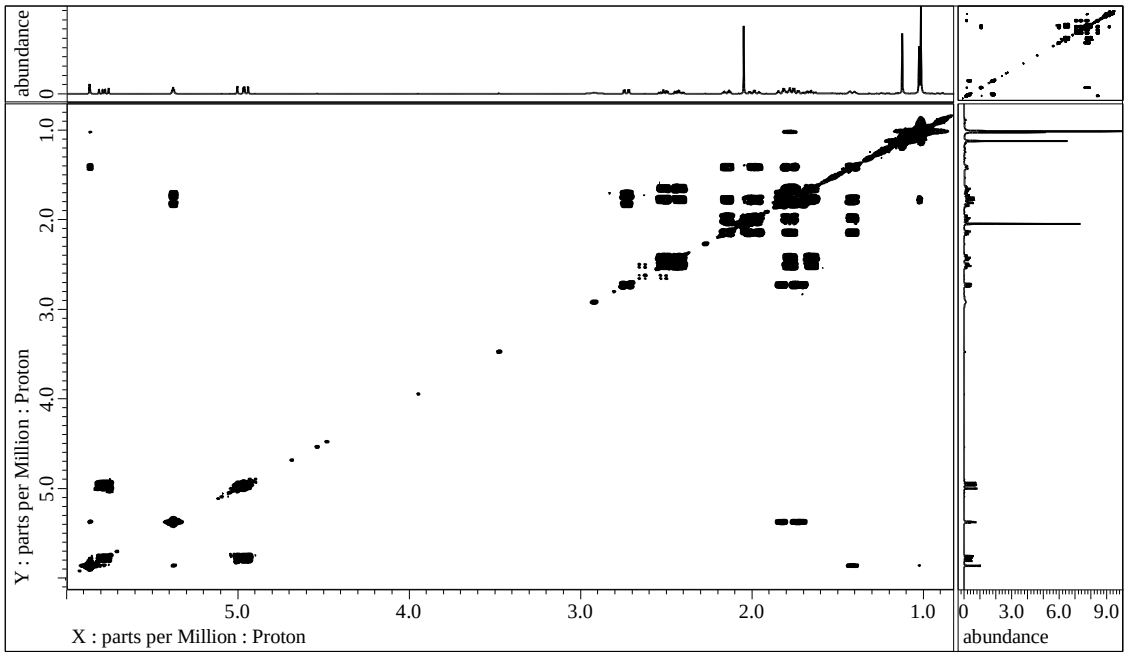

Figure S48. $^{1}H–^{1}H$ COSY spectrum of **7** in $CDCl_3$

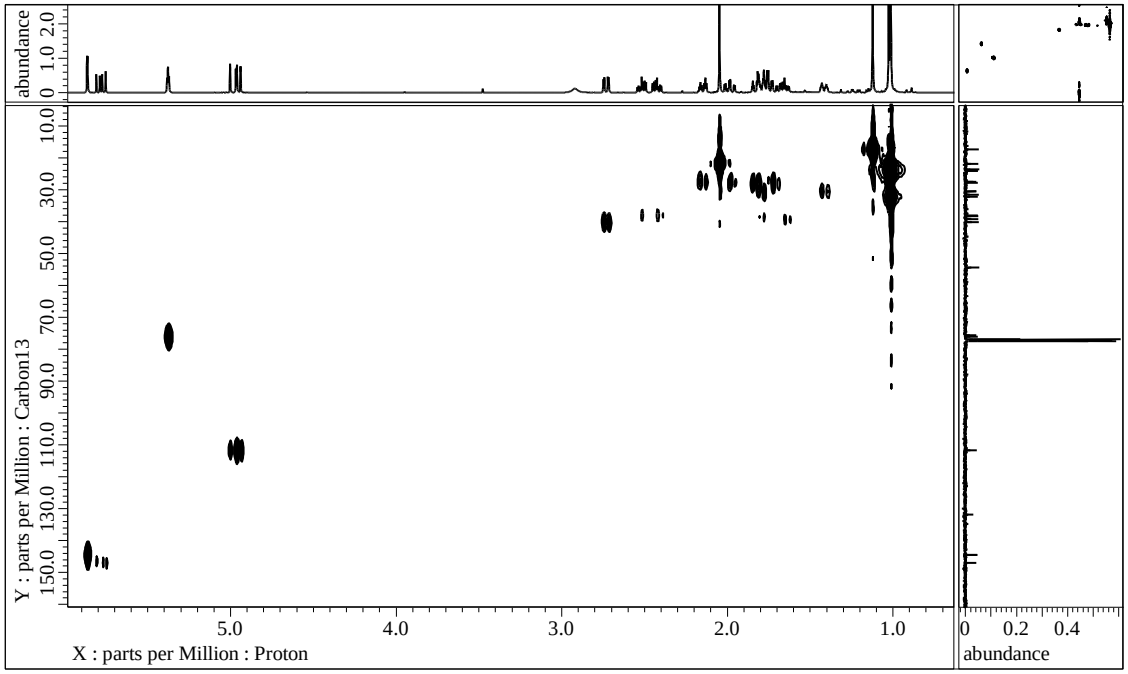

Figure S49. HMQC spectrum of **7** in $CDCl_3$

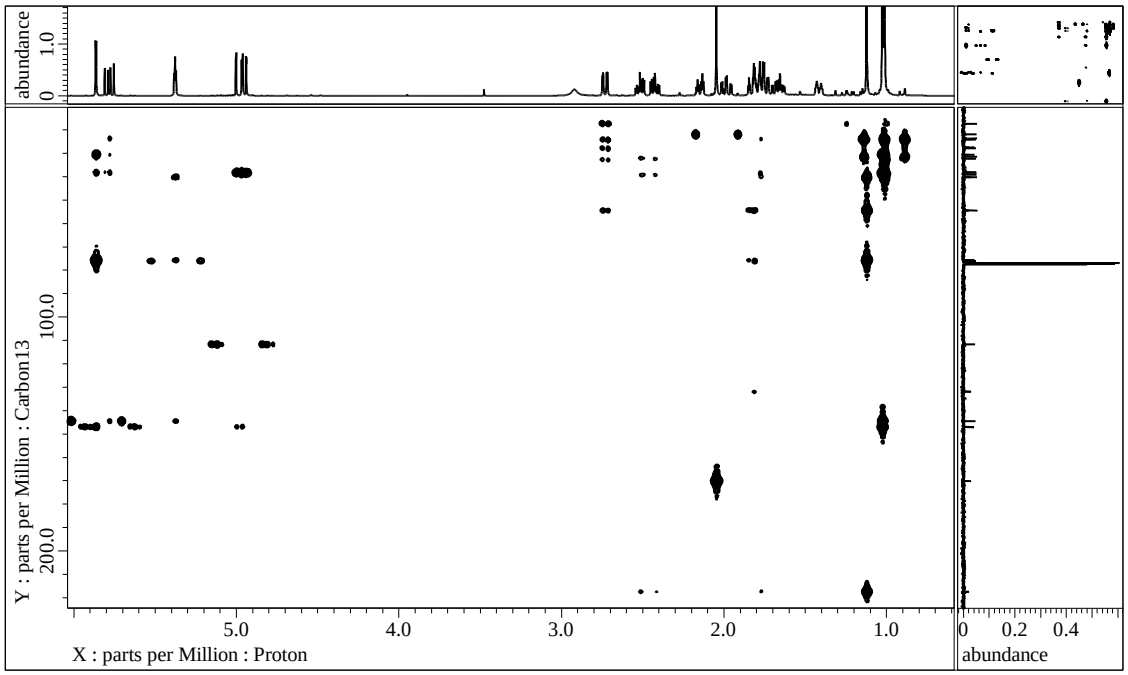

Figure S50. HMBC spectrum of **7** in $CDCl_3$

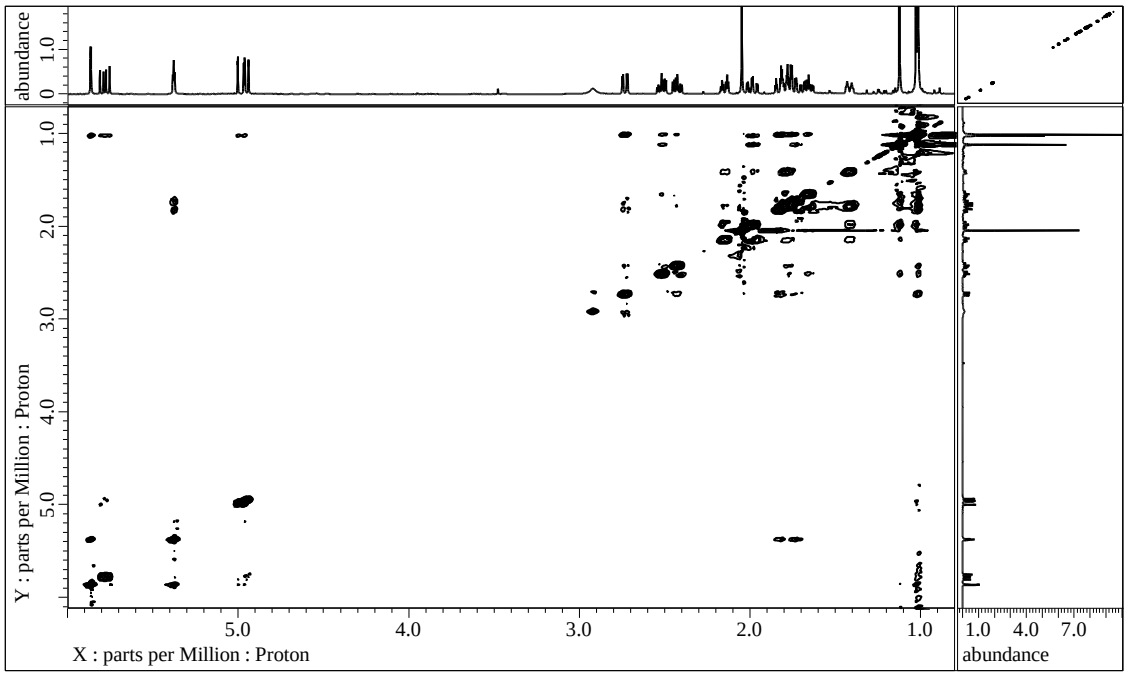

Figure S51. NOESY spectrum of **7** in $CDCl_3$

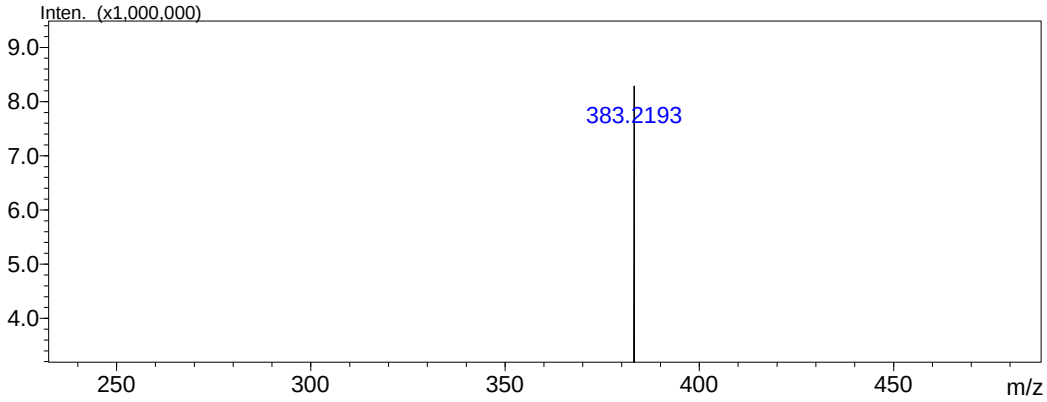

Figure S52. HRESIMS of **7**

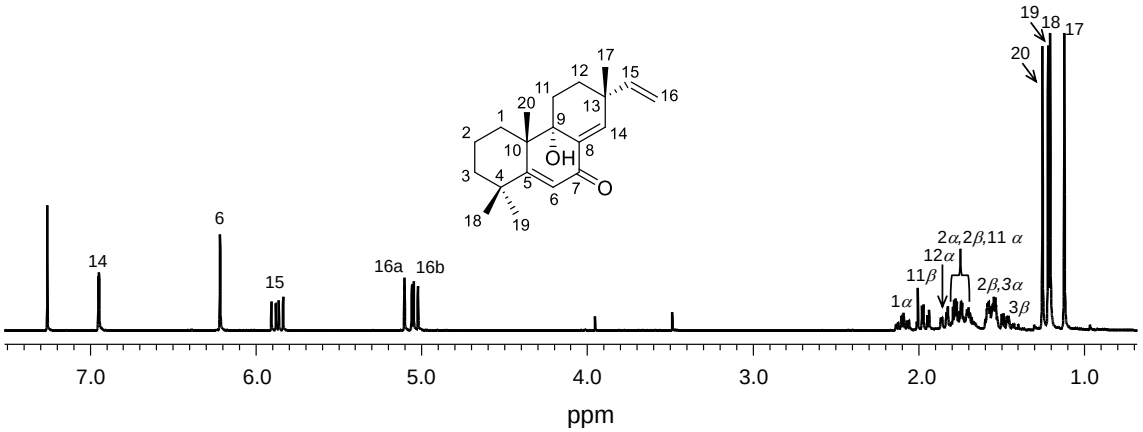

Figure S53. ^{1}H NMR spectrum ($CDCl_3$, 500 MHz) of **8**

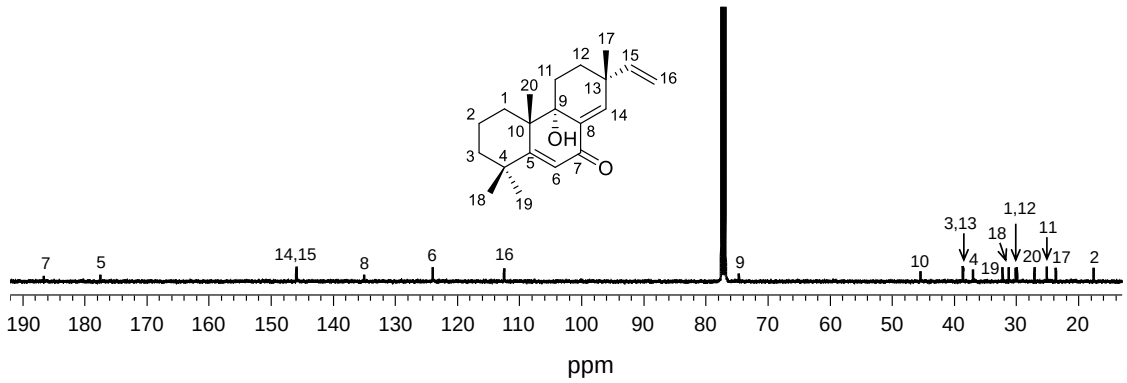

Figure S54. ^{13}C NMR spectrum ($CDCl_3$, 125 MHz) of **8**

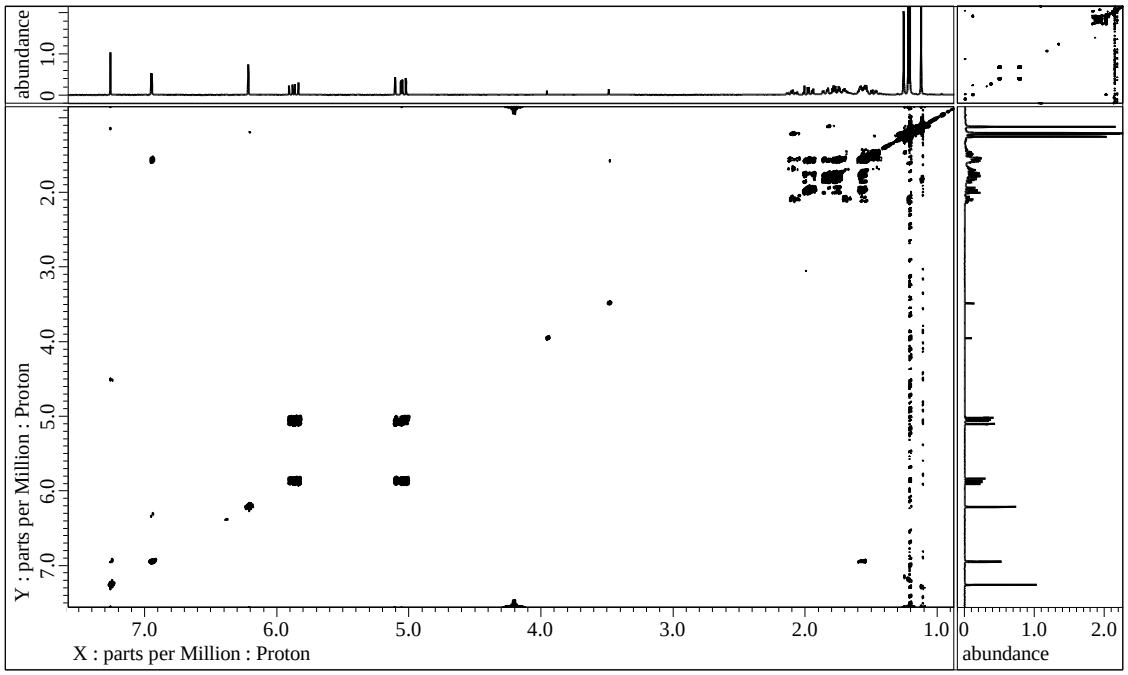

Figure S55. $^{1}H–^{1}H$ COSY spectrum of **8** in $CDCl_3$

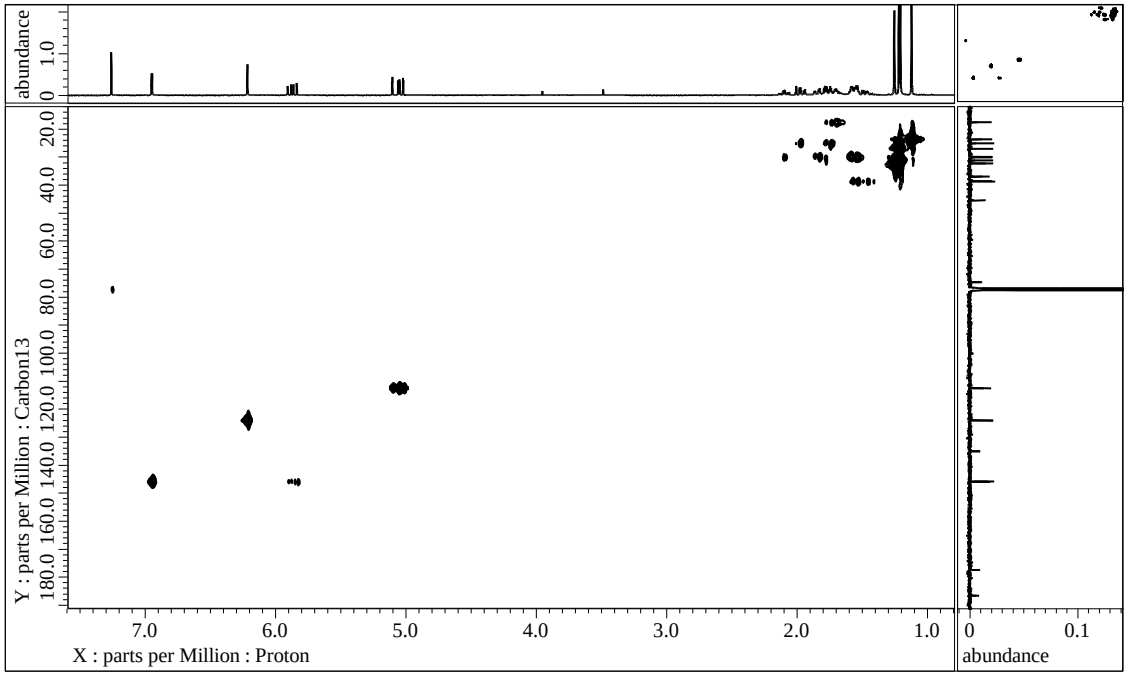

Figure S56. HMQC spectrum of **8** in $CDCl_3$

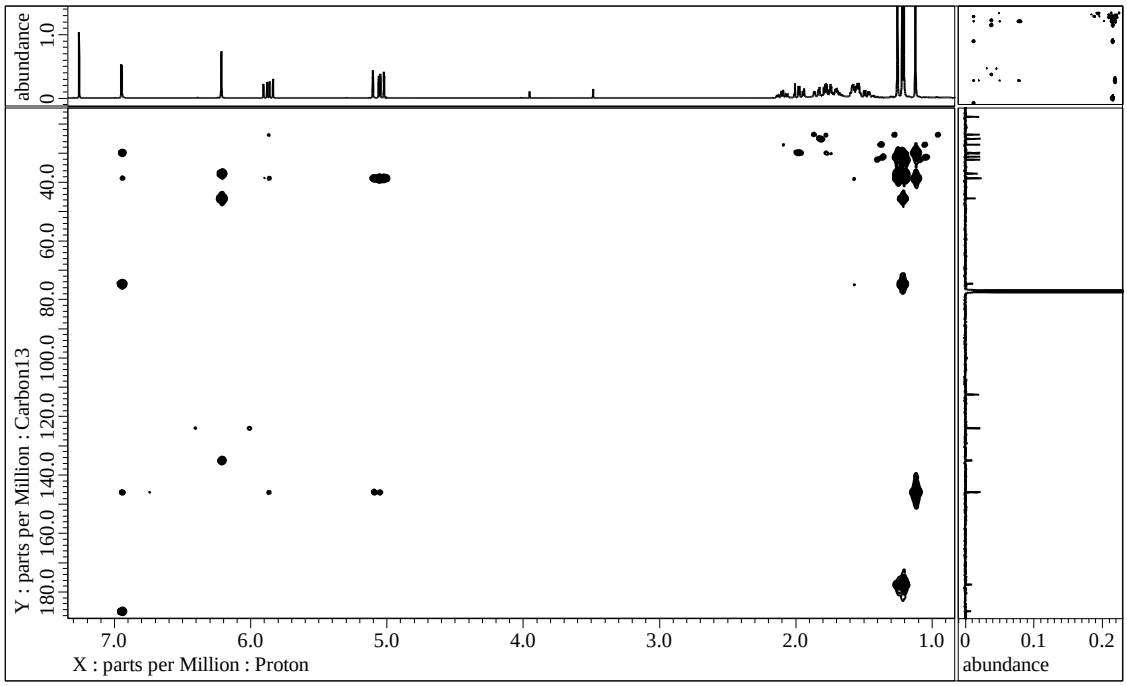

Figure S57. HMBC spectrum of **8** in $CDCl_3$

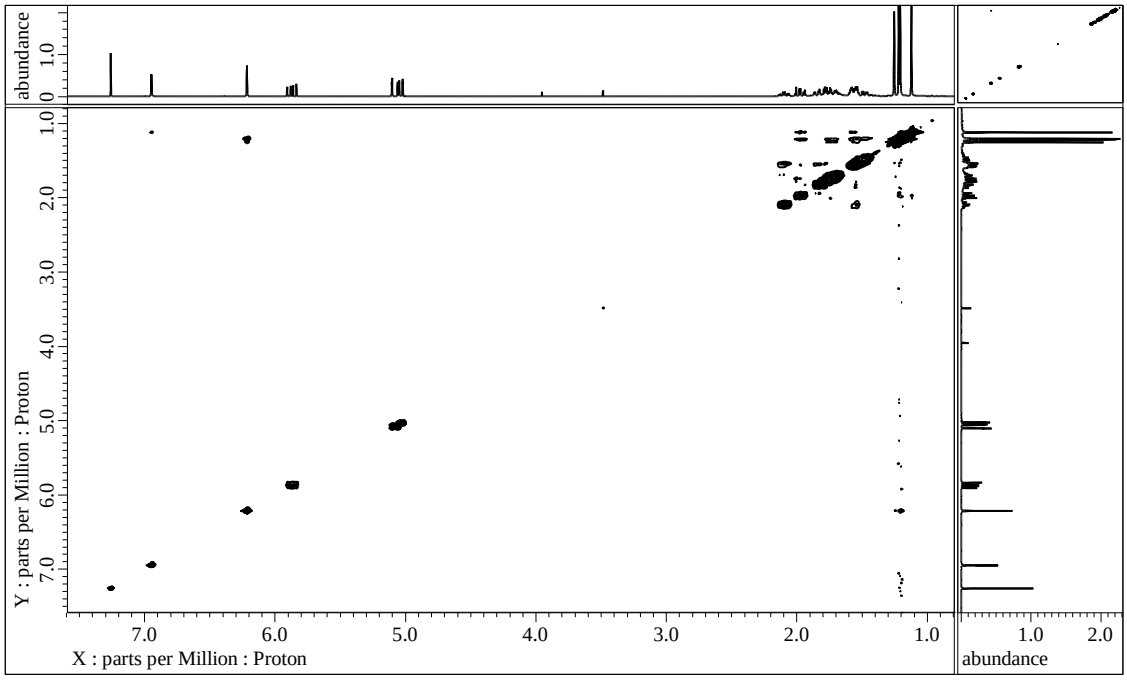

Figure S58. NOESY spectrum of **8** in $CDCl_3$

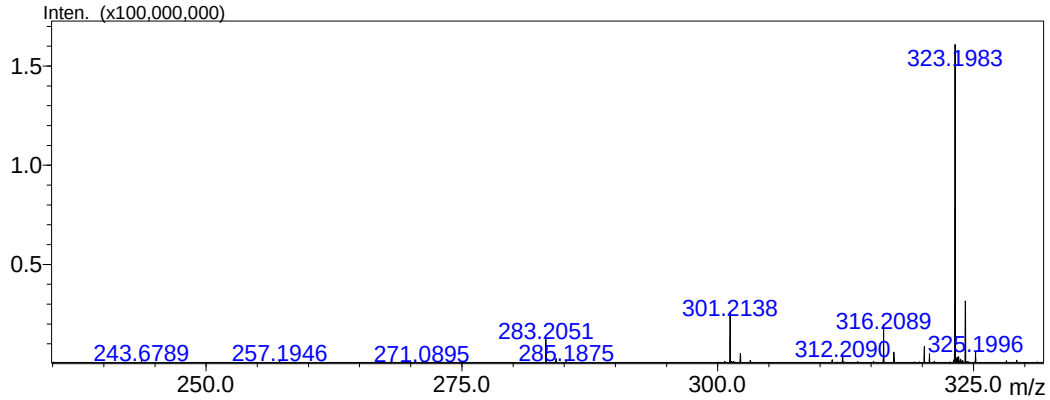

Figure S59. HRESIMS of **8**

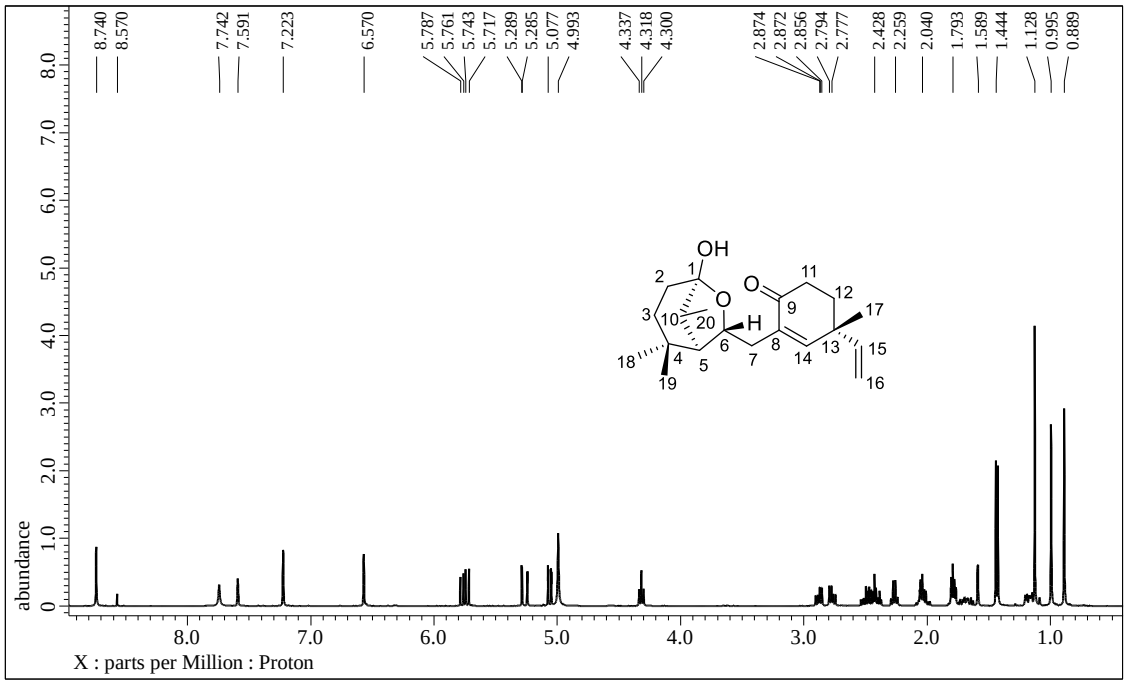

Figure S60. ^{1}H NMR spectrum (pyridine-d_5, 400 MHz) of **9**

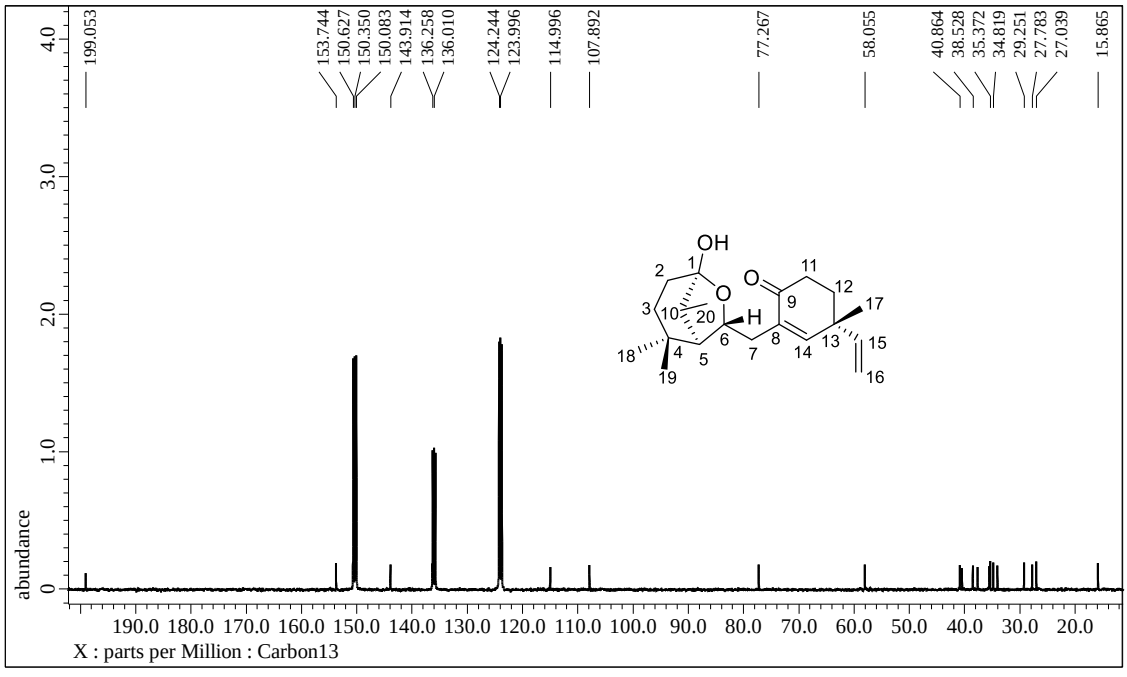

Figure S61. ^{13}C NMR spectrum (pyridine-d_5, 100 MHz) of **9**

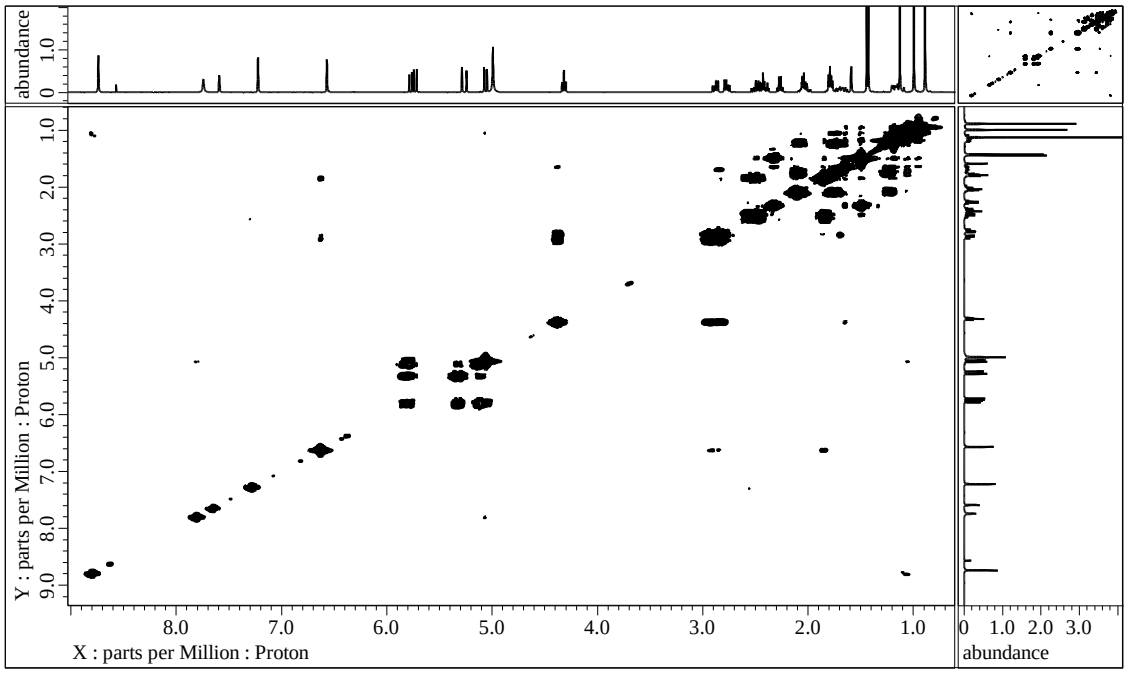

Figure S62. ^{1}H–^{1}H COSY spectrum of **9** in pyridine-d_5

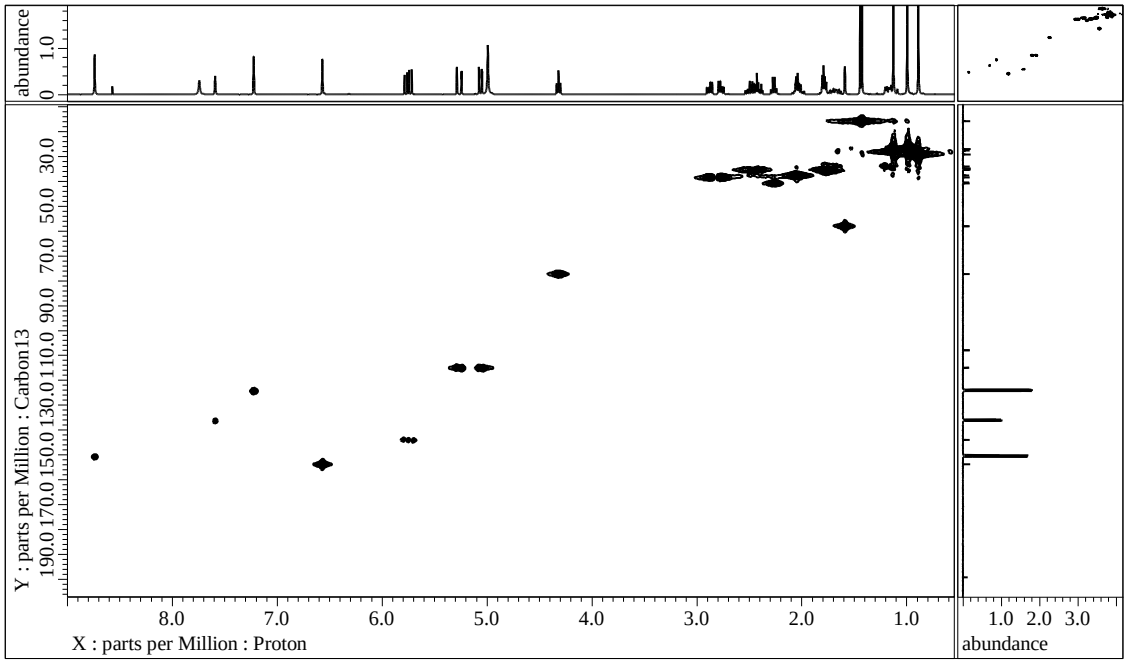

Figure S63. HMQC spectrum of **9** in pyridine-d_5

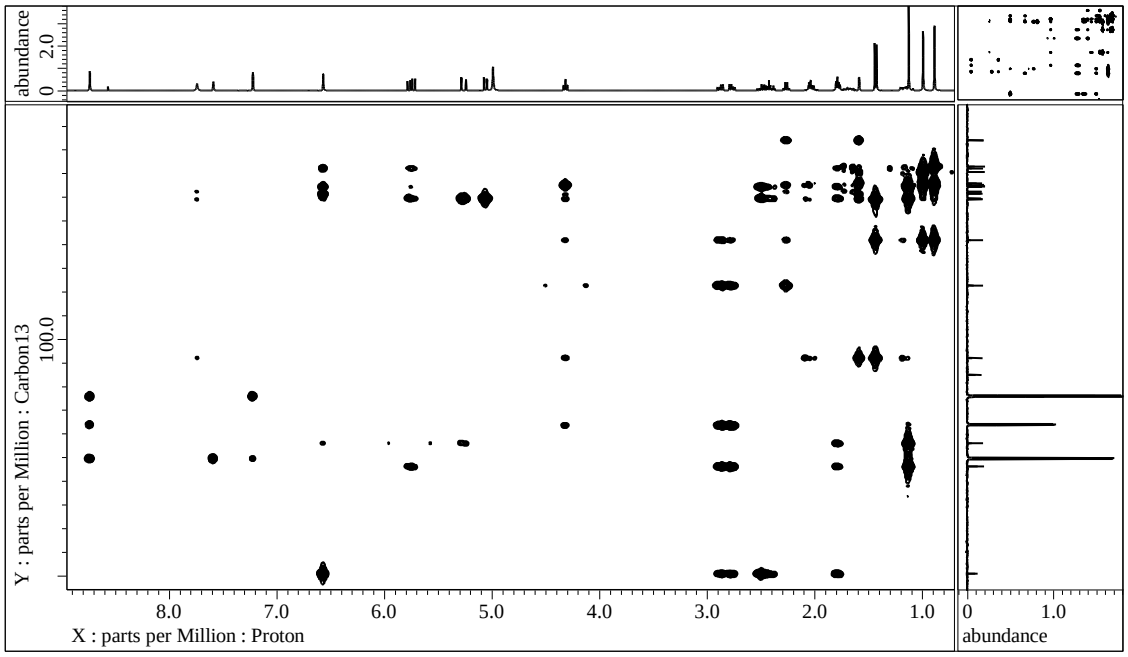

Figure S64. HMBC spectrum of **9** in pyridine-d_5

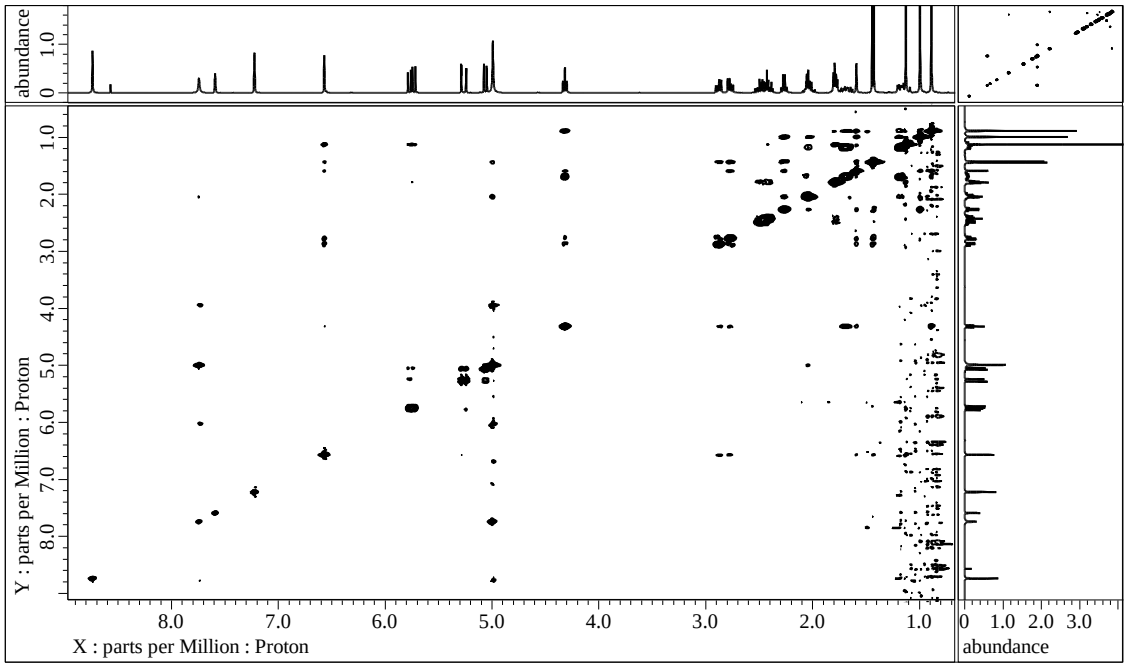

Figure S65. NOESY spectrum of **9** in pyridine-d_5

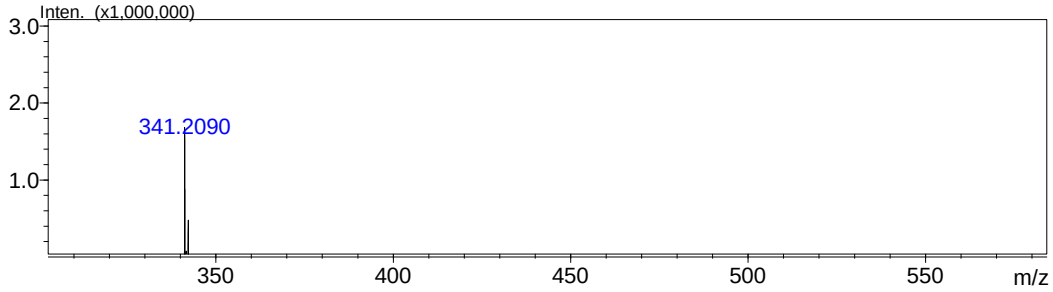

Figure S66. HRESIMS of **9**

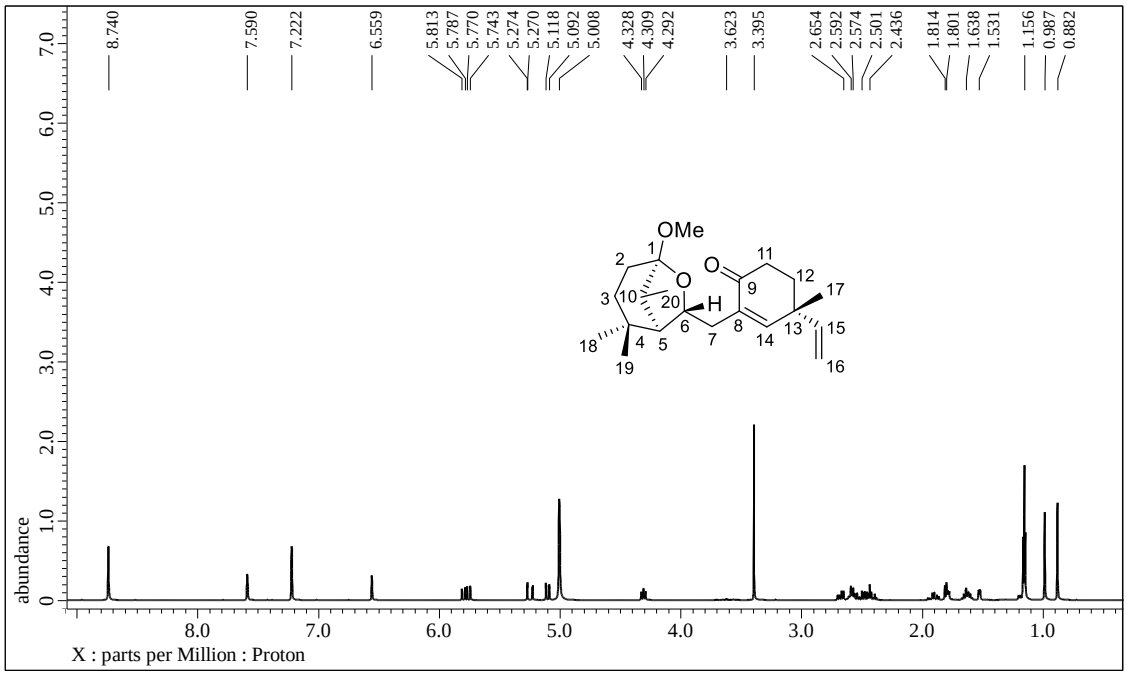

Figure S67. ^{1}H NMR spectrum (pyridine-d_5, 400 MHz) of **10**

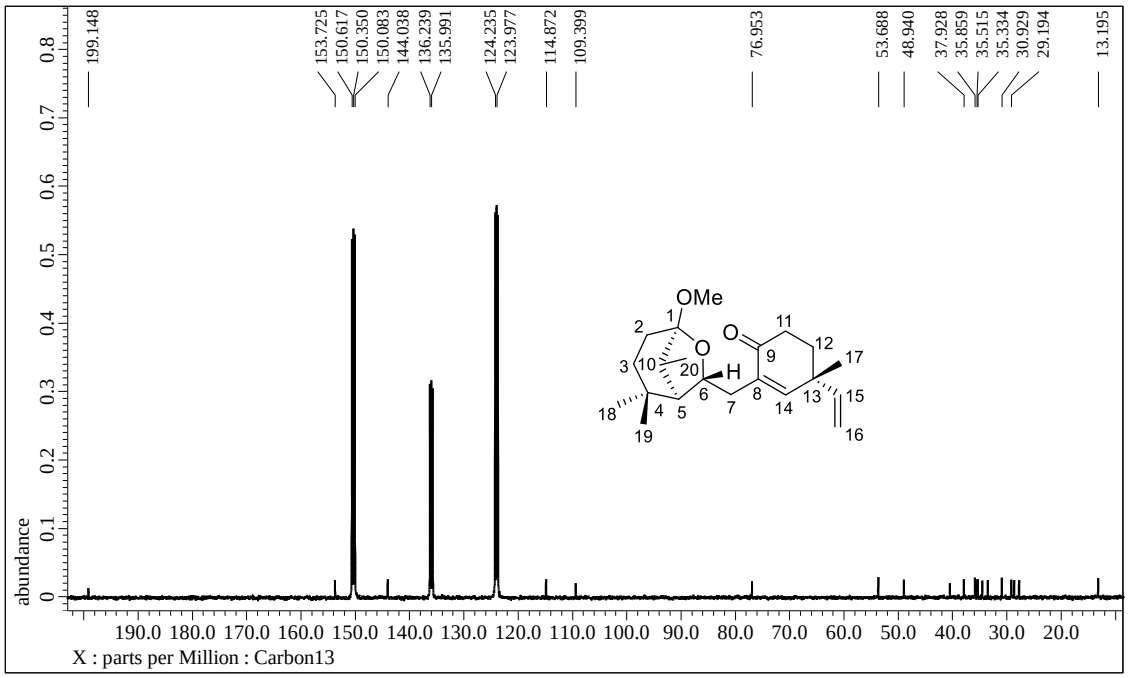

Figure S68. ^{13}C NMR spectrum (pyridine-d_5, 100 MHz) of **10**

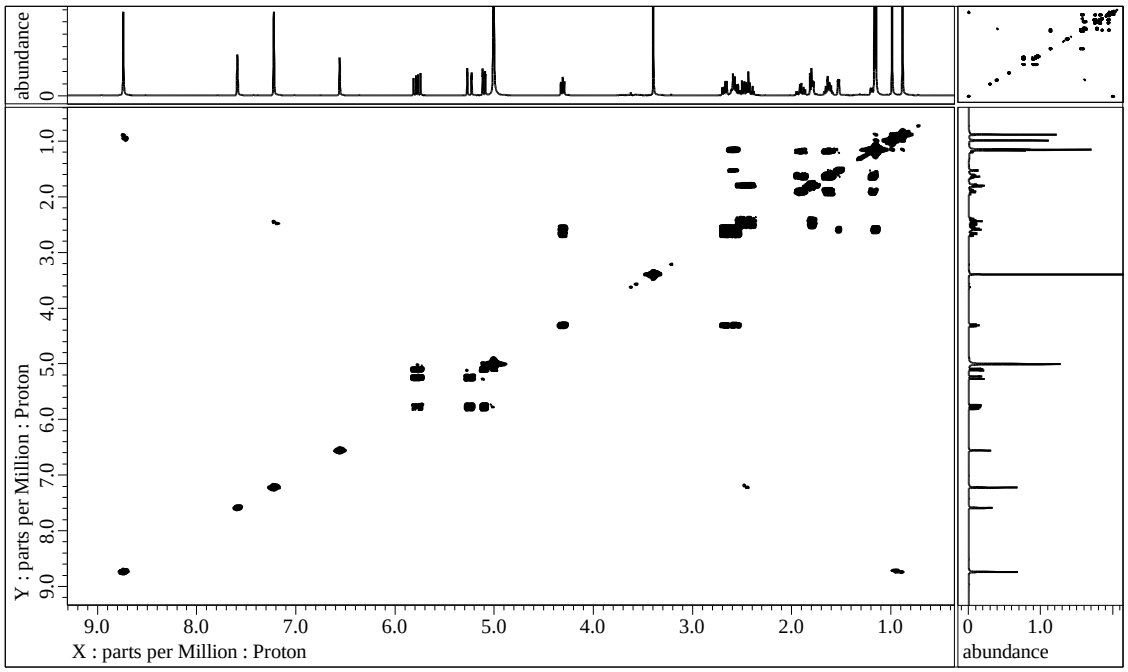

Figure S69. ^{1}H–^{1}H COSY spectrum of **10** in pyridine-d_5

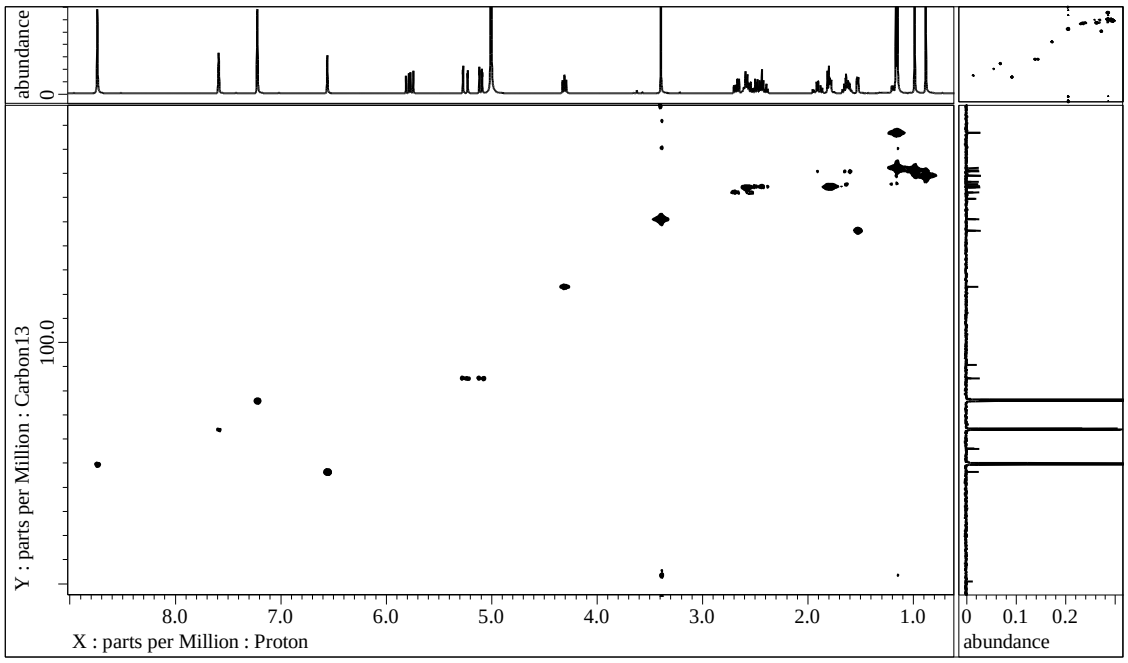

Figure S70. HMQC spectrum of **10** in pyridine-d_5

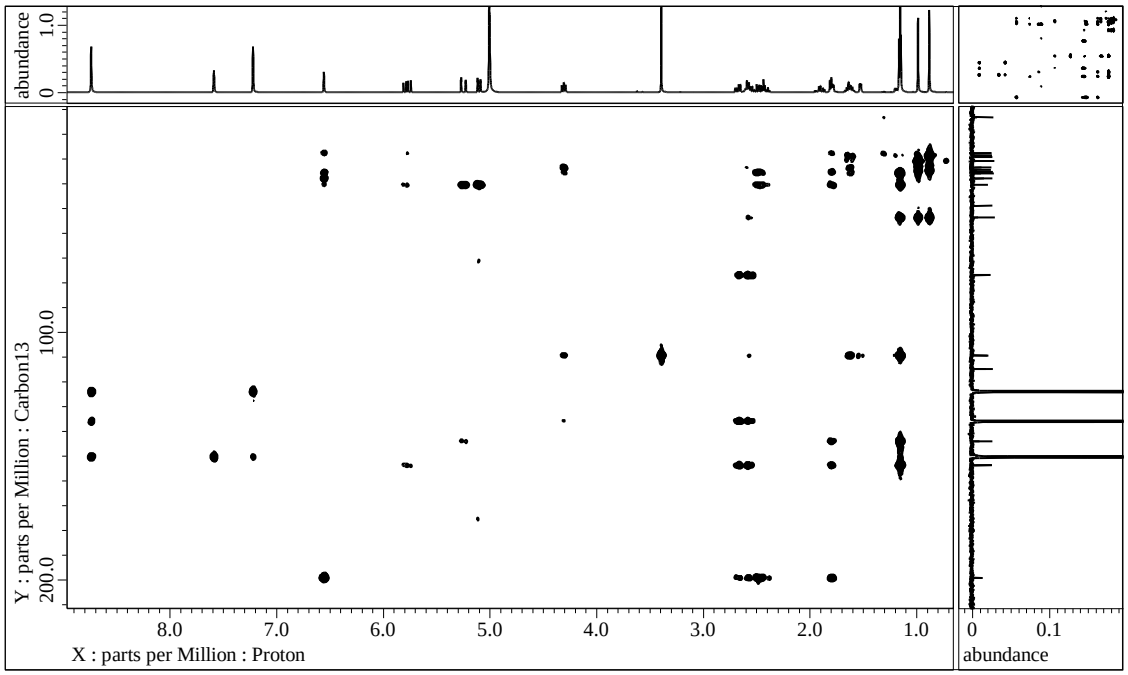

Figure S71. HMBC spectrum of **10** in pyridine-d_5

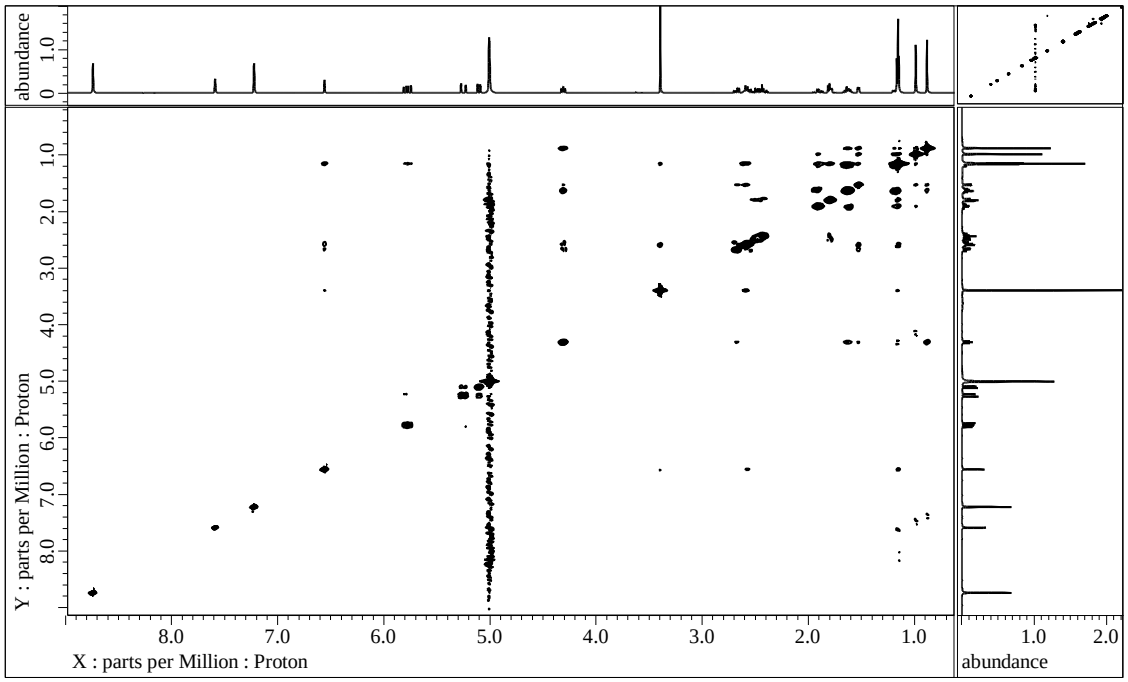

Figure S72. NOESY spectrum of **10** in pyridine-d_5

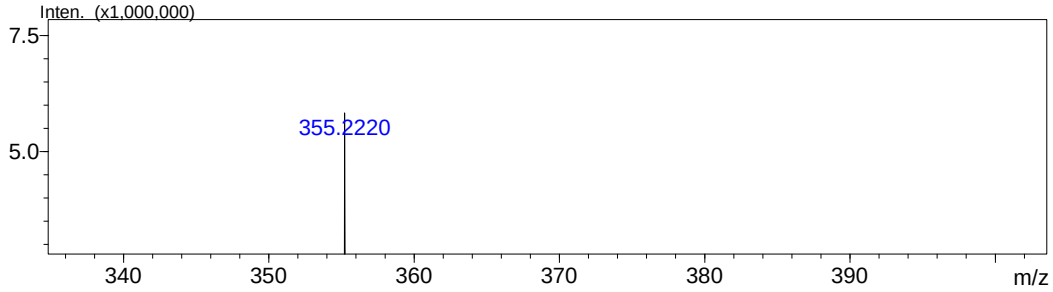

Figure S73. HRESIMS of **10**

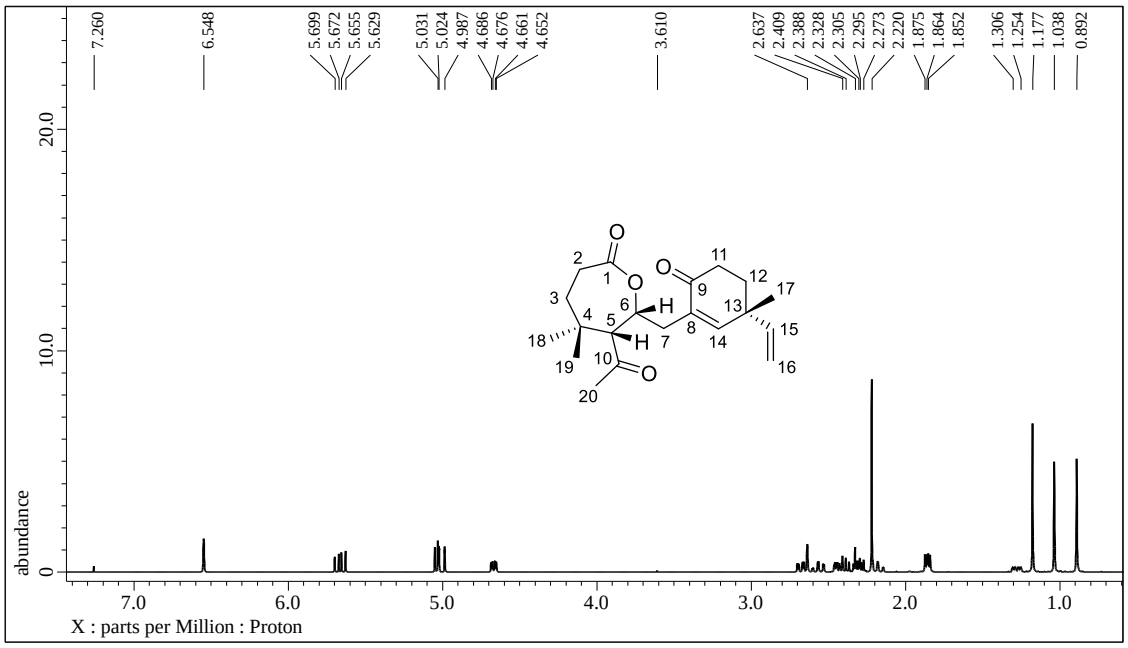

Figure S74. ^{1}H NMR spectrum ($CDCl_3$, 400 MHz) of **11**

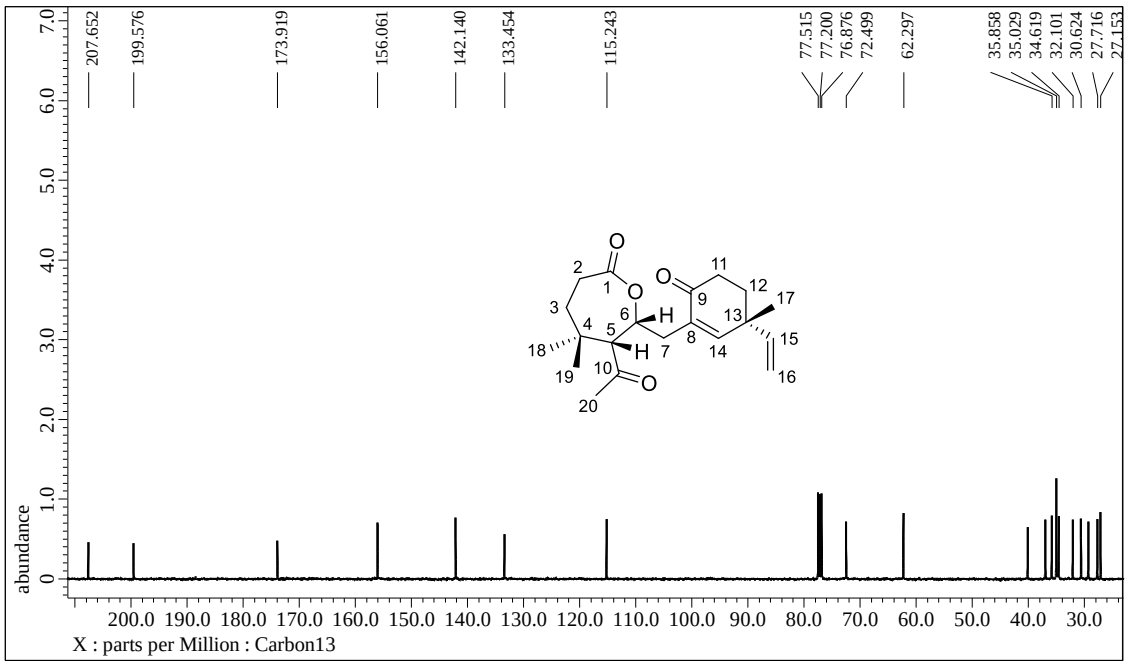

Figure S75. ^{13}C NMR spectrum ($CDCl_3$, 100 MHz) of **11**

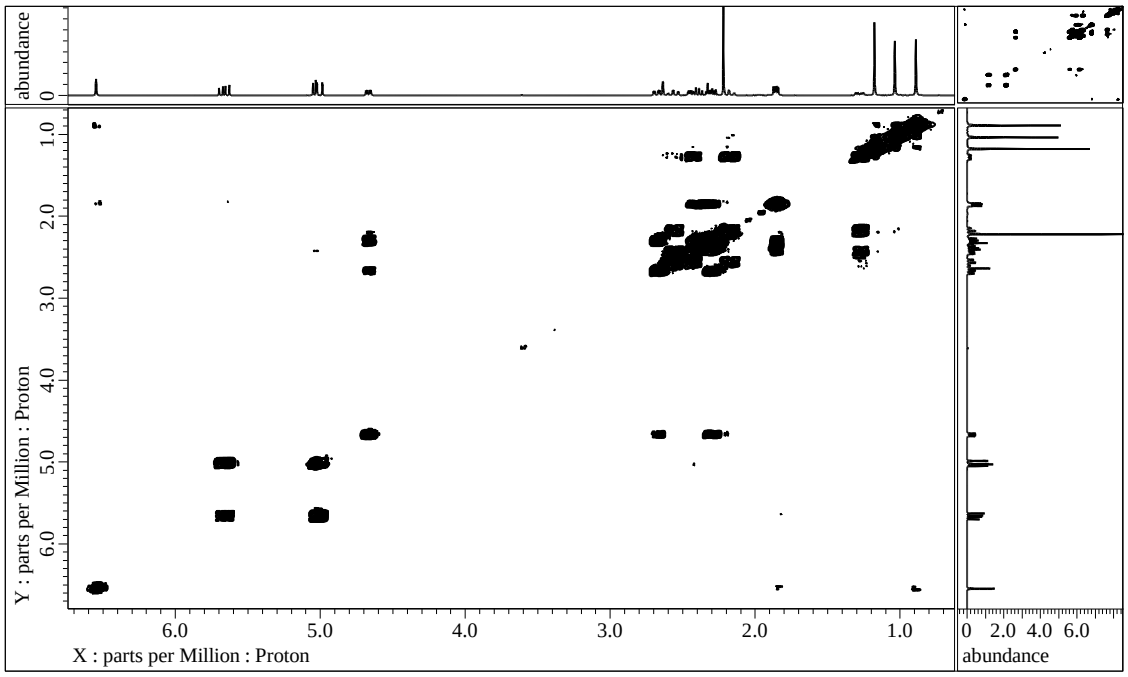

Figure S76. $^{1}H–^{1}H$ COSY spectrum of **11** in $CDCl_3$

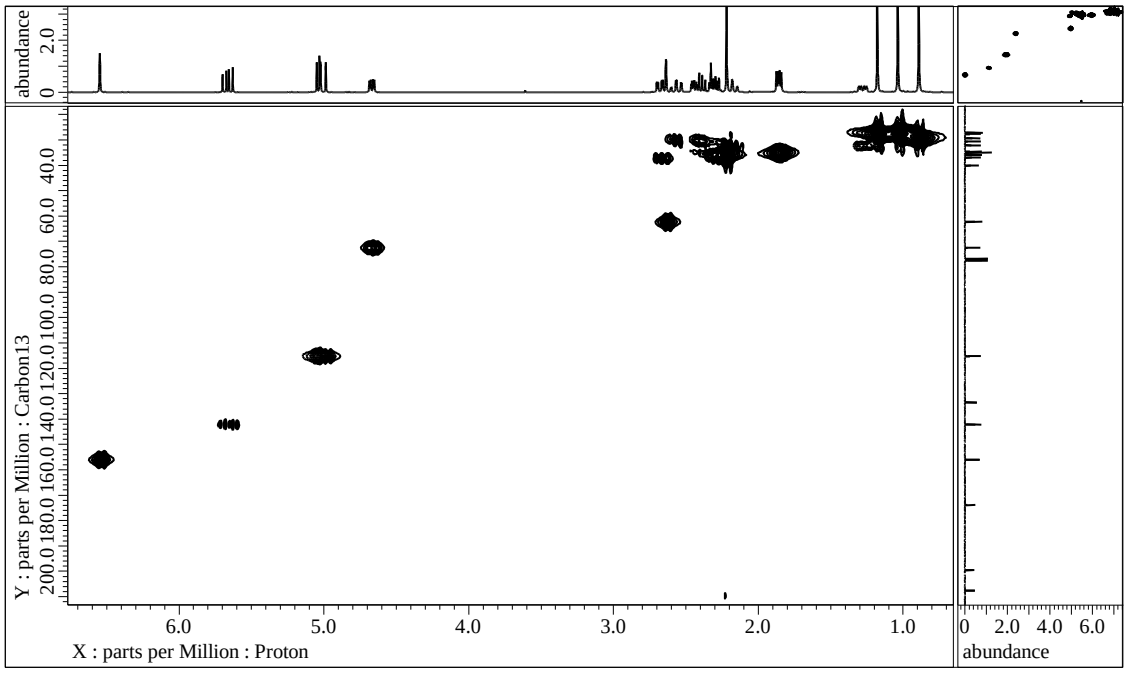

Figure S77. HMQC spectrum of **11** in $CDCl_3$

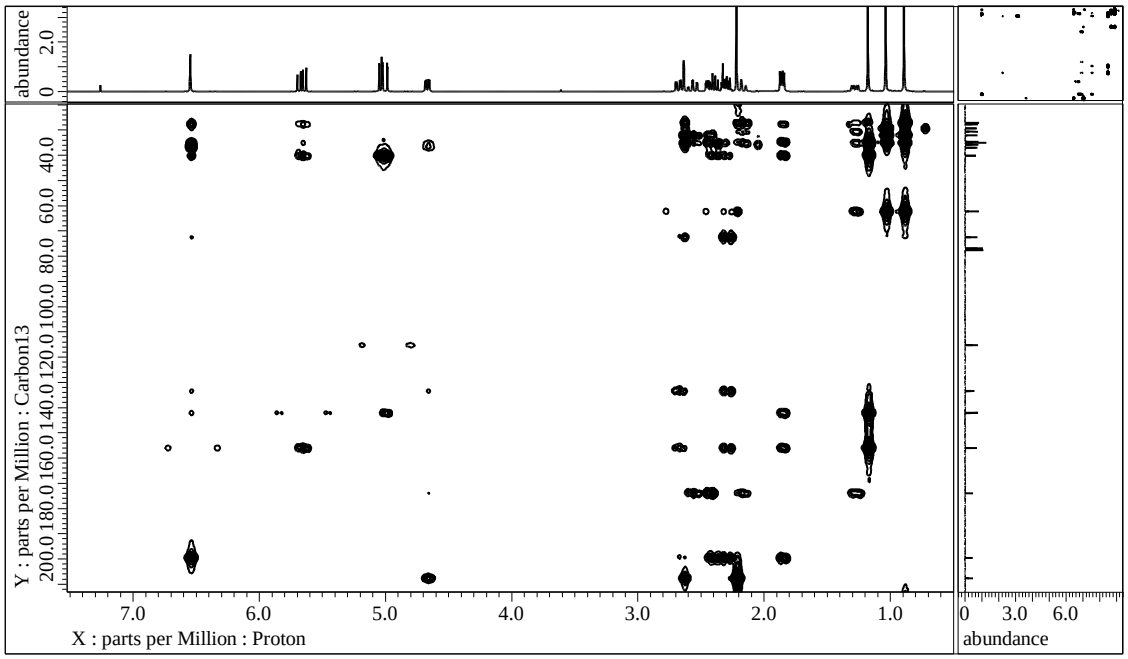

Figure S78. HMBC spectrum of **11** in $CDCl_3$

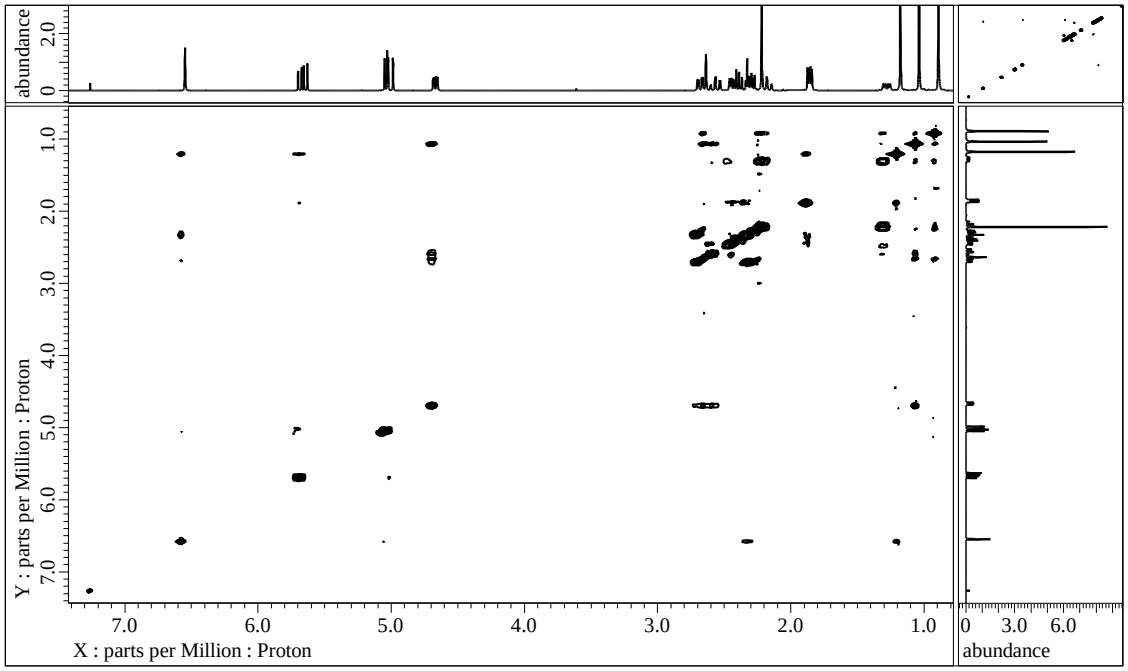

Figure S79. NOESY spectrum of **11** in $CDCl_3$

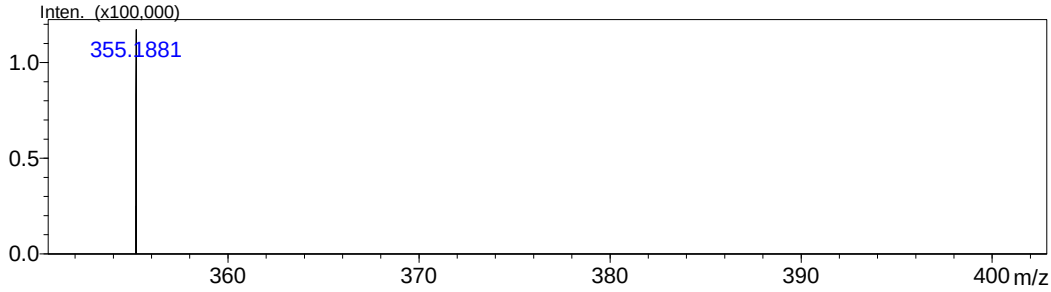

Figure S80. HRESIMS of **11**

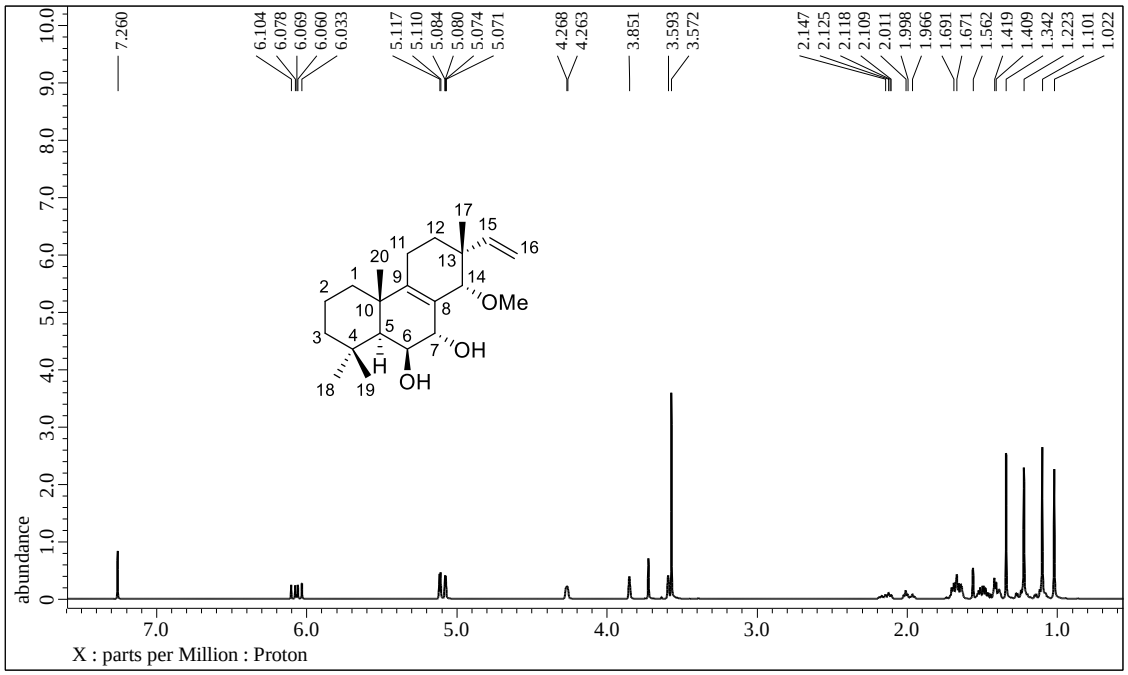

Figure S81. ^{1}H NMR spectrum ($CDCl_3$, 400 MHz) of **12**

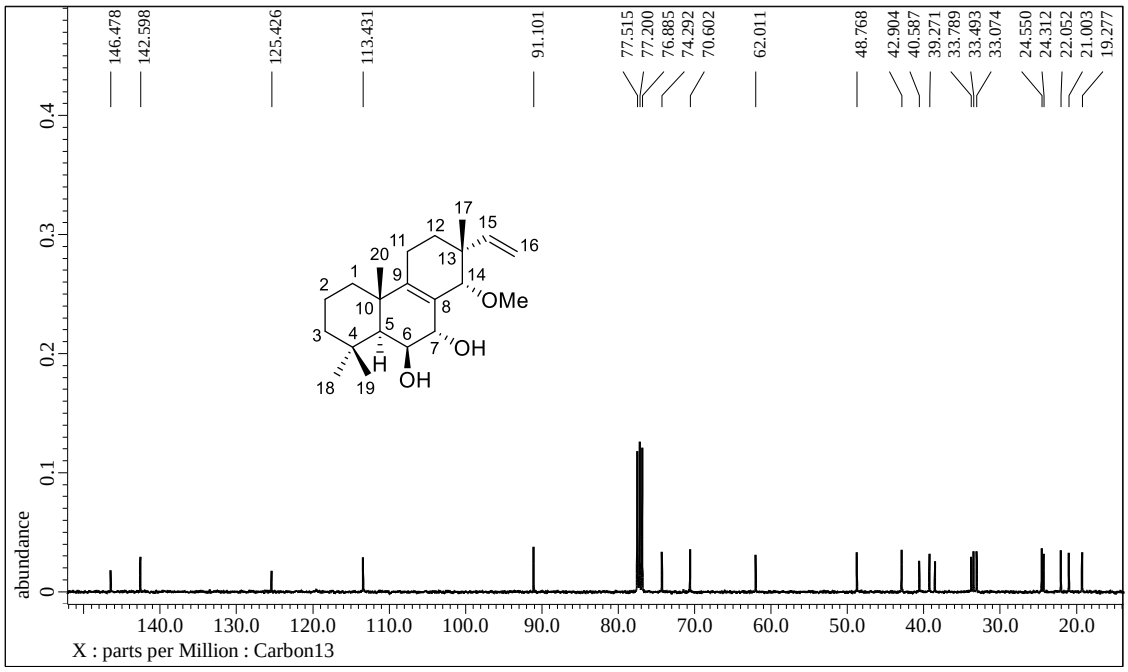

Figure S82. ^{13}C NMR spectrum ($CDCl_3$, 100 MHz) of **12**

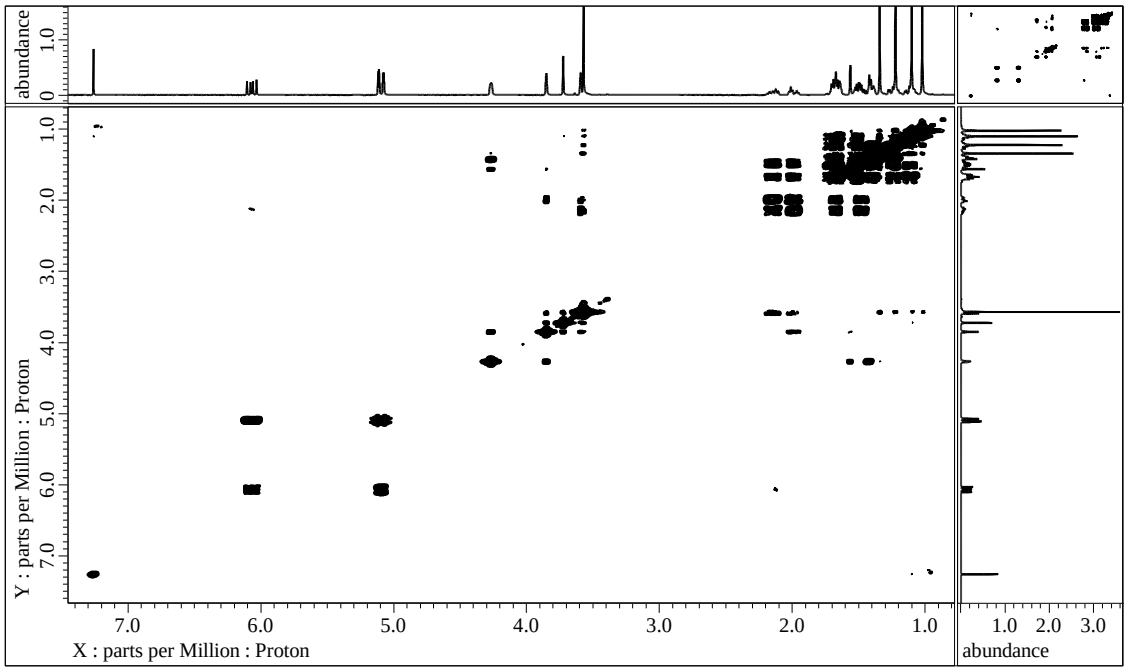

Figure S83. $^{1}H–^{1}H$ COSY spectrum of **12** in $CDCl_3$

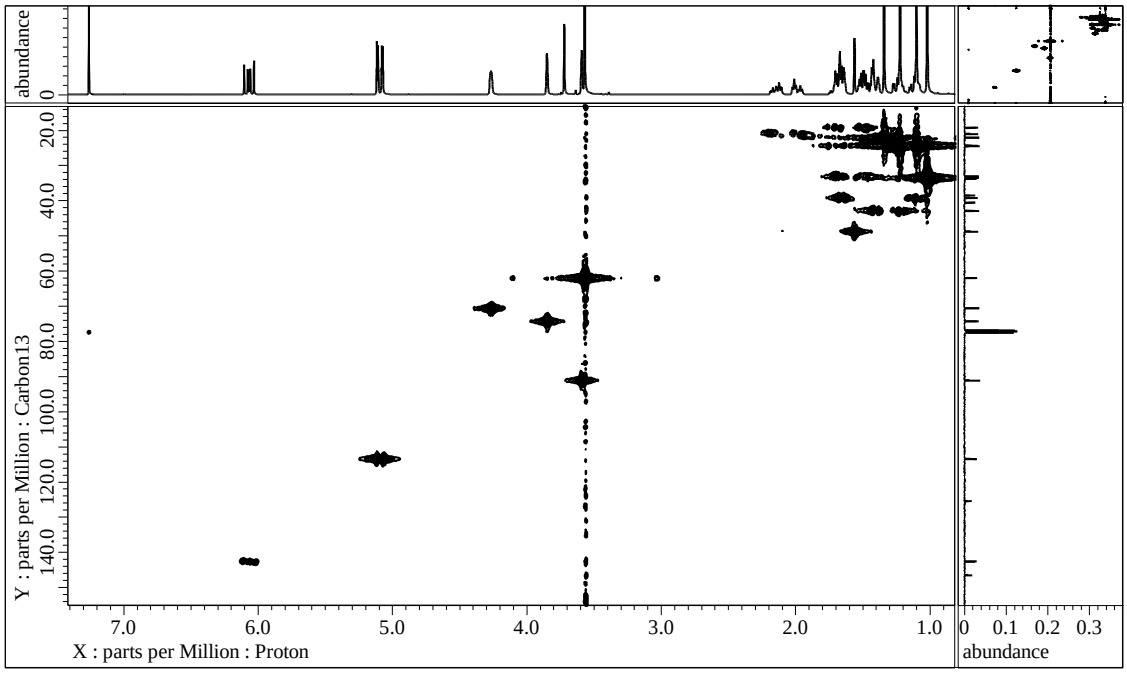

Figure S84. HMQC spectrum of **12** in $CDCl_3$

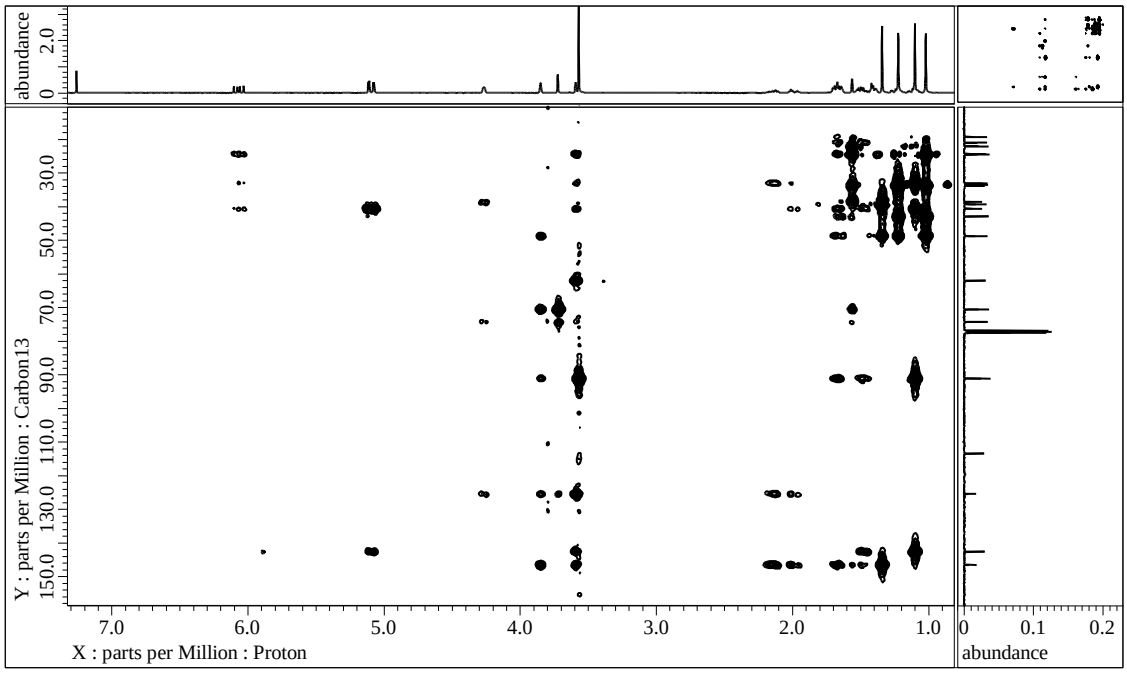

Figure S85. HMBC spectrum of **12** in $CDCl_3$

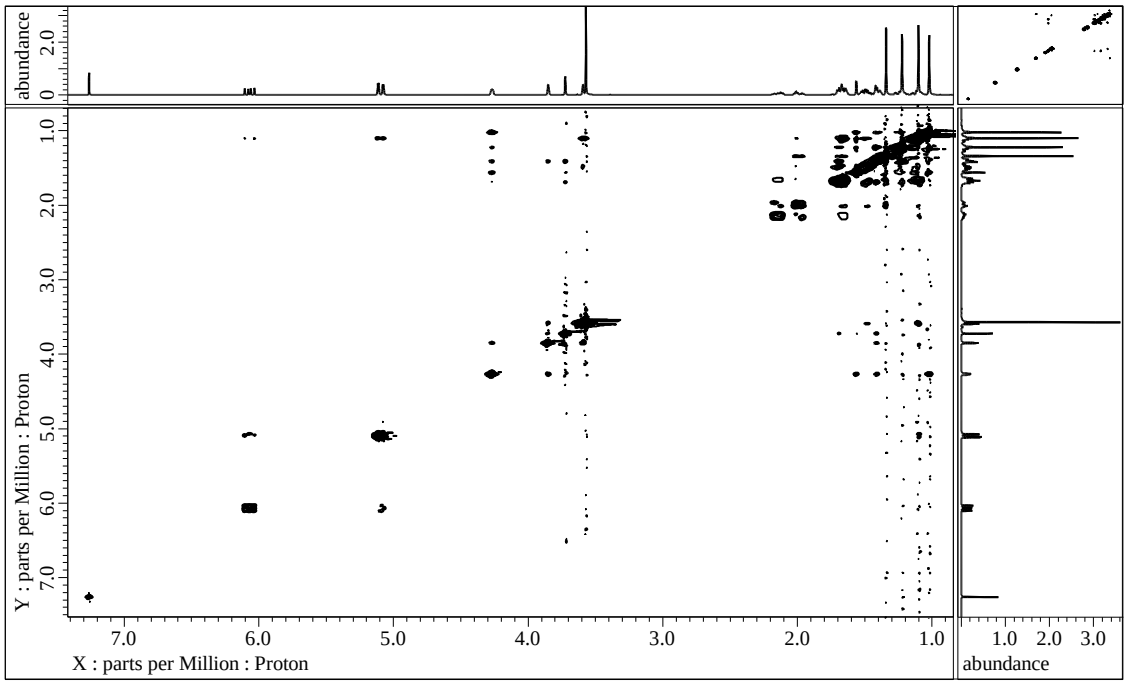

Figure S86. NOESY spectrum of **12** in $CDCl_3$

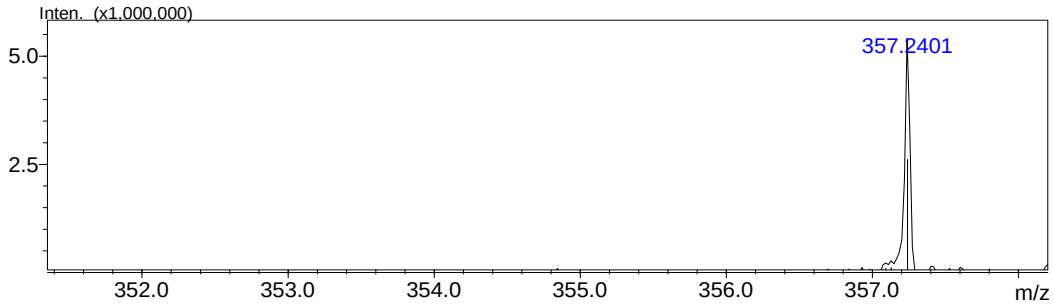

Figure S87. HRESIMS of **12**

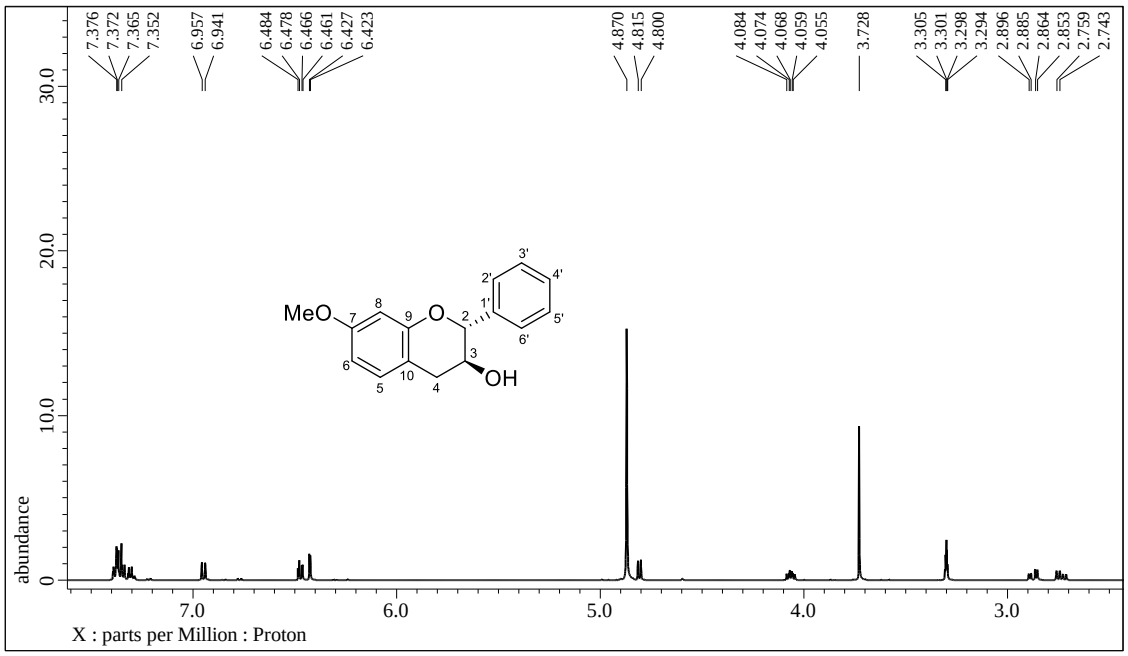

Figure S88. ^{1}H NMR spectrum (methanol-d_4, 500 MHz) of **32**

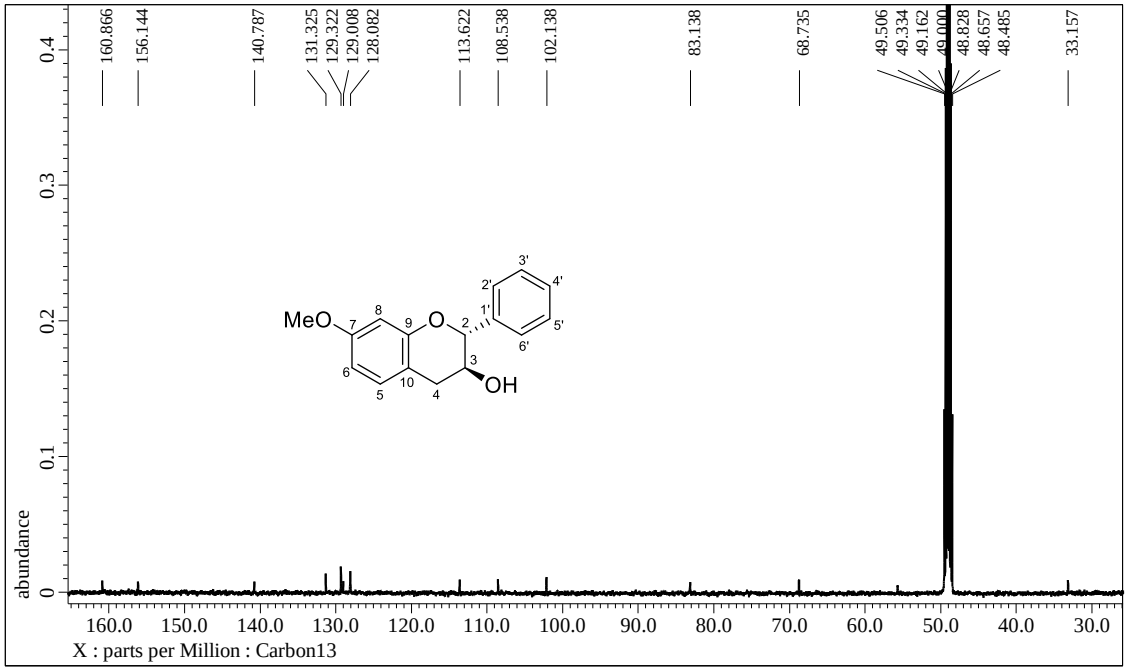

Figure S89. ^{13}C NMR spectrum (methanol-d_4, 125 MHz) of **32**

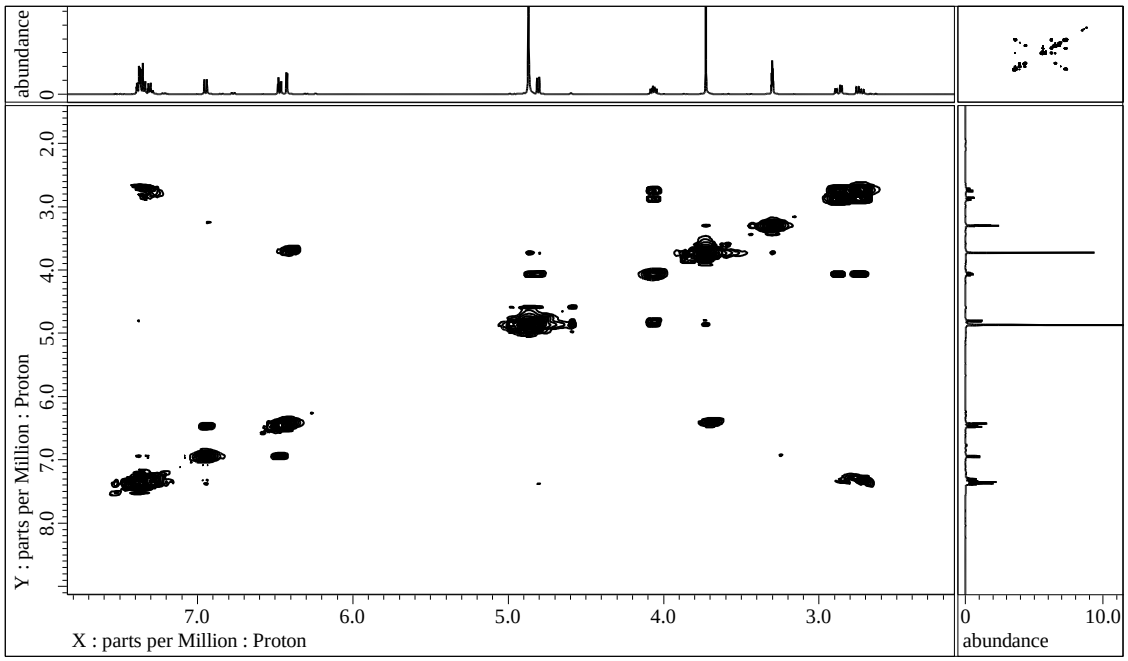

Figure S90. $^{1}H–^{1}H$ COSY spectrum of **32** in methanol-d_4

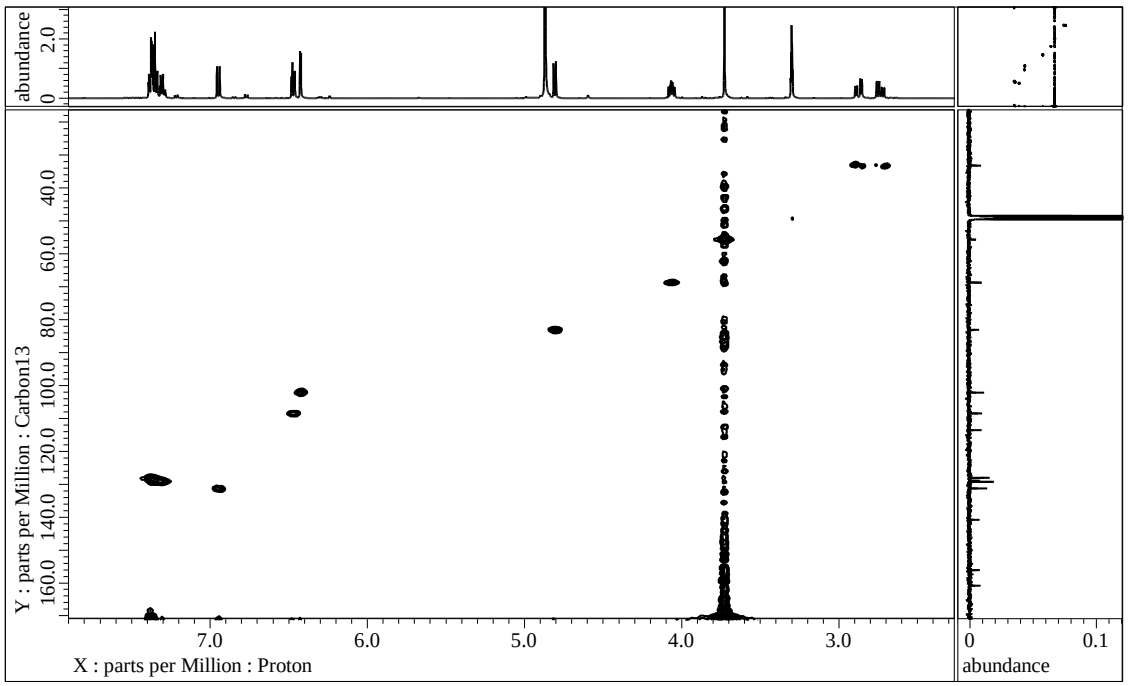

Figure S91. HMQC spectrum of **32** in methanol-d_4

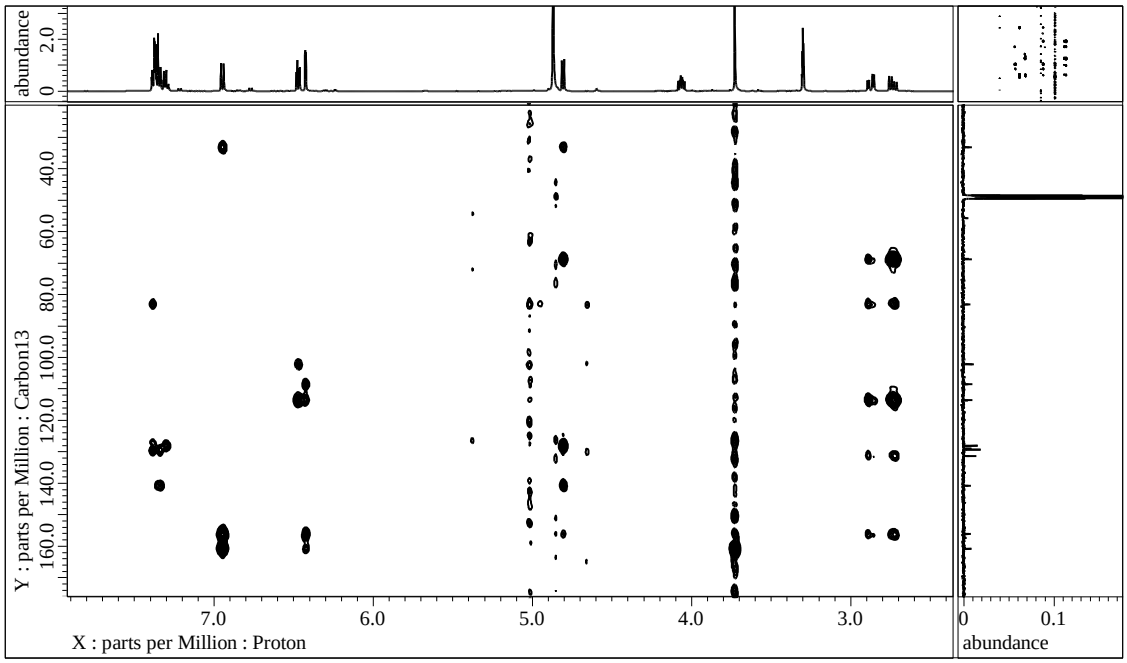

Figure S92. HMBC spectrum of **32** in methanol-d_4

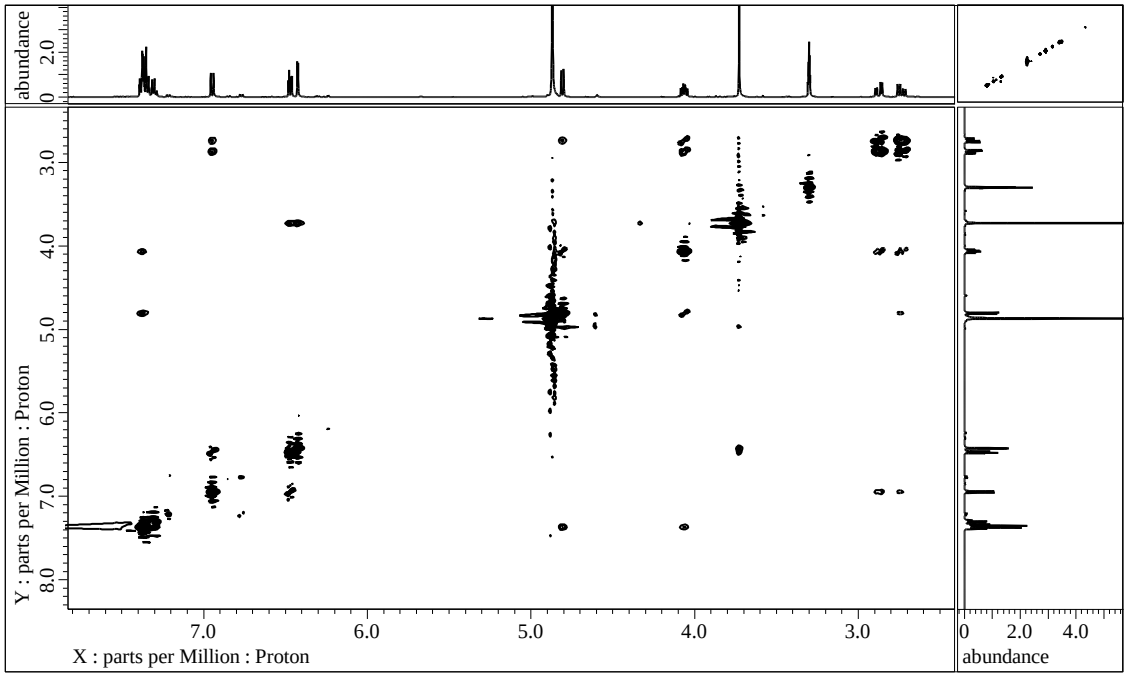

Figure S93. NOESY spectrum of **32** in methanol-d_4

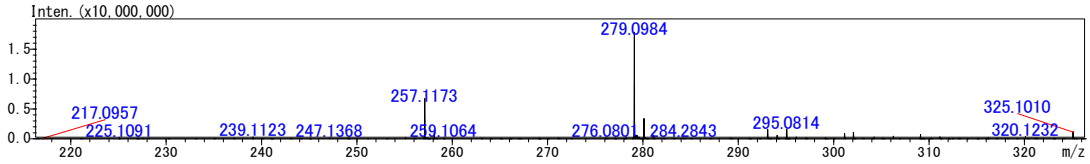

Figure S94. HRESIMS of **32**

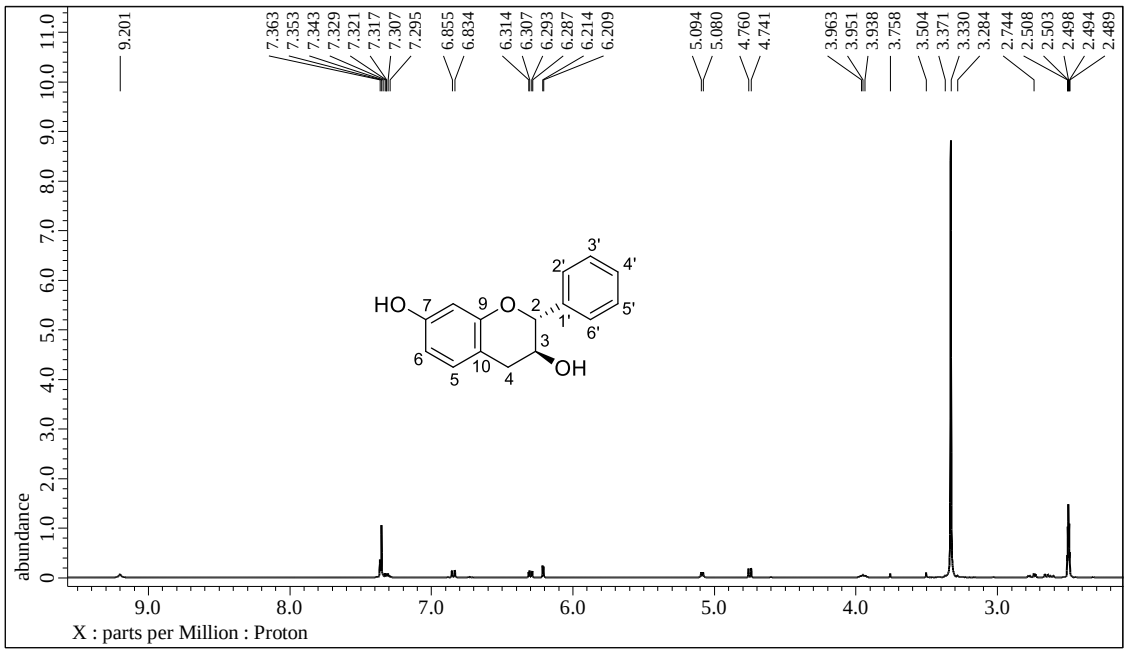

Figure S95. ^{1}H NMR spectrum (DMSO-d_6, 400 MHz) of **33**

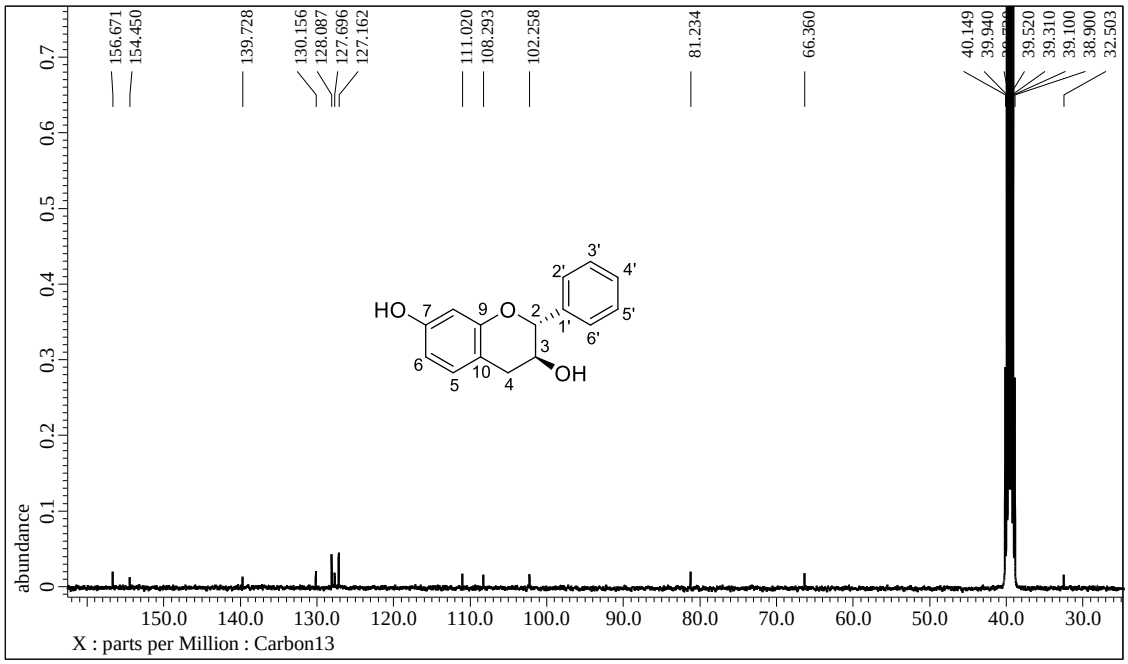

Figure S96. ^{13}C NMR spectrum (DMSO-d_6, 100 MHz) of **33**

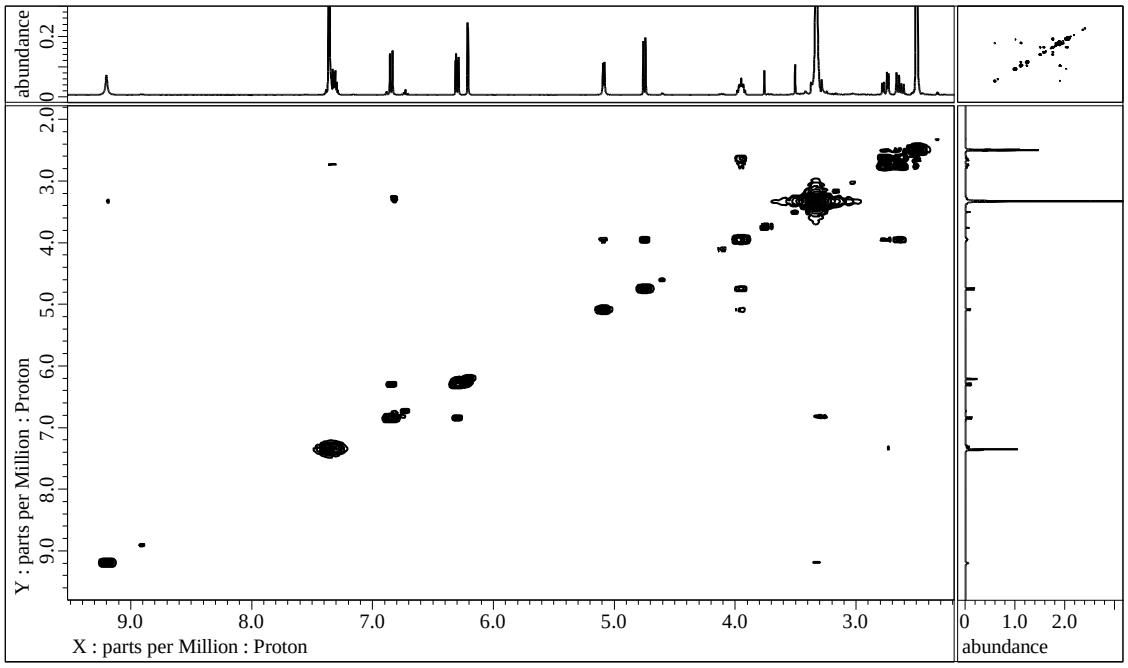

Figure S97. $^{1}H–^{1}H$ COSY spectrum of **33** in DMSO-d_6

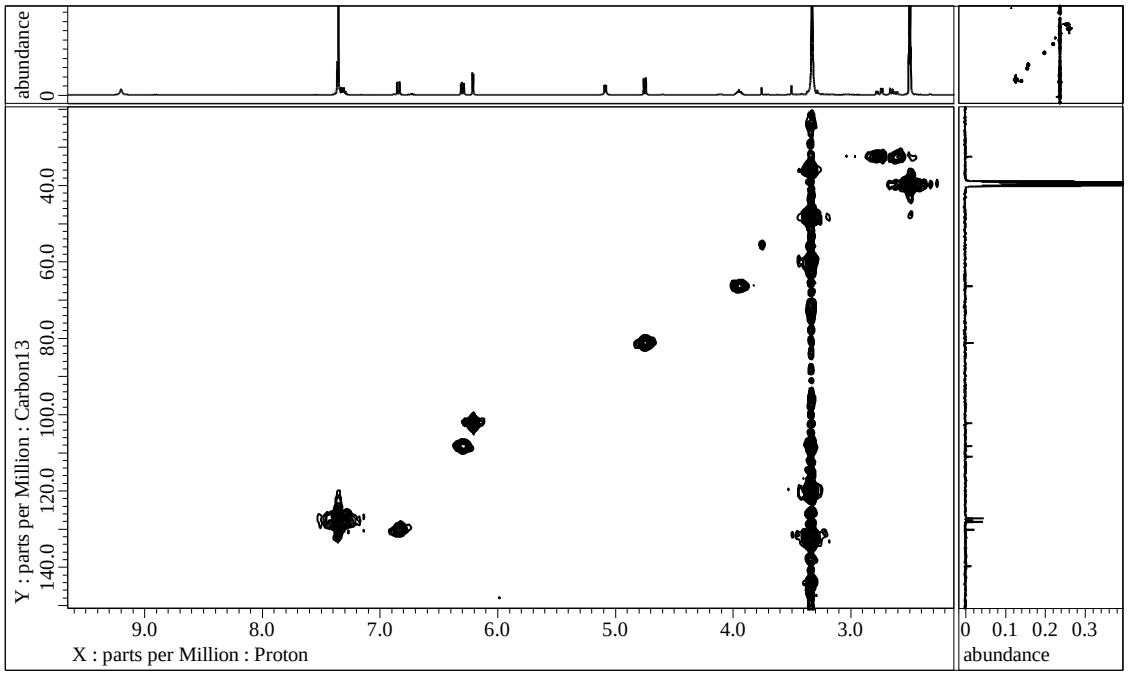

Figure S98. HMQC spectrum of **33** in DMSO-d_6

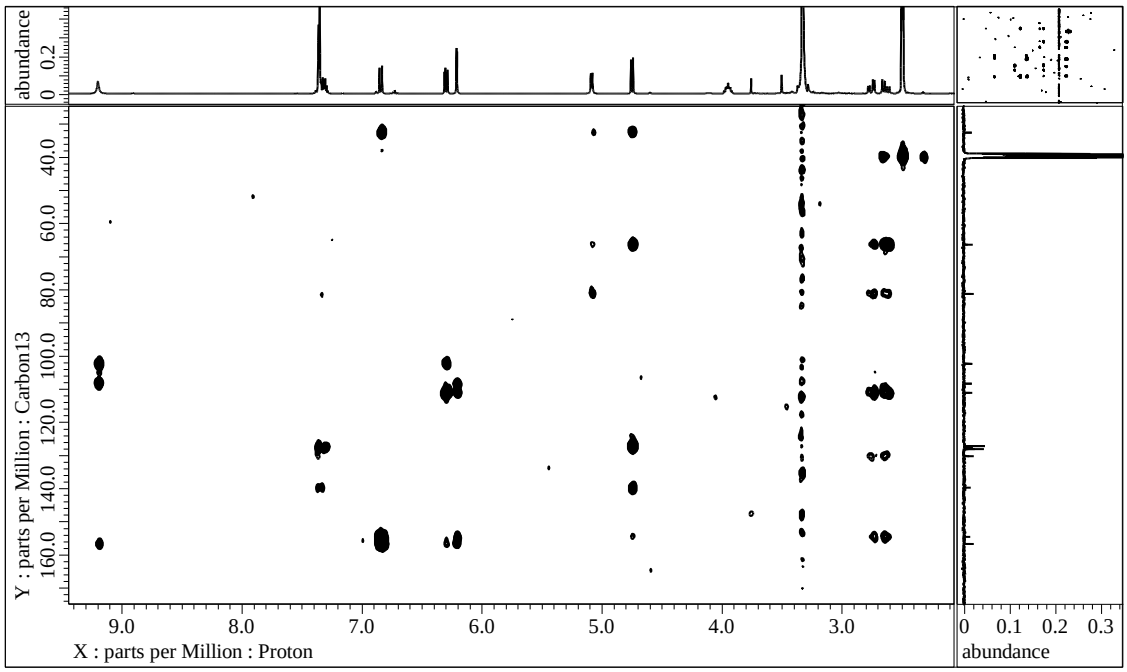

Figure S99. HMBC spectrum of **33** in DMSO-d_6

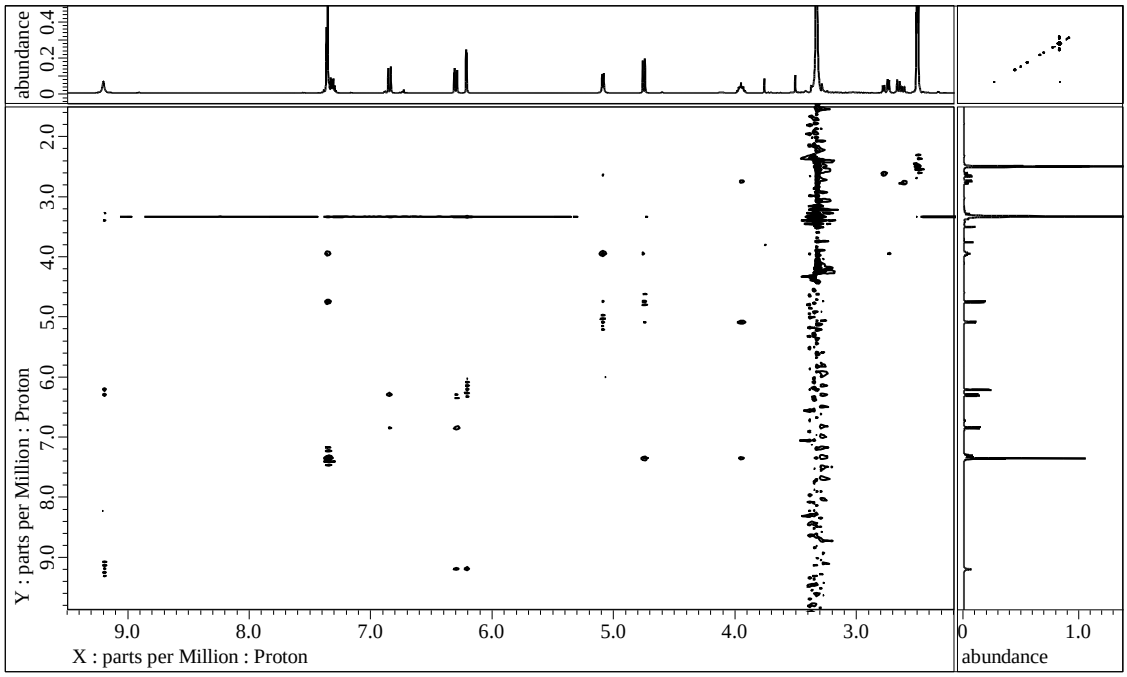

Figure S100. NOESY spectrum of **33** in DMSO-d_6

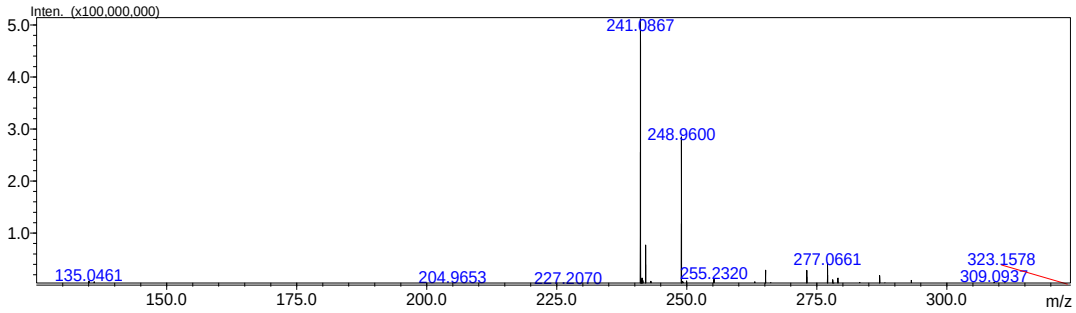

Figure S101. HRESIMS of **33**

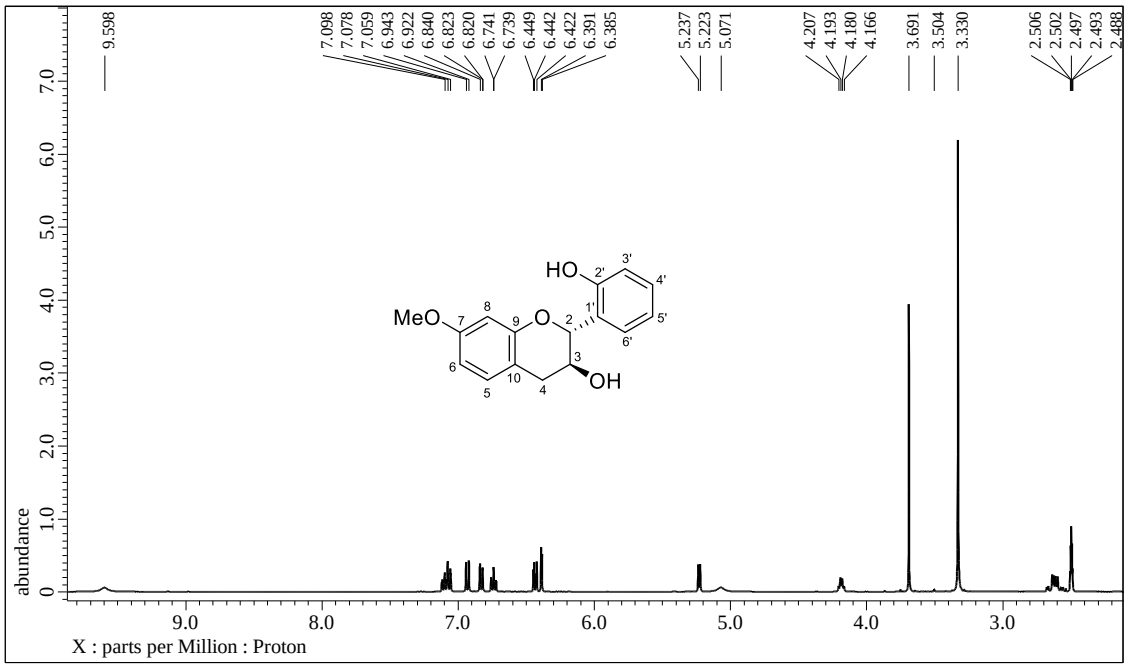

Figure S102. ^{1}H NMR spectrum (DMSO-d_6, 400 MHz) of **34**

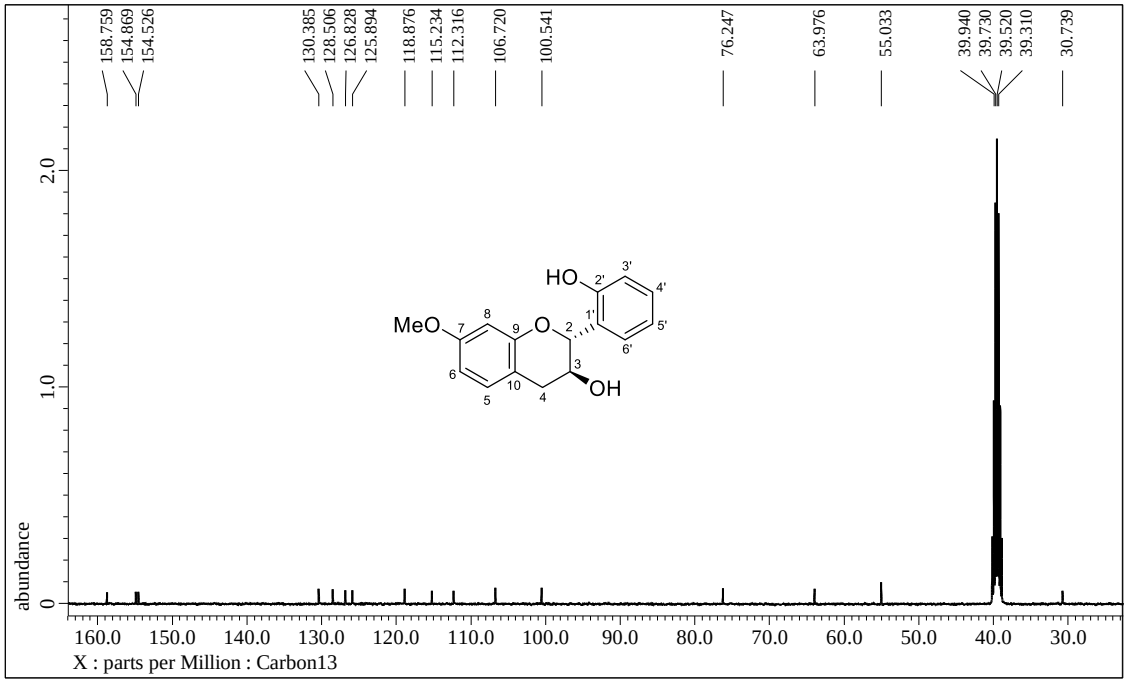

Figure S103. ^{13}C NMR spectrum (DMSO-d_6, 100 MHz) of **34**

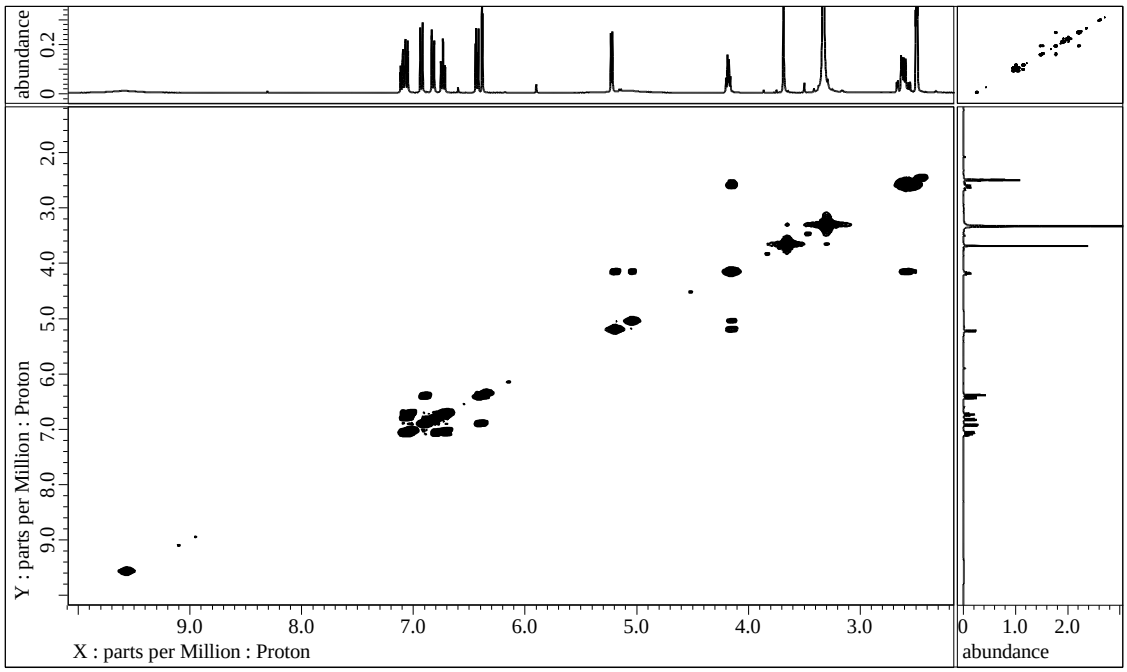

Figure S104. ^{1}H–^{1}H COSY spectrum of **34** in DMSO-d_6

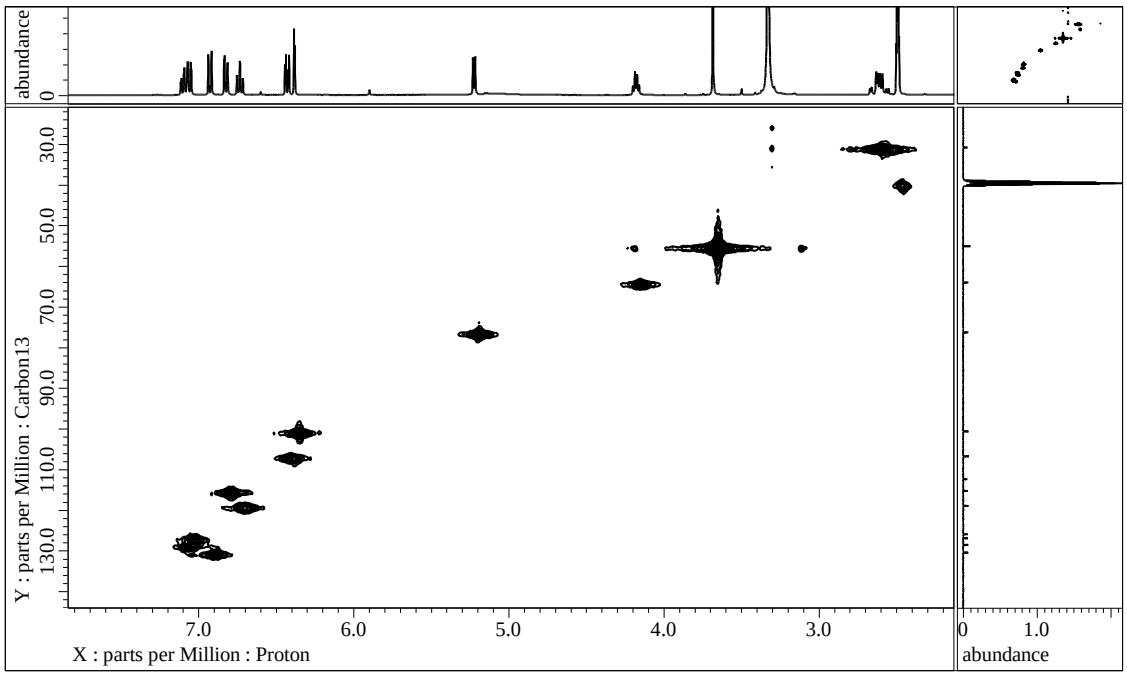

Figure S105. HMQC spectrum of **34** in DMSO-d_6

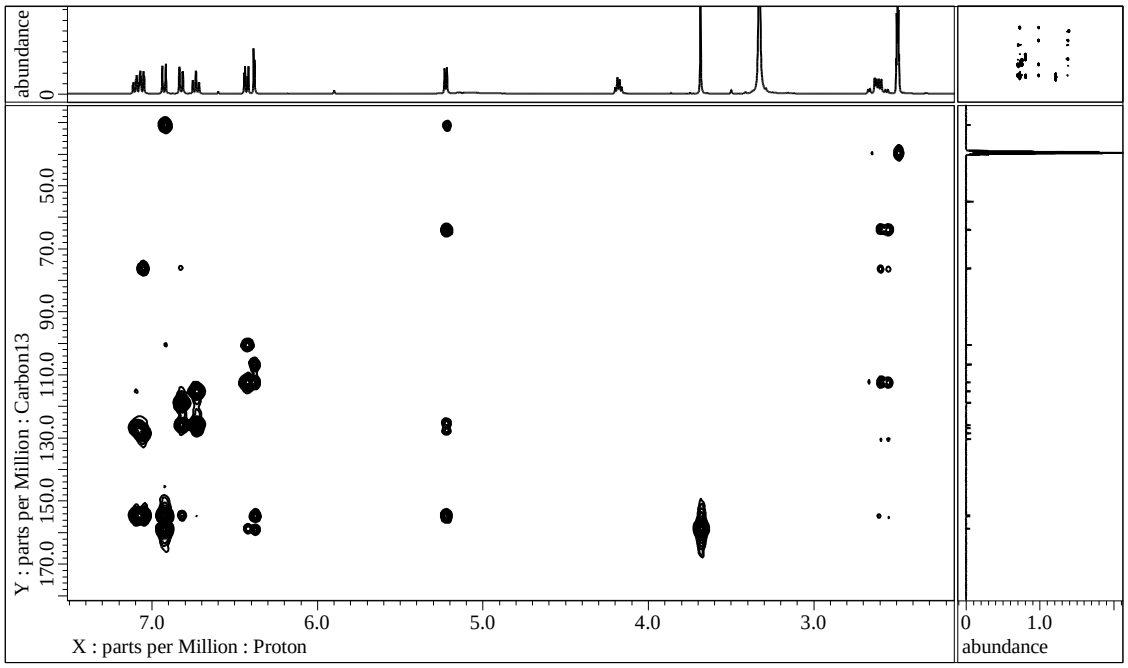

Figure S106. HMBC spectrum of **34** in DMSO-d_6

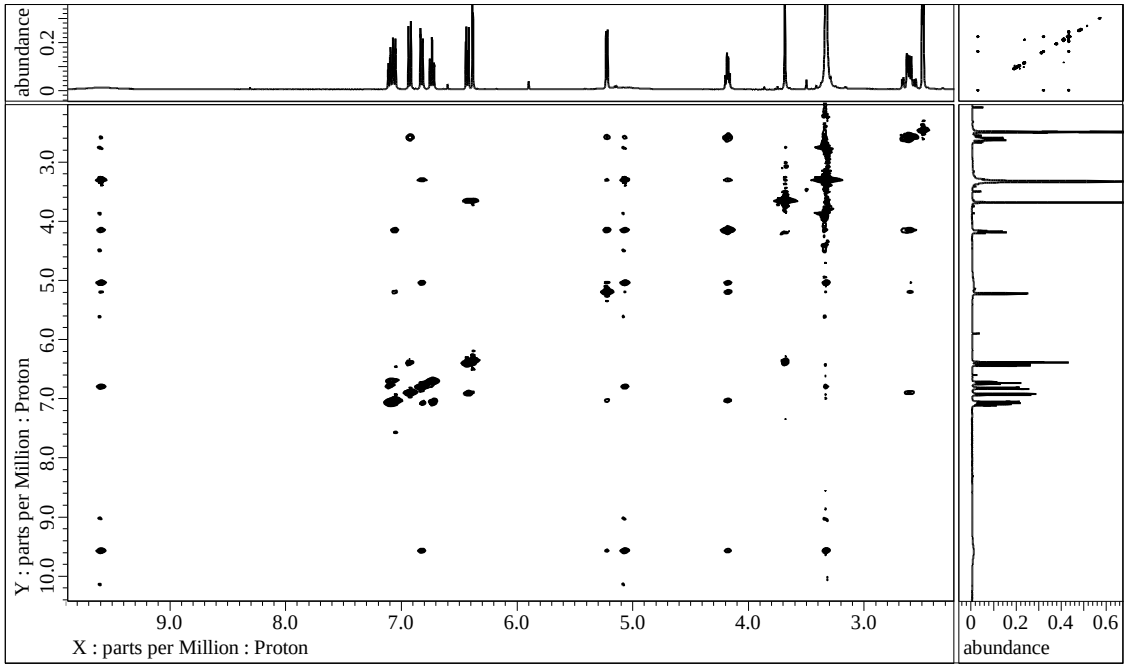

Figure S107. NOESY spectrum of **34** in DMSO-d_6

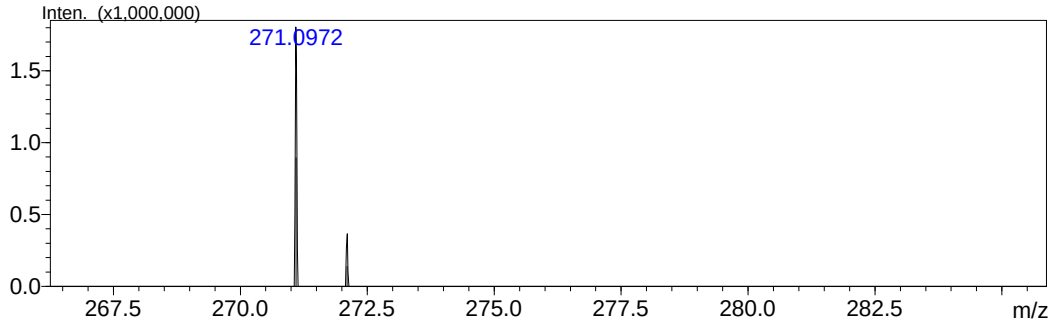

Figure S108. HRESIMS of **34**